

THIRD SLOPE TECTONICS CONFERENCE

TRONDHEIM, 8-12 SEPTEMBER 2014
GEOLOGICAL SURVEY OF NORWAY,

Organizers

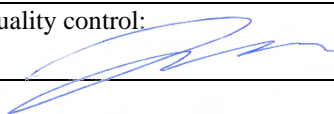


Supporters



NGU Report 2014.031

3rd Slope Tectonics conference –
Field excursion guide

Report no.: 2014.031		ISSN: 0800–3416		Grading: Open	
Title: 3rd Slope Tectonics conference – Field excursion guide					
Authors: T. Oppikofer, R.L. Hermanns, G. Sandøy			Client: -		
County: Møre og Romsdal			Commune: -		
Map-sheet name (M=1:250.000) Ålesund, Røros & Sveg			Map-sheet no. and -name (M=1:50.000) -		
Deposit name and grid-reference: -			Number of pages: 167		Price (NOK): 315
			Map enclosures: 0		
Fieldwork carried out: -	Date of report: 05.09.2014		Project no.: 355400		Quality control: 
<p>Summary:</p> <p>The field trip of the 3rd Slope Tectonics conference visits areas of past rock slope failures and present-day unstable rock slopes and aims to discuss the structural and geological conditions of these sites, the morphologies and tectonic fabrics induced by slope movements and the role of glaciers, isostatic uplift and major faults in the development of rock slope failures.</p> <p>The trip leads from Trondheim to the glacially over steepened Sunndal and Romsdal Valleys in western Norway including following stops:</p> <ol style="list-style-type: none"> 1. Geological and structural control on slope deformation of the rockslide scar and unstable rock slope at Ivasnasen and unstable rock slope at Vollan 2. Rockfall-prone road section at Oppdølstranda 3. Multiple rock avalanche deposits in the Innerdal Valley, incl. Younger Dryas supra-glacial rock avalanche deposits and a lake dammed by a rock avalanche 4. Petroglyphs at Bogge in the Eresfjord, 6000 years old rock engravings 5. Back-analysis of the 1756 Tjellefonna rock avalanche, the largest historic rock avalanche in Norway 6. Role of a post-Caledonian fault in the development of a large deep-seated gravitational slope at Middagstinden in the Innfjorddal Valley 7. Multiple rock avalanche deposits in the Innfjorddal Valley, incl. rock avalanching into fjord that is now exposed due to isostatic rebound 8. Trollveggen cliff in the Romsdal Valley, the tallest vertical rock wall in Europe 9. Continuous monitoring and early-warning instrumentation of the Mannen rockslide in the Romsdal Valley and the combination of multiple data sources to improve the geological model 10. Rock avalanche deposits and present unstable rock slopes at Flatmark in the Romsdal Valley <p>This field trip would not have been possible in its present form without the generous sponsorship of Åknes/Taffjord Beredskap IKS, University of Lausanne, Naturfare - Infrastruktur, Flom og Skred (NIFS, joint programme of NVE, Vegvesen and NSB), Nordnorsk Fjellovervåking, C.S.G. S.r.l, LisaLab, NavSys AS and RIEGL Laser Measurement Systems.</p>					
Keywords: Rock avalanche		Unstable rock slope		Hazard and risk classification	
Deposits		Dating		Monitoring	
Structural control		Rockfall			

CONTENTS

Introduction	1
Slope Tectonics in a Norwegian perspective	3
Geographical and geological setting	9
Stop 1: Ivasnasen & Vollan.....	14
Stop 2: Oppdølstranda.....	23
Stop 3: Innerdal Valley	27
Stop 4: Petroglyphs at Bogge	29
Stop 5: Tjellefonna	30
Stop 6: Middagstinden	41
Stop 7: Innfjorddal Valley.....	44
Stop 8: Trollveggen cliff	47
Stop 9: Mannen	49
Stop 10: Flatmark.....	54
Acknowledgements	57

APPENDIXES

Appendix 1: Hermanns et al. (2014) Approach for Systematic Rockslide Mapping of Unstable Rock Slopes in Norway.	A1
Appendix 2: Hermanns et al. (2013a) Hazard and Risk Classification for Large Unstable Rock Slopes in Norway.	A9
Appendix 3: Saintot et al. (2012) Large gravitational rock slope deformation in Romsdalen valley (Western Norway).	A21
Appendix 4: Schleier et al. (2013) Spatial distribution of rockslide deposits and their morphological features suggest timing and paleo-environmental conditions for rock slope failures in Innerdalen and Innfjorddalen, Møre og Romsdal County, Western Norway.	A41
Appendix 5: Krieger et al. (2013) The Berill fault and its relation to a deep-seated gravitational slope deformation (DSGSD).	A57
Appendix 6: Blikra & Kristensen (2012) Mannen (Norway).	A69
Appendix 7: Kristensen & Blikra (2013) Monitoring displacement on the Mannen rockslide in Western Norway.	A85
Appendix 8: Hermanns et al. (2013b) Rockslide Dams in Møre og Romsdal County, Norway.	A93

INTRODUCTION

The field trip of the 3rd Slope Tectonics conference will bring us from Trondheim to the glacially over steepened Sunndal and Romsdal Valleys in western Norway (Figure 1). Here we will observe where catastrophic collapses of large rock masses have taken place in historic time causing displacement waves in the fjords. We will visit unstable rock slopes that are periodically or continuously monitored. We will also visit sites to discuss rock slope failures onto a decaying glacier, and sites where rock slope failures run into a fjord and deposits are now exposed due to isostatic rebound. Other sites will allow discussion about the influence of post-Caledonian faulting on rock slope stability today.

Day 1

Depart Trondheim towards Sunndal Valley and Innerdal Valley:

- Stop 1: field trip to the currently unstable rock slope and a past rock avalanche Ivasnasen (incl. ca. 1h walk to the top of the rockslide & 1h back to the bus)
- Stop 2: road stop at the rockfall prone road section at Oppdølstranda
- Stop 3: ca. 1h walk through rock avalanche deposits in Innerdal Valley towards the overnight accommodation at Innerdalshytta

Day 2

Leave Innerdalshytta towards the Langfjord, Innfjorddal Valley and Åndalsnes:

- Stop 3 (continued): visit of the rock avalanche deposits in Innerdal Valley (incl. Younger Dryas supra-glacial rock avalanche deposits, ca. 1h walk back to the bus)
- Stop 4: road stop for 6000-year old stone carvings at Bogge
- Stop 5: road stop for the 1756 Tjellefonna rock avalanche and displacement wave (site of the largest historic rock avalanche in Norway)
- Stop 6: field visit of the Middagstinden DSGSD controlled by a post-Caledonian fault
- Stop 7: road stops at the rock avalanche deposits in Innfjorddal Valley (rock avalanching into fjord, exposed due to isostatic rebound)

Day 3

Depart towards Romsdal Valley, the Dovrefjell mountain plateau and Trondheim:

- Stop 8: road stop at the Trollveggen cliff (tallest vertical rock face in Europe)
- Stop 9: field visit of the Mannen rockslide (permanently monitored rockslide, visit of monitoring instrumentation in the valley)
- Stop 10: road stop at the rock avalanche deposits and present unstable rock slopes at Flatmark

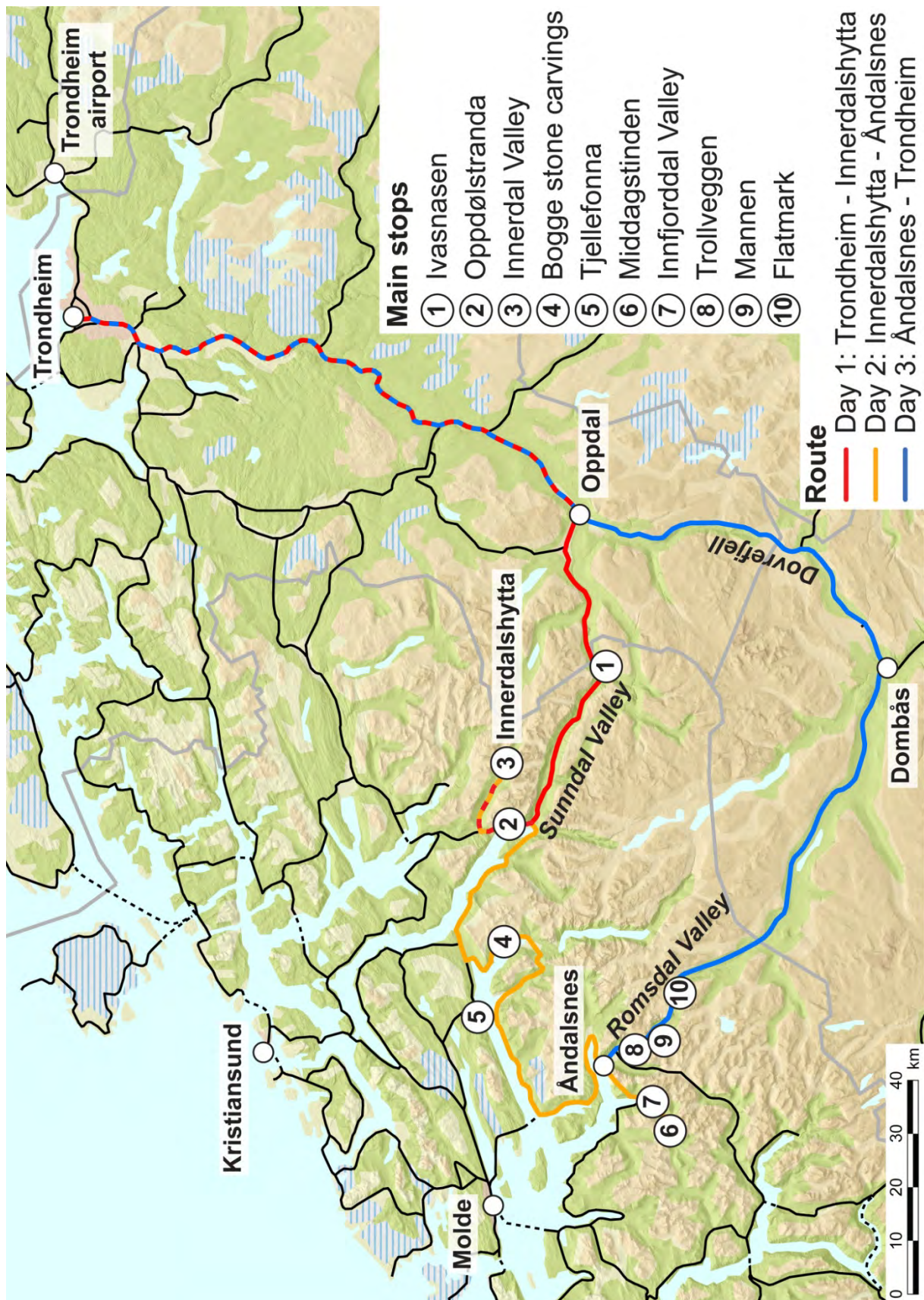


Figure 1: Map of the field trip route for the 3rd Slope Tectonics conference.

SLOPE TECTONICS IN A NORWEGIAN PERSPECTIVE

Deep erosion during multiple glacial cycles, together with Holocene isostatic rebound, produced an extensive fjord system in Western Norway (Vorren and Mangerud 2008), with the result that the coastline is more than one hundred thousand kilometres long. This geologic history lead to Norway having both high, steep coastline sections with rock exposures and low relief coastline sections with sensitive marine sediments. The first are prone to massive rock slope failures that might drop into water bodies, while the latter are prone to form slides in sensitive clays. Not many places around the globe have a similar landslide exposure. Due to topographic and climatic factors, the population of Norway tends to be concentrated in most fjords and valleys at low elevation close to lakes, marine shorelines and rivers. Consequently, Norway's population is more exposed to displacement waves generated by impact of catastrophic rock slope failures and quick clay slides than any other nation. Indeed, seven out of the ten largest landslide disasters in the Norwegian history have been related to either catastrophic rock slope failures in combination with displacement waves (five) or quick clay slides (two) (Hermanns et al. 2012a).

Catastrophic rockslope failures are destructive due to the high release of energy in a short time, and normally they cannot be mitigated by any physical measures. As long as they are of smaller volume (30,000 to 100,000 m³), the impact area can be indicated by rockfall hazard maps, and building restrictions in those areas would ensure that nobody settles in the hazard zone. However if the volume becomes larger, those failures can have excessive run-out length that can increase the hazard zone significantly. Worse is the situation when a rock slope failure hits a water body and creates a displacement wave. These waves can be tens to more than 100 m high in the near-field (<10 km) and several metres to more than 10 m high in the far field (>10 km) (Hermanns et al. 2014a). Even rock slope failures with smaller volumes (30,000 to 100,000 m³) have produced displacement waves in Norway with destructive or even fatal consequences (Hermanns et al. 2014a).

Catastrophic rock slope failures can be triggered by earthquakes, intense precipitation or result from progressive failure due to the fatigue of rock bridges through time. In general, a catastrophic rock slope failure event is preceded by a long period of progressive failure (Hermanns et al. 2012b). In Norway there is no conclusive account of a catastrophic rock slope failure being triggered by a seismic event, although this was discussed for the Tjellefonna event in 1756 (Redfield & Osmundsen 2009). Detailed mapping of the Tjellefonna rockslide scarp area in combination with numerical slope stability modelling rather suggest that the strong rainfall preceding the event had caused the final failure of that slope (Sandøy, 2012). This is consistent with the observation that the seismic activity of Norway, positioned at a passive continental margin, is relatively low (Bungum et al. 2000). Extreme weather conditions prior to catastrophic failures have been reported for some of the historic events, but most of the historic events have not been linked to any special meteorological conditions (Furseth 2006). However, for all recorded events, there are accounts of visible rock slope deformation with opening of cracks for several month, years or decades in advance of the event. This makes mapping for rock slopes with gravitational slope deformation and monitoring of deforming rock slopes a promising mitigation measure to prevent loss of life during future events.

In Norway, mapping of rock slope failures and rock slope instability started in the last decade of the 20th century (e.g., Blikra and Anda 1997, Braathen et al. 2004, Blikra et al. 2006a). Since 2005 it has become more systematic, beginning in three counties (Møre og Romsdal, Sogn og Fjordane and Troms; e.g. Böhme et al. 2011, Henderson and Saintot 2011, Saintot et al. 2011, Bunkholt et al. 2011, 2013, Hermanns et al. 2011, Oppikofer et al. 2013). More than 300 unstable rock slopes (rock slopes with rock deformation) or potential unstable rock slopes

(rock slopes with structural precondition for rock slope failures that were mapped under the systematic mapping for unstable slopes) have been identified so far (Hermanns et al. 2014b) (see Appendix 1). In the past years, six unstable rock slopes at four localities have been classified as high-risk sites or were recommended for permanent monitoring and early-warning without a risk classification (Blikra et al. 2006b, Dahle et al. 2008, Blikra et al. 2009). The Norwegian building code (Byggteknisk forskrift 2010) requires such early-warning systems in areas where a rockslide-induced displacement wave is likely in the next 1000 to 5000 years (depending on the type of building that is exposed). Today, these localities are continuously monitored and early-warning practices are in place. Periodical displacement measurements are carried out at ca. 60 other sites with one to several years interval. On some of these sites, we are increasing the frequency of observation by installing corner reflectors that are observed by Synthetic Aperture Radar (InSAR) from space. The Sentinel-1A satellite will provide a new SAR image every 11 days from late 2014 onward. In early 2016, the Sentinel-1B satellite will be launched and our measurement frequency will then increase to every six days. These monitoring and displacement measurement procedures are established in order to reduce the possibility that a catastrophic rock slope failure will occur unforeseen and result in loss of life.

The large number of unstable and potential unstable slopes necessitates a systematic mapping approach that focuses on the relevant geological data for assessing the likelihood of failure. Furthermore, it requires prioritization of follow-up activities, such as periodic or permanent monitoring, early-warning systems, and other mitigation measures. A first guideline on the mapping approach and a hazard and risk classification was given in a geological report (Hermanns et al. 2012) and was summarized in Hermanns et al. (2013) (see Appendix 2). The earlier mapping approach was revised based on this risk hazard and risk classification in order to focus expensive field work and displacement measurements only on potential medium and high risk sites (Hermanns et al. 2014b) (see Appendix 1). The first site classified following this hazard and risk classification is the Stampa unstable area above the village of Flåm (Blikra et al. 2013). Mapping as well as hazard and risk classification in Norway in the upcoming years will follow these guidelines and procedures until a large number of sites are classified and related geological data and data on potential consequences stored in a related database (Bunkholt et al. 2013). Then the classification system can be reviewed based on real data. As the likelihood of failure cannot be given quantitatively in hundreds or thousands of years with today's scientific knowledge, the risk analysis is built on a qualitative hazard analysis and a quantitative consequence analysis. The goal is to assemble enough data on historic and prehistoric rock slope failures in Norway to allow a calibration of the qualitative hazard analyses. The Storfjord region in Møre og Romsdal is the first region where this could be realized (Oppikofer et al. 2014, Böhme et al. submitted).

Mapping, displacement measurements, monitoring, early warning and research on unstable rock slopes is well distributed over several institutions in Norway that interact closely with each other through cooperation, knowledge exchange and projects in common. It is the Geological Survey of Norway that carries out mapping of unstable rock slopes. Complex sites that require more intensive mapping and that are useful for MSc projects are often mapped by students from the Norwegian University of Science and Technology (NTNU) or the University of Troms (UiT) in collaborative projects or in close connection (e.g. Tukkensæter 2010, Sandøy 2012, Dreiås 2012, Hannus 2012, Skrede 2013, Sollie 2014). Research on a PhD level has been carried out at the NTNU, UiT and the University of Bergen (e.g. Kveldsvik 2008, Ganerød 2008, Grøneng 2010, Laukens 2010, Böhme 2014). Monitoring of unstable rock slopes has been carried out by the Åknes/Tafjord Early-Warning Centre (Åknes/Tafjord Beredskap IKS) in western Norway and the Nordnorsk Fjellovervåking in northern Norway, mainly financed through the Norwegian Water and Energy directorate

(NVE). Those companies will be merged into NVE in 2015. Modelling of rockslide triggered displacement waves has been carried out by the Norwegian Geotechnical Institute (NGI) (e.g., NGI 1992, 1999, Harbitz et al. 2001, 2014). The Earth Observation group at NORUT research institute in Tromsø has developed software and techniques for satellite InSAR observations of unstable areas (e.g. Lauknes et al. 2010, 2011). Researchers at these institutes collaborate broadly within Norway and the rest of the research community in the world giving an important contribution to today's scientific understanding of the failure process of rock slopes (e.g. Anda et al. 2002, Bhasin & Kaynia 2004, Blikra et al. 2005, Hermanns et al. 2006, Kveldsvik 2006, Ganerød et al. 2008, Fenton et al. 2010, Grøneng et al. 2010, Oppikofer et al. 2011, Böhme et al. 2011, Kristensen & Blikra 2011, Saintot et al. 2011, Blikra 2012, Hermanns and Longva 2012, Böhme et al. 2013, Krieger et al. 2013, Schleier et al. 2013, Blikra and Christiansen 2014, Booth et al. 2014, Dehls et al. 2014, Harbitz et al. 2014).

During the field trip it will be possible to discuss the mapping approach for unstable rock slopes in Norway as well as the monitoring and early-warning practices with real cases. We will visit a site where a post-Caledonian fault strongly contributes controlling a rock slope deformation. In addition, we will visit sites where rock avalanches caused secondary effects such as displacement waves and landslide dams and sites where the late Pleistocene and Holocene landscape development controls the distribution of deposits of rock slope failures.

Cited references: Slope Tectonics in a Norwegian perspective

- Anda, E., Blikra, L.H. and Braathen, A. (2002). The Berill fault - first evidence of neotectonic faulting in southern Norway. *Norwegian Journal of Geology* 82, p. 175-182.
- Bhasin, R. and Kaynia, A.M. (2004). Static and Dynamic Simulation of a 700 m High Rock Slope in Western Norway. *International Journal of Engineering Geology*, 71, p. 213-226.
- Blikra, L.H., Anda, E. (1997) Rock-avalanche hazard in Møre og Romsdal, western Norway. Norwegian Geotechnical Institute Publication, 2003, 53-57.
- Blikra, L.H., Longva, O., Harbitz, C.B. and Løvholt, F. (2005). Quantification of rock-avalanche and tsunami hazard i Storfjorden, western Norway. In: Senneset, K., Flaate, K. & Larsen, J.O. (eds): *Landslides and Avalanches. ICFL 2005 Norway. Proceedings of the 11th International Conference and Fiel Trip on Landslides, Norway, 1-10 September 2005*. Taylor & Francis Group, London, p. 57-63.
- Blikra, L.H., Longva, O., Braathan, A., Anda, E., Dehls, J.F. & Stalsberg, K. (2006a). Rock slope failures in Norwegian fjord areas; examples, spatial distribution and temporal pattern. In: EVANS, S.G., Scarascia Mugnozza, G., Strom, A., and Hermanns R.L., *Landslides from massive rock slope failures::* 475-496. NATO Science Series IV (49), Earth and Environmental Sciences, Springer, Dordrecht, Netherland.
- Blikra, L.H., Anda, E., Belsby, S., Jogerud, K. & Klempe, Ø. (2006b) Åknes/Tafjord prosjektet, Satusrapport for Arbeidsgruppe 1 (undersøking og overvakning). Åknes/Tafjord-Prosjektet, 57p.
- Blikra, L.H., Henderson, I.H.C., Norvik, T. (2009) Faren for fjellskred fra Nordnesfjellet i Lyngenfjorden, Troms, NGU rapport: 2009.026.
- Blikra, L.H. (2012) The Åknes rockslide, Norway. In: Clague J.J. and Stead D. (Eds.) - *Landslides: Types, Mechanisms and Modeling*: Cambridge University Press, p. 323-335.
- Blikra, L.H., Böhme, M., Dehls, J.F., Hermanns, R.L., Oppikofer, T., Redfield, T., Rønning, J.S., Yugsi, Molina, F., Domaas, U., Pfaffenhuber, A., Henriksen, H., Hole, J., Kristensen, L. (2013) The unstable phyllitic rocks in Stampa - Flåm, western Norway: Compilation, scenarios, risk and recommendations. NVE rapport 35-2013, 55p.
- Blikra, L.H., Christiansen, H.H. (2014) A field-based model of permafrost-controlled rockslide deformation in northern Norway, *Geomorphology*, 208, p. 34-49.
- Böhme, M., Saintot, A., Henderson, I.H.C., Henriksen, H. and Hermanns, R.L. (2011) Rock-slope instabilities in Sogn & Fjordane County, Norway: a detailed structural and geomorphological analysis. *Geological Society, London, Special Publications*, 351, p. 97-111.
- Böhme, M., Hermanns, R.L., Oppikofer, T., Fischer, L., Bunkholt, H.S.S., Eiken, T. Pedrazzini, A., Derron, M.-H. Jaboyedoff, M., Blikra, L.H., and Nilsen, B. (2013) Analyzing complex rock slope deformation at Stampa, western Norway, by integrating geomorphology, kinematics and numerical modelling. *Engineering Geology*, doi: 10.1016/j.enggeo.2012.11.016.
- Böhme, M., Oppikofer, T., Longva, O., Jaboyedoff, M., Hermanns, R.L. and Derron, M.-H. (submitted) Analyses of past and present rock slope instabilities in a fjord valley: implications for hazard assessment. Submitted to *Geomorphology*.

- Böhme, M. (2014) Spatial and temporal variability of rock slope instability in western Norway: Implications for susceptibility and hazard assessment. Doctoral theses at NTNU, 2014:82.
- Booth, A.M., Dehls, J., Eiken, T., Fischer, L., Hermanns, R.L., Oppikofer, T. (2014) Integrating diverse geologic and geodetic observations to determine failure mechanisms and deformation rates across a large bedrock landslide complex: the Osmundneset landslide, Sogn og Fjordane, Norway, *Landslides*, DOI 10.1007/s10346-014-0504-y.
- Braathen, A., Blikra, L.H., Berg S.S., Karlsen F. (2004) Rock-slope failures in Norway; type, geometry, deformation mechanisms and stability. *Norwegian Journal of Geology*, 84, 67-88.
- Bungum, H., Lindholm, C.D., Dahle, A., Woo, G., nadim, F., Holme, J.K., Gudmestad, O.T., Hagberg, T., Karthigeyan, K. (2000) New seismic zoning maps for Norway, the North Sea and the UK, *Seismological Research Letters* 71, 687-697.
- Bunkholt H, Osmundsen PT, Redfield T, Oppikofer T, Eiken T, L'Heureux J-S, Hermanns R, Lauknes TR (2011) ROS Fjellskred i Troms: status og analyser etter feltarbeid 2010. Norwegian Geological Survey Report. No. 2011-031, 135 p.
- Bunkholt H., Nordahl, B., Hermanns, R.L., Oppikofer, T., Fischer, L., Blikra, L.H., Anda, E., Dahle, H., Sætre, S. Database of unstable rock slopes of Norway. In: Margottini, C., Canuti, P., Sassa, K. (eds): *Landslide science and practice*, Vol. 3: Spatial Analysis and Modelling. Springer-Verlag, Berlin Heidelberg, Germany, p. 423-428.
- Bunkholt, H., Otterå, S., Yugsi Molina, F.X., Hermanns, R.L., Dehls, J.F., Osmundsen, P.T., Redfield, T.F. and Eiken, T. (2013) Undersøkelser av ustabile eller potensielt ustabile fjellpartier i Troms – status og planer etter feltarbeid 2011 og 2012. NGU report 2013.021, Geological Survey of Norway, Trondheim, Norway.
- Byggteknisk forskrift (Tek 10) (2010) <http://www.lovdata.no/cgi-wift/ldeles?doc=/sf/sf/sf-20100326-0489.html>.
- Dahle, H., Anda, E., Saintot, A., Sætre, S. (2008) Faren for fjellskred fra Mannen i Romsdalen. NGU-rapport 2008.087.
- Dehls, J.F., Laukens, T.R., Hermanns, R.L., Bunkholt, H., Grydeland, T., Larsen, Y., Eriksen, H.Ø., Eiken, T. (2014) Use of satellite and ground based InSAR in hazard classification of unstable rock slopes. Eds. Sassa, K., Canuti, P., Yin, Y. *Landslide science for a safer geoenvironment*, Vol. 2, Springer, 389-392.
- Dreiås, G.M. (2012) Engineering geological assessment and structural comparison of the Vollan and Ivasnasen rock slopes in Sunndalen, Norway. MSc thesis, Norwegian University of Science and Technology, Trondheim, Norway.
- Fenton, C.R., Hermanns, R.L., Blikra, L.H., Kubik, P.W., Bryant, C., Niedermann, S., Meixner, A., and Goethals, M.M. (2010) Regional ^{10}Be production rate calibration for the past 12 ka deduced from the radiocarbon-dated Grøtlandsura and Russenes rock avalanches at 69° N, Norway. *Quaternary Geochronology*, 6(5), p. 437-452.
- Furseth, A. (2006) - Skredulykker i Norge. Tun Forlag, Oslo.
- Ganerød, G.V. (2008) Applied Structural Geology – Case Studies of Underground Constructions and Rockslides. Doctoral thesis at University of Bergen, Norway.
- Ganerød, G.V., Grøneng, G., Rønning, J.S., Dalsegg, E., Elvebakk, H., Tønnesen, J.F., Kveldsvik, V., Eiken, T., Blikra, L.H., and Braathen, A. (2008) Geological model of the Åknes rockslide, western Norway. *Engineering Geology*, 102, p. 1-18.
- Grøneng, G., Christiansen, H.H., Nilsen, B., Blikra, L.H. (2010) Meteorological effects on seasonal displacements of the Åknes rockslide, western Norway. *Landslides*, Vol. 8, pp. 1-15.
- Grøneng, G. (2010) Stability analyses of the Åknes rock slope, Western Norway. Doctoral theses at NTNU, 2010:30.
- Hannus, M. (2012) Structural geometry and controlling factors for a rock slope failure area at Hompen/Várás, Signaldalen, Troms, north Norway. MSc thesis, University of Tromsø, Tromsø, Norway.
- Harbitz, C.B., Domaas, U., Varlid, E., 2001. Flodbølger etter fjellskred — Sannsynlighet og faresoner i Åfjorden, Hyllestad. Norsk Jord og Fjellteknisk Forbund, Bergmekanikkdagen 23. November 2001, Oslo (in Norwegian with English abstract).
- Harbitz, C.B., Glimsdal, S., Løvolt, F., Kveldsvik, V., Pedersen, G.K., Jensen, A. (2014). Rockslide tsunamis in complex fjords: From an unstable rock slope at Åkneset to tsunami risk in western Norway. *Coastal engineering* 88: 101-122.
- Henderson I.H.C., and Saintot A. (2011) Regional spatial variations in rockslide distribution from structural geology ranking: an example from Storfjorden, western Norway. *Slope tectonics*. Jaboyedoff M (ed.) Geological Society, London. Special Publication, 351. (ISBN 978-1-86239-324-0). 79-96.
- Hermanns, R.L., Blikra, L.H., Naumann, M., Nilsen, B., Panthi, K.K., Stromeyer, D., Longva, O. (2006) Examples of multiple rock-slope collapses from Köfels (Ötztal valley, Austria) and western Norway. *Engineering Geology*, 83: 94-108.
- Hermanns, R.L., Fischer L., Oppikofer, T., Böhme, M., Dehls, J.F., Henriksen H., Booth, A., Eilertsen, R., Longva, O., and Eiken, T. (2011) Mapping of unstable and potentially unstable rock slopes in Sogn og Fjordane, NGU rapport 2011.055, (ISSN 0800-3416). 195 p.

- Hermanns R.L. & Longva O. (2012) - Rapid rock-slope failures. In: Clague J.J. and Stead D. (2012 Eds.) - *Landslides: Types, Mechanisms and Modeling*: 59-70, Cambridge University Press.
- Hermanns, R.L., Hansen, L., Sletten, K., Böhme, M., Bunkholt, H., Dehls, J.F., Eilertsen, R., Fischer, L., L'Heureux, J.-S., Høgaas, F., Nordahl, B., Oppikofer, T., Rubensdotter, L., Solberg, I.-L., Stalsberg K., Yugsi Molina, F.X. (2012a). Systematic geological mapping for landslide understanding in the Norwegian context. Eds. Eberhardt, E., Froese, C., Turner, A.K., Leroueil, S., *Landslide and engineered slopes: Protecting society through improved understanding*, Taylor & Francis Group, London. pp. 265-271.
- Hermanns, R.L., Oppikofer, T., Anda, E., Blikra, L.H., Böhme, M., Bunkholt, H., Crosta, G.B., Dahle, H., Devoli, G., Fischer, L., Jaboyedoff, M., Loew, S., Sætre, S., & Yugsi Molina, F. (2012b) Recommended hazard and risk classification system for large unstable rock slopes in Norway. NGU-rapport 2012.029, <http://www.ngu.no/no/hm/Publikasjoner/Rapporter/2012/2012-029/>
- Hermanns, R.L. and Longva, O. (2012) - Rapid rock-slope failures. In: Clague J.J. and Stead D. (Eds.) - *Landslides: Types, Mechanisms and Modeling*: Cambridge University Press, p. 59-70.
- Hermanns, R.L., Oppikofer, T., Anda, E., Blikra, L.H., Böhme, M., Bunkholt, H., Crosta, G.B., Dahle, H., Devoli, G., Fischer, L., Jaboyedoff, M., Loew, S., Sætre, S., Yugsi Molina, F. (2013) Hazard and risk classification system for large unstable rock slopes in Norway. In: Genevois R, Prestininzi A, (eds) *International conference on Vajont - 1963-2013. Italian Journal of Engineering Geology and Environment*, Book series 6, DOI 10.4408/IJEGE.2013-06.B-22, Rome, Italy, p. 245-254.
- Hermanns, R.L., Oppikofer, T., Roberts, N.J., Sandøy, G. (2014a). Catalogue of historical displacement waves and landslide-triggered tsunamis in Norway. Ed. Lollino, G. *Engineering geology for society and territory*, Vol. 4, Springer, DOI: 10.1007/978-3-319-08660-6_13, in press.
- Hermanns, R.L., Oppikofer, T., Yugsi Molina, F.X., Dehls, J.F., Böhme, M. (2014b) Approach for systematic rockslide mapping of unstable rock slopes in Norway. Eds. Sassa, K., Canuti, P., Yin, Y. *Landslide science for a safer geoenvironment*, Vol. 3, Springer, 129-134.
- Krieger, I., Hermanns, R.L., Schleier, M., Yugsi Molina, F.X., Oppikofer, T., Rønning, J.S., Eiken, T., Rohn, J. The Berill fault and its relation to deep seated gravitational slope deformation (DSGSD). I: Genevois R, Prestininzi A, (eds) *International conference on Vajont - 1963-2013. - Italian Journal of Engineering Geology and Environment*, Book series 6, DOI 10.4408/IJEGE.2013-06.B-24, Rome, Italy. p. 265-273.
- Kristensen, L., Blikra, L.H. (2013). Monitoring displacement on the Mannen rockslide in Western Norway. In: Margottini, C., Canuti, P., Sassa, K. (eds): *Landslide science and practice*.
- Kveldsvik, V., Eiken, T., Ganerød, G.V., Grøneng, G., and Ragvin, N. (2006) Evaluation of movement data and ground conditions for the Åknes rock slide. *International Symposium on Stability of Rock slopes in open Pit Mining and civil Engineering. The South African Institute of Mining and Metallurgy*, p. 279-300.
- Kveldsvik, V. (2008) Static and dynamic stability analyses of the 800 m high Åknes rock slope, western Norway. Doctoral theses at NTNU, 2008:128.
- Lauknes, T.R. (2010) Rockslide mapping in Norway by means of interferomagnetic SAR time series analysis. Doctoral theses at UIT, 2008:128.
- Lauknes, T.R., Shanker, A.P., Dehls, J.F., Zebker, H.A., Henderson, I.H.C., and Larsen, Y.. (2010). Detailed rockslide mapping in northern Norway with small baseline and persistent scatterer interferometric SAR time series methods. *Remote Sensing of Environment*, 114(9), 2097-2109.
- Lauknes, T.R., Zebker, H.A., and Larsen, Y. (2011). InSAR Deformation Time Series Using an L_1 -Norm Small-Baseline Approach. *IEEE Transactions on Geoscience and Remote Sensing*, 49(1), 536-546.
- NGI, 1992. Skredgenererte bølger — En teoretisk gjennomgang med praktiske eksempler. Norwegian Geotechnical Institute report 894031-1. (in Norwegian).
- NGI, 1999. Hyllestad kommune — Vurdering av skredfare og bølgehøyder i Åfjorden. Norwegian Geotechnical Institute report 981014-1 (in Norwegian).
- Oppikofer, T., Jaboyedoff, M., Pedrazzini, A., Derron, M.-H. and Blikra, L.H. (2011) Detailed DEM analysis of a rockslide scar to characterize the basal sliding surface of active rockslides. *J. of Geophysical Research*, Vol. 116, F02016, doi:10.1029/2010JF001807.
- Oppikofer, T., Saintot, A., Otterå, S., Hermanns, R.L., Anda, E., Dahle, H. and Eiken, T. (2013) Investigations on unstable rock slopes in Møre og Romsdal – status and plans after field surveys in 2012. NGU report 2013.014, Geological Survey of Norway, Trondheim, Norway.
- Oppikofer, T., Böhme, M., Saintot, A., Hermanns, R.L. and Longva, O. (2014) Hazard assessment of unstable and potential unstable rock slopes in Storfjord (Western Norway). In: Lollino, G., Giordan, D., Crosta, G., et al. (eds.) *Engineering Geology for Society and Territory - Volume 2: Landslide processes*, Springer, Berlin Heidelberg.
- Redfield, T.F., Osmundsen, P.T. (2009) The Tjellefonna fault system of Western Norway: Linking late-Caledonian extension, post-Caledonian normal faulting, and Tertiary rock column uplift with the landslide-generated tsunami event of 1756. *Tectonophysics* 474, 106 - 123.
- Sandøy, G. (2012) Back-analysis of the 1756 Tjellefonna rockslide, Langfjorden. MSc thesis, Norwegian University of Science and Technology, Trondheim, Norway.

- Saintot, A., Henderson, I.H.C. and Derron, M.H. (2011) Inheritance of ductile and brittle structures in the development of large rock slope instabilities: examples from Western Norway. Geological Society of London, Special Publications, 351, p. 27-78.
- Schleier, M., Hermanns, R.L., Rohn, J. (2013) Spatial distribution of rockslide deposits and their morphological features suggests timing and paleo-environmental conditions for rock slope failures in Innerdalen and Innfjorddalen, Møre og Romsdal county, western Norway. In: Genevois R, Prestininzi A, (eds) International conference on Vajont - 1963-2013. - Italian Journal of Engineering Geology and Environment, Book series 6, DOI 10.4408/IJEGE.2013-06.B-24, Rome, Italy. p. 493-505.
- Skrede, I. (2013) Jettan, Nordnesfjellet, Kåfjord, Troms - indre geometri og struktur, kinematikk og styrande faktorar av eit ustabil fjellparti, basert på strukturellanalyse, geomorfologi og overvakningsdata. MSc thesis, University of Tromsø, Tromsø, Norway.
- Sollie, I.L. (2014) The Håkåneset rockslide, Tinnsjø: Stability analysis of a potential rock slope instability. MSc thesis, Norwegian University of Science and Technology, Trondheim, Norway.
- Tukkensæter, Å. (2010) Stability analysis of deformed rock slope at Flomsdalen in Aurland, Norway, MSc thesis, Norwegian University of Science and Technology, Trondheim, Norway.
- Vorren, T.O., Mangerud, J. (2008) Glaciations come and go. In: Ramberg, I.B., Bryhni, I., Nøttvedt, A., Rangnes, K. (Eds.), The making of land: Geology of Norway, Geological Society of Norway, Trondheim. pp. 481-533.

GEOGRAPHICAL AND GEOLOGICAL SETTING

The field excursion of the 3rd Slope Tectonics conference leads through several previously glaciated valleys and the coastal fjords in the Møre og Romsdal county in western Norway (see map in Figure 1). The following description of the geographical and geological setting of the field excursion area is modified from Saintot et al. (2011; 2012) (see Appendix 3).

Caledonian Orogeny

The valleys and fjord visited during the field trip cut into the crystalline basement of the Western Gneiss Region of Norway, which is formed by a large variety of mostly Lower Palaeozoic and Precambrian metamorphic rocks (Figure 2). During the Caledonian Orogeny, the rocks were severely reworked by a general NW-SE-oriented bulk crustal shortening that resulted in a SE-directed nappe transport, in regimes ranging from the deepest ductile domain to the brittle-ductile transition (Roberts and Gee 1985, Hossack and Cooper 1986, Roberts 2003). The abundant gneissic rocks in the Western Gneiss region are found in both autochthonous (or para-autochthonous) and allochthonous positions.

Most of the area visited during the field trip is covered by the typical, and probably the oldest, granitic to dioritic gneiss unit of the basement. Other main gneiss types in the field trip area are coarse-grained granitic and augengneiss of Proterozoic age (e.g. in the north-eastern part of the Romsdal Valley and the lower Sunndal Valley); quartz-rich gneiss characterized by sillimanite and kyanite (widespread in the Romsdal Valley); amphibolite, hornblende gneiss and mica-rich gneiss (encountered for example in the upper Sunndal Valley). Mica schist, mica-rich gneiss and amphibolite form a widespread unit in the upper Sunndal Valley and narrow bands along the coastal fjords (e.g. the Langfjord).

Exhumation and brittle deformation

After the Caledonian Orogeny, the basement of the Western Gneiss region was significantly exhumed during the Devonian semi-ductile syn- or post-orogenic collapse of the chain (Hossack 1984, Fossen 2000, Hossack and Cooper 1986, Roberts 2003). The age of the major brittle structures observed in the area of the field trip is not constrained. They can pertain to this Devonian tectonic phase as well as to other intense brittle tectonic events that affected western Norway, including the Permo-Triassic and Jurassic rifting phases and the opening of the North Atlantic Ocean (Torsvik et al. 1997, Valle et al. 2002, Mosar 2003).

Starting from a recent but still debated time, an ongoing high-rated uplift brought the intensively tectonized rocks to the surface. Regardless, the drainage river system was surely installed during the Tertiary and already shaped the present-day landscape.

Quaternary glaciations & rock slope failures

The Quaternary geology of the region is marked by glaciation episodes. The ice extended to the outer part of the continental shelf during the maximum of the last glaciation in the Weichselian (Mangerud 2004). During the Younger Dryas last severe cooling event, the glaciers re-advanced close to the coast. Moraines and tills of the last Younger Dryas ice sheet are conspicuous in these valleys, which were probably ice-free approximately 10,000 years ago (Mangerud 2004). The work of glaciers enhanced the relief to produce the spectacular landscape (fjords, cirques, lakes) of Western Norway. Etzelmüller et al. (2007) summarized well the relief of Western Norway with these words: alpine; steep slopes; heavily over-deepened glacial valleys.

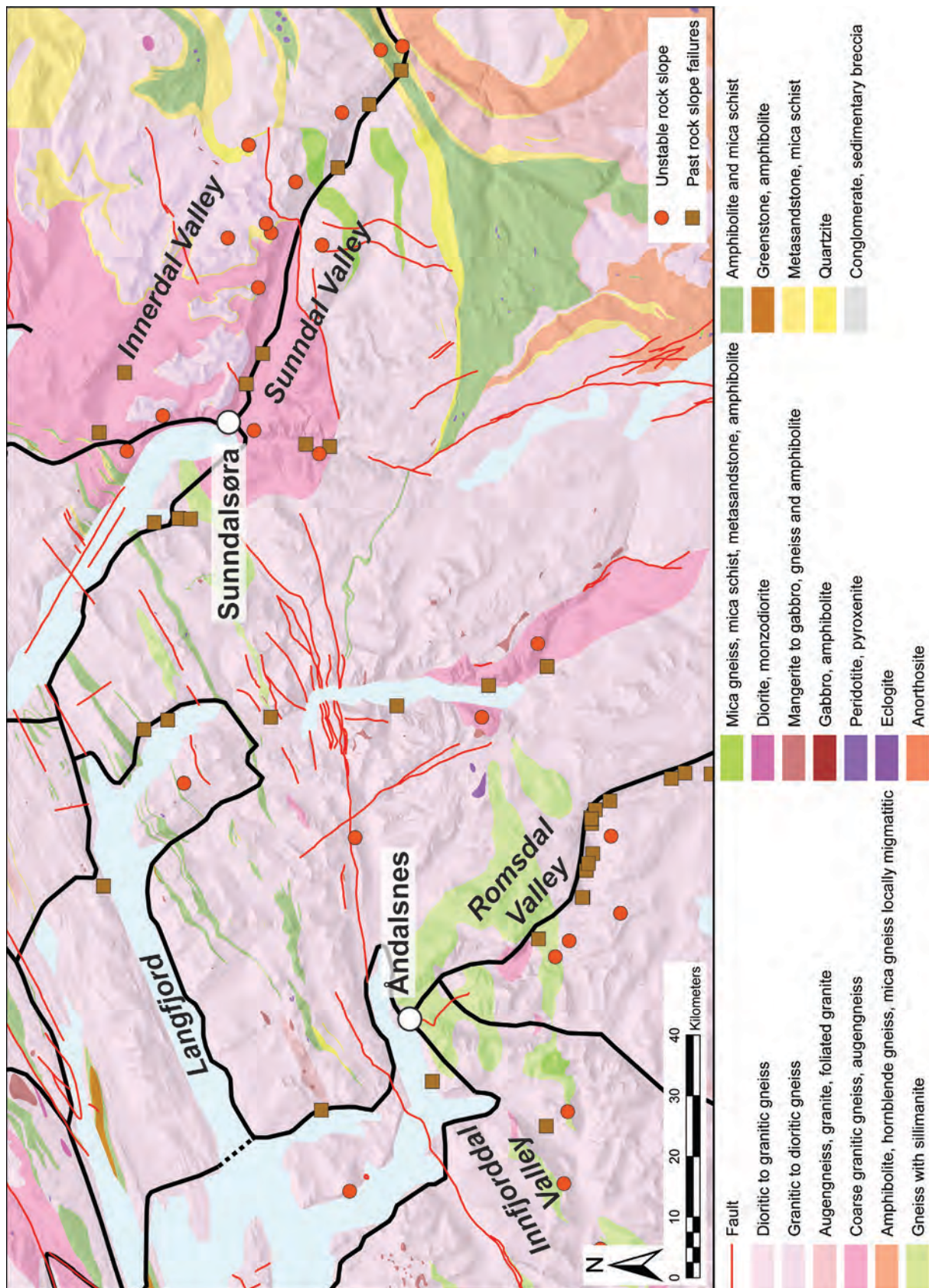


Figure 2: Bedrock map of the field trip area (original scale 1:250,000; Geological Survey of Norway database: <http://geo.ngu.no/kart/berggrunn>) showing also historical rock slope failures (data from the Norwegian national landslide database: www.skrednett.no) and present unstable rock slopes (data from NGU's unstable rock slope database).

The ice cap melting generated a regional isostatic rebound, large-magnitude earthquakes and further neotectonic activity (Olesen et al. 2000, 2004). In the field trip area, the present-day uplift rates range from 1.5 mm/year in the West to 3.5 mm/year in the East (see Figure 2 in Saintot et al. 2011).

Past rock slope failures

A large number of rock slope failures and gravitational structures in Norway were generated shortly (i.e. 1000 to 2000 years) after the deglaciation (Blikra et al. 2002, 2006, Longva et al. 2009, Böhme et al. submitted). These were likely triggered by this neotectonic activity combined with the sudden unloading of the steep slopes due to the rapid glacier retreat and the associated large discharge of water into the fractures (Blikra et al. 2002, 2006). Blikra et al. (2006) invoked frost wedging (i.e. opening of pre-existing fractures due to the ice expansion) as a primary factor of rock slope instability development. In the recent past, permafrost covered most of the slopes of western Norway and, during a Younger Dryas dramatic cooling event, it even occurred down to sea level (Blikra and Longva 1995) causing ice wedging at the largest possible scale [the lower limit of permafrost today is at c. 1500 m a.s.l. in western Norway].

Most of the unstable rock slopes in Norway are believed to have been structured in syn- and post-glacial times and to be presently dormant or inactive. The extreme Alpine relief of the coastal fjord areas of Norway, combined with the high concentration of pre-existing geological structures, seasonal heavy precipitation, snow melting and frost periods, makes these areas prone to rock slope failures (Blikra et al. 2006).

Conversely to rock avalanche deposits in fjords (e.g. Longva et al. 2009, Böhme et al. submitted), no deposits linked to the ice debuttressing of the slopes are preserved on the low-altitude valley floors of the Sunndal, Innfjorddal and Romsdal Valleys, due to remobilization by the remnant glaciers and/or coverage by marine and fluvial sediments that filled the valley in post-glacial times. Nonetheless, many rock avalanche deposits have been mapped in all the valleys visited during this field trip and are therefore the most recent significant infill of the valley bottom. Many historical rock slope failures have been recorded in the area of the field trip (Figure 2), including the largest historic rock avalanche at Tjellefonna in the Langfjord in 1756.

Several large unstable rock slopes are currently identified and mapped in the area of the field trip (Figure 2). Nine of them are located in the Sunndal Valley, three in the Innfjorddal Valley and four unstable rock slopes are identified along the southern slope of the Romsdal Valley. The unstable rock slopes Ivasnasen, Vollan, Middagstinden, Mannen and Flatmark will be visited during the field trip and are further described in this field trip guide book.

Studies of large rock slope instabilities in similar intrinsically strong rocks as here in the Western Gneiss Region have demonstrated the quasi-systematic reactivation of inherited structures in the gravity-driven deformation and large volumes of these types of rocks effectively destabilize where the pre-existing structures favorably dip relatively to the slope (e.g. Giraud et al. 1990, Agliardi et al. 2001, Eberhardt et al. 2004, Brideau et al. 2005, 2009, Jaboyedoff et al. 2009, Welkner et al. 2010). The same conclusion is drawn from extensive studies on the development of large rock slope instabilities over Western Norway with, in many cases, the metamorphic foliation accommodating a prominent part of the deformation (e.g. Braathen et al. 2004, Henderson et al. 2006, Ganerød et al. 2008, Oppikofer 2009, Böhme et al. 2011, Henderson and Saintot 2011, Jaboyedoff et al. 2011, Oppikofer et al. 2011, Saintot et al. 2011, 2012, Booth et al. 2014).

Cited references: Geographical and geological setting

- Agliardi, F., Crosta, G. and Zanchi, A. (2001) Structural constraints on deep-seated slope deformation kinematics. *Engineering Geology*, **59**, 1-2, 83-102.
- Blikra, L. H. and Longva, O. (1995) Frost-shattered debris facies of Younger Dryas age in the coastal sedimentary successions in western Norway: palaeoenvironmental implications. *Palaeogeography, Palaeoclimatology, Palaeoecology*, **118**, 89-110.
- Blikra, L.H., Braathen, A., Anda, E., Stalsberg, K. and Longva, O. (2002) Rock avalanches, gravitational bedrock fractures and neotectonic faults onshore northern West Norway: Examples, regional distribution and triggering mechanisms. NGU report 2002.016, Geological Survey of Norway, Trondheim, Norway.
- Blikra, L.H., Longva, O., Braathen, A., Anda, E., Dehls, J.F. and Stalsberg, K. (2006) Rock Slope Failures in Norwegian Fjord Areas: Examples, Spatial Distribution and Temporal Pattern. In: Evans, S.G., Scarascia Mugnozza, G., Strom, A. and Hermanns, R.L. (eds.) *Landslides from Massive Rock Slope Failure; NATO Science Series, IV. Earth and Environmental Sciences, Vol 49*. Springer, Dodrecht, Netherlands, pp. 475-496.
- Böhme, M., Saintot, A., Henderson, I., Henriksen, H. and Hermanns, R.L. (2011) Slope instabilities in Sogn og Fjordane County, Norway. In: Jaboyedoff, M. (ed.) *Slope Tectonics. Geological Society, London, Special Publications*, **351**, 97-111.
- Böhme, M., Oppikofer, T., Longva, O., Jaboyedoff, M., Hermanns, R.L. and Derron, M.-H. (submitted) Analyses of past and present rock slope instabilities in a fjord valley: implications for hazard assessment. Submitted to *Geomorphology*.
- Booth, A.M., Dehls, J., Eiken, T., Fischer, L., Hermanns, R.L., Oppikofer, T. (2014) Integrating diverse geologic and geodetic observations to determine failure mechanisms and deformation rates across a large bedrock landslide complex: the Osmundneset landslide, Sogn og Fjordane, Norway, Landslides, DOI 10.1007/s10346-014-0504-y.
- Braathen, A., Blikra, L.H., Berg, S.S. and Karlsen, F. (2004) Rock-slope failure in Norway; type, geometry, deformation mechanisms and stability. *Norwegian Journal of Geology*, **84**, 1, 67-88.
- Brideau, M., Yan, M. and Stead, D. (2009) The role of tectonic damage and brittle rock fracture in the development of large rock slope failures. *Geomorphology*, **103**, 1, 30-49.
- Brideau, M., Stead, D., Kinakin, D. and Fecova, K. (2005) Influence of tectonic structures on the Hope Slide, British Columbia, Canada. *Engineering Geology*, **80**, 3-4, 242-259.
- Eberhardt, E., Stead, D. and Coggan, J.S. (2004) Numerical analysis of initiation and progressive failure in natural rock slopes - the 1991 Randa rockslide. *International Journal of Rock Mechanics & Mining Sciences*, **41**, 1, 69-87.
- Etzelmüller, B., Romstad, B. and Fjellanger, J. (2007) Automatic regional classification of topography in Norway. *Norwegian Journal of Geology*, **87**, 167-180.
- Fossen, H. (2000). Extensional tectonics in the Caledonides: synorogenic or postorogenic? *Tectonics*, **19**, 213-224.
- Ganerød, G.V., Grøneng, G., Rønning, J.S., Dalsegg, E., Elvebakk, H., Tønnesen, J.F., Kveldsvik, V., Eiken, T., Blikra, L.H. and Braathen, A. (2008) Geological model of the Åknes rockslide, western Norway. *Engineering Geology*, **102**, 1-18.
- Giraud, A., Rochet, L. and Antoine, P. (1990) Processes of slope failure in crystallophyllian formations. *Engineering Geology*, **29**, 241-253.
- Henderson, I.H.C., Saintot, A. and Derron, M. (2006) Structural mapping of potential rockslide sites in the Storfjorden area, western Norway: the influence of bedrock geology on hazard analysis. NGU report 2006.052, Geological Survey of Norway, Trondheim, Norway.
- Henderson, I.H.C. and Saintot, A. (2011) Regional spatial variations in rockslide distribution from structural geology ranking: an example from Storfjorden, western Norway. In: Jaboyedoff, M. (ed.) *Slope Tectonics. Geological Society, London, Special Publications*, **351**, 79-95.
- Hossack, J. R. (1984) The geometry of listric growth faults in the Devonian basins of Sunnfjord, west Norway. *Journal of the Geological Society, London*, **135**, 705-711.
- Hossack, J.R. and Cooper, M.A. (1986) Collision tectonics in the Scandinavian Caledonides. *Geological Society of London, Special Publications*, **19**, 287-304.
- Jaboyedoff, M., Oppikofer, T., Derron, M., Blikra, L.H., Böhme, M. and Saintot, A. (2011) Complex landslide behaviour and structural control: a three-dimensional conceptual model of Åknes rockslide, Norway. In: Jaboyedoff, M. (ed.) *Slope Tectonics. Geological Society, London, Special Publications*, **351**, 147-161.
- Jaboyedoff, M., Couture, R. and Locat, P. (2009) Structural analysis of Turtle Mountain (Alberta) using digital elevation model: Toward a progressive failure. *Geomorphology*, **103**, 5-16.
- Longva, O., Blikra, L.H. and Dehls, J. (2009) Rock avalanches - distribution and frequencies in the inner part of Storfjorden, Møre og Romsdal County, Norway. NGU report 2009.002, Geological Survey of Norway, Trondheim, Norway.

- Mangerud, J. (2004) Ice sheet limits in Norway and on the Norwegian continental shelf. In: Ehlers, J. and Gibbard, P.L. (eds.) *Quaternary Glaciations Extent and Chronology Part I: Europe*, Elsevier, , pp. 271-294.
- Mosar, J. (2003) Scandinavia's North Atlantic passive margin. *Journal of Geophysical Research*, **108**, B8, 2360, doi:10.1029/2002JB002134.
- Olesen, O., Dehls, J., Bungum, H., Riis, F., Hicks, E., Lindholm, C., Blikra, L.H., Fjeldskaar, W., Olsen, L., Longva, O., Faleide, J.I., Bockmann, L., Rise, L., Roberts, D., Braathen, A. and Brekke, H. (2000) Neotectonics in Norway, Final Report. NGU report 2000.002, Geological Survey of Norway, Trondheim, Norway.
- Olesen, O. (2004) Neotectonic deformation in Norway and its implications:a review. *Norwegian Journal of Geology*, **84**, 3-34.
- Oppikofer, T. (2009) Detection, analysis and monitoring of slope movements by high-resolution digital elevation models. PhD thesis, Institute of Geomatics and Analysis of Risk, University of Lausanne, Lausanne, Switzerland.
- Oppikofer, T., Jaboyedoff, M., Pedrazzini, A., Derron, M.H. and Blikra, L.H. (2011) Detailed DEM analysis of a rockslide scar to improve the basal failure surface model of active rockslides. *Journal of Geophysical Research*, **116**, F02016.
- Roberts, D. and Gee, D.G. (1985). An introduction to the structure of the Scandinavian Caledonides. In: Gee, D.G. and Sturt B.A. (eds.) *The Caledonide Orogen - Scandinavia and related areas*. John Wiley and Sons, Chichester, pp. 55-68.
- Roberts, D. (2003) The Scandinavian Caledonides: event chronology, palaeogeographic settings and likely modern analogues. *Tectonophysics*, **363**, 283-299.
- Saintot, A., Henderson, I.H.C. and Derron, M.-H. (2011) Inheritance of ductile and brittle structures in the development of large rock slope instabilities: examples from western Norway. In: Jaboyedoff, M. (ed.) *Slope Tectonics*. Geological Society, London, *Special Publications*, **351**, 27-78.
- Saintot, A., Oppikofer, T., Derron, M.-H. and Henderson, I. (2012) Large gravitational rock slope deformation in Romsdalen valley (Western Norway). *Revista de la Asociación Geológica Argentina*, **69**, 3, 354-371.
- Torsvik, T.H., Andersen, T.B. Eide, E.A. and Walderhaug, H.J. (1997) The age and tectonic significance of dolerite dykes in western Norway. *Journal of Geological Society of London*, **154**, 961-973.
- Valle, P., Faereth, R. B. and Fossen, H. (2002) Devonian–Triassic brittle deformation based on dyke geometry and fault kinematics in the Sunnhordland region, SW Norway. *Norwegian Journal of Geology*, **82**, 3-17.
- Welkner, D., Eberhardt, E. and Hermanns, R.L. (2010) Hazard investigation of the Portillo Rock Avalanche site, central Andes, Chile, using an integrated field mapping and numerical modelling approach. *Engineering Geology*, **114**, 3-4, 278-297.

STOP 1: IVASNASSEN & VOLLAN

At this first stop in the upper part of the Sunndal Valley (Figure 3) we have the opportunity to look at the failure surface and deposits of a past rock avalanche at Ivasnasen, as well as at the sliding surface of a current unstable rock slope. We will also observe the large unstable rock slope of Vollan located on the opposite slope and discuss the differences in deformation style related to lithological and structural differences between the opposing slopes. The following contribution of the excursion guide is based on a MSc thesis by G.M. Dreiås finished in 2012 at the Norwegian University of Science and Technology (NTNU, Trondheim, Norway) (Dreiås 2012) and on several reports and articles (Henderson and Saintot 2007, Saintot et al. 2008, 2013).

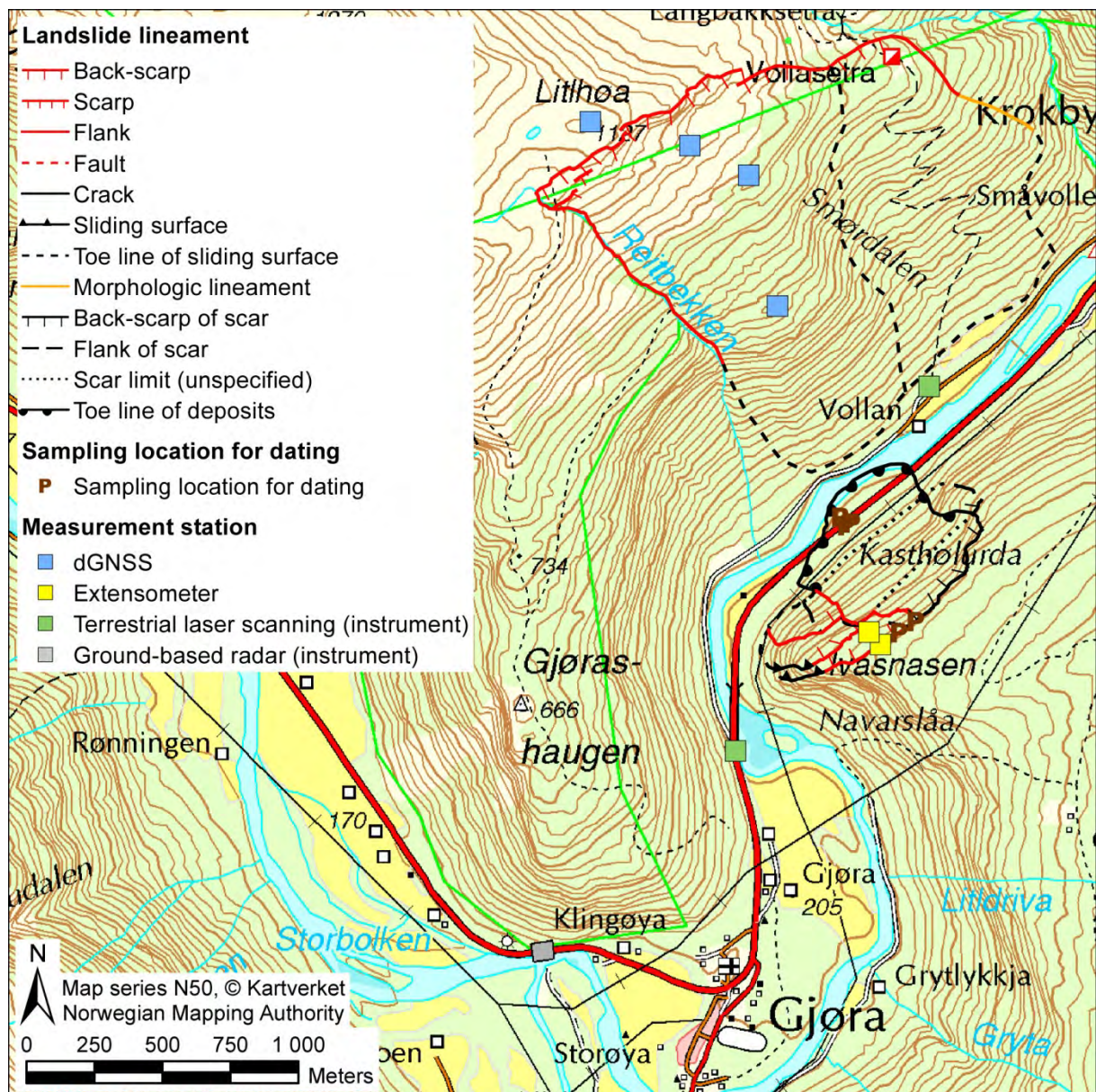


Figure 3: Situation map of stop 1: the Ivasnasen rockslide scar, the Ivasnasen unstable rock slope and the Vollan unstable rock slope.

GEOLOGICAL AND STRUCTURAL CONTROL OF THE IVASNASEN AND VOLLAN UNSTABLE ROCK SLOPES (WESTERN NORWAY)

By T. Oppikofer

Summary

The Ivasnasen and Vollan unstable rock slopes are located on opposite slopes in the upper part of the Sunndal Valley (western Norway). Vollan lies on a SE-facing slope composed of quartzite in the upper part and calcareous phyllite and garnet micaschist in the lower part while Ivasnasen faces NW and exposes competent augengneiss. These different lithological units belong to different nappes or nappe complexes, which were thrust over the gneissic basement during the Caledonian orogeny and folded into a large syncline forming the valley.

The rock slope deformation at Vollan is characterized by a steep back-scarp along the subvertical valley-parallel SW-NE metamorphic foliation in the quartzites and a series of parallel counterscarps in the phyllites. Field observations and a kinematic analysis indicate toppling as possible failure mechanism along the back-scarp, while the counterscarps are most likely formed by compression in the relatively incompetent phyllites induced by the toppling movement of the quartzites. Extremely slow have been detected by periodic differential global navigation satellite system (dGNSS) measurements over the past five years.

A post-glacial rock avalanche occurred at Ivasnasen with a reconstructed volume of 1.2 million m³. Failure occurred along a single planar sliding surface formed by the 45°-55° NW-dipping metamorphic foliation in the augengneiss. The same structure forms the back-scarp and sliding surface of the present unstable rock slope only a few tens of metres to the west. Extremely slow displacements are currently recorded by periodic terrestrial laser scanning and extensometer measurements, and the site is considered as unstable rock slope owing to the offset of the mass along the sliding surface. The current unstable area is estimated to have a volume of 2.1 to 4.1 million m³.

Introduction

Ivasnasen is located on a west- to northwest-facing slope 295 m above the Sunndal Valley close to Gjøra in the upper part of the Sunndal Valley in western Norway (Figure 3). Ivasnasen is an unstable rock slope and in addition it hosted a post-glacial rock slope failure whose deposits are well preserved in the valley bottom. This rock avalanche was postulated as having occurred in 1789 (Henderson and Saintot 2007, Saintot et al. 2008), but the historic sources do not allow a definitive confirmation of that assumption: on 22 to 23 July 1789 a sudden debris flood partly destroyed a farm downstream of the rock avalanche deposits (NVE 2014). However, the debris flood likely originated from the hillslopes directly west of the farm under an extreme rainfall event (known as “Stor-oksen”) (NVE 2014) and not from an outburst flood of a rock avalanche dam breach.

On the opposite, southeast-facing valley side lies the unstable rock slope Vollan at 840 m above the valley. Both sites show clear signs of post-glacial deformation and have been mapped and are periodically monitored within NGU’s systematic mapping program of unstable rock slopes (Henderson and Saintot 2007, Saintot et al. 2008). The investigations include detailed geomorphic, structural and geological field mapping, along with interpretation of high-resolution digital elevation models (DEM) and orthophotos, terrestrial laser scanning for structural analysis and displacement measurements, and numerical slope stability modelling.

Geographical and geological setting

The study area is located close to the village of GjØra. At GjØra, the valley orientation suddenly changes from the general WNW-ESE-trend to a SW-NE-direction and changes from a typical wide glacial valley to a much narrower valley. This change in valley direction and morphology is likely related to a zone of intense tectonic deformation, with several nappes that were overthrust during the Caledonian orogeny (Figure 4) (Henderson and Saintot 2007, Saintot et al. 2008). The valley direction north of GjØra matches the trend of these tectonic limits. The bedrock map (Nilsen and Wolff 1989) distinguishes five main units in the study area from NW to SE: undifferentiated gneiss and quartzite of the Åmotdal nappe (lower nappe series); calcareous phyllites and garnet-bearing micaschists of the BlåhØ nappe (upper nappe series); quartzite and quartz schists of the Sætre nappe and augengneiss of the Risberg nappe (middle nappe series), and finally again quartzite and undifferentiated gneiss of the Åmotdal nappe (Figure 4).

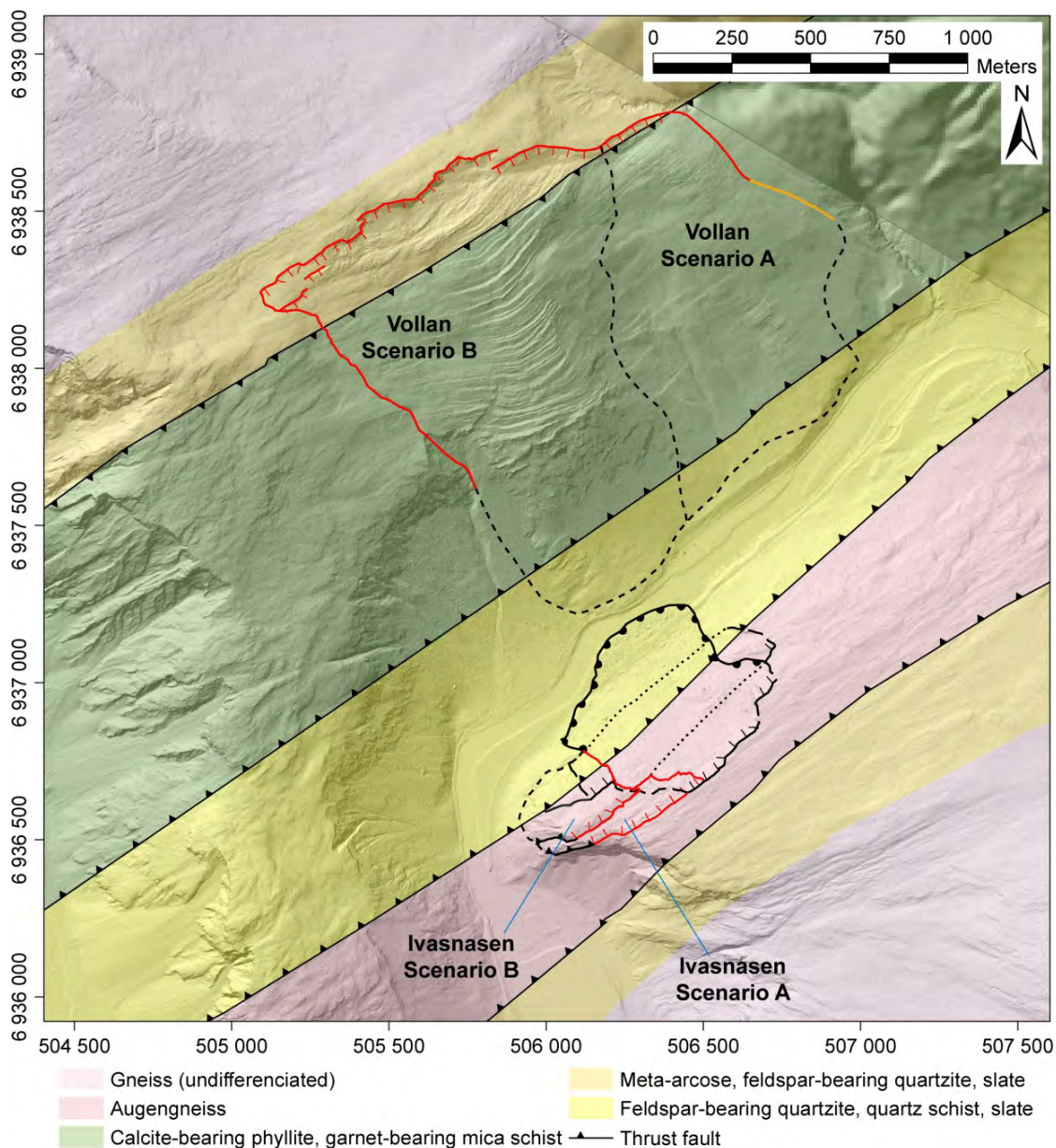


Figure 4: Geological and morphological map of the Ivasnasen and Vollan rock slopes (1:250,000 bedrock map by Nilsen and Wolff 1989). See Figure 3 for the symbology of landslide lineaments.

The lower nappe series is formed of metamorphosed rocks of Proterozoic age, while the middle nappe series is of Proterozoic to Ordovician age (ca. 1600 Ma for the augengneiss). All nappe series were overthrust and emplaced in Early Ordovician. In the study area the overthrust units form a synform, whose axis is parallel to the NW-SE-trending valley (Nilsen and Wolff 1989).

The unstable rock slope Ivasnasen developed in augengneisses on the NW-facing slope, while the unstable rock slope Vollan formed in quartzites (back-scarp) and phyllites and micaschists (main landslide body).

Ivasnasen rockslide scar

The post-glacial rockslide at Ivasnasen has a well-exposed basal failure surface that is formed by the gneiss foliation dipping 45° - 55° to the NW (Figure 5a). The flanks are also well visible, especially in the NE (Figure 5b). The rockslide scar is ca. 400 m wide and ca. 150 m long and the exposed flanks are up to 40 m high. The back-scarp of the rockslide lies at an altitude of 510 m a.s.l. and the toe of the rock avalanche lies at an elevation of 200 m a.s.l. The run-out distance is measured to 530 m, which results in an angle of reach of 30° .

The orientations of main discontinuity sets are based on field measurements along with an analysis of terrestrial laser scanning data in the software Coltop3D (Terranum 2013). These discontinuity sets enable a planar sliding mechanism for the Ivasnasen rockslide (Figure 6a).

The ante-rockslide topography was reconstructed manually in the 3D software PolyWorks by following the slope orientation in the surroundings of the rockslide scar. The rock avalanche deposits were removed from the present topography using the Sloping Local Base Level (SLBL) technique (Jaboyedoff et al. 2004, 2009). The volume of rockslide is then computed using the altitude differences between the ante-rockslide topography and the present digital elevation model, resulting in a volume of 1.2 million m^3 (Figure 7). The present morphology of the Ivasnasen rock slope suggests that other rock slope failures occurred prior to this event. These were likely of pre- or syn-glacial age since no deposits are found in the valley floor. These rock slope failures had a total volume of approximately 4 million m^3 .

Ivasnasen unstable rock slope

An unstable rock slope is located on a topographic promontory directly southwest of the rockslide scar at Ivasnasen. The sliding surface of the unstable rock slope follows the basal sliding surface of the past rockslide, i.e. the 45° - 55° NW-dipping metamorphic foliation (Figure 8a). The back-scarp formed by past sliding along the sliding surface is up to 10 m long (Figure 8b). The unstable rock slope is divided into two scenarios by another foliation-parallel sliding surface that also forms a small scarp on top of the unstable area (Figure 4).

Kinematic feasibility tests with the measured discontinuity sets indicate a planar failure mechanism (Figure 6b). The lateral view of the unstable rock slope (Figure 8a) shows that the observed sliding surfaces do not daylight and field measurements at the toe of the unstable area indicate that the metamorphic foliation steepens to 60° - 70° . This steepening of structures impedes planar sliding and no simple failure mechanism is thus possible. Breaking of rock bridges at the rockslide toe is thus necessary in order to create a continuous failure surface, and there are at present indications of higher fracturing and disintegration of the rock mass at the foot of the unstable rock slope (Figure 8b). The volume of the Ivasnasen unstable rock slope is computed using the SLBL technique, giving a volume of 2.1 to 4.1 million m^3 for the total unstable rock slope (scenario A) and 1.2 to 3.2 million m^3 for scenario B that is delimited by the middle scarp (upper sliding surface in Figure 8a).



Figure 5: Photographs of the Ivasnasen rockslide scar: left) overview photograph of the scar and the unstable rock slope; right) along the moderately NW-dipping sliding surface and the northeastern flank (photographs: T. Oppikofer / G.M. Dreiaås) (Dreiaås 2012).

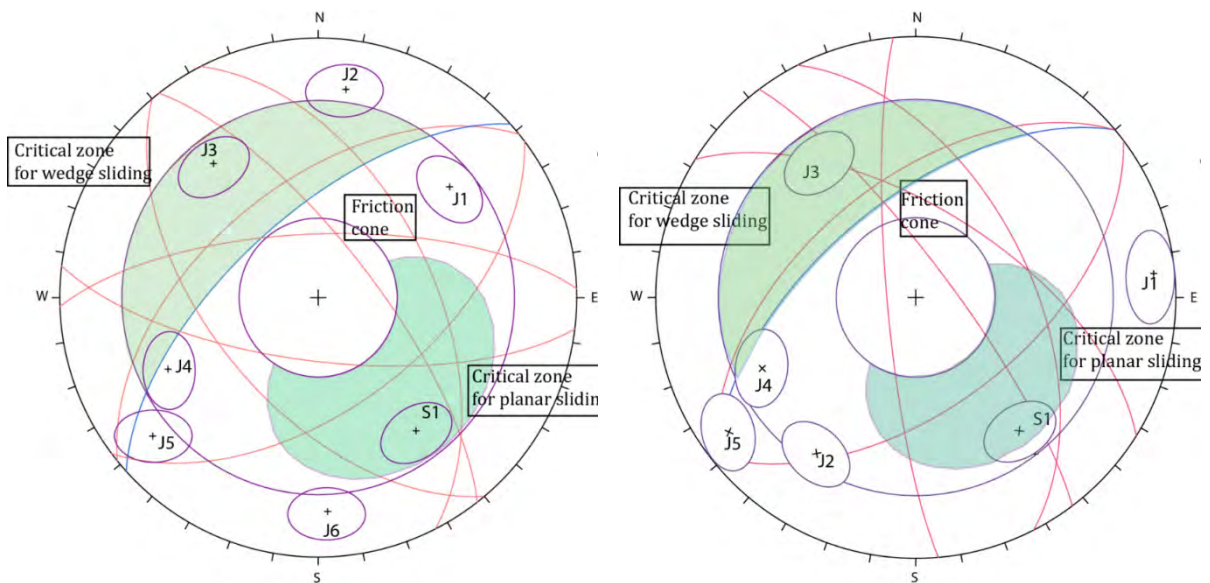


Figure 6: Kinematic analysis of possible failure mechanisms for the past Ivasnasen rockslide (left) and the Ivasnasen unstable rock slope (right) (Dreiaås 2012).

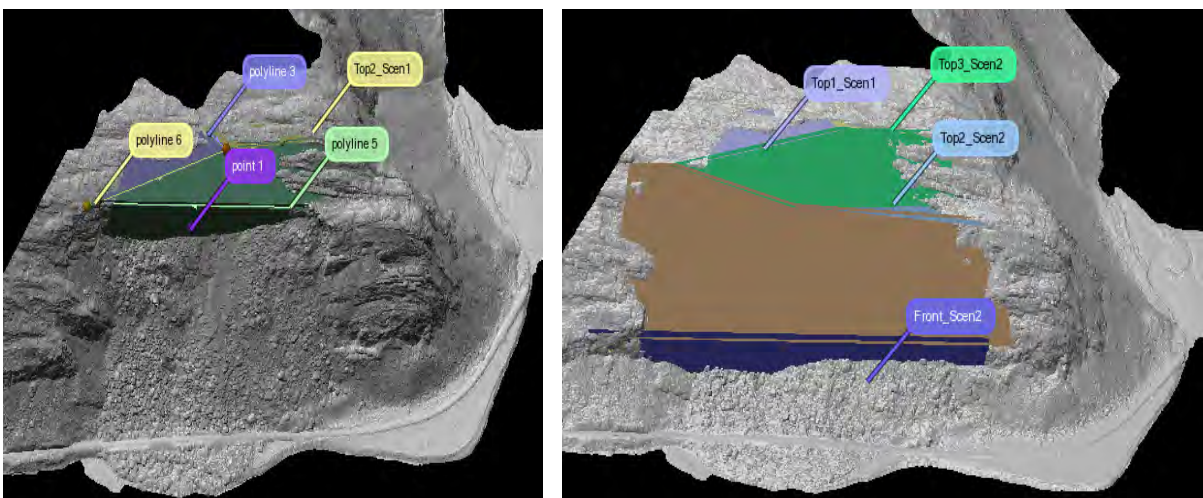


Figure 7: Reconstruction of the past Ivasnasen rockslide (Dreiaås 2012).



Figure 8: Photograph of the Ivasnasen unstable rock slope: left) lateral view of the SW-facing cliff with the location of foliation-parallel basal sliding surfaces (photograph: A. Saintot); right) fractured rock mass at the foot of the unstable rock slope (photograph: G.M. Dreiß)

The Ivasnasen unstable rock slope has been periodically measured since 2010 using terrestrial laser scanning and tape extensometers at two locations (Figure 4). Both tape extensometer points were measured again in 2011 and 2014, but only small displacements (approximately 1.5 mm/year) are detected along the back-scarp, while no significant displacement are measured over an internal secondary scarp. Repetitive TLS data acquired in 2011 and 2012 did not reveal any significant displacements or rockfall activity.

Numerical slope stability modelling indicates that the unstable rock slope at Ivasnasen might be stable, while failure was achieved for the past rockslide when using the same modelling parameters (Dreiß 2012).

The hazard and risk classification for unstable rock slopes in Norway (Hermanns et al. 2012, 2013) is applied to both scenarios of the present unstable rock slope. On the hazard score scale ranging from 0 (very low hazard) to 12 (very high hazard), scenario A (failure of the whole unstable area) has a hazard score of 6.1 (medium hazard). The smaller scenario B has a lower hazard score of 4.6 (low hazard). The absence of clear kinematic failure mechanism and morphologic evidences of a continuous sliding surface, along with the low displacement rates and lack of other signs of activity (rockfalls) lead to these relatively low hazard scores.

For both scenarios (A and B) a rock avalanche from Ivasnasen would affect the National road Rv70 and likely dam the river Driva with the consequence of upstream flooding and also downstream flooding in the event of a dam breach (Dahle et al. 2011). On the other hand there are no inhabitants living in the run-out area of a possible rock avalanche. Combined with the hazard score, this results in a low risk for both scenarios of the Ivasnasen unstable rock slope.

Vollan

Vollan is a complex unstable rock slope that affects the entire SE-facing slope (Figure 3, Figure 4 and Figure 9). The unstable rock slope is approximately 1400 m wide and 1420 m long, but the most deformed area in the western part of the slope is only 1030 m wide. The back-scarp is well developed and forms a high escarpment in the central part of the unstable rock slope, with decreasing height towards the lateral limits. There are no visible flanks to the unstable rock slope, however the deformed area can be delimited based on a hillshade of the digital elevation model (Figure 4). The toe of the unstable rock slope cannot be mapped out due to colluvium and vegetation in the lower part of the slope.

The back-scarp is located in competent quartzites of the Åmotdal nappe with a well-developed subvertical foliation. Past slope movements formed an up to 130 m wide graben-like structure, which is filled with rockfall material. Toppling along the subvertical to overhanging foliation is identified as the principal failure mechanism (Dreiß 2012). Below

this back-scarp and graben-like structure, the bedrock changes to less competent calcareous phyllites and mica schists of the Blåhø nappe. This lithological change is associated with a clear change in deformation style with a more plastic deformation of the phyllites leading to flow-like structures on the slope surface with multiple parallel counter-scarps and depressions (Figure 4, Figure 9 and Figure 10). Field measurements of discontinuities rule out any of the classical kinematic failure mechanisms (planar or wedge sliding or toppling). This suggests that the deformation of the phyllites is caused by the toppling movements along the back-scarp. Flexural toppling is evoked as possible failure mechanism as illustrated at outcrop-scale at the southeastern part of the back-bounding graben (Figure 9).

The volume of the Vollan unstable rock slope is computed using the SLBL technique. Two possible scenarios are considered based on the differences in degree of deformation: scenario A encompasses the entire unstable rock slope, while scenario B is restrained to the more deformed area in the western part. The volume assessment yields a volume of 57 to 105 million m³ for scenario A, and 39 to 55 million m³ for scenario B. A sudden failure of such large volumes of rock seems, however, unlikely given the observed deformation style and mechanism.



Figure 9: Photographs of the Vollan unstable rock slope: a) overview of the back-scarp in quartzites and the more plastic deformation of the phyllites (photograph: T. Oppikofer); b) back-scarp formed by the vertical foliation (photographs: G.M. Dreiaås); c) outcrop-scale representation of a possible flexural toppling mechanism for the unstable rock slope (photographs: G.M. Dreiaås).

Three dGNSS-points for periodic displacements measurement were installed in 2008 and measured again in 2009, 2011 and 2013. Between 2009 and 2013, the three measurement points indicate a significant and coherent displacement ranging from 1.5 to 3 mm/year towards the ESE (Figure 10). This displacement direction is oblique by about 45° to the dip direction of the slope and the counter-scarps in the phyllites. However, the displacement direction is uncertain since the measured displacements are close to the significance limit.

The hazard and risk classification for unstable rock slopes in Norway (Hermanns et al. 2012, 2013) gives a hazard score of 2.6 for scenario A and 4.0 for scenario B (low hazard level). The lack of clear lateral and basal delimitations, along with small displacements rates and absence of other signs of activity (rockfalls or past events) explains these low hazard scores.

A massive rock slope failure from Vollan would destroy several buildings in the run-out area, affect the National road Rv70 and dam the river Driva with the consequence of upstream flooding and also downstream flooding in the event of a dam breach (Dahle et al. 2011). A preliminary risk assessment estimates the average life losses to 24. Combined with the above hazard assessment, this results in a low risk for scenario A and medium risk for scenario B.

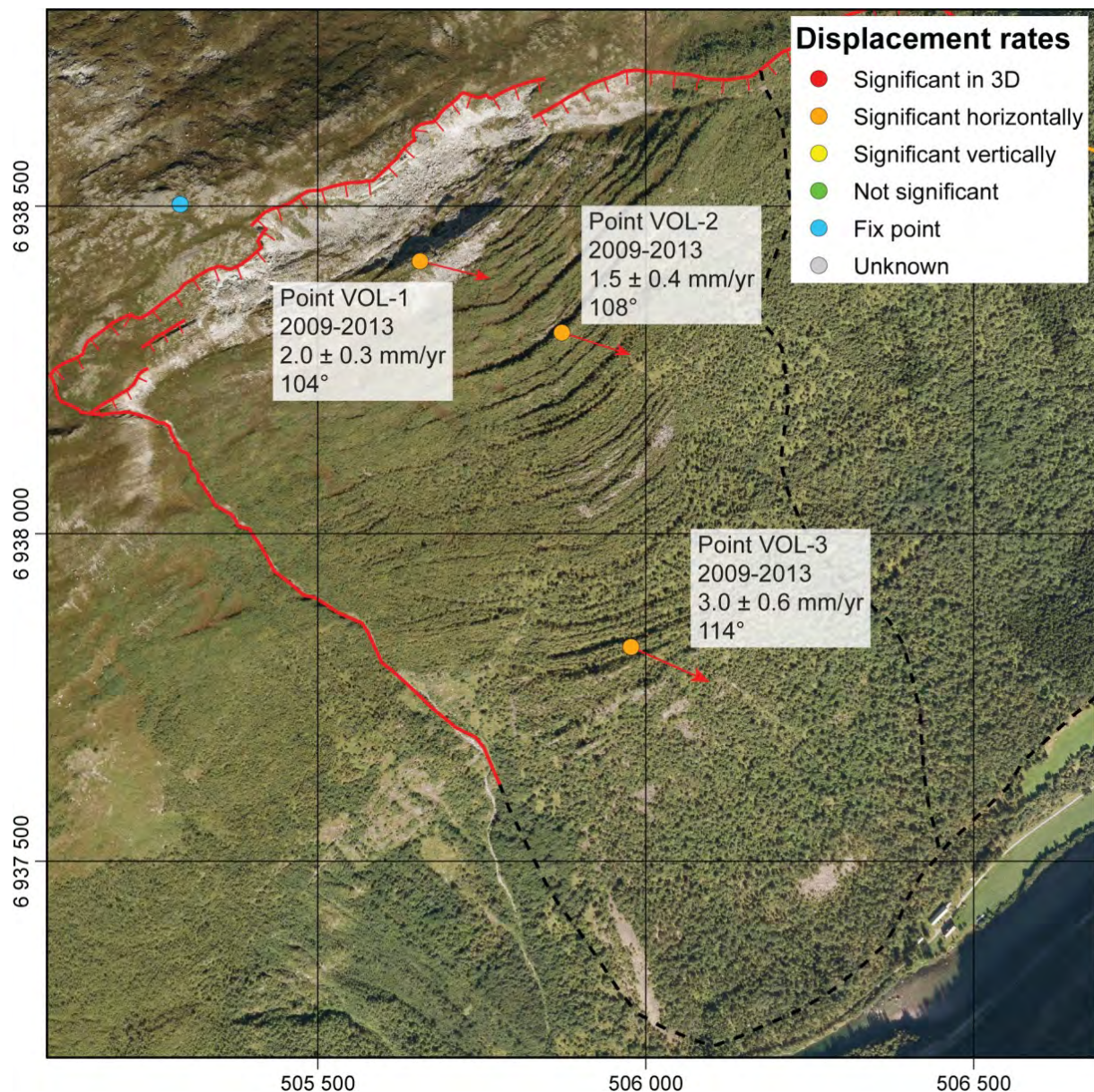


Figure 10: Map of the measured displacement rates by dGNSS for the time period from 2009 to 2013.

Cited references for stop 1: Ivasnasen & Vollan

- Dahle, H., Anda, E., Sætre, S., Saintot, A., Hermanns, R.L. and Oppikofer, T. (2011) Risiko- og sårbarhetsanalyse for fjellskred i Møre og Romsdal - FylkesROS-fjellskred. Fylkesmannen i Møre og Romsdal, Møre og Romsdal Fylkeskommune, Geological Survey of Norway, Molde, Norway.
- Dreiås, G.M. (2012) Engineering geological assessment and structural comparison of the Vollan and Ivasnasen rock slopes in Sunndalen, Norway. MSc thesis, Norwegian University of Science and Technology, Trondheim, Norway.
- Henderson, I. and Saintot, A. (2007) Fjellskredundersøkelser i Møre og Romsdal. NGU report 2007.043, Geological Survey of Norway, Trondheim, Norway.
- Hermanns, R.H., Oppikofer, T., Anda, E., Blikra, L.H., Böhme, M., Bunkholt, H., Crosta, G.B., Dahle, H., Devoli, G., Fischer, L., Jaboyedoff, M., Loew, S., Sætre, S. and Yugsi Molina, F.X. (2013) Hazard and Risk Classification for Large Unstable Rock Slopes in Norway. In: Genevois, R. and Prestininzi, A. (eds.) *International Conference Vaiont, 1963-2013 - thoughts and analyses after 50 years since the catastrophic landslide*, Italian Journal of Engineering Geology and Environment - Book Series 6, Sapienza University, Rome, Italy, pp. 245-254.
- Hermanns, R.L., Oppikofer, T., Anda, E., Berg, H., Blikra, L.H., Böhme, M., Bunkholt, H., Crosta, G.B., Dahle, H., Devoli, G., Eikenæs, O., Fischer, L., Jaboyedoff, M., Loew, S., Sætre, S. and Yugsi Molina, F.X. (2012) Recommended hazard and risk classification system for large unstable rock slopes in Norway. NGU report 2012.029, Geological Survey of Norway, Trondheim, Norway.
- Jaboyedoff, M., Baillifard, F., Couture, R., Locat, J. and Locat, P. (2004) Toward preliminary hazard assessment using DEM topographic analysis and simple mechanical modeling by means of sloping local base level. In: Lacerda, W.A., Ehrlich, M., Fontoura, A.B. and Sayão, A. (eds.) *Landslides: Evaluation and Stabilization*, Taylor & Francis Group, London, pp. 199-205.
- Jaboyedoff, M., Couture, R. and Locat, P. (2009) Structural analysis of Turtle Mountain (Alberta) using digital elevation model: Toward a progressive failure. *Geomorphology*, 103, 1, 5-16.
- Nilsen, O. and Wolff, F.C. (1989) Bedrock map Røros & Sveg. Bedrock map scale 1:250,000, Geological Survey of Norway, Trondheim, Norway.
- NVE (2014) Skrednett. Norwegian Water Resources and Energy Directorate (NVE), Oslo, Norway. Available: <http://www.skrednett.no/>.
- Oppikofer, T., Saintot, A., Otterå, S., Hermanns, R.L., Anda, E., Dahle, H. and Eiken, T. (2013) Investigations on unstable rock slopes in Møre og Romsdal – status and plans after field surveys in 2012. NGU report 2013.014, Geological Survey of Norway, Trondheim, Norway.
- Saintot, A., Böhme, M., Redfield, T.F. and Dahle, H. (2008) Field studies of unstable slopes in Sunndalen Valley. NGU report 2008.049, Geological Survey of Norway, Trondheim, Norway.
- Terranum (2013) Coltop3D - LIDAR data processing and analyzing software for geologists. Terr@num SàRL, Bussigny, Switzerland . Available: <http://www.terranum.ch/coltop3d-features>.

STOP 2: OPPDØLSTRANDA

Oppdølstranda, a 6.5 km-long road section of the National road Rv70 between Oppdøl and Sunndalsøra (Figure 11), is a well known rockfall-prone area. At this stop we have the opportunity to discuss some of the monitoring and mitigation measures that were undertaken by the National Road Authorities, including rockfall protection fences above the road, periodic ground-based radar measurements and finally a new road tunnel. The following summary is based on the final report on the radar measurements by the Åknes/Tafjord Early-Warning Centre (Kristensen 2013).

The National road Rv70 between Oppdøl and Sunndalsøra follows the shoreline of the fjord for about 6.5 km. The road goes through several tunnels, but about 3.3 km is open and exposed to rockfalls. The topography rises from sea level to around 1400-1550 m a.s.l. with a mean slope of 40-50° and locally vertical cliffs, which are the main rockfall sources.

There have been several incidences of large rockfalls in the past years (Figure 11) and the rockfall risk along the road was determined to be high (Moen 2009). Therefore, the National Road Authority undertook various monitoring and mitigation measures, including installation of rockfall protection fences, inducing rockfalls by helicopter with a wrecking ball (Norwegian Public Roads Administration 2009), periodic measurements of the rock walls by ground-based radar (made by the Åknes/Tafjord Early-Warning Centre) (Kristensen 2011, 2013) and terrestrial laser scanning (made by the University of Lausanne and NGU). In August 2014 the National Road Authority opened a new tunnel that bypasses the rockfall-prone road section as a permanent mitigation.

Ground-based radar measurements

The Åknes/Tafjord Early-Warning Centre conducted periodic measurements between 2010 and 2012 using a LiSALab (Ellegi Srl) ground-based radar system. The system uses the Synthetic Aperture technique, where the radar moves automatically on a 2.5 m-long steel rail during the measurements, in order to simulate a larger antenna separation and thereby obtain a better resolution (Figure 12) (Kristensen 2013). The same ground-based radar system is currently used by the Åknes/Tafjord Early-Warning Centre to monitor the unstable rock slopes at Åknes, Mannen, Børa, Stampa and Nordnesfjellet.

The radar system was installed on four different sites (A-D in Figure 11), where the measurements had a duration of about a week per site and measurement campaign. A total of 6-7 campaigns were conducted during the period 2010-2012. The goal of these periodic measurements was to determine if small displacements of small and large instabilities in the rock wall can be detected (Kristensen 2013).

Rockfall event on 8 June 2011

The periodic radar measurements detected displacements in the range of approximately 1 cm between autumn 2010 and spring 2011 at site C (Figure 13). These displacements turned out to be pre-failure deformation of a 15-20 m³ rockfall that occurred on 8 June 2011 (Figure 14). The rockfall blocks were so big that they destroyed and crossed the rockfall protection fence built above the road (visible in Figure 12). Ground-based radar measurements immediately after the event revealed no further displacements in the rock walls. Based on this information along with observations from helicopter, the road was opened again. The radar measurements after the event revealed slight displacements of a small potential unstable area just south of the 8 June 2011 rockfall scar (Figure 15) (Kristensen 2013).



Figure 11: Situation map of stop 2: the rockfall-prone section of the National road Rv70 at Oppdølstranda between Sunndalsøra and Oppdøl. A newly opened tunnel now bypasses this hazardous road section.

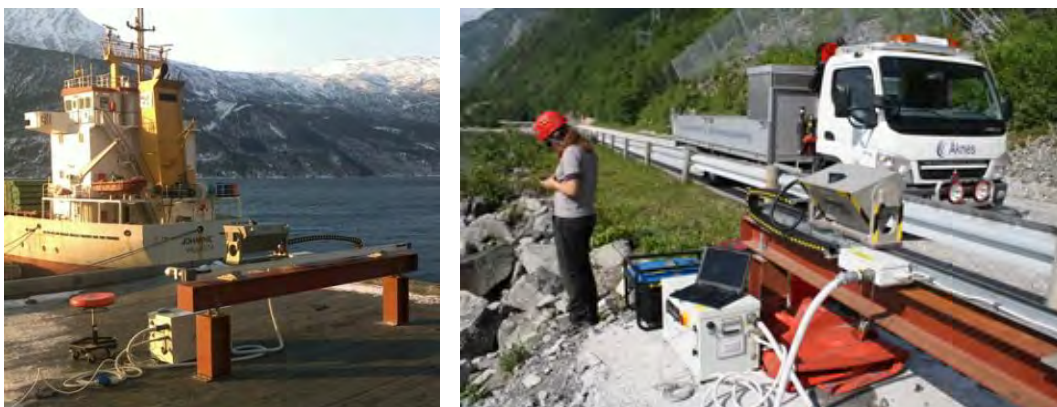


Figure 12: Photographs of the ground-based radar installation on 2.5 m-long steel rails (Kristensen 2013).

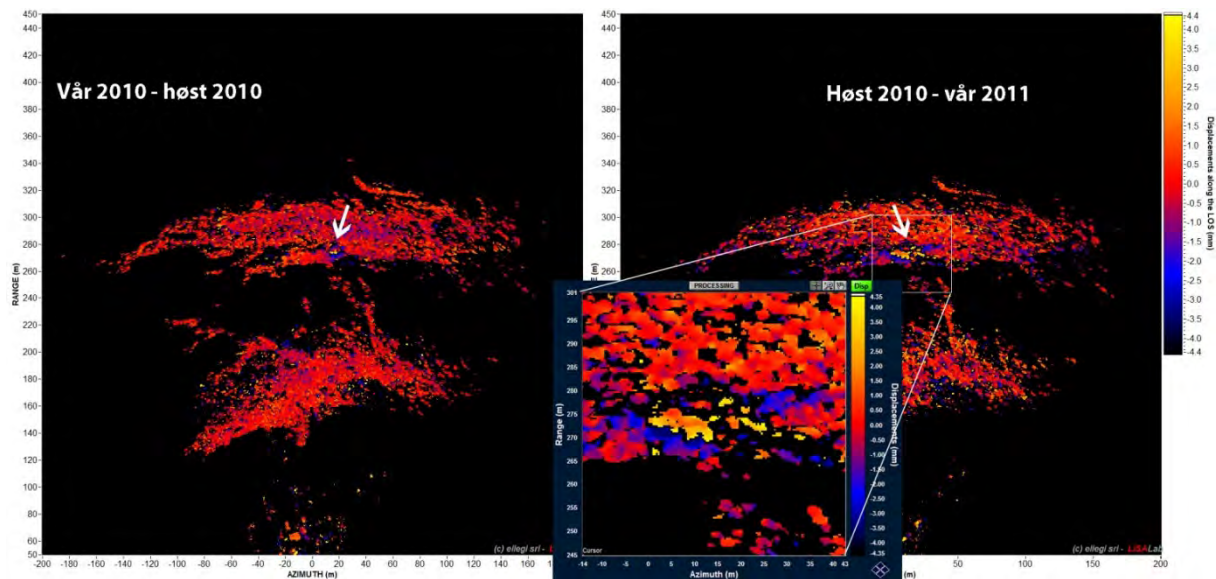


Figure 13: Ground-based radar measurements prior to the 8 June 2011 rockfall: left) between spring and autumn 2010; right) between autumn 2010 and spring 2011. Red color equal no movements and blue about -4 mm, yellow and orange about 6-8 mm. The pre-failure deformation in the rockfall release area is clearly visible (Kristensen 2013).



Figure 14: Pictures of the 8 June 2011 rockfall scar and rockfall blocks on the road. The blocks destroyed and crossed the rockfall protection fence above the road (photographs: T. Humstad, Norwegian Public Roads Administration) (Kristensen 2013).

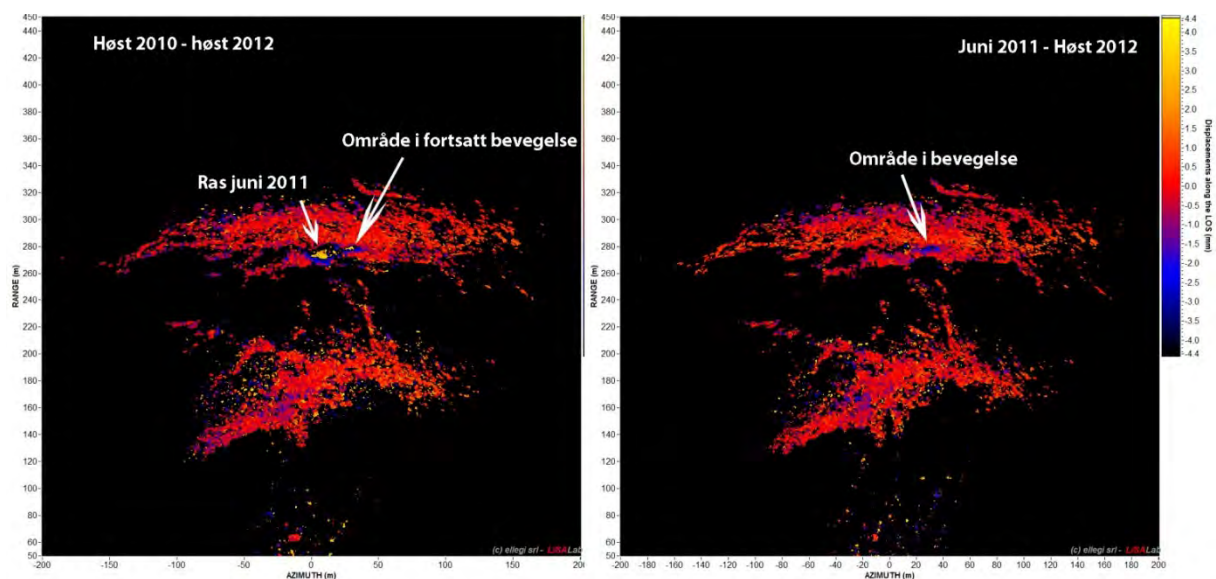


Figure 15: A small potential unstable area is detected at site C just south of the 8 June 2011 rockfall scar (Kristensen 2013).

Conclusions

The periodic ground-based radar measurements were able to measure pre-failure deformation and displacements prior to the rockfall event on 8 June 2011. The displacements increased during the winter 2010/2011 compared to summer 2010. This suggests that the release process takes place in a relative short time-frame. However, it was possible still to identify the movement almost one year in advance (Kristensen 2013).

Ground-based radar has a good potential for detecting displacements in steep rock slopes. The measurements show that small unstable blocks have periods of increased movement, which is possible to detect by radar and thereby to predict. After the rockfall event, the radar can be rapidly deployed and used to quickly conclude that the slope was now stable and the road could be reopened. This demonstrates that the radar is an effective method to use in rockfall monitoring, especially in critical situation (Kristensen 2013).

No large unstable rock slopes were detected by the periodic radar measurements, but minor active rockfall areas were found. The main advantage of the radar is that it covers large areas, but it is still important to combine radar data with other mapping methods in order to verify possible unstable areas. Additionally, it is important to evaluate the data accuracy to distinguish noise from vegetation and atmosphere from real displacements (Kristensen 2013).

Cited references for stop 2: Oppdølstranda

- Kristensen, L. (2013) Radarkartlegging av potensielle løseområder for steinskred på rv. 70 Oppdølstranda – Sluttrapport. Åknes report 01.2013, Åknes/Taffjord Early-Warning Centre, Stranda, Norway.
- Kristensen, L. (2011) Radarmålinger viste bevegelser før steinraset på rv 70, Oppdølstranda 8. juni. Available: <http://aknes.no/?q=nb/node/48>, accessed 02.09.2014.
- Moen, K. (2009) Risikovurdering av rv. 70 forbi Oppdølstranda. Rapportnr.119654-1, Multiconsult, Oslo, Norway.
- Norwegian Public Roads Administration (2009) Norwegian Helicopter Induces a Rock Fall beside a Fjord. Available: <https://www.youtube.com/watch?v=afI58PRmTJ0>, accessed 02.09.2014.

STOP 3: INNERDAL VALLEY

At this stop in Innerdal Valley (Figure 16) we have the opportunity to observe and discuss the deposits of multiple rock avalanches, incl. Younger Dryas supra-glacial rock avalanche deposits and a lake dammed by a rock avalanche. An inventory of rock avalanche deposits in Innerdalen Valley was made by M. Schleier (University of Erlangen, Germany). Preliminary results are summarized in Schleier et al. (2013) (see Appendix 4) and the following summary is modified from Oppikofer et al. (2013).



Figure 16: Situation map of stop 3: the rock avalanche deposits from Skarfjellet dammed the Innerdalsvatna Lake; remnants of multiple other rock avalanches can be found further up and down the valley.

Multiple rock avalanche deposits composed of rock boulders several meters in diameter occur in Innerdalen Valley. The blocky deposits are divided into six units (A to F in Figure 17). The main rock avalanche deposits (A) have an estimated volume of 39 million m³ and typical lateral levees and frontal rims. The rock avalanche crossed the valley, ran-up on the opposite valley side by up to 65 m and dammed the river to form Innerdalvatnet Lake. Boulders are several meters to tens of meters in diameter and cover the entire surface of the deposits.

Other boulder deposits are interpreted to be related to another rock avalanche that would have occurred in Innerdalen Valley when it was filled by a glacier at the end of the Younger Dryas. This rock avalanche would have travelled over the glacier and deposited patches of boulders (D) on the slope at 270–370 m above the valley floor. However, most of the material would have been deposited onto the glacier and then redeposited with the normal supra- and subglacial load into three closely spaced 12–15 m high frontal moraine ridges covered with metric boulders (B) and isolated hills composed of rock boulders surrounded by fluvial sediments (C). Two distinctive valley-parallel ridges (E) 30–50 m above Innerdalvatnet Lake are likely related to rock avalanche debris deposited onto the glacier. This protects the ice from melting and leads to an accumulation of boulders by washing out of fine-grained material by supraglacial processes. A flat boulder patch within moraine deposits southeast of Innerdalvatnet Lake (F) should be related to transported rockfall and rock avalanche material from upstream the Innerdalen Valley.

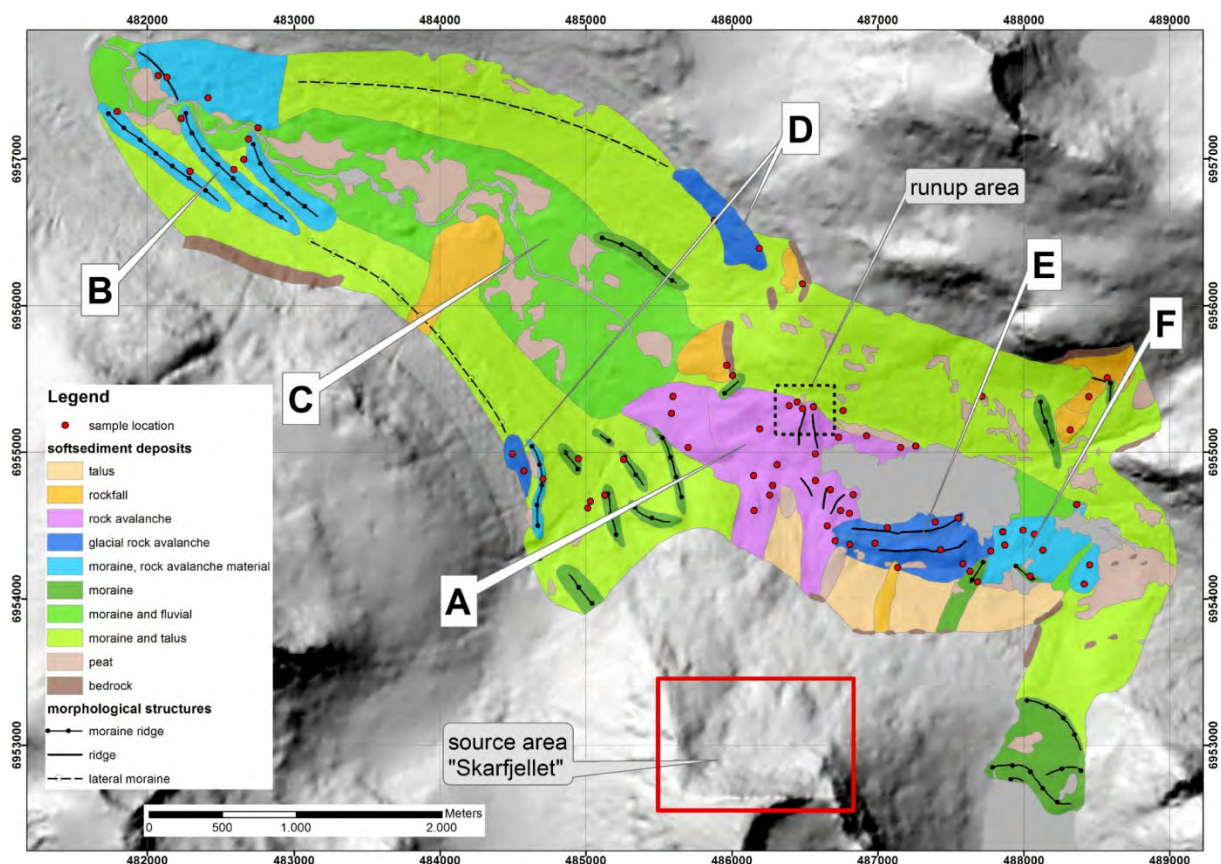


Figure 17: Rock avalanche inventory map in Innerdalen Valley (Schleier et al. 2013).

Cited references for stop 3: Innerdal Valley

- Oppikofer, T., Saintot, A., Otterå, S., Hermanns, R.L., Anda, E., Dahle, H. and Eiken, T. (2013) Investigations on unstable rock slopes in Møre og Romsdal – status and plans after field surveys in 2012. NGU report 2013.014, Geological Survey of Norway, Trondheim, Norway.
- Schleier, M., Hermanns, R.L. and Rohn, J. (2013) Spatial distribution of rockslide deposits and their morphological features suggest timing and paleo-environmental conditions for rock slope failures in Innerdalen and Innfjorddalen, Møre og Romsdal County, Western Norway. In: Genevois, R. and Prestininzi, A. (eds.) *International Conference Vaiont, 1963-2013 - thoughts and analyses after 50 years since the catastrophic landslide*, Italian Journal of Engineering Geology and Environment - Book Series 6, Sapienza University, Rome, Italy, pp. 493-505.

STOP 4: PETROGLYPHS AT BOGGE

This short touristic stop presents you prehistoric petroglyphs (or rock engravings) at Bogge, located in the scenic Eresfjord.

Motifs of elks, fishes and boats were engraved by the fishers and hunters into rocks at the shoreline that were newly exposed due to the isostatic rebound. The oldest petroglyphs are located at 24 m a.s.l. and are dated to approximately 6000 years, while younger drawings are located closer to the present shoreline (VisitNorway.com, 2014).



Figure 18: Photographs of the petroglyphs at Bogge (photographs by R. Hermanns, NGU).

Cited reference for stop 4: Petroglyphs at Bogge

VisitNorway.com (2014) The petroglyphs at Bogge - Official Travel Guide to Norway. Available: <http://www.visitnorway.com/en/product/?pid=32981>, accessed 02.09.2014.

STOP 5: TJELLEFONNA

This stop along the shoreline of the Langfjord (Figure 19) allows us to observe the largest historical rock avalanche in Norway, which took place at Tjellefonna in 1756. We will discuss the back-analysis of this ca. 10 million m³ rock avalanche, including structural features, kinematics, volume reconstructions, as well as numerical slope stability modelling, in order to propose a geological model for the Tjellefonna rock avalanche and discuss possible triggering factors. The following contribution of the excursion guide is based on a MSc thesis by G. Sandøy finished in 2012 at the Norwegian University of Science and Technology (NTNU, Trondheim, Norway) (Sandøy 2012).

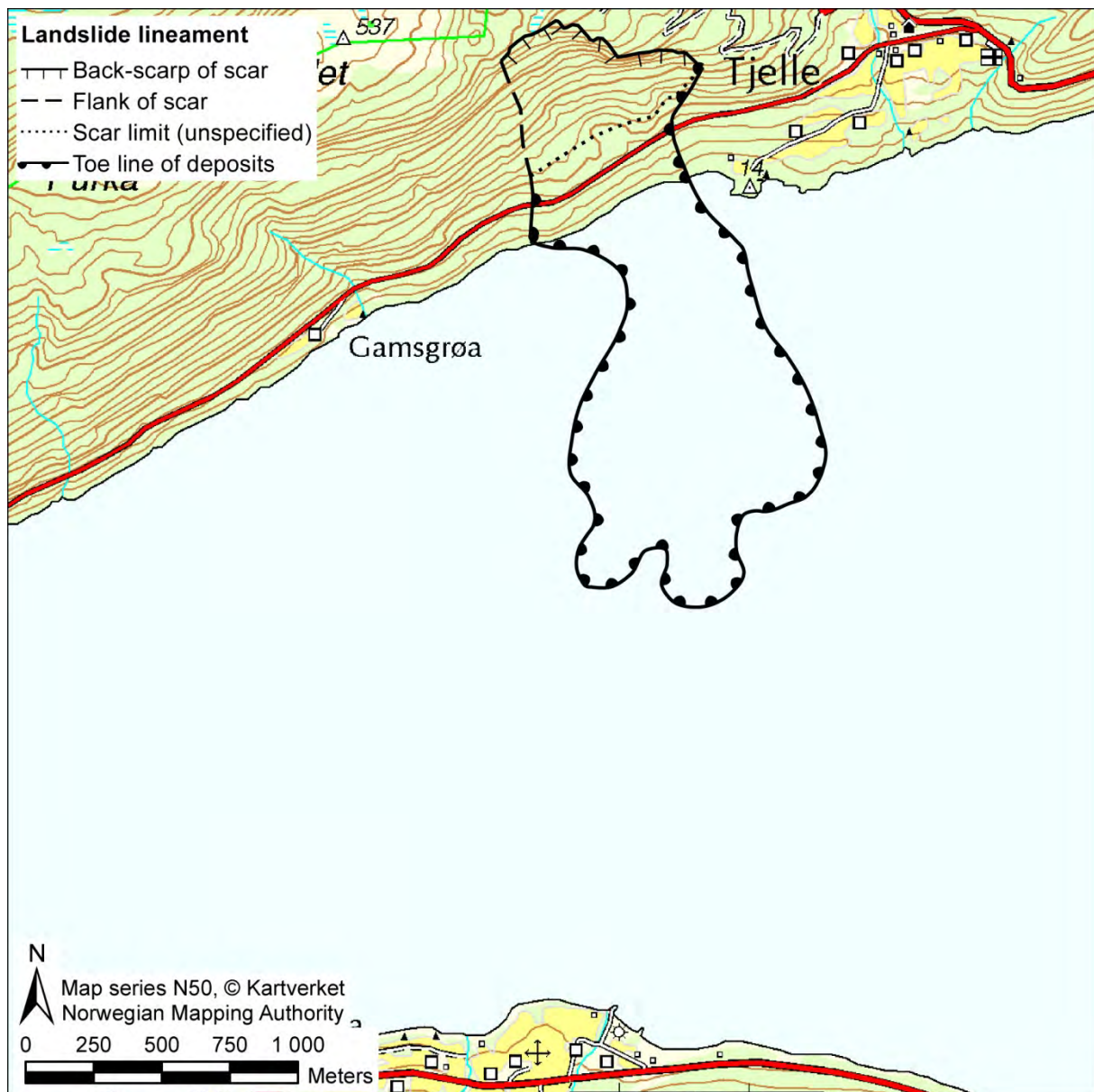


Figure 19: Situation map of stop 5: the Tjellefonna rock avalanche in 1756 triggered a displacement wave that affected the entire Langfjord area.

BACK-ANALYSIS OF THE 1756 TJELLEFONNA ROCKSLIDE

By Gro Sandøy (NGU)

Summary

On 22 February 1756 the largest historically recorded rockslide in Norway took place at Tjelle in the Langfjord. The displacement waves that were created as the rock mass hit the water caused 32 casualties and destroyed most houses and boats along the shores of Langfjord.

The initial rockslide volume was recalculated to 9.3 to 10.4 million m³, of which only 3.9 million m³ entered the fjord. This volume is significantly lower than what has been reported previously (15 million m³).

Structural analysis shows that the foliation is folded and dips steeply towards the fjord and into the slope. Two prominent fault zones are present in close proximity to Tjellefonna; one dipping steeply towards the fjord with dipdirection/dip 153/80 and one sub-horizontal varying from 350/20, 172/12 to 000/03. Additionally, there are in total four persistent joint sets with orientations 157/59, 076/81, 352/47 and 211/88.

Kinematic feasibility testing indicates that there is no simple kinematic failure mechanism that can explain the collapse, suggesting that failure must be related to a complex mechanism. It is concluded that the Tjellefonna rockslide was not composed of a uniform plane, but of a complex surface consisting of joints, faults, foliation and intact rock bridges. The Tjellefonna failure was closely related to the tectonic deformation of the rocks in this area.

Trigger factors and strain softening parameters have been investigated using the 2D numerical slope stability modelling software Phase². Modelling results suggest that strain softening must have preceded failure. In addition a sub-horizontal structure is critical in order to induce slope instability and an external trigger is required. Sensitivity tests show that a high groundwater level is the most likely trigger, while even high magnitude earthquakes seem to have a minor effect.

1. Background

The Tjellefonna rockslide is located at Tjelle between Molde and Sunndalen, in the municipality of Neset in Møre & Romsdal County (Figure 20). The site collapsed on 22 February 1756 and formed three displacement waves causing run-ups of up to 40-50 meters in the Langfjord (Morsing 1756, Jørstad 1968). Thirty two people were killed and 168 houses and 196 boats were destroyed (Morsing 1756, Jørstad 1968, Furseth, 2006a).

Only five years after the event, Captain Johan Chr. Von Richelieu documented the rockslide in more details in the "Topografisk Journal" (published 1784) with the first drawing of the Tjellefonna rockslide (Figure 21). Von Richelieu noted the composite configuration of the back walls as well as the presence of a fault-like feature at mid-height of the failed area (Redfield et al. 2011). Prior to the failure, the Tjellefonna crown was used as grazing land by local farmers (Svendsen and Werswick 1961). They observed a growing tension crack on the top of the slope (Schøning 1778) and water running from the marsh into the crack (Svendsen and Werswick 1961). Before the rockslide occurred, there had been two weeks of heavy rainfall and a storm was building up on the day of the event (Furseth 2006a).

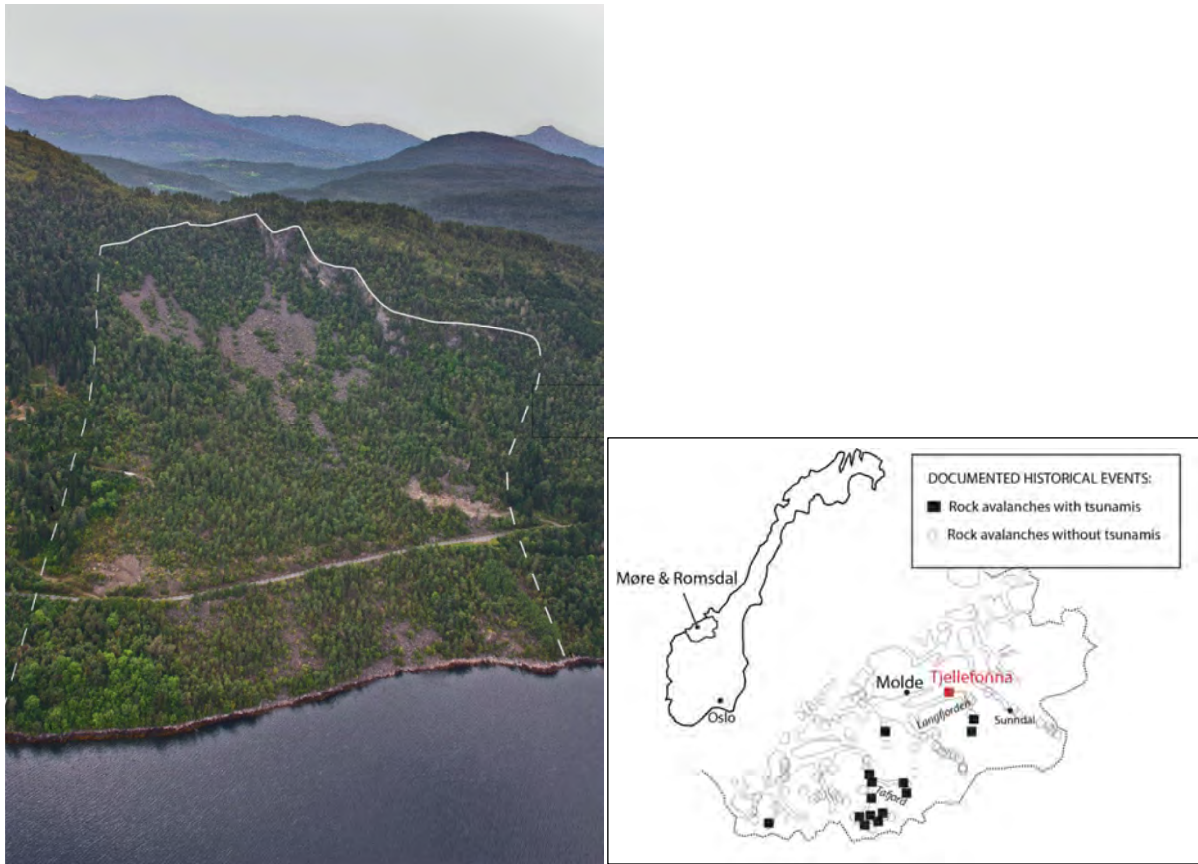


Figure 20: Overview photograph and location of Tjellefonna, Møre & Romsdal. The figure also gives an overview of known historical large rockfalls and rock avalanches with and without displacement waves (tsunamis), based on the national landslide database (modified from Blikra et al. 2006).

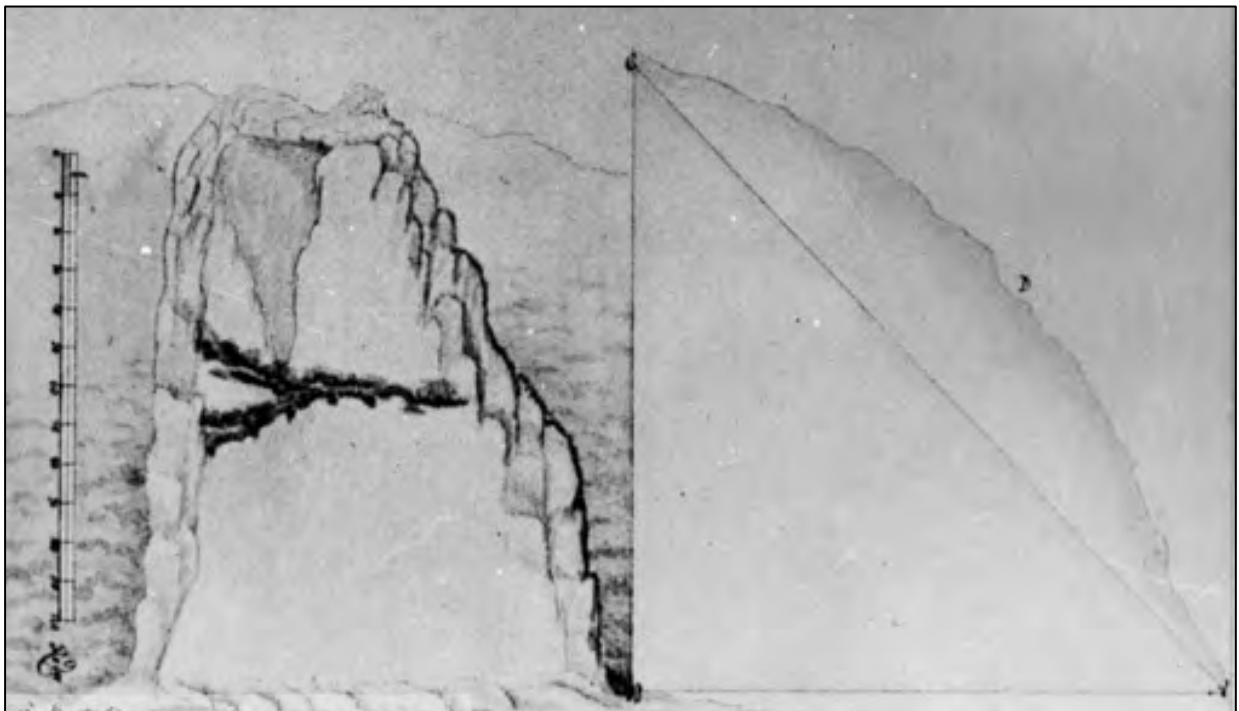


Figure 21: First drawing of the Tjelle rockslide by Captain Johan Chr. von Richelieu in 1761, (Romsdalsmuseets fotoarkiv; Austrigard 1976). Note the thick dark lines crossing at mid-height, which might be a fault-like feature (Redfield et al. 2011).

2. Methods

This work is based on extensive fieldwork, including mapping of morphological features, bedrock and structural mapping. Rock samples were collected for laboratory tests (tilt test, uniaxial compressive strength, Young's modulus, point load test, Brazilian test). In addition, the back walls were scanned with Terrestrial Laser Scanning (TLS) because the area is heavily vegetated and difficult to access.

The Ante-Rockslide Topography (ART) is reconstructed using both the Sloping Local Base Level technique (2D) (Jaboyedoff et al. 2004, 2005) and a manual reconstruction in the PolyWorks (3D).

Numerical modelling of Tjellefonna was conducted using Phase² (Rocscience). The modelling includes various set ups of the different joint sets and fault zones (e.g. Figure 27). By using a shear strength reduction (SSR) method, the Strength Reduction Factor (SRF) can be determined. The analyses include investigation of strain softening parameters (friction angle and cohesion) and trigger factors such as groundwater and earthquake. Input parameters were based on laboratory analysis results, RocLab (Rocscience) and literature.

3. Geological and structural setting

Western Gneiss Region (WGR)

Figure 22 gives an overview of the geology of the area. The study area is situated in the Precambrian bedrock-province referred to as the Western Gneiss Region (WGR). Field mapping reveals that the bedrock at Tjelle consists predominantly of a granitic to granodioritic gneiss. It is locally banded with mafic layers rich in biotite and amphibole, and felsic layers rich in quartz and feldspar.

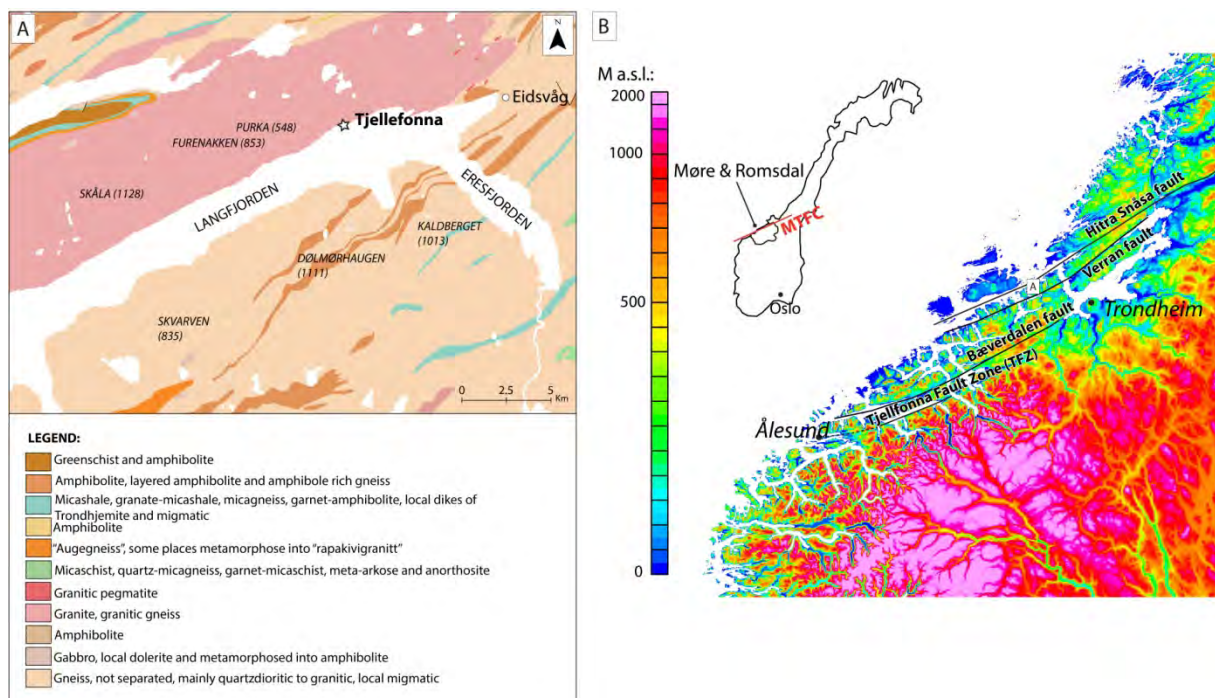


Figure 22: A) Geological bedrock map of the Langfjord area (modified from Lutro et al. 1996). B) Map of proven and suggested fault strands of the NW-ES-trending Møre Trøndelag Fault Complex (MTFC) (modified from Redfield and Osmundsen 2009).

The Tjellfonna Fault Zone (TFZ) and Tjelle fault

The topographic lineament defined by the Langfjord represents the trace of the Tjellefonna Fault Zone (TFZ) (Figure 22). Apatite fission-track (AFT) ages across the TFZ provide evidence for post-Cretaceous normal-offset across the TFZ. Quaternary deposits and the sea (Langfjord) cover the major trace of the Tjellefonna fault. It is regularly covered by quaternary deposits and the sea (Langfjorden), however, several damage zones exposed north of the Langfjord are interpreted to be second order faults to the main TFZ. (Redfield and Osmundsen 2009). One of these damage zones is called the Tjelle fault, and crops out also in the back scarp of the Tjellfonna slide (Bauck 2010).

The structures of the Tjelle fault have been mapped by Bauck (2010). It is described as a steep south-dipping fault, which is sub-parallel to the main hillside gneissic foliation. The youngest lineaments seem to indicate normal dip slip movement. The Tjelle Fault is on strike with a normal fault exposed at Rød (between Tjelle and Eidsvåg), and is likely a structure linked to that fault (Redfield et al. 2011).

Structural geology of Tjellefonna

The study area consists of four persistent joint sets, documented by both field mapping and terrestrial laser scanning (Table 1) (Sandøy 2011). The foliation (dip direction/dip angle: 155/69, 338/70), fault (153/80) and joint sets J1 (158/62) and J3 (352/47) are all sub-parallel to each other, as well as to the Langfjord and the Møre Trøndelag Fault Complex (MFTC) lineament (see Figure 4). The main foliation is sometimes poorly developed, and it is folded into open folds with sub-horizontal axial plane and fold axes. The flanks of the scar are defined by joint set J2 (076/81), locally in combination with joint set J4 (211/88). A combination of the foliation, faults, and joint sets J1 and J3 makes up the back-scarp of the Tjellefonna crown.

Table 1: Summary of the discontinuity sets from terrestrial laser scanning (TLS) and field mapping. Data in dip direction and dip angle with 1 σ variability.

Discontinuity set	TLS		Field data	
J1	164/71	± 17	157/59	± 21
J2	089/59	± 13	076/81	± 17
J3	339/79	± 9	352/47	± 27
J4	050/82	± 26	211/88	± 19
MF1	-	-	158/62	± 19
MF2	-	-	388/70	± 13

Phenomena map

Figure 23 shows an overview of the rockslide phenomena map. Geomorphologic features like tension cracks and doubled ridges are mapped on the crown. The map also shows the mapped faults and the average block-volume distribution. Note also the Tjelle fault in the back walls, striking parallel to the Langfjord and back walls.

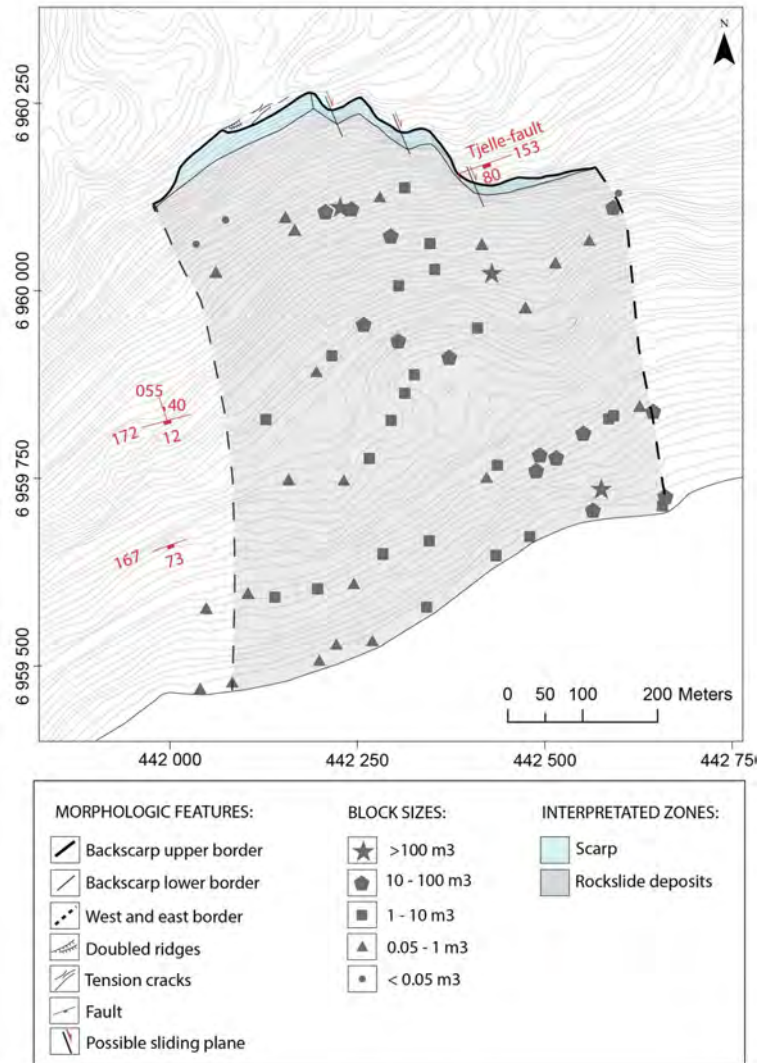


Figure 23: Rockslide phenomenological map of the Tjellefonna rockslide (Sandøy 2012).

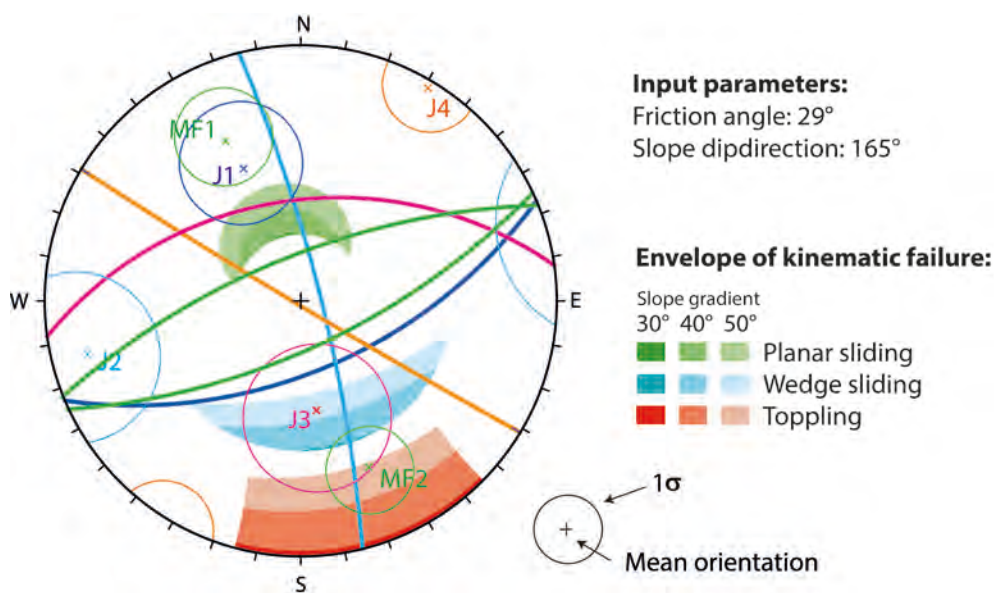


Figure 24: Results of the kinematic feasibility test based on measured discontinuity sets and for different slope gradients (Sandøy 2012).

4. Kinematic feasibility test

The kinematic feasibility tests reveal that there is no clear failure mechanism (Figure 24). This is even the case when using a low friction angle of 29° (e.g. smooth surface, gouge-filled fault). The analysis includes variation of slope angles. The topography of the area surrounding Tjellefonna has a mean slope gradient of 30° , with local bands striking parallel to the Langfjord having gradients between $40\text{--}50^\circ$.

5. Ante-rockslide topography reconstruction and volume estimations

The reconstructed topography is illustrated in Figure 25, and results of the volume calculation are given in Table 2. The final volume of deposits onshore and in the fjord is chosen based on an expected volume increase of 25% based on other rock avalanche events (Hungr and Evans 2004).

ART reconstruction gives an initial rockslide volume between 9.3 and 10.4 million m^3 , which is lower than previous estimates of 12 to 15 million m^3 (Jørstad 1965; Furseth 2006b). The onshore deposits are estimated to 7.6 million m^3 , and only 3.9 million m^3 of the rock avalanche was deposited in the fjord.

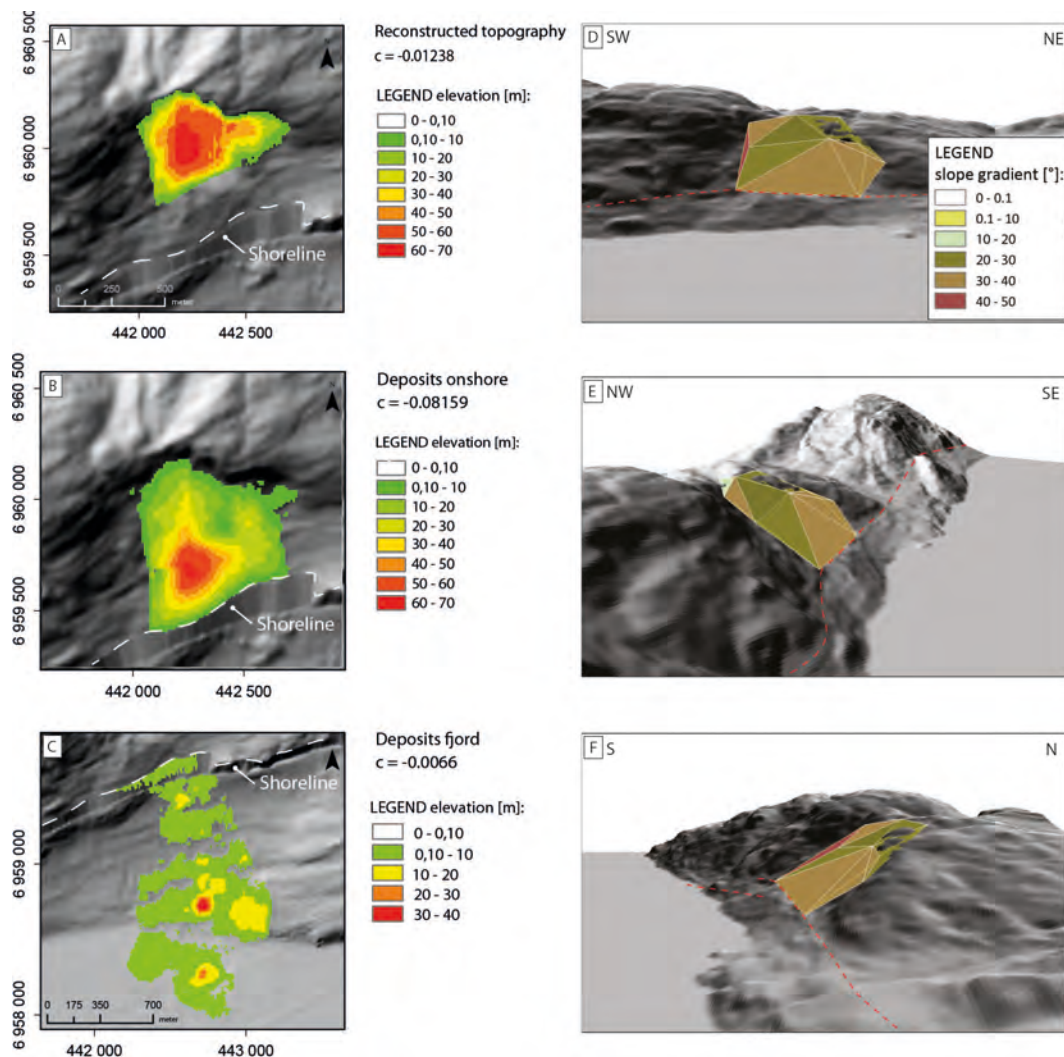


Figure 25: A), B) and C) Reconstruction of the volume of the Tjellefonna rockslide using the Sloping Local Base Level (SLBL) technique. D), E) and F) Volume reconstruction using manual reconstruction in PolyWorks. The red dashed line marks a marked change in slope angle (Sandøy 2012).

Table 2: Results of volume estimations from the SLBL and PolyWorks methods (Sandøy 2012).

Method:		Volume [m3]	Volume total [m3]
SLBL	ART-1	6 066 000	9 248 800
	Deposits ART-1	3 182 800	
	Onshore deposits	7 562 000	11 485 800
	Deposits fjord	3 923 800	*24% increase
PolyWorks	ART-2	7 232 150	10 414 950
	Deposits ART-2	3 182 800	

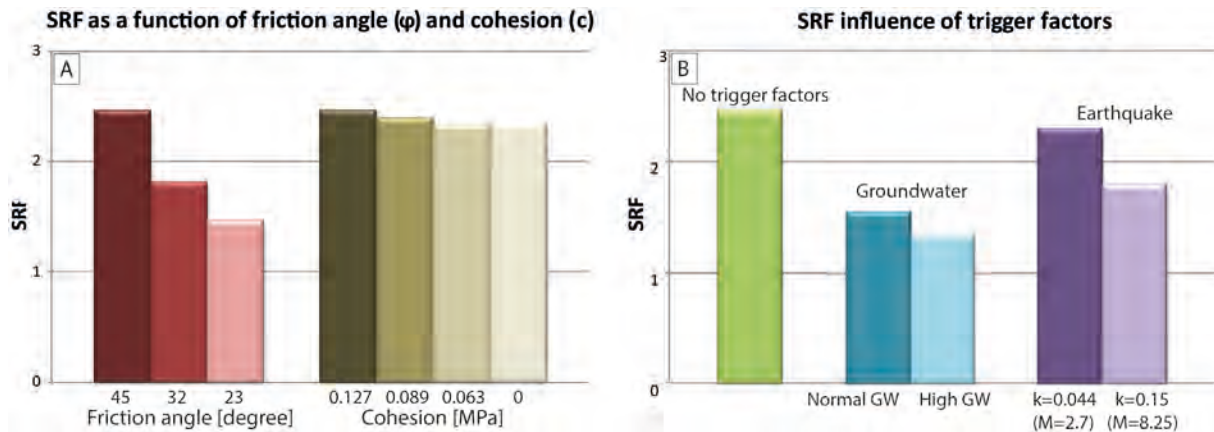


Figure 26: Strength Reduction Factor (SRF) influence of A) friction angle and cohesion and B) trigger factors (Sandøy 2012).

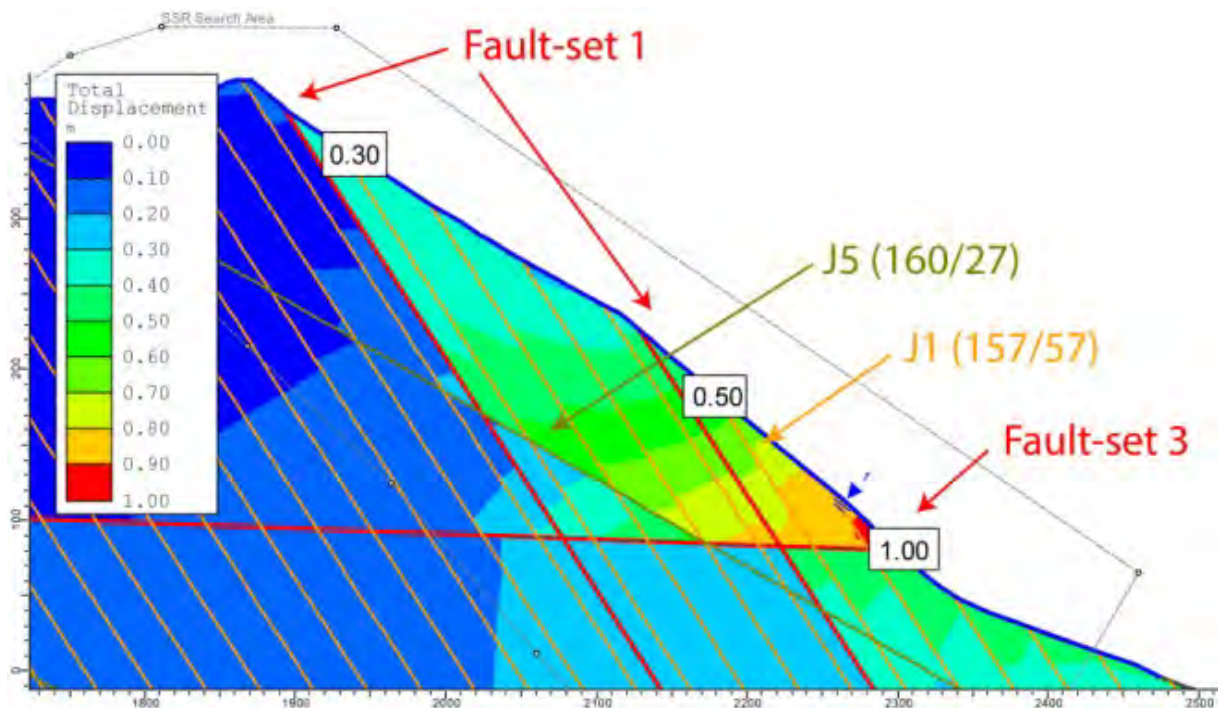


Figure 27: Result of Shear Strength Reduction (SSR) by using a strain softening model of 10%. Critical SRF is 0.86 in this case (Sandøy 2012).

6. Numerical slope stability modelling

The parameter study shows that the friction angle has significantly more influence on the critical SRF value than the cohesion (Figure 26). Additionally, the influence of groundwater is considerably higher than the effect of earthquake load (Sandøy 2012). This suggests that an elevated groundwater level could have been the sole triggering mechanism. An earthquake as triggering factor, suggested as a mechanism by Redfield and Osmundsen (2009), has only a minor effect on the SRF (Figure 26).

The most important implication of the modelling is that a sub-horizontal structure and some strain softening are required in order that failure can occur (Figure 27). The rockslide model used in the strain softening set-up includes the mapped structures (a persistent J1, faults and a non-persistent J5) and groundwater. Notice that the highest displacement is along the sub-horizontal fault (fault-set 3).

7. Conclusions

The lack of a clear kinematic failure mechanism and the high mechanical strength of the rock mass at Tjellefonna both suggest both failure must be related to a complex mechanism. This result is supported by field observations, which reveal that the intact rock strength is compromised by the collective contribution of a variably developed foliation, fault zones and four persistent joint sets.

According to the modelling results, a sub-horizontal structure is also required for failure to occur. This is most likely represented by the sub-horizontal fault (Fault-set 3) observed close to the slide area (Figure 28, Figure 29).

Furthermore, numerical modeling shows that failure must have required strain softening in combination with elevated groundwater level. Groundwater has a much larger influence on the shear reduction factor (SRF) than the seismic load from an earthquake. Modelling shows that an earthquake with magnitude of 2.7 (mean seismic magnitude in the area) and magnitude 8 (tested as a worst cause scenario) could not be a trigger on its own. An earthquake magnitude of 6 is normally required to trigger a rockslide and there are no accounts of such an event in Møre & Romsdal at this time. The people living close and around Langfjorden would notice an earthquake of 6 to 8 magnitude, but no written sources have described such experience.

Field mapping and numerical modelling indicate that the basal failure surface must be composed of a complex sliding surface consisting of joints, faults, foliation and intact rock bridges (Figure 29). It is obvious that the Tjellefonna failure was closely depended on the presence of weak fault zones.

The Tjellefonna failure is most likely a consequence of progressive accumulation of weakening, leading to fracturing of the intact rock bridges and generating hillside creep. This might have been attained through long-term infiltration of water, freezing-thawing cycles and low-magnitude earthquakes. This progressive creep would explain the observation of growing tension cracks located at the present crown prior to the failure. The intense rainfall in the weeks prior to the failure was the crucial factor to trigger the slope to fail.

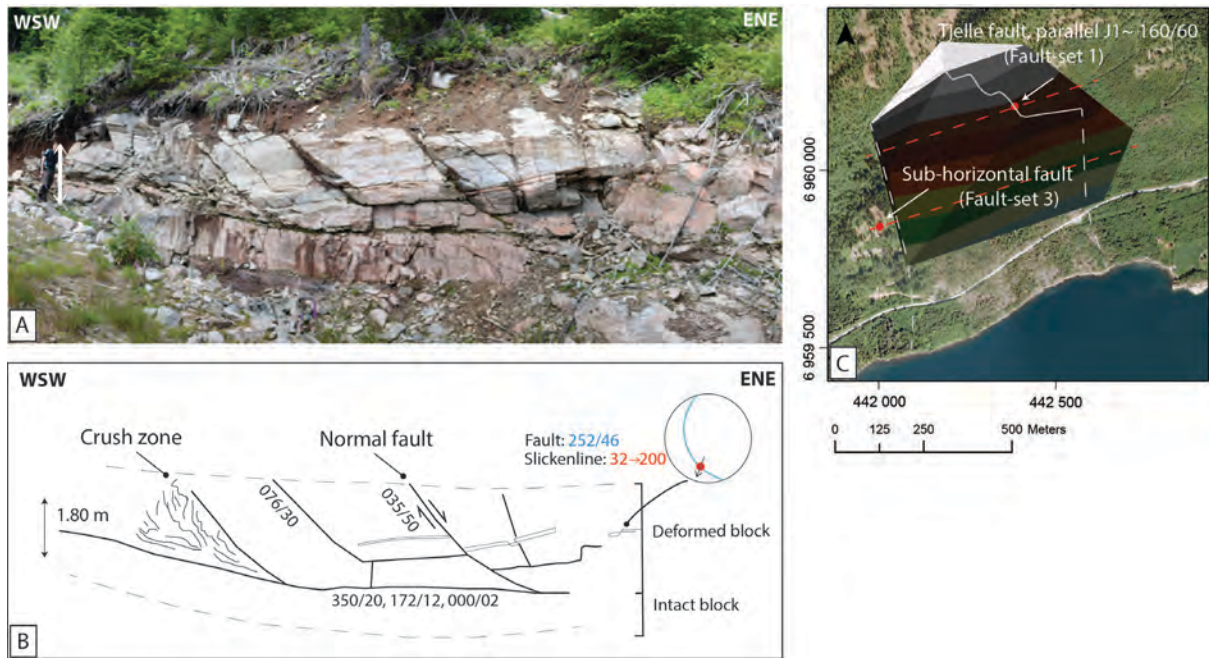


Figure 28: An illustration of the sub-horizontal fault, where A) is an overview picture, B) sketch of the block structures, and C) the location of this sub-horizontal fault (Fault-set 3), SW of rockslide limit (Sandøy 2012).

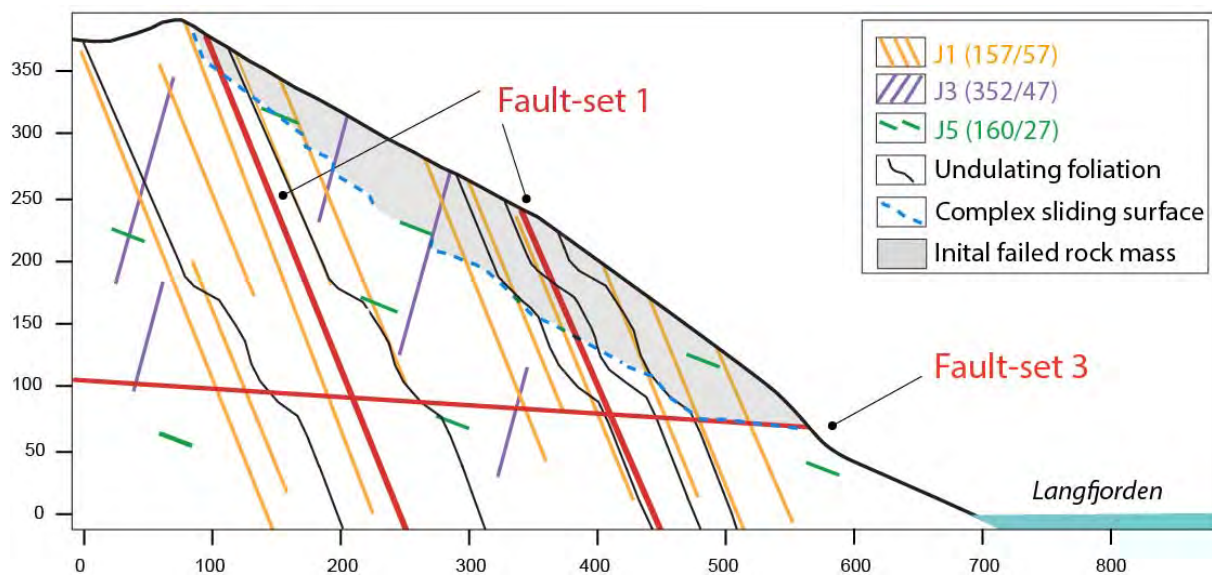


Figure 29: A conceptual model of the basal surface based on field work and numerical modelling results (Sandøy 2012).

Cited references for stop 5: Back-analysis of the 1756 Tjellefonna rockslide

- Austrigard, B. (1976) Nytt om Tjellefonna. In: Høla, O. (Ed.) *Romsdalsmuseets årbok 1976*, pp. 45-51.
- Bauck, S.M. (2010) Fault rock assemblages and fault architecture in the Møre - Trøndelag Fault Complex. MSc thesis, NTNU, Trondheim, 97 p.
- Blikra, L.H., Longva, O., Braathen, A., Anda, E., Dehls, J.F. and Stalsberg, K. (2006) Rock slope failures in Norwegian fjord areas: examples, spatial distribution and temporal pattern. In: Evans, S.G., Mugnozza, G.S., Strom, A., Hermanns, R.L. (Eds.) *Landslides from Massive Rock Slope Failure*. Springer, pp. 475-496.
- Furseth, A. (2006a) Tjellefonna - norgeshistoriens største fjellskred. In: Furseth, A., *Skredulykker i Norge*. Tun Forlag, pp. 151-155.
- Furseth, A. (2006b). Tjellefonna – 250 år etter, In: *Årbok for Romsdal Sogelag*, Molde, pp. 7-30.

- Hungr, O. and Evans, S.G. (2004) Entrainment of debris in rock avalanches: An analysis of a long run-out mechanism. *Geological Society of America Bulletin*, **116**, 1240-1252.
- Jaboyedoff, M., Baillifard, F., Couture, R., Locat, J. and Locat, P. (2004) Toward preliminary hazard assessment using DEM topographic analysis and simple mechanical modeling by means of sloping local base level. In: Lacerda, W.A., Ehrlich, M., Fontoura, A.B. and Sayão, A. (eds.) *Landslides: Evaluation and Stabilization*, Taylor & Francis Group, London, pp. 199-205.
- Jaboyedoff, M. and Derron, M.-H. (2005) A new method to estimate the infilling of alluvial sediment of glacial valleys using a sloping local base level. *Geografica Fisica e Dinamica Quaternaria*, **28**, 37-46.
- Jørstad, F. (1968) Waves generated by landslides in Norwegian fjords and lakes. Technical report, Norwegian Geotechnical Institute, Oslo, pp. 13-32.
- Morsing, C. (1756) *En kortleg beskrivelse over Jordskiælv, og Fieldets Nedfald Som skede udj Nettet Præstegjæld i Romsdahls Provstie, og Trondhiems Stift udj Norge, nest afvigte Aar, Natten til dend 23 February 1756*. Norsk Historisk Kjedskrift Institutt, København.
- Redfield, T.F. and Osmundsen, P.T. (2009) The Tjellefonna fault system of Western Norway: Linking late-Caledonian extension, post-Caledonian normal faulting, and Tertiary rock column uplift with the landslide-generated tsunami event of 1756. *Tectonophysics*, **474**, 1-2, 106.
- Redfield, T.F., Osmundsen, P.T., Gradmann, S., Bauck, S.M., Ebbing, J. and Nasuti, A. (2011) TopoScandiaDeep Field Trip, Tectonic Topography of Norway's MTFC. NGU report 2011.033, Geological Survey of Norway, Trondheim, 47 p.
- Sandøy, G. (2011) Tjellefonna – Mapping of factors affecting rock slope stability. Project thesis, Norwegian University of Science and Technology, Trondheim, Norway.
- Sandøy, G. (2012) Back-analysis of the 1756 Tjellefonna rockslide, Langfjorden. MSc thesis, Norwegian University of Science and Technology, Trondheim, Norway.
- Schøning, G. (1778). Reise igiennem en Deel af Norge i de Aar 1773 - 75.
- Svendsen, G. and Werswick, K. (1961) Tjeldefjellet går ut. In: *Fjellene dreper*. Tiden Norsk Forlag, Oslo, pp. 83-85.
- Tveten, E., Lutro, O. and Thorsnes, T. (1998) Bedrock map Ålesund. 1:250,000, Geological Survey of Norway, Trondheim, Norway.

STOP 6: MIDDAGSTINDEN

This stop at the deep-seated gravitational slope deformation of Middagstinden in the Innfjorddal Valley (Figure 30) opens for discussion about the role of a post-Caledonian fault in the development of a large unstable rock slope. Here, we present results from NGU's investigations and periodic displacement measurements along with findings from an ongoing PhD thesis by M. Schleier and an MSc thesis by I. Krieger (Krieger et al. 2013), both from the University of Erlangen, Germany (see Appendix 5). The following summary is modified from Oppikofer et al. (2013).

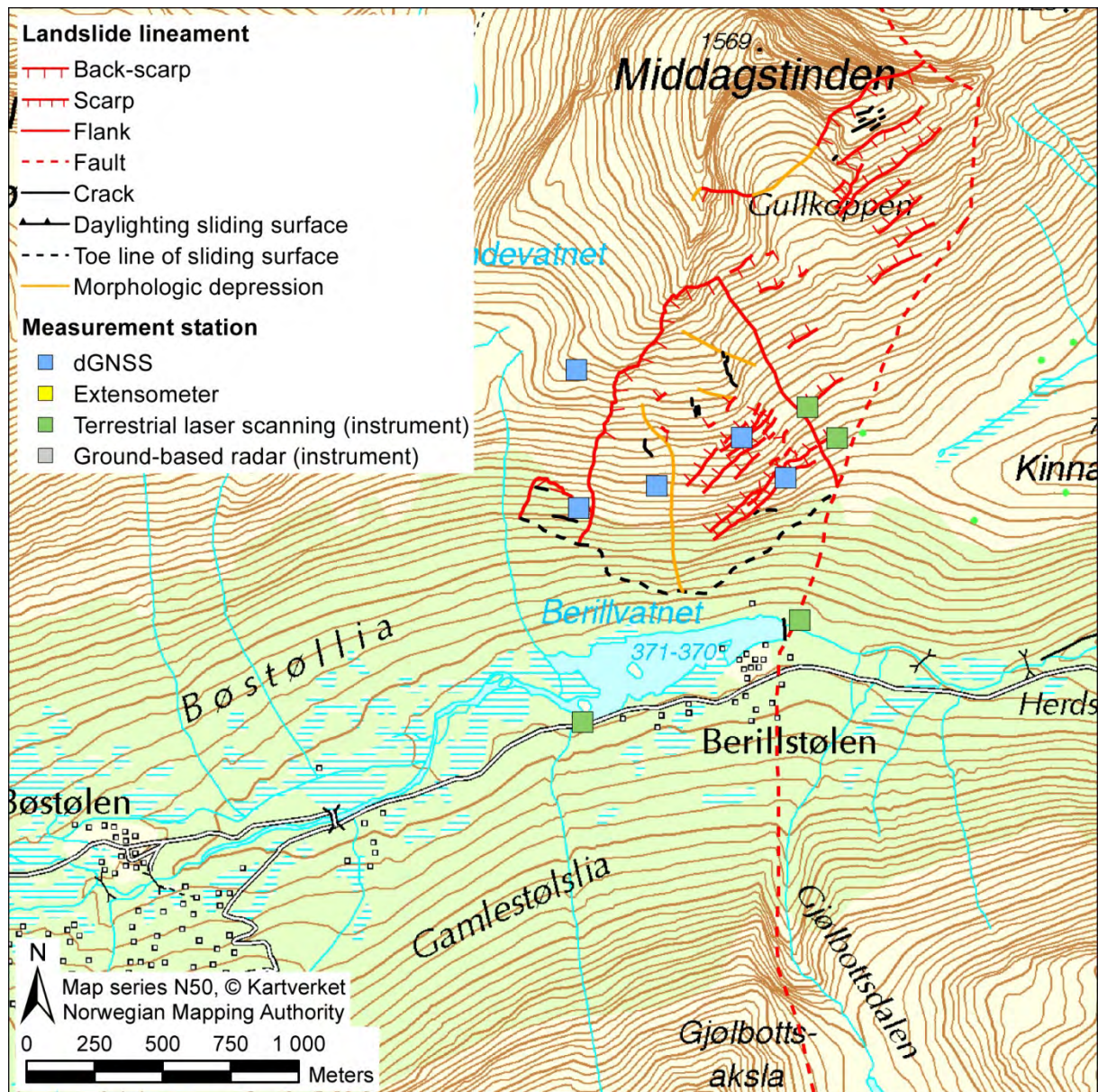


Figure 30: Situation map of stop 6: the Middagstinden deep-seated gravitational slope deformation.

Middagstinden is located on a south-facing slope 700 m above Berillvatnet Lake in the Innfjorddal Valley. A complex unstable rock slope was identified in the early 2000s in relation with the Berill fault (Anda et al. 2002, Blikra et al. 2002), which is SSW-NNE-trending and delimits the unstable rock slope to the SE (Figure 31). The back-scarp is formed by moderately S-dipping gneiss foliation surfaces and shows several tens of meters of displacement. These past movements have led to strong deformation of the instability with

open cracks, depressions, counter-scarps and ridges (Figure 31). Past rock slope failures have likely occurred from the western part of the unstable rock slope, which is heavily disintegrated and covered by debris. Directly west of the large unstable rock slope is a smaller instability with a relatively newly opened back-crack (Anda et al. 2002, Blikra et al. 2002). A strong post-glacial earthquake along the Berill fault is discussed as possible trigger of the Middagstinden rockslide (Anda et al. 2002, Blikra et al. 2002), but geophysical investigations and trenches dug out by NGU in the valley sediments did not reveal post-glacial seismic activity along the Berill fault (Krieger et al. 2013).

The unstable rock slope has been periodically measured using dGNSS since 2008 and TLS since 2010. Four dGNSS measurement points were set out in 2008 and 2009 on the Middagstinden unstable rock slope (Figure 31). Repetitive measurements were made in 2009, 2010 and 2011 and all four points show significant horizontal and vertical displacements: the points BER-1, BER-2 and BER-3 are located on the main part of the unstable rock slope and

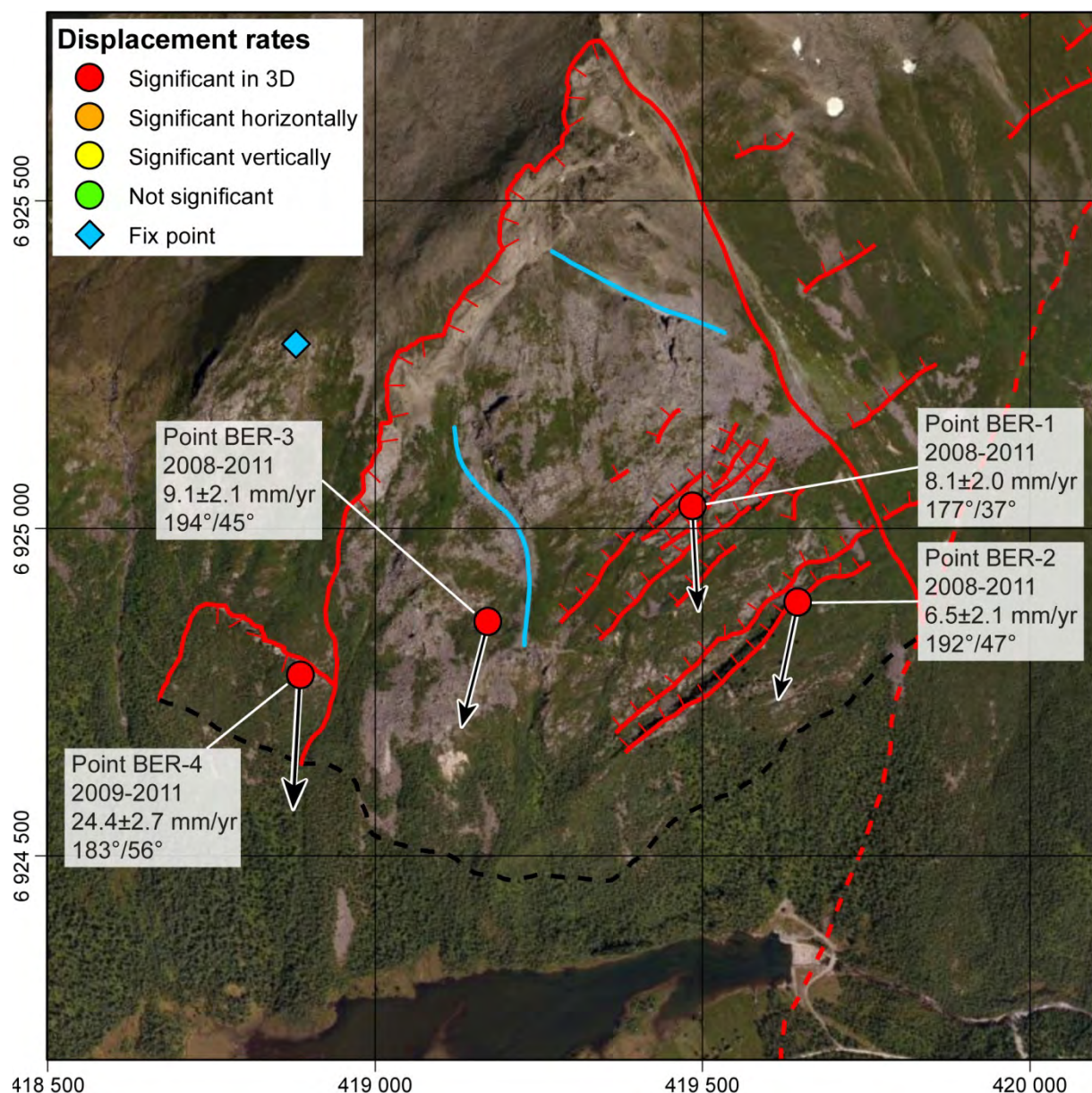


Figure 31: Map of the Middagstinden unstable rock slope with the location of dGNSS points for periodic displacement measurements and average displacement vectors for the 2008–2011 measurement period (Oppikofer et al. 2013).

move with 6.5 to 9.1 mm/year towards the S to SSW with a plunge angle ranging from 37° to 47° (Figure 31). Point BER-4 is located on the located instability west of the main unstable rock slope and moves with 24.4 mm/year towards the S with a plunge angle of 56°.

TLS acquisitions were made in 2010 and 2012 from the valley bottom along Berillvatnet Lake and from the eastern lateral release surface. Structural analyses based on the 2010 TLS dataset show a steeply SSE-dipping foliation that forms a basal sliding surface cropping out in the upper part of the slope due to downward motion of the rock mass. Other discontinuity sets are all very steep to subvertical and delimit the unstable rock slope into different compartments. One of these discontinuity set forms overhanging cliffs and the uphill facing counter-scarps.

Field measurements of the fault orientation show that the fault forms an intersection line with the metamorphic foliation. This intersection line is parallel to the displacement vectors recorded by the periodic dGNSS measurements (Krieger et al. 2013). The volume of the Middagstinden unstable rock slope is estimated to 26 to 35 million m³, but is somewhat speculative due to the uncertain location of the toe zone of the unstable rock slope.

A catastrophic of the Middagstinden rockslide would cross and possibly dam the narrow Innfjorddalen Valley, create a displacement wave in the shallow Berillvatnet Lake and affect several buildings (Dahle et al. 2011).

Cited references for stop 6: Middagstinden

- Anda, E., Blikra, L.H. and Braathen, A. (2002) The Berill Fault-first evidence of neotectonic faulting in southern Norway. *Norsk Geologisk Tidsskrift*, **82**, 3, 175-182.
- Blikra, L.H., Braathen, A., Anda, E., Stalsberg, K. and Longva, O. (2002) Rock avalanches, gravitational bedrock fractures and neotectonic faults onshore northern West Norway: Examples, regional distribution and triggering mechanisms. NGU report 2002.016, Geological Survey of Norway, Trondheim, Norway.
- Dahle, H., Anda, E., Sætre, S., Saintot, A., Hermanns, R.L. and Oppikofer, T. (2011) Risiko- og sårbarhetsanalyse for fjellskred i Møre og Romsdal - FylkesROS-fjellskred. Fylkesmannen i Møre og Romsdal, Møre og Romsdal Fylkeskommune, Geological Survey of Norway, Molde, Norway.
- Krieger, I., Hermanns, R.L., Schleier, M., Yugsi Molina, F.X., Oppikofer, T., Rønning, J.S., Eiken, T. and Rohn, J. (2013) The Berill fault and its relation to a deep-seated gravitational slope deformation (DSGSD). In: Genevois, R. and Prestininzi, A. (eds.) *International Conference Vaiont, 1963-2013 - thoughts and analyses after 50 years since the catastrophic landslide*, Italian Journal of Engineering Geology and Environment - Book Series 6, Sapienza University, Rome, Italy, pp. 265-273.
- Oppikofer, T., Saintot, A., Otterå, S., Hermanns, R.L., Anda, E., Dahle, H. and Eiken, T. (2013) Investigations on unstable rock slopes in Møre og Romsdal – status and plans after field surveys in 2012. NGU report 2013.014, Geological Survey of Norway, Trondheim, Norway.

STOP 7: INNFJORDDAL VALLEY

At this stop in the Innfjorddal Valley we will observe the deposits of multiple rock avalanches that originated from the Gråfonnfjellet on the southeastern valley flank (Figure 32). The oldest of these rock avalanches is dated to approximately 3000 years ago and partly deposited in the Innfjord that was at that time ca. 20 m higher. The deposits are now exposed due to the isostatic rebound. An inventory of rock avalanches in Innfjorddalen Valley was made by S. Seljesæter (Norwegian University of Science and Technology (NTNU), Trondheim, Norway) and M. Schleier (University of Erlangen, Germany). Preliminary results are summarized in Schleier et al. (2013) (see Appendix 4) and the following summary is modified from Oppikofer et al. (2013).

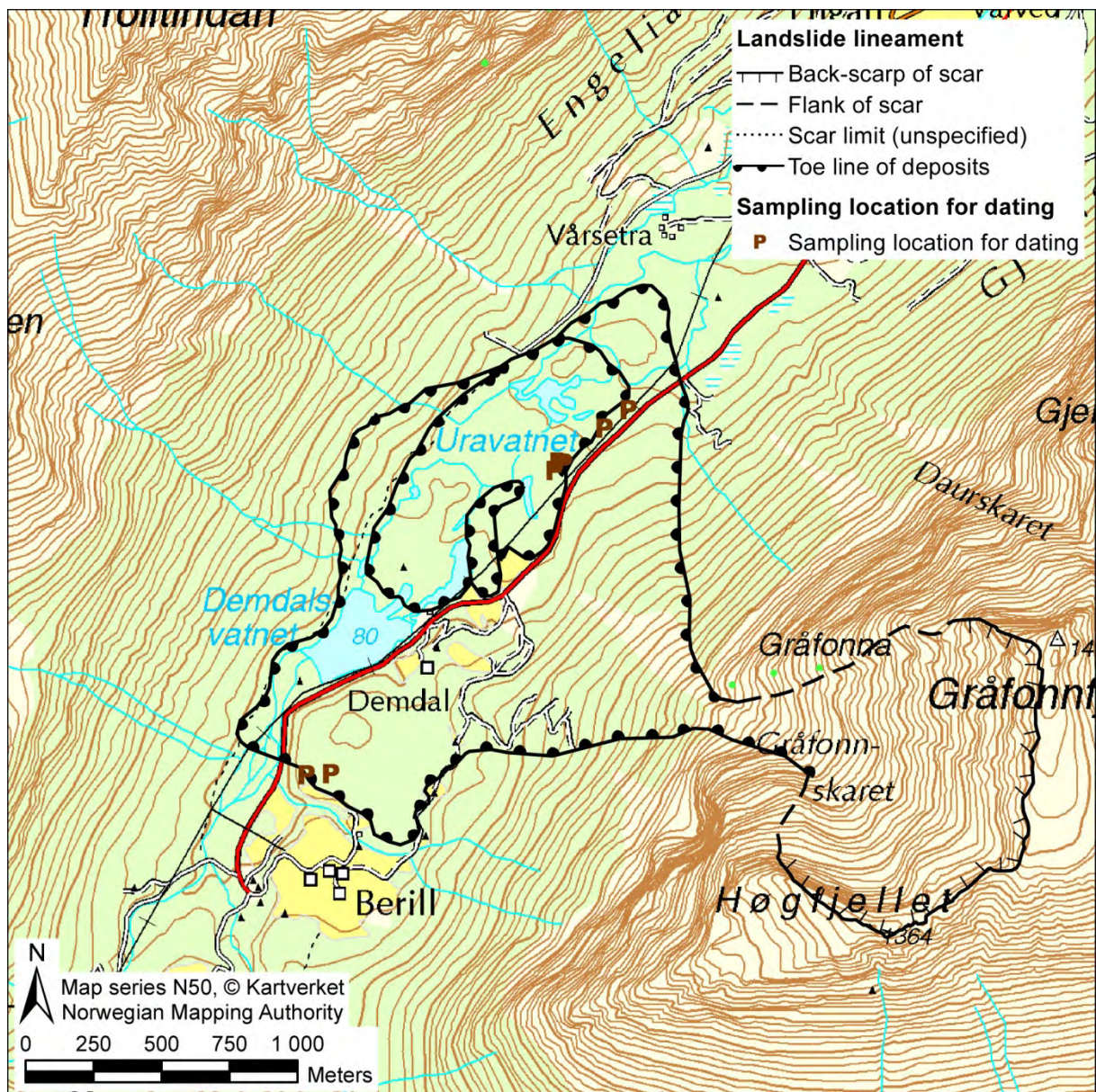


Figure 32: Situation map of stop 7: rock avalanche deposits in the Innfjorddal Valley.

In the lower Innfjordalen Valley a succession of three rock avalanche deposits is mapped. The deposits have lobate forms and overlay each other. Boulders up to several meters in diameter occur (Figure 33). Several distinguishable morphological features can be mapped: a terrace of a marine delta at an altitude of 120 m a.s.l. (A), which is overlain by a first rock avalanche

deposit (B). It has a volume of approximately 21 million m³ and the rock avalanche ran-up the opposite valley side by 110 m. These deposits can be divided into a continuous deposit located between 130 and 35 m a.s.l. (B) and a distal part at 15 m a.s.l. showing only isolated hills of boulder deposits (E). In between there is an area of deformed valley fill deposits with isolated boulders (C) and undisturbed valley fill deposits without boulders (D) (Figure 33). The distal part of the oldest rock avalanche in Innfjorddalen Valley (E) is interpreted to have deposited into the fjord approximately 3000 years ago when the shoreline was still approximately 20 m higher than today. The main part of that rock avalanche (B), however, is deposited onshore. The limit between disturbed and undisturbed valley fill sediments (C and D) is supposed to mark the shoreline at that time and the disturbed sediments were liquefied and deformed by the rock avalanche.

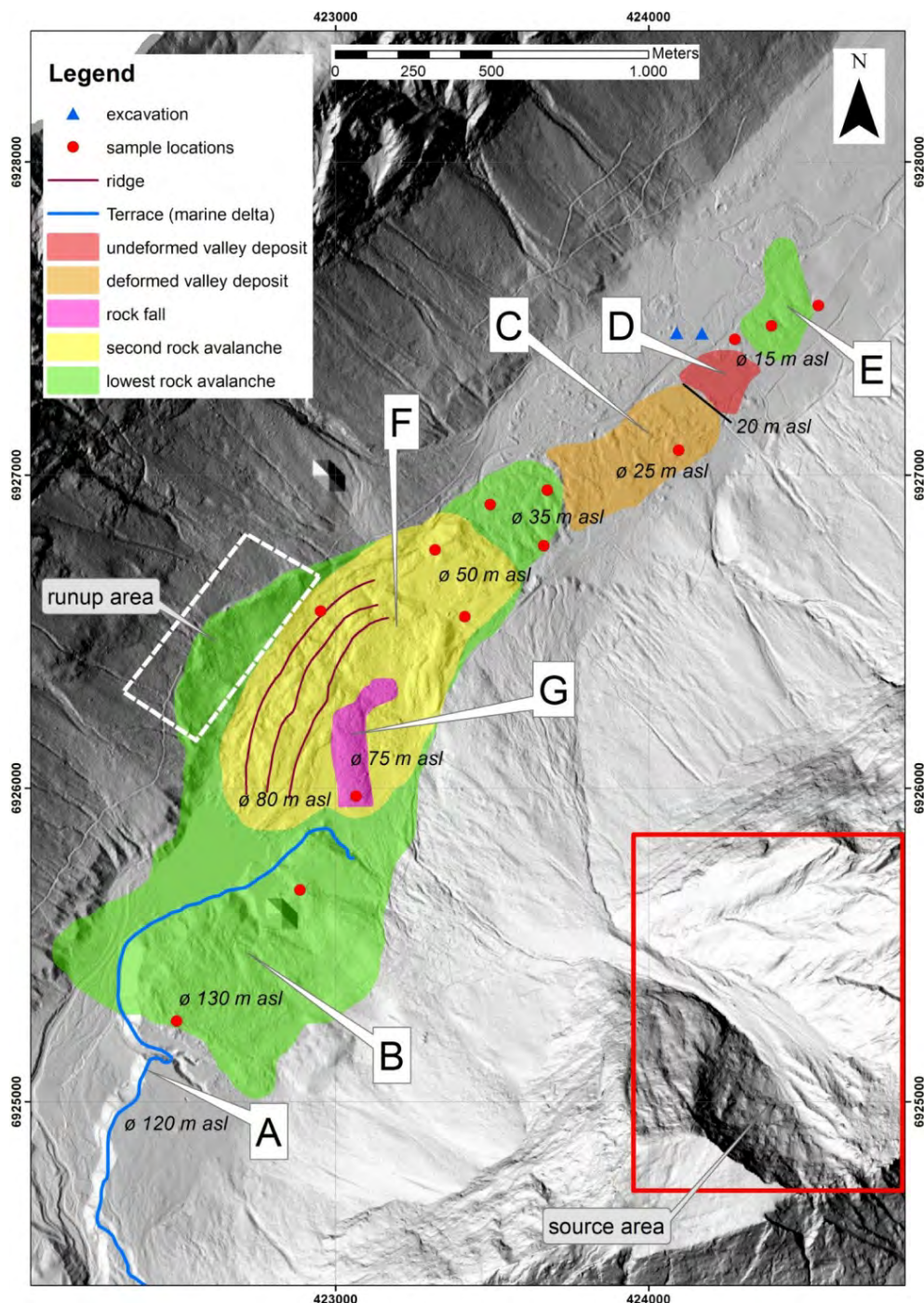


Figure 33: Rock avalanche inventory map in Innfjorddalen Valley (Schleier et al. 2013).

The proximal part of first rock avalanche deposit is overlain by a second rock avalanche deposit with an estimated volume of 5.4 million m³ (F), which dammed the river and formed a lake. These deposits are overlain by a third rockfall deposit (G), which has a relatively small volume (190 000 m³) and occurred in 1611 or 1612 (Furseth 2006).

Cited references for stop 7: Innfjorddal Valley

- Furseth, A. (2006) *Skredulykker i Norge*, Tun Forlag, Oslo, Norway, 207 p. (in Norwegian).
- Oppikofer, T., Saintot, A., Otterå, S., Hermanns, R.L., Anda, E., Dahle, H. and Eiken, T. (2013) Investigations on unstable rock slopes in Møre og Romsdal – status and plans after field surveys in 2012. NGU report 2013.014, Geological Survey of Norway, Trondheim, Norway.
- Schleier, M., Hermanns, R.L. and Rohn, J. (2013) Spatial distribution of rockslide deposits and their morphological features suggest timing and paleo-environmental conditions for rock slope failures in Innerdalen and Innfjorddalen, Møre og Romsdal County, Western Norway. In: Genevois, R. and Prestininzi, A. (eds.) *International Conference Vaiont, 1963-2013 - thoughts and analyses after 50 years since the catastrophic landslide*, Italian Journal of Engineering Geology and Environment - Book Series 6, Sapienza University, Rome, Italy, pp. 493-505.

STOP 8: TROLLVEGGEN CLIFF

This short touristic stop is at the foot of the impressive Trollveggen cliff (or Troll wall) in the Romsdal Valley. With its 1100 m height, it is the tallest vertical or even overhanging rock face in Europe.

The Trollveggen cliff is part of the Trolltindene peaks (maximum altitude at 1770 m a.s.l.) with many spires and pinnacles at their summit (Figure 34). Large parts of the northeast-facing cliff are overhanging and the summit overhangs the foot of the cliff by up to 50 m. This stunning rock wall is a very popular place for base jumpers, which is, however, illegal in the Trollveggen cliff (Wikipedia 2014).



Figure 34: Photographs of the Trollveggen cliff (Photographs by M. Böhme, NGU).

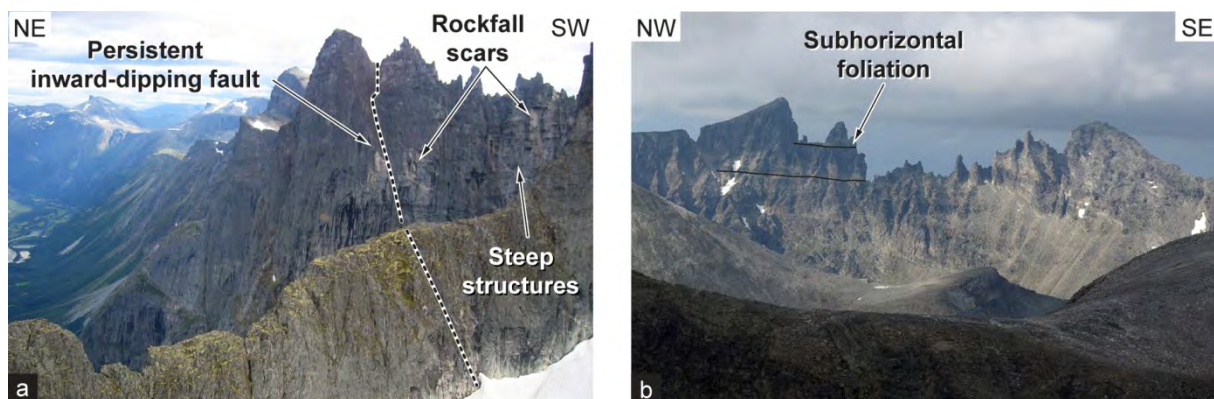


Figure 35: Photographs of the Trolltindene rock slope: a) lateral view showing the inward-dipping fault and other steep structures on the Trollveggen cliff; b) view from the back-side of Trolltindene showing the subhorizontal foliation (Photographs by A. Saintot, NGU).

Several rock slope failures occurred in the past, mainly in the form of rockfalls, but also as larger failures. In 1998, a volume of approximately 75,000 m³ collapsed and formed a small rock slope failure (Furseth 2006) that did not have an excessive run-out distance. The foliation is subhorizontal, while other discontinuity sets are very steeply dipping to subvertical (Figure 35). A persistent fault is inward-dipping and crosses the Trolltindene mountain (Figure 35a). This structural setting delimits relatively small volumes that may fail as rockfalls or small rock slope failures. On the other hand, there is a moderately valley-dipping structure at the foot of the Trollveggen cliff, which is formed by a lithological contact between two gneiss units. At present there are no morphologic evidences to define an unstable rock slope large enough to form a rock avalanche (Oppikofer et al. 2013).

Cited references for stop 8: Trollveggen cliff

- Furseth, A. (2006) *Skredulykker i Norge*, Tun Forlag, Oslo, Norway, 207 p. (in Norwegian).
- Oppikofer, T., Saintot, A., Otterå, S., Hermanns, R.L., Anda, E., Dahle, H. and Eiken, T. (2013) Investigations on unstable rock slopes in Møre og Romsdal – status and plans after field surveys in 2012. NGU report 2013.014, Geological Survey of Norway, Trondheim, Norway.
- Wikipedia (2014) Troll Wall. Available: http://en.wikipedia.org/wiki/Troll_Wall, accessed 02.09.2014.

STOP 9: MANNEN

Mannen is an unstable rock slope in the Romsdal Valley that is under continuous monitoring and early-warning by the Åknes/Tafjord Early-Warning Centre. We will observe the slope from Rønningen down in the valley and discuss latest monitoring results from dGNSS, ground-based radar and borehole instrumentation, as well as the newest geological model of the Mannen rockslide. The following summary is modified from Blikra and Kristensen (2012) (see Appendix 6), Kristensen and Blikra (2013) (see Appendix 7) and Oppikofer et al. (2013).

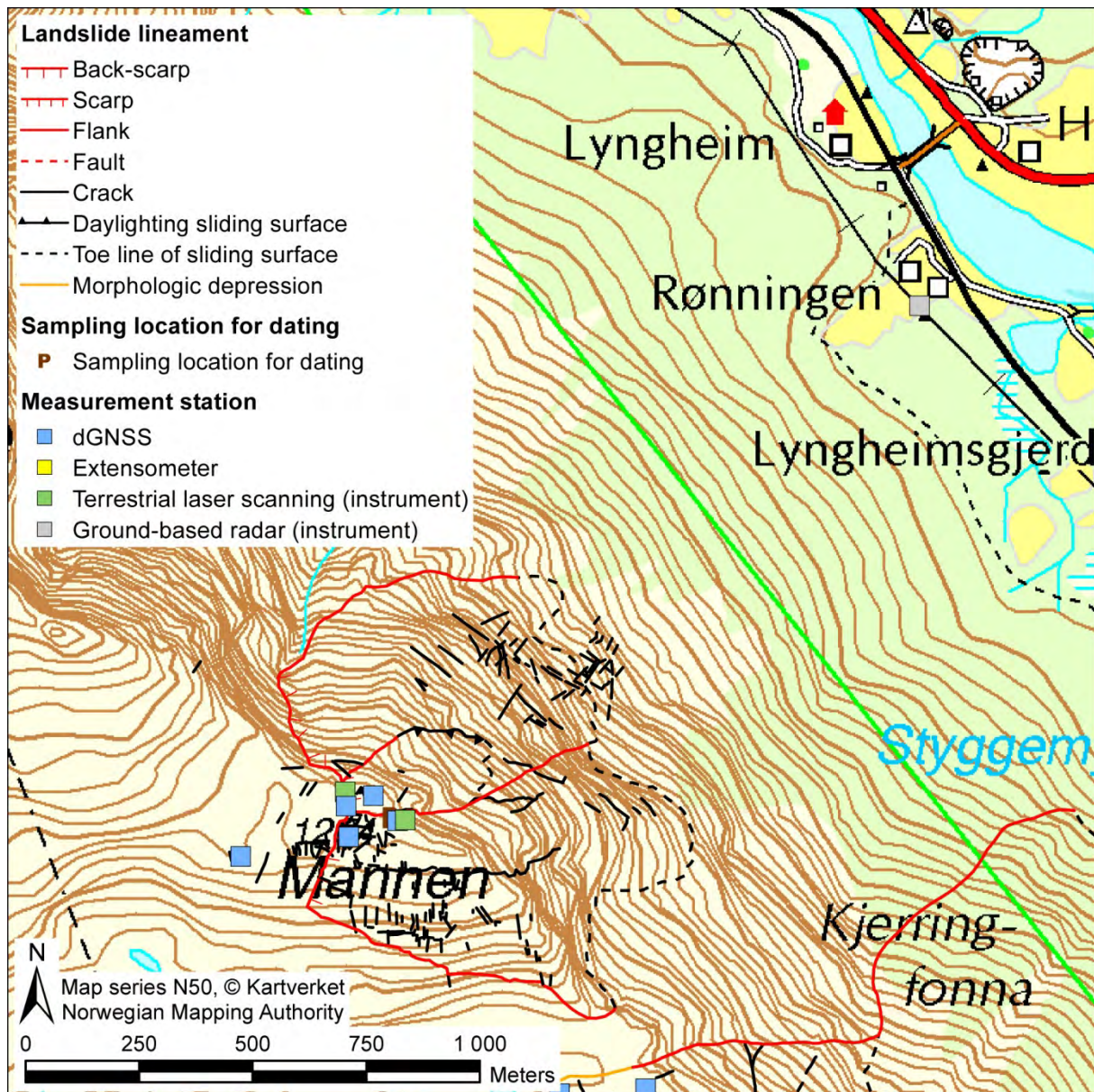


Figure 36: Situation map of stop 9: the permanently monitored unstable rock slope Mannen. The ground-based radar instrument is located in a small house in Rønningen in the valley floor.

Mannen is located on a northeast-facing slope 1215 m above Rønningen in the Romsdal Valley. This large, complex unstable rock slope is one of six continuously monitored unstable rock slopes in Norway. It has the potential of creating a rock avalanche of 2-20 million m³ with catastrophic consequences for houses and infrastructure in the valley, in particular as a landslide dam may be formed, including upstream and downstream flooding (Hermanns et al.

2013; see Appendix 8). An early-warning system has been established, which is based on continuous displacement measurements and a well-defined alarm chain. The monitoring sensors are a dGNSS network, lasers, extensometers, a ground-based radar system and borehole instruments; all data are checked daily (modified from Blikra and Kristensen 2012).

The site has been extensively studied since the 2000s with:

- field mapping and geomorphic interpretations (Henderson and Saintot 2007, Dahle et al. 2008, 2011a, 2011c, Saintot et al. 2011, 2012, Blikra and Kristensen 2012, Kristensen and Blikra 2013);
- geophysical investigations of the unstable rock slope (Dalsegg and Rønning 2012) and deposits in the valley (Tønnesen 2009);
- borehole investigations (Saintot et al. 2011a, Oppikofer et al. 2012, Elvebakk 2012);
- numerical slope stability modelling (Farsund 2011);
- run-out modelling (Dahle et al. 2011b);
- modelling of rockslide damming and outburst floods (Hermanns et al. 2013)
- continuous monitoring instrumentation (Blikra and Kristensen 2012, Kristensen and Blikra 2013).

The bedrock consists of Proterozoic sillimanite-bearing gneisses with inherited structural weaknesses from the tectonic deformation. Specifically, the metamorphic foliation surfaces are prone to be reactivated where favorable orientation occurs in regards to the gravitational forces (Saintot et al. 2011).

At the top, where the main back-scarp is developed, foliation is near-vertical. In the upper part of the unstable area, a borehole showed foliation dipping about 30° to the north and downslope, but further down the pattern is more complex as the gneisses are intensely folded. Inside the instability, the bedrock is extremely fractured and weathering products of soil cover much of the surface. The morphology is characterized by the well-defined back-scarp and numerous smaller slide scars (Figure 37). The scars bear witness to multiple recent rockfalls or smaller rock avalanches on the slope (modified from Blikra and Kristensen 2012).

A block of possibly 15-20 million m³ (scenario B in Figure 37) has been lowered by 15-20 m from the plateau (Figure 38). The upper part of scenario B with a volume of 2-3 million m³ forms an individual scenario (A in Figure 37) and has been measured periodically with dGNSS, showing a yearly movement of 4.5 cm dipping 45-50° towards ENE (modified from Blikra and Kristensen 2012).

NGU and the county governor of Møre og Romsdal have estimated that the annual probability of a rock avalanche to about 1/100 for scenario A and 1/100 to 1/1000 for scenario B (Dahle et al. 2008). Run-out modelling shows that a rock avalanche of a magnitude of either scenarios A or B would destroy the road and railroad at the valley bottom as well as several houses (Figure 39) (Dahle et al. 2011b, Hermanns et al. 2013). Furthermore, the rock debris may dam the river Rauma, with a subsequent risk of dam collapse and flooding downstream of the river (Figure 39) (Hermanns et al. 2013) (modified from Blikra and Kristensen 2012).

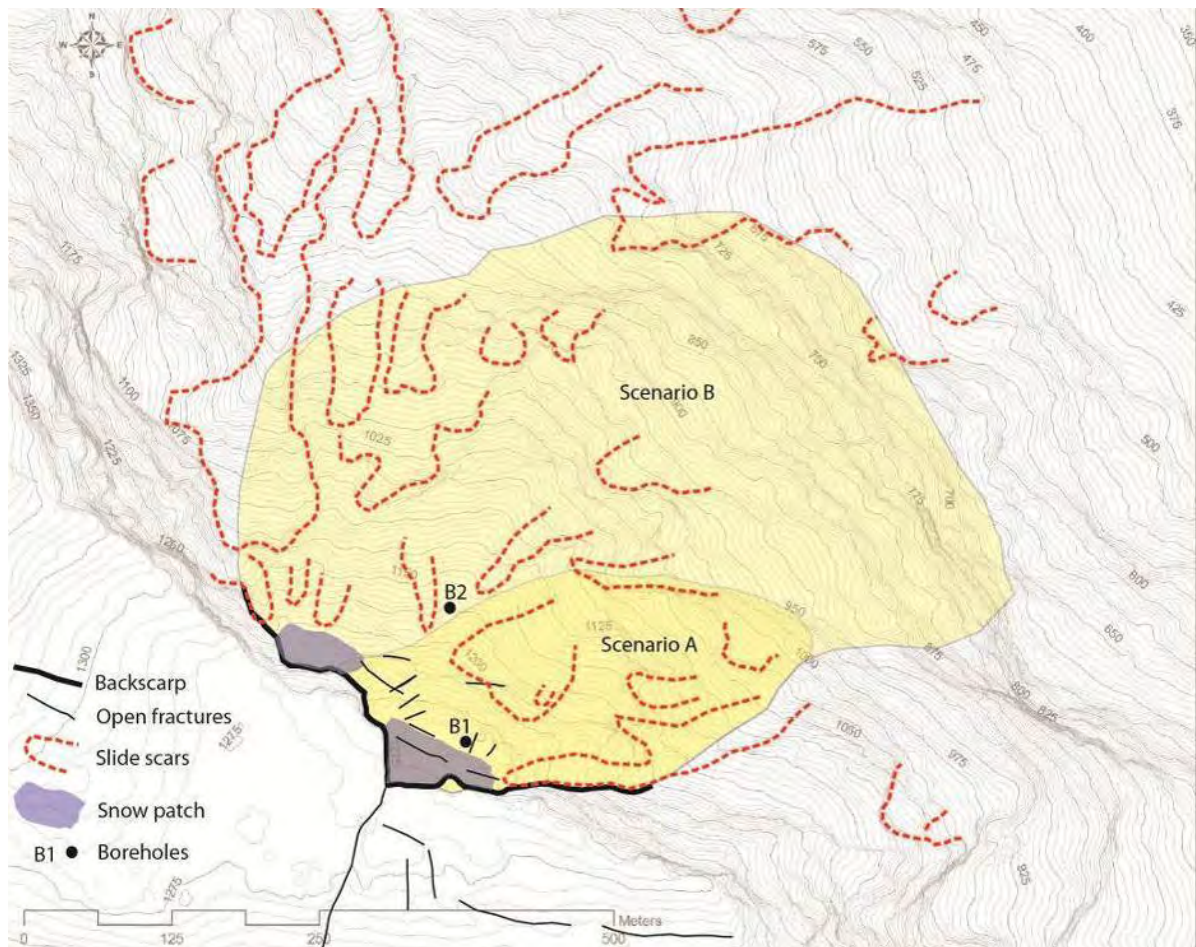


Figure 37: Morphological map of the Mannen rockslide displaying multiple slide scars within the unstable rock slope. The extent of scenarios A and B, as well as the location of two cored boreholes are shown (Blikra and Kristensen 2012).



Figure 38: Photo of the upper part of Mannen, showing the block that has been lowered from the plateau. Some instruments from the upper part of the rock slope instability are shown (Blikra and Kristensen 2012).

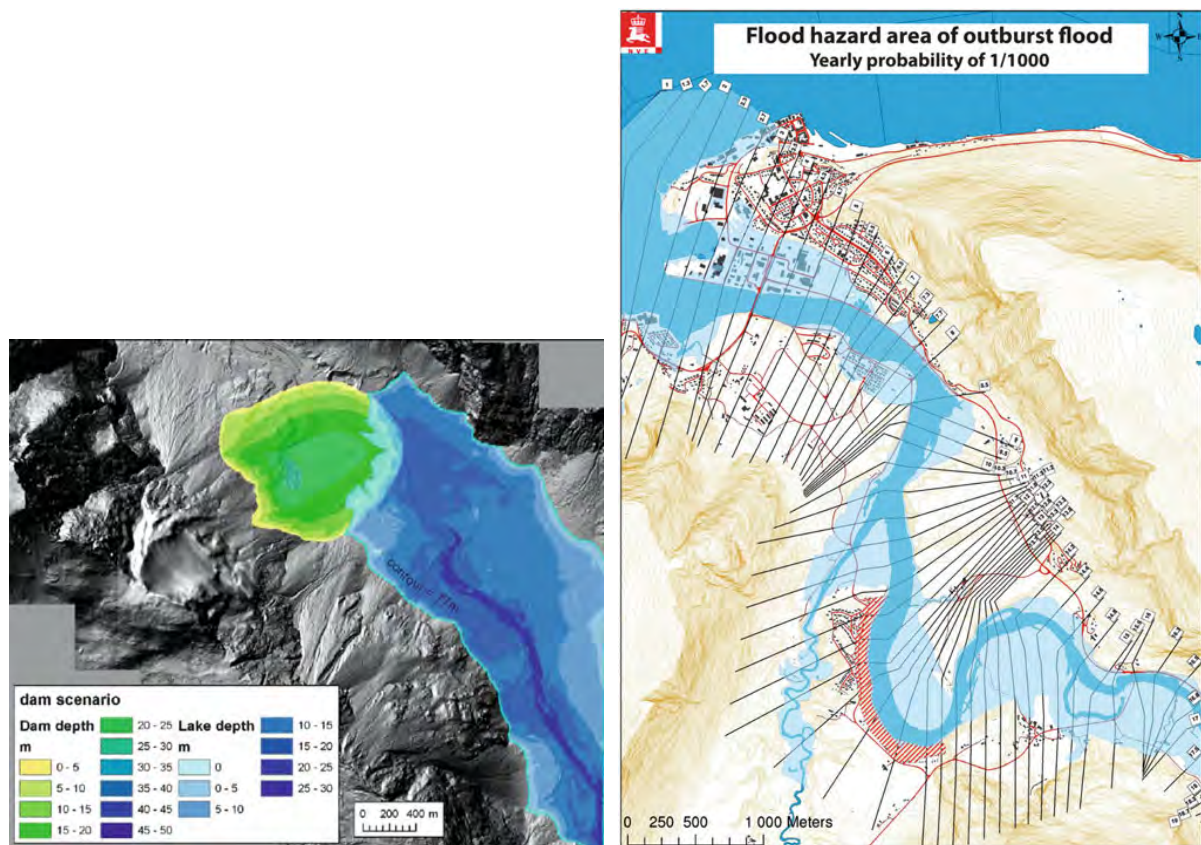


Figure 39: Rock avalanche run-out, landslide dam and dam breach modelling: left) map showing the extent of the simulated rock avalanche deposits for the Mannen rockslide (scenario B) made by the University of Milano-Bicocca, as well as the flooding area upriver the dam; right) simulated flooding area of the lower river section in the area of Åndalsnes made by P.L. Bjerke, NVE (figures from Hermanns et al. 2013).

Instrumentation at the Mannen instability consists of two lasers, seven extensometers, eight GNSS antennas, two DMS borehole instruments (Differential Monitoring of Stability columns from C.S.G. S.r.l) in two ca. 130 m-deep boreholes, and a meteorological station. At the valley bottom, a ground-based radar system is in place that measures displacement of the entire slope and provides the only information we obtain from the lower, inaccessible part of the rock instability. A diesel generator inside a bunker at the top provides power to the sensors, and the data signals are collected in dataloggers in the bunker as well. The bunker is connected to the internet by a radio link to the valley. Thus, the generator control system, dataloggers, routers and other equipment in the bunker are accessible from everywhere via VPN. The data is transferred to a database and this database has a web-interface that permits a display of the measurements of flexible intervals.

The latest monitoring results and a new geological model of the Mannen unstable rock slope will be presented during this field trip.

Cited references for stop 9: Mannen

- Blikra, L.H. and Kristensen, L. (2012) Mannen (Norway). In: Baron, I., Supper, R. and Ottowitz, D. (eds.) *SafeLand deliverable D4.6 - Report on evaluation of mass movement indicators*, SafeLand European project, available at <http://www.safeland-fp7.eu>, pp. 271-283.
- Dahle, H., Anda, E., Sætre, S., Saintot, A., Hermanns, R.L. and Oppikofer, T. (2011a) Risiko- og sårbarhetsanalyse for fjellskred i Møre og Romsdal - FylkesROS-fjellskred. Fylkesmannen i Møre og Romsdal, Møre og Romsdal Fylkeskommune, Geological Survey of Norway, Molde, Norway.
- Dahle, H., Anda, E., Saintot, A. and Sætre, S. (2008) Faren for fjellskred fra fjellet Mannen i Romsdalen. NGU report 2008.087, Geological Survey of Norway, Trondheim, Norway.

- Dahle, H., Bjerke, P.L., Crosta, G.B., Hermanns, R.L., Anda, E. and Saintot, A. (2011b) Faresoner for utløp, oppdemming og flom som følge av fjellskredfare ved Mannen. NGU report 2011.058, Geological Survey of Norway, Trondheim, Norway.
- Dahle, H., Saintot, A., Blikra, L.H. and Anda, E. (2011c) Geofagleg oppfølging av ustabilt fjellparti ved Mannen i Romsdalen. NGU report 2010.022, Geological Survey of Norway, Trondheim, Norway.
- Dalsegg, E. and Rønning, J.S. (2012) Geofysiske målinger på Mannen i Rauma kommune, Møre og Romsdal. NGU report 2012.024, Geological Survey of Norway, Trondheim, Norway.
- Elvebakk, H. (2012) Borhullslogging med optisk televiwer KH-02-11, Mannen, Rauma kommune, Møre og Romsdal. NGU report 2012.032, Geological Survey of Norway, Trondheim, Norway.
- Farsund, T.Ø (2011) Geological and numerical stability modelling of Mannen, Romsdalen. MSc thesis, Norwegian University of Science and Technology, Trondheim, Norway.
- Henderson, I. and Saintot, A. (2007) Fjellskredundersøkelser i Møre og Romsdal. NGU report 2007.043, Geological Survey of Norway, Trondheim, Norway.
- Hermanns, R., Dahle, H., Bjerke, P., Crosta, G., Anda, E., Blikra, L., Saintot, A. and Longva, O. (2013) Rockslide Dams in Møre og Romsdal County, Norway. In: Margottini, C., Canuti, P. and Sassa, K. (eds.) *Landslide Science and Practice*, Springer, Berlin Heidelberg, pp. 3-12.
- Kristensen, L. and Blikra, L.H. (2013) Monitoring displacement on the Mannen rockslide in Western Norway. In: Margottini, C., Canuti, P. and Sassa, K. (eds.) *Landslide Science and Practice*, Springer, Berlin Heidelberg, pp. 251-256.
- Oppikofer, T., Bunkholt, H., Ganerød, G.V. and Engvik, A.K. (2012) Mannen unstable rock slope (Møre og Romsdal): Geological and engineering geological logging of drill core KH-02-11 & grain size distribution and XRD analysis of fine-grained breccia. NGU report 2012.036, Geological Survey of Norway, Trondheim, Norway.
- Oppikofer, T., Saintot, A., Otterå, S., Hermanns, R.L., Anda, E., Dahle, H. and Eiken, T. (2013) Investigations on unstable rock slopes in Møre og Romsdal – status and plans after field surveys in 2012. NGU report 2013.014, Geological Survey of Norway, Trondheim, Norway.
- Saintot, A., Elvebakk, H., Oppikofer, T., Ganerød, G.V. and Farsund, T.Ø (2011a) Mannen unstable rock slope (Møre & Romsdal): Logging of borehole and drill core KH-01-10, geomorphologic digital elevation model interpretation & displacement analysis by terrestrial laser scanning. NGU report 2011.026, Geological Survey of Norway, Trondheim, Norway.
- Saintot, A., Henderson, I.H.C. and Derron, M.-H. (2011b) Inheritance of ductile and brittle structures in the development of large rock slope instabilities: examples from western Norway. In: Jaboyedoff, M. (ed.) *Slope Tectonics*, pp. 27-78.
- Saintot, A., Oppikofer, T., Derron, M.-H. and Henderson, I. (2012) Large gravitational rock slope deformation in Romsdalen valley (Western Norway). *Revista de la Asociación Geológica Argentina*, **69**, 3, 354-371.
- Tønnesen, J.F. (2009) Georadarmålinger ved Rønningen og Horgheim i Romsdalen for undersøkelse av løsmassetyper i dalbunnen under det ustabile fjellpartiet Mannen. NGU report 2009.062, Geological Survey of Norway, Trondheim, Norway.

STOP 10: FLATMARK

At this final stop we will observe impressive deposits of a rock avalanche that occurred shortly after the deglaciation. Several unstable rock slopes are found in the source area of this rock avalanche and we will discuss their structural setting and failure mechanisms. The following summary is modified from Saintot et al. (2012) and Oppikofer et al. (2013).

Old rock avalanche deposits have dammed the Rauma River at Skiri and Flatmark in the Romsdal Valley (Figure 40). Cosmogenic nuclide dating of three rock avalanche deposit samples give an age of $11\,700 \pm 1000$ years. The source area of this rock avalanche is most probably the 920 m high north-facing slope above Skiri and Flatmark. Five unstable rock slopes still remain on this slope (Henderson and Saintot 2007, Saintot et al. 2011, 2012).

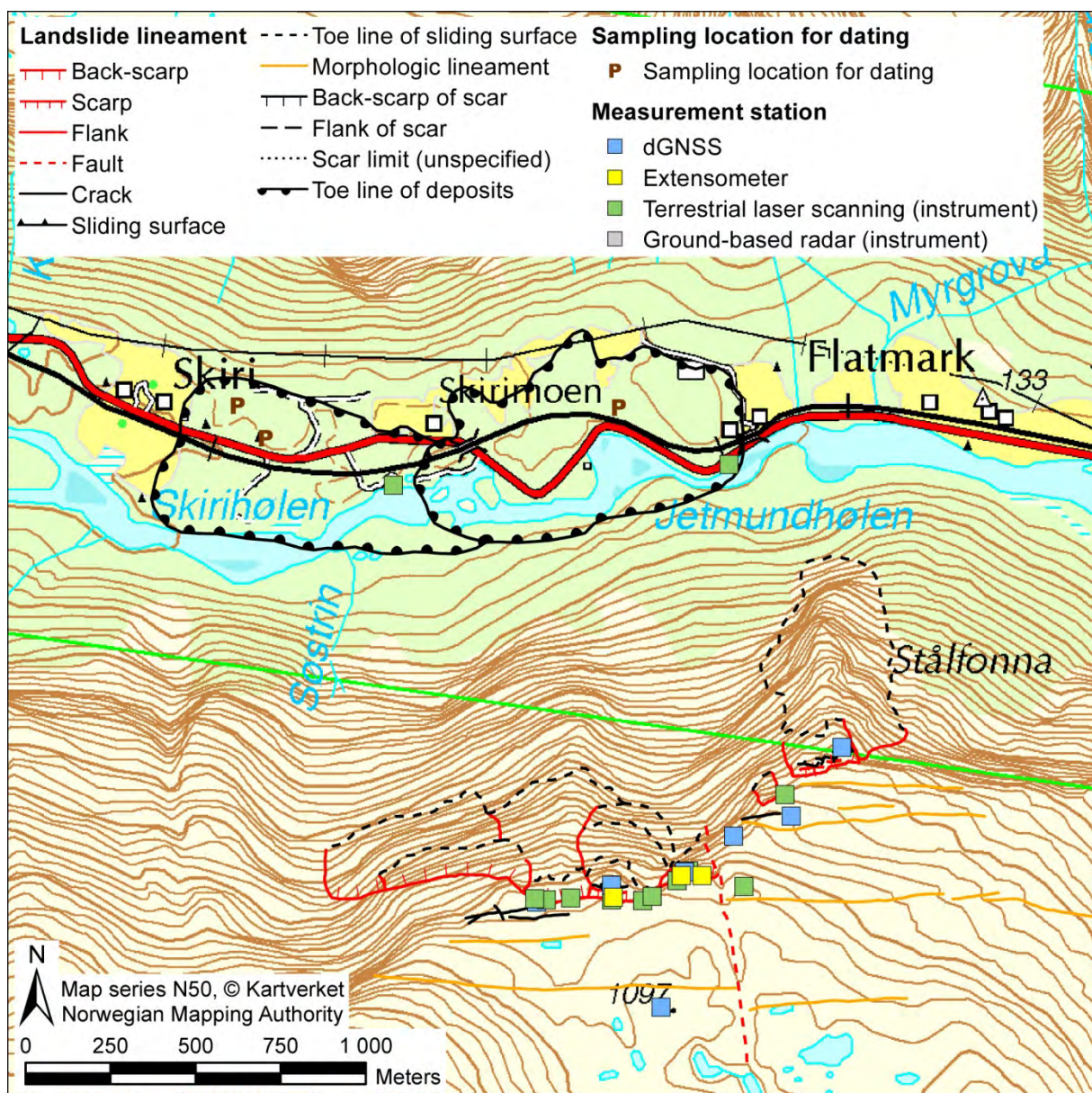


Figure 40: Situation map of stop 10: the Flatmark unstable rock slopes and rock avalanche deposits.

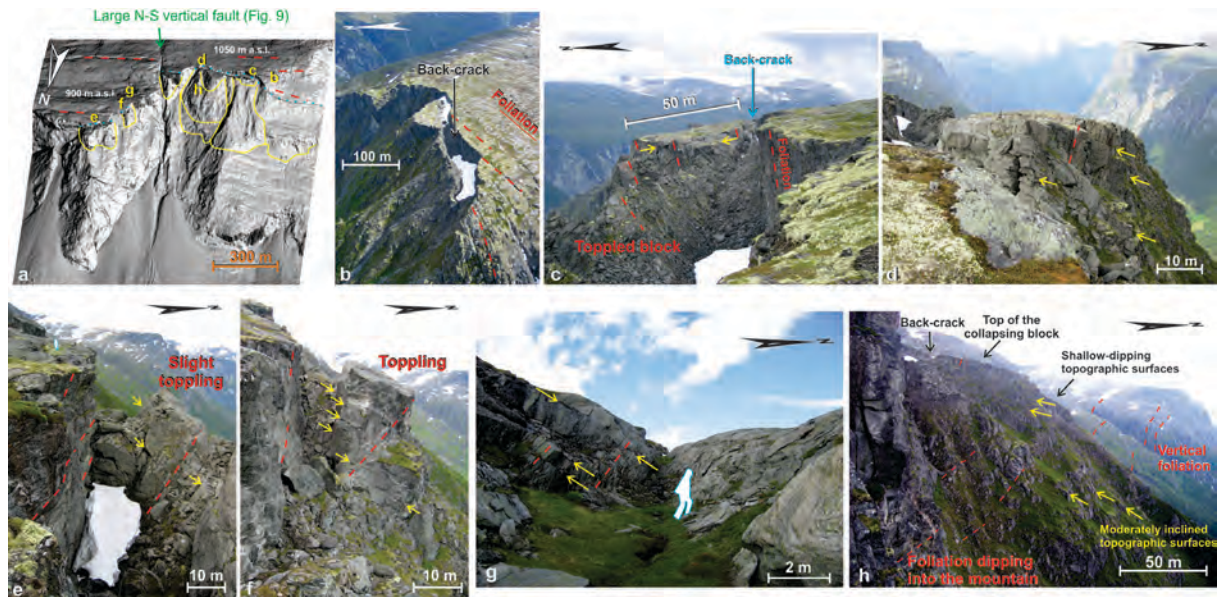


Figure 41: Photographs of the Flatmark unstable rock slopes (the metamorphic foliation is shown as red dashed lines; the shallow to moderately valley-dipping joints as yellow arrows): a) 3D view of the hillshaded digital elevation model (locations of photos in b)-h) are shown); b) the back-scarp of the largest instability is partly guided by the quasi-vertical metamorphic foliation; c) close view to the east of the 20 m wide back-scarp largely filled by debris and of toppling movements within the instability; d) close view to the west of the largest instability; e) and f) toppling movements observed at the top of two instabilities in the eastern part of the Flatmark plateau; g) surface depression in the eastern part of the plateau; h) shallow to moderately valley-dipping topographic surfaces on the largest rock slope instability corresponding to joints that systematically developed perpendicular to the foliation dip line and are thus favorably orientated toward the valley where the foliation steeply dips into the mountain (modified from Saintot et al. 2012).

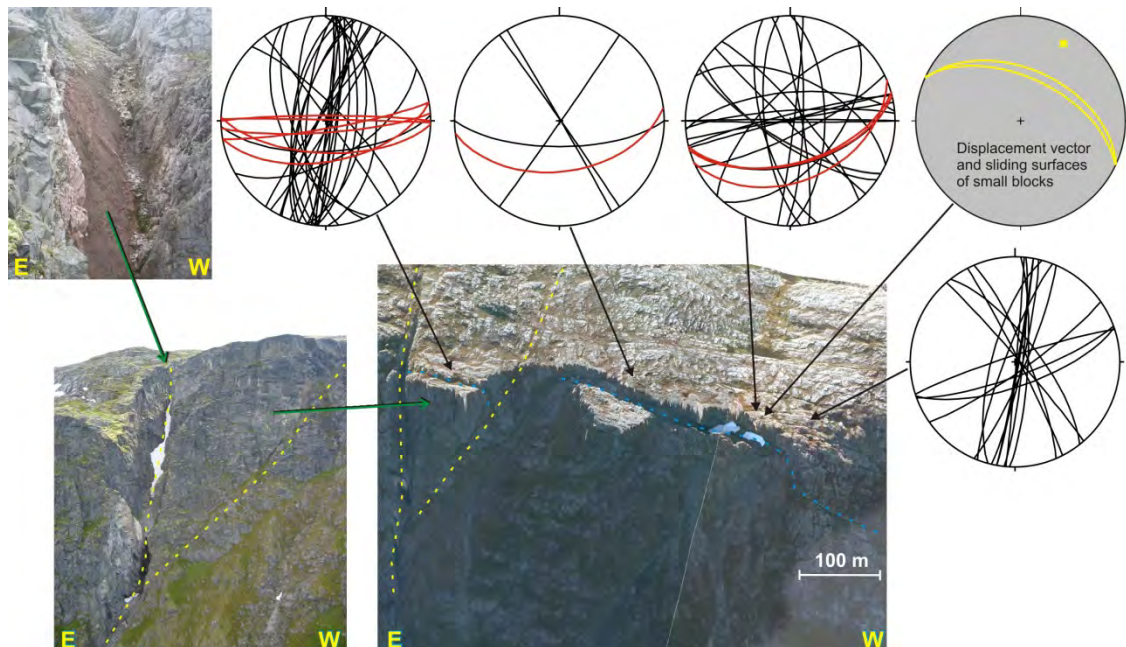


Figure 42: Stereoplots of field measurements at the edge of the Flatmark plateau where the largest instability developed: metamorphic foliation in red and joints in black, two surfaces at the base of small detached blocks have an orientation favorable for sliding. Locations of field measurements on a 3D view of the top of the largest instability (aerial photograph draped on DEM). Photographs taken from helicopter of one of the instabilities, delimited by a foliation-parallel back-crack (blue line) and two pre-existing tectonic faults (yellow lines), one being largely hematite-rich cataclastic (located on Figure 41a) (modified from Saintot et al. 2012).

The unstable rock slopes at Flatmark are delimited by wide vertical back-scarps that have partly smooth walls parallel to the quasi-vertical metamorphic foliation and partly stepped walls shaped by the same foliation and steep joints (Figure 41). For the uppermost and largest instability, the width of the back-crack is 20–25 m. Only few open fractures of low persistence are observed inward the plateau at the back of the rock slope instabilities (modified from Saintot et al. 2012).

The structures that may represent the basal failure surfaces of the instabilities are not clearly identified, but a few favorably orientated, valley-dipping planes were observed (Figure 42). Field measurements show a discontinuity set that systematically developed perpendicular to the dip line of the metamorphic foliation (Figure 41). Variations of the foliation orientation from quasi-vertical to clearly inward-dipping might thus lead to discontinuities that are favourably oriented for sliding (Figure 41g and Figure 42). The sharp topographic surfaces at the foot of the largest instability may actually reflect the foliation dipping into the mountain and moderately valley-dipping topographic surfaces would correspond to such basal sliding surfaces (Figure 41h) (modified from Saintot et al. 2012).

The possible failure mechanism of the large rock slope instabilities at Flatmark is likely a sliding and/or a sagging on these valley-dipping basal failure surfaces yielding back-crack opening along the cliff-parallel steep metamorphic foliation surfaces. Locally, toppling affects small blocks within the unstable rock slopes (Figure 41). However, the vertical extents of the back-cracks and the continuity of the basal failure surfaces are speculative and stepped surfaces cannot be ruled out (modified from Saintot et al. 2012).

Six dGNSS measurement points were installed at Flatmark in 2006. Three points are located on detached unstable rock slopes that have obviously moved in the past. All points were measured again in 2007, 2008 and 2011, but no significant displacements were recorded over the 5 years measurement period. This is in agreement with (1) the important infill of the back-cracks with deposits (Figure 41a, b) and with (2) the absence of rockfall activity at the front of the unstable rock slopes, as well as of well-developed bulges due to slope deformation (modified from Saintot et al. 2012 and Oppikofer et al. 2013).

Cited references for stop 10: Flatmark

- Henderson, I. and Saintot, A. (2007) Fjellskredundersøkelser i Møre og Romsdal. NGU report 2007.043, Geological Survey of Norway, Trondheim, Norway.
- Oppikofer, T., Saintot, A., Otterå, S., Hermanns, R.L., Anda, E., Dahle, H. and Eiken, T. (2013) Investigations on unstable rock slopes in Møre og Romsdal – status and plans after field surveys in 2012. NGU report 2013.014, Geological Survey of Norway, Trondheim, Norway.
- Saintot, A., Henderson, I.H.C. and Derron, M.-H. (2011) Inheritance of ductile and brittle structures in the development of large rock slope instabilities: examples from western Norway. In: Jaboyedoff, M. (ed.) *Slope Tectonics*, pp. 27-78.
- Saintot, A., Oppikofer, T., Derron, M.-H. and Henderson, I. (2012) Large gravitational rock slope deformation in Romsdalen valley (Western Norway). *Revista de la Asociación Geológica Argentina*, **69**, 3, 354-371.

ACKNOWLEDGEMENTS

This field trip would not have been possible in its present form without the generous sponsorship of Åknes/Tafjord Beredskap IKS, University of Lausanne, Naturfare - Infrastruktur, Flom og Skred (NIFS, joint programme of NVE, Vegvesen and NSB), Nordnorsk Fjellovervåking, C.S.G. S.r.l, LisaLab, NavSys AS and RIEGL Laser Measurement Systems.

The authors would like to thank A. Saintot from the University of Bochum (Germany) for geological background information and data on the Flatmark unstable rock slope (stop 10), G.M. Dreiås from NTNU for providing field measurements and investigations on the Ivasnasen and Vollan unstable rock slopes (stop 1), H. Dahle from the Norwegian Public Road Authorities and L. Kristensen from the Åknes/Tafjord Early-Warning Centre for data on Oppdølstranda (stop 2), M. Schleier and I. Krieger for their investigations on the rock avalanche deposits in the Innerdal Valley (stop 3), the Middagstinden unstable rock slope (stop 6) and the rock avalanche deposits in the Innfjorddal Valley (stop 7), and L.H. Blikra and L. Kristensen from the Åknes/Tafjord Early-Warning Centre for data on the continuously monitored unstable rock slope Mannen.

Organizers



Supporters



APPENDIX 1: HERMANNNS ET AL. (2014) APPROACH FOR SYSTEMATIC ROCKSLIDE MAPPING OF UNSTABLE ROCK SLOPES IN NORWAY

Full citation: Hermanns, R., Oppikofer, T., Yugsi Molina, F., Dehls, J. and Böhme, M. (2014) Approach for Systematic Rockslide Mapping of Unstable Rock Slopes in Norway. In: Sassa, K., Canuti, P. and Yin, Y. (eds.) *Landslide Science for a Safer Geoenvironment*, Springer International Publishing, pp. 129-134.



Approach for Systematic Rockslide Mapping of Unstable Rock Slopes in Norway

Reginald L. Hermanns, Thierry Oppikofer, Freddy X. Yugsi Molina, John F. Dehls, and Martina Böhme

Abstract

Systematic mapping of unstable rock slopes has been carried out in Norway since 2005. More than 300 unstable or potential unstable rock slopes have been detected and characterized so far. This utilises a standardized hazard and risk classification system that was established in 2012. The determination of the hazard and risk level follows a new standard approach for the systematic mapping of the analyzed sites that is iterative, starting with simple assessments. However the higher the hazard/risk level of a site is, the larger the amount of geological information collected, and the more detailed the run-out models and consequence analyses that will be carried out. This approach allows mapping resources to be focused on sites with higher risk level, delivering products with different levels of detail. Rock slope failures that would not result in any loss of life, as there is no life line or building in the run-out area, are mapped without a probability assessment. These analyses thus have no scale for the hazard class. Rock slope failures that can result in loss of life are analyzed using qualitative hazard analyses, thus the mapping products are hazard maps with qualitative probability classes. The work on this mapping approach is still ongoing; methods for assessment of the occurrence and consequences of secondary processes (e.g., triggering of displacement waves in water bodies, river damming and outburst floods) need still to be defined. An iterative approach will also be developed to analyze those processes.

Keywords

Rock slope instability • Detection • Mapping • Displacement measurements • Run-out analysis • Consequence analysis • Hazard classification • Risk classification

Introduction

Although rock slope failures are relatively rare events on a global scale, with its 100,000 km long coastline, Norway has historically experienced 2–6 large rockslides per century

that have produced several tens of meters high displacement waves and resulted in the death of dozens of people (e.g., Hermanns et al. 2006; Devoli et al. 2011). In response to this high rockslide exposure, the Geological Survey of Norway (NGU) began in 2005 to map unstable rock slopes (e.g., Böhme et al. 2011; Bunkholt et al. 2011; Henderson and Saintot 2011; Oppikofer et al. 2013). Since 2009, this activity has been financed through the Norwegian Water Resources and Energy Directorate (NVE).

Standardization of the mapping approach is crucial in order to guarantee that the products of the hazard and risk classification are comparable and reproducible. The establishment of the hazard and risk classification for unstable

R.L. Hermanns (✉) • T. Oppikofer • F.X. Yugsi Molina • J.F. Dehls • M. Böhme
Geological Survey of Norway, P.O. Box 6315 Sluppen, 7491
Trondheim, Norway
e-mail: reginald.hermanns@ngu.no; thierry.oppikofer@ngu.no;
freddy.molina.yugsi@ngu.no; john.dehls@ngu.no; martina.bohme@ngu.no

rock slopes in 2012 (Hermanns et al. 2012, 2013a) has set the frame work to define the level of detail required for the mapping of unstable rock slopes according to their level of hazard. This paper describes that approach, which is also summarized in a flowchart diagram in Fig. 1.

Mapping Approach

Goals

Goals of these ongoing mapping activities are to find all rock slopes that could fail catastrophically and to determine areas that would be affected by their failure in order to communicate possible consequences to Norwegian society. Catastrophic failures are here defined as rock slope failures that involve substantial fragmentation of the rock mass during run-out and that impact an area larger than that of a rockfall, hence also include rock slope failures that might cause a displacement wave or damming of valleys (Hermanns and Longva 2012).

Since the beginning of 2013, mapping activities have focused on collecting information to be used for the implementation of the hazard and risk classification system (Hermanns et al. 2012) recently developed by a team of Norwegian and international experts. This classification became the standard procedure for defining the risk level that will be used to decide on further actions (that will be specified in an upcoming NVE document) on the investigated sites. The consequence analysis within this classification system focuses on loss of life only.

The results of the evaluation using this classification system have allowed developing a systematic mapping approach, as presented in Fig. 1. This approach is set up so that mapping activities for sites that cannot cause catastrophic rock slope failures, or that do not show signs of past deformation or do not have consequences in case of failure, are discarded from further investigations after the reconnaissance phase. This allows detailed, costly investigations to be focused on the medium- and high-risk sites.

This mapping approach guarantees a similar level of geological information for all sites with the same risk level over the entire country. However, detail of geological information is not even for sites with different risk levels. Additional geological data will have to be collected in future at sites where the risk level changes due to external factors (e.g., increase in potential consequences due to new buildings).

Due to the difference in the amount and detail of geological data, outcomes will be different too: maps of the run-out area of the majority of low-risk sites will represent hazard maps without a hazard class (qualitative probability of

failure), while they will represent hazard maps with qualitative hazard classes for all medium- and high-risk sites and some of the low-risk sites.

Investigation Stages

Detection of Unstable Rock Slopes

Detection of (potential) unstable rock slopes is carried out using expert-based analysis of optical remote sensing imagery to search for morphological features of unstable slopes such as opening of cracks, displacement of blocks, high fracture density of bedrock, and satellite-based radar interferometry (InSAR) (Fig. 1).

Reconnaissance

On steep slopes and high mountain plateaus in Norway the bedrock is often bare or covered only by thin Quaternary deposits. Old inherited tectonic structures are thus readily visible and may appear as cracks, especially on slopes where they are subject to preferential erosion. However, superficial processes such as solifluction can be detected by InSAR techniques and mistaken for signs of rock slope deformation. Therefore, all detected sites undergo an initial reconnaissance.

Reconnaissance is carried out from any spot with easy access to the site and good visibility or from a helicopter. In this step, rock slopes with no real signs of deformation of large rock volumes are divided in three categories: (A) unstable rock slopes that are too small to cause a catastrophic failure in the above-defined sense. These sites are however prone to rockfalls, and other available mapping products such as the national rockfall susceptibility map or rockfall hazard maps define the susceptibility/hazard levels of those areas (see <http://www.skrednett.no>). (B) Rock slopes that have no structural or lithological conditions that could lead to a catastrophic rock slope failure in the future. (C) Rock slopes that have the structural or lithological conditions for failure in the future, but no sign of past or present displacements or deformation (potential unstable rock slopes). Category C sites have to be followed up by a revision after several years to decades, as they might become active unstable rock slopes. The fast development of remote sensing data with increasing resolution and acquisition cycles will make this possible.

Preliminary Consequence Analyses

At the end of the reconnaissance phase a preliminary consequence analysis will be carried out for all unstable rock slopes. Sites with evidently no consequences (no buildings or life lines in the potential run-out area) are evident low-risk sites and no further investigations will be made. Nonetheless, the volume will be assessed and an automated run-out

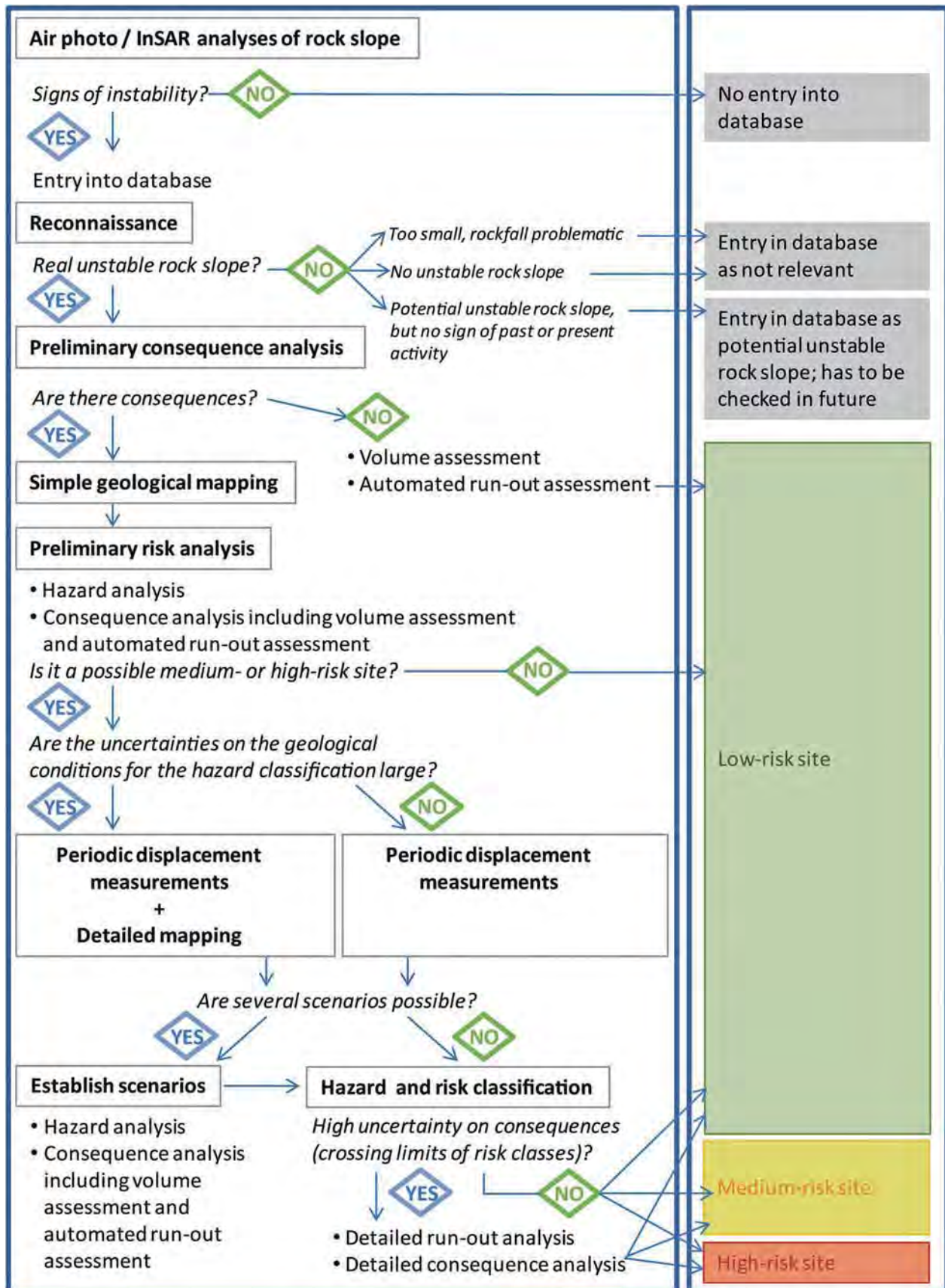


Fig. 1 The flowchart shows the mapping approach for unstable rock slopes in Norway. Potential unstable rock slopes that do not display signs of past displacements and sites without possible consequences are discarded from more intensive geological studies at an early stage

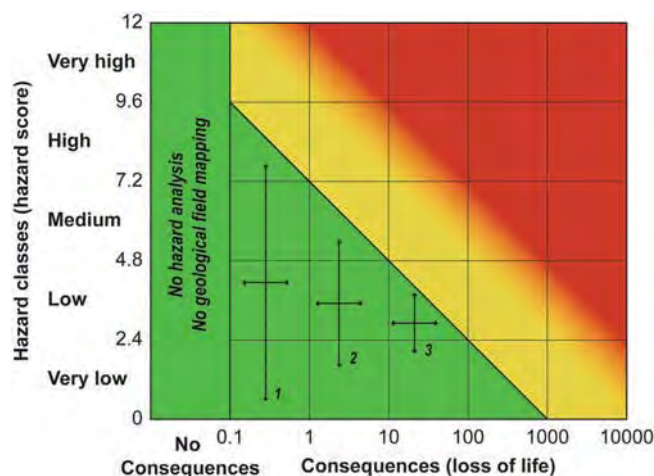


Fig. 2 Risk matrix, showing the risk classes (green is low, yellow is moderate and red is high). The diagram also shows under which conditions no geological field mapping will be carried out (no consequences) and 3 examples with increasing consequences (1–3) that require decreasing uncertainty levels and hence increasing certainty of geological observations

analysis will be calculated to indicate areas that could potentially be hit by a catastrophic failure (hazard map without a qualitative probability assessment) (Figs. 1 and 2). Unstable rock slopes with evident consequences (buildings, life lines or water bodies in the run-out area) will be further investigated according to the flowchart in Fig. 1.

Simple Geological Mapping

During simple geological mapping geological information on all criteria that are necessary for the hazard classification are collected, including morphological and structural development (e.g., back scarp, potential sliding structures, lateral release surfaces, morphological expression of rupture surface, kinematic analysis) and signs of activity (displacement rates, acceleration, increase of rockfall activity, past events) (see also: Hermanns et al. 2012, 2013a). Uncertainty on these observations might be high (especially for the displacement rates, since no monitoring data are being collected at that stage of investigation). A first hazard analysis will be performed as indicated in Hermanns et al. (2012, 2013a). For all sites an automated run-out analysis is calculated and consequences are assessed. Sites with no consequences are categorized as low-risk sites. For all other sites a preliminary risk analysis is carried out following Hermanns et al. (2012, 2013a). Low-risk sites with low consequences might have large uncertainty on the geological observations (example 1 in Fig. 2). For all possible medium- or high-risk sites, i.e., the yellow and red zones in the chart presented in Fig. 2, the amount of geological observations has to be increased to reduce the uncertainty margins (examples 2 and 3 in Fig. 2). Two situations are possible

based on this simple geological mapping: (A) the geological conditions are well understood, or (B) the geological criteria could not entirely be assessed by the simple geological mapping. For the former, periodic displacement measurements need to be carried out, while for the latter further geological mapping is necessary, in addition to periodic displacement measurements.

Periodic Displacement Measurements and Detailed Geological Mapping

At all sites that are assessed as potential medium- or high-risk sites, local conditions have to be understood better in order to reduce uncertainties in the hazard analysis. In general the easiest way to reduce uncertainties is to use monitoring equipment in order to assess the current displacement rates. A wide variety of monitoring techniques is currently used by NGU, including extensometers, differential Satellite Global Navigation Systems (dGNSS), satellite- and ground-based InSAR with and without reflectors, terrestrial laser scanning and photogrammetry.

In addition, sites with complex geology require additional geological field mapping. These are sites where simple kinematic models (planar sliding, wedge sliding, flexural or block toppling) cannot explain the observed deformation and more complex kinematic models have to be developed. These could be sites with a combination of two failure mechanisms, such as bi-planar sliding, slide toppling, or a combination of sagging and rock slide. Sites with a strong change in the structural conditions over the slope (e.g., folding) also fall into this group.

Establish Scenario and Hazard and Risk Classification

Scenarios are developed following structural and morphological mapping, in combination with results of displacement measurements. A single failure scenario is likely if the structures over the entire unstable slope do not vary and the entire unstable slope deforms uniformly. In contrast, if the displacement rates vary over the instability and the whole unstable rock slope is divided in compartments with different behaviour, different failure scenarios have also to be taken into account. Two general cases of scenarios exist: (A) individual compartments of a larger unstable rock slope lie beside each other and each one could fail independently of the other, or (B) individual compartments are subareas within a larger unstable rock slope and could fail without causing the failure of the total unstable rock slope; the failure of the total unstable rock slopes however includes also its subareas.

For each scenario the hazard and automated run-out analyses followed by consequence analyses have to be performed, leading to the risk classification. If the

uncertainties on the consequences are high, detailed run-out analyses become necessary.

Mapping Products

The information product will be published through the existent database of unstable rock slopes in Norway (Bunkholt et al. 2013) and includes the location and extent of the unstable area, mapping status and recommendations for follow-up activities. This information will become of public access through <http://www.skrednett.no> in 2014. The result of the hazard and risk classification will be added once all necessary data have been collected and the classification performed. In addition, run-out areas for each site will be published once the analysis is carried out. These run-out areas present different quality levels. They represent hazard maps with no qualitative probability analysis for those sites where today consequences are zero (no building or life lines are in the run-out area) and qualitative hazard maps for those areas where loss of life might occur. More specific geological information will continue to be in the category of restricted access. Information for each site will be downloadable in 2014 as factsheets.

Discussion

Due to the geomorphologic conditions of Norway, with one of the world's longest coastlines characterized by high mountains deeply incised by fjords, large rock slope failures occurred repeatedly in the past, often accompanied by secondary effects such as displacement waves and damming of valleys (Blikra et al. 2006; Hermanns et al. 2013b). Therefore, in contrast to other mountain belts in the world, these long-distance effects resulted in a larger death toll than from just the direct impact of the rock slope failure itself. As such events will also occur in the future, and in order to attenuate their deadly consequences, systematic mapping of rock slopes has started in the first decade of the twenty-first century, and today more than 300 (potential) unstable rock slopes are known. This high number of sites necessitated a quantitative hazard and risk classification system to assist in deciding on follow-up activities. This system was elaborated in a large effort combining national and international experts from various disciplines in earth sciences and presented in Hermanns et al. (2012, 2013a).

Subsequently, in order to establish the hazard and risk classification system, it became necessary to adapt the national mapping approach to this system. The goal of this mapping approach is to be cost-effective and to focus mapping resources on sites that are most critical. This goal is met by using an iterative approach: the amount of

collected geological data, quality of run-out modelling, and detail of consequence analyses increase respectively, improving with the increasing risk level for each site and scenario. Hence for high-risk sites, various cycles of hazard analysis, run-out-analysis, consequence analysis and risk analysis are carried out. This leads in parallel to a reduction of the uncertainties in the hazard and risk classification. However, using this approach, the level of detail of the mapping products is not even. Sites where run-out models are calculated from a volume estimate alone do not include an assessment of the hazard level. Also the run-out areas of low-risk sites represent hazard zones with relatively high uncertainties in the likelihood of an event. Uncertainties in the likelihood of an event are smaller for medium- and high-risk sites. This will lead in general to the situation that mapping products for unstable slopes that can cause a larger number of casualties will rely on a sound knowledge of their geological characteristics.

The work on this mapping approach is not finalized and it is an ongoing project. So far it has been decided that secondary effects such as rockslide-triggered displacement waves and rockslide damming will be included. Detail of analysis for these secondary effects should also increase with risk level and follow an iterative approach; however, practises are still under development.

References

- Blikra LH, Longva O, Braathan A, Anda E, Dehls JF, Stalsberg K (2006) Rock slope failures in Norwegian fjord areas; examples, spatial distribution and temporal pattern. In: Evans SG, Scarascia Mugnozza G, Strom A, Hermanns RL (eds) Landslides from massive rock slope failures, NATO science series IV (49), Earth and environmental sciences. Springer, Dordrecht, pp 475–496
- Böhme M, Henderson I, Saintot A, Hermanns RL, Henriksen H (2011) Rock-slope instability investigations in Sogn & Fjordane County, Norway: a detailed structural and geomorphological analysis. In: Jaboyedoff M (ed) Slope tectonics. Geological Society, London. Special Publication, 351, pp 97–112. ISBN:978-1-86239-324-0
- Bunkholt H, Osmundsen PT, Redfield T, Oppikofer T, Eiken T, L'Heureux J-S, Hermanns R, Lauknes TR (2011) ROS Fjellskred i Troms: status og analyser etter feltarbeid 2010. Norwegian Geological Survey Report No. 2011-031, 135 p
- Bunkholt H, Nordahl B, Hermanns RL, Oppikofer T, Fischer L, Blikra LH, Anda E, Dahle H, Sætre S (2013) Database of unstable rock slopes of Norway. In: Margottini C, Canuti P, Sassa K (eds) Landslide science and practice, Volume 3: Spatial analysis and modelling. Springer, Berlin, pp 423–428
- Devoli G, Eikenæs O, Taurisano A, Hermanns RL, Fischer L, Oppikofer T, Bunkholt H (2011) Plan for skredfarekartlegging – Delrapport steinsprang, steinskred og fjellskred. NVE rapport 15/2011. Norgesvassdrags- og energidirektorat, Oslo, 110 p
- Henderson IHC, Saintot A (2011) Regional spatial variations in rockslide distribution from structural geology ranking: an example from Storfjorden, western Norway. In: Jaboyedoff M (ed) Slope tectonics. Geological Society, London. Special Publication, 351, pp 79–96. ISBN:978-1-86239-324-0

- Hermanns RL, Longva O (2012) Rapid rock-slope failures. In: Clague JJ, Stead D (eds) *Landslides: types, mechanisms and modeling*. Cambridge University Press, Cambridge, UK, pp 59–70
- Hermanns RL, Blikra LH, Naumann M, Nilsen B, Panthi KK, Stromeyer D, Longva O (2006) Examples of multiple rock-slope collapses from Köfels (Ötztal valley, Austria) and western Norway. *Eng Geol* 83(1–3):94–108
- Hermanns RL, Oppikofer T, Anda E, Blikra LH, Böhme M, Bunkholt H, Crosta GB, Dahle H, Devoli G, Fischer L, Jaboyedoff M, Loew S, Sætre S, Yagci Molina F (2012) Recommended hazard and risk classification system for large unstable rock slopes in Norway. NGU-rapport 2012.029, 53 p
- Hermanns RL, Oppikofer T, Anda E, Blikra LH, Böhme M, Bunkholt H, Crosta GB, Dahle H, Devoli G, Fischer L, Jaboyedoff M, Loew S, Sætre S, Yagci Molina F (2013a) Hazard and risk classification system for large unstable rock slopes in Norway. In: Genevois R, Prestininzi A (eds) *International conference on Vajont – 1963-2013*. Italian Journal of Engineering Geology and Environment, Book series 6, Rome, Italy, pp 245–254
- Hermanns RL, Dahle H, Bjerke PL, Crosta GB, Anda E, Blikra LH, Saintot A, Longva O, Eiken T (2013b) Rock slide dams in Møre og Romsdal county, Norway: examples for the hazard and potential of rock slide dams. In: Margottini C, Canuti P, Sassa K (eds) *Landslide science and practice, Volume 6: Risk assessment, management and mitigation*. Springer, Berlin
- Oppikofer T, Saintot A, Otterå S, Hermanns RL, Anda E, Dahle H, Eiken T (2013) Investigations on unstable slopes in Møre og Romsdal - status and plans after field surveys in 2012. NGU rapport 2013.014 (ISSN 0800-3416), 169 p

APPENDIX 2: HERMANN'S ET AL. (2013A) HAZARD AND RISK CLASSIFICATION FOR LARGE UNSTABLE ROCK SLOPES IN NORWAY

Full citation: Hermanns, R.H., Oppikofer, T., Anda, E., Blikra, L.H., Böhme, M., Bunkholt, H., Crosta, G.B., Dahle, H., Devoli, G., Fischer, L., Jaboyedoff, M., Loew, S., Sætre, S. and Yugsi Molina, F.X. (2013a) Hazard and Risk Classification for Large Unstable Rock Slopes in Norway. In: Genevois, R. and Prestininzi, A. (eds.) *International Conference Vaiont, 1963-2013 - thoughts and analyses after 50 years since the catastrophic landslide*, Italian Journal of Engineering Geology and Environment - Book Series 6, Sapienza University, Rome, Italy, pp. 245-254.

HAZARD AND RISK CLASSIFICATION FOR LARGE UNSTABLE ROCK SLOPES IN NORWAY

REGINALD L. HERMANN^(*), THIERRY OPIKOFER^(*), EINAR ANDA^(**), LARS H. BLIKRA^(*),
MARTINA BÖHME^(*), HALVOR BUNKHOLT^(*), GIOVANNI B. CROSTA^(***), HALGEIR DAHLE^(****),
GRAZIELLA DEVOLI^(****), LUZIA FISCHER^(*), MICHEL JABOYEDOFF^(*****),
SIMON LOEW^(*****), STINE SÆTRE^(*****) & FREDDY XAVIER YUGSI MOLINA^(*)

^(*) Geological Survey of Norway (NGU) - Trondheim, Norway

^(**) Åknes Tafford Beredskap

^(***) University of Milano-Bicocca - Milan, Italy

^(****) Norwegian Road Authorities

^(*****) Norwegian Water and Energy Directorate

^(*****) University of Lausanne - Lausanne, Switzerland

^(*****) ETH Zurich - Zurich, Switzerland

^(*****) The county of Møre og Romsdal

ABSTRACT

We present a classification system for hazard and risk that is posed by unstable rock slopes in Norway that might undergo catastrophic failure in future and can cause loss of life. The system is scenario-based as the intensity and rate of displacement, as well as the geological structures activated by the sliding rock mass vary significantly on the slopes. In addition, for each scenario the secondary effects, such as generation of displacement waves or landslide damming of valleys with the potential of later outburst floods, are evaluated. The hazard analysis is based on two types of criteria: 1) Structural site investigations including analysis of the development of a back-scarp, lateral boundaries and basal sliding surface. This includes a kinematic analysis for sliding and toppling based on slope orientation, persistence of main structures and morphologic expressions of the sliding surface. 2) Analysis of slope activity primarily based on slide velocity, change of deformation rates, observation of rockfall activity, and historic or prehistoric events. The analysis of consequences focuses on the potential fatalities to the rock slide scenarios and secondary effects. Based on the hazard and consequence analysis each scenario is classified in a risk matrix into category low, medium or high risk.

KEY WORDS: *catastrophic rock slope failure, secondary effects, hazard analysis, consequence analysis, risk matrix*

INTRODUCTION

Catastrophic failure of large rock slopes in Norway has several times per century led to rock avalanches or large rock falls, which directly affected settlements, but also caused either a displacement wave when impacting a water body with often fatal consequences or damming of narrow valleys with a high loss of property (BLIKRA *et alii*, 2006a; FURSETH, 2006). Such events will also occur in the future. For catastrophic failure we follow here the definition given by HERMANN & LONGVA (2012) as rock slope failures that could involve substantial run-out and fragmentation of the rock mass and could impact with high velocity an area larger than that of a rockfall with typical shadow angles of ca. 28-34° (e.g. EVANS & HUNGR, 1993). This limitation is permissible as there are other mapping products in Norway that characterize the source and invasion areas and its likelihood for small scale rock slope failures (rockfall susceptibility map, detailed hazard maps) (e.g. HØST *et alii*, 2013).

The Geological Survey of Norway (NGU), following its obligation towards society and the Norwegian Water and Energy Directorate (NVE) carries out systematic geologic mapping of potentially unstable rock slopes that might fail catastrophically (HERMANN *et alii*, 2013a). Within the last years mapping in only three of the 17 relevant counties of Norway has revealed more than 300 sites of potential future rock slope failures. This number necessitates a systematic mapping approach that focuses on the relevant geological data

R.L. HERMANN, T. OPPIKOFER, E. ANDA, L.H. BLIKRA, M. BÖHME, H. BUNKHOLT, G.B. CROSTA,
H. DAHLE, G. DEVOLI, L. FISCHER, M. JABOYEDOFF, S. LOEW, S. SÆTRE & F.X. YUGSI MOLINA

for assessing the likelihood of failure. Furthermore, it requires prioritization of follow-up activities, such as periodic or permanent monitoring, early-warning systems, and other mitigation measures. A first guideline on the mapping approach and a hazard and risk classification is given in a geological report (HERMANN *et alii*, 2012) and is summarized in this publication. Mapping as well as hazard and risk classification will follow in Norway in the upcoming years these guidelines until a large number of sites are classified and related geological data and data on potential consequences stored in a related database (BUNKHOLT *et alii*, 2013). Then the classification system can be reviewed based on real data. As the likelihood of failure cannot be given quantitatively in hundreds or thousands of years with today's scientific knowledge, the risk analysis is built on a qualitative hazard analysis and a quantitative consequence analysis. The goal is to assemble enough data on historic and pre-historic rock slope failures in Norway that will allow for a calibration of the qualitative hazard analyses.

The working approach for the elaboration of this classification system was to combine a broad national and international experience on large rock slope failures and a group of 18 Norwegian and 5 international experts had participated in the discussion preceding this classification system (see summary in HERMANN *et alii*, 2012). Furthermore, earlier proposed classification systems that focus on long term slope stability of large rock slopes have been taken as guide (HANTZ *et alii*, 2002; HUNGR & EVANS, 2004; GLASTONBURY & FELL, 2008; JABOYEDOFF *et alii*, 2012).

Examples of 32 historic catastrophic rock slope failures from Norway and around the world show that unstable rock slopes do not fail under aseismic conditions without any pre-failure slope deformation (HERMANN *et alii*, 2012). This classification system only focuses on aseismic failures because the timing of earthquakes cannot be predicted up to now, making early-warning of earthquake-triggered rockslides impossible. We have to highlight here that in Norway seismicity rates over the 20th century suggest that the region typically reveals one magnitude (M) 5 earthquake every 10 years and one M 7 earthquake every 1100 years (BUNGUM *et alii*, 1998, 2000, 2005). However, there are clear regional differences with most of the seismic activity concentrated in small areas located in the near-shore or off shore area (STANDARD NORGE, 2008) that should be considered in the risk management of rock slope fail-

ures. This has to be taken into account when assessing spontaneous (seismically-triggered rockslides) for that a minimum magnitude of M 6 was established by KEEFER (1984) based on 40 historical earthquakes. Historic observations over the past 200 years indicate that with the premise of an acceleration phase prior to collapse we could capture the vast amount of rock slope failures in Norway (FURSETH, 2006). Said that, triggers (e.g. seismic activity) with a longer recurrence period are not captured in this observational period, highlighting that this classification system cannot be used as a risk management tool alone, but has to be used especially in areas with higher levels of seismic activity in connection with seismic hazard maps as presented by STANDARD NORGE (2008).

Hence the hazard analysis focuses on capturing unfavorable geological conditions, morphological features expressing slope deformations and changes within the slope that can give a hint of the stability state of the slope as well as on the area that will be impacted by the direct impact of the rockslide or a related secondary effect. The risk classification focuses on the potential loss of life only.

This classification system is built for the special geographic and geological conditions in Norway that is dominated by crystalline rock and does not present large rock slopes with weak sedimentary rocks such as the Alps, Apennine or the Rocky Mountains. Other observations would have to be included in mountain terrains with thick weakly consolidated sedimentary or volcanic rocks. The classification system might also be applied in other areas in the world, but needs to be adapted to local geologic, geographic and climatic conditions. The classification system is flexible for such adaptations by giving the possibility to exclude some of the criteria used in Norway and to add new ones. We especially underline that today there is insufficient quantity of information on geological occurrences to support the prediction of large rock slope failures on geological conditions alone and that instrumental monitoring is the appropriate tool for monitoring changes in rock slope.

DEFINING FAILURE SCENARIOS

Deformation of unstable rock slopes can be either uniform over the entire slope or spatially distributed. In the latter case, deformation varies between different compartments of an unstable rock slope (also called parts, blocks or similar). This difference in deforma-

HAZARD AND RISK CLASSIFICATION FOR LARGE UNSTABLE ROCK SLOPES IN NORWAY

tion style also becomes evident when looking back into geological records indicating that some unstable slopes collapsed repeatedly while others slopes failed in a single event (e.g. HERMANN *et alii*, 2001; WILLENBERG, 2004; HERMANN *et alii*, 2006 and references there in, AA *et alii*, 2007). These multiple failure sites suggest that at some rock slopes parts of the rock mass can get to a critical state at different moments in time. These compartments may have different failure probabilities, different consequences and pose therefore also different levels of risk. One can define a scenario by a compartment of the unstable rock slope, which might fail in a single event and individually from other compartments. An additional hint to define failure scenarios is the analyses of historic and prehistoric failures along slope sections built by the same lithologies and controlled by the same structures.

Different scenarios are therefore justified and need to be analyzed at slopes that show a combination of:

- Different deformation rates
- Varying structural conditions
- Internal scarps, cracks and depression which dissect the unstable rock slope

Based on the combination of those observations the hazard and risk classification for each potential scenario has to be carried out independently.

In order to reduce costs, the development of scenarios has to be an iterative process in which detail of analysis increases stepwise following the principles outlined in Fig. 1. The term assessment is here used to describe a semi-quantitative evaluation carried out by the mapping geologist, while the term "analysis" is used here for more thorough, quantitative investigations.

HAZARD CLASSIFICATION

ORGANIZATION OF THE HAZARD CLASSIFICATION SYSTEM

The classification system uses nine criteria describing the present state of an unstable rock slope (Fig. 2). They can be arranged into two main groups: 1. the structural development of the unstable rock slope; 2. displacement rates and other signs of activity. For each criterion (κ_i) several conditions (χ_{ij}) are possible to choose from and a score (v_{ij}) is assigned to each condition. The sum of scores for the chosen conditions gives the total score, which is called hazard

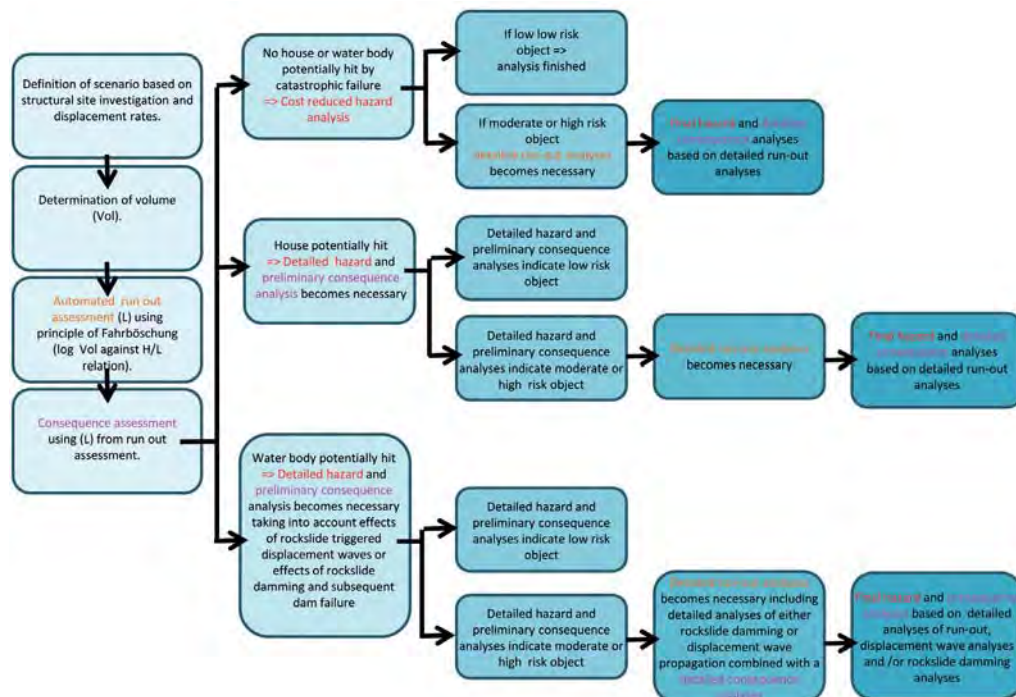


Fig. 1 - Development of the scenario based hazard and risk assessment by gradually increasing detail (from left to right) of hazard and consequence analyses in an iterative approach. The term assessment is here used for a semi-quantitative evaluation during project development, while analysis is a quantitative evaluation

R.L. HERMANN, T. OPPIKOFER, E. ANDA, L.H. BLIKRA, M. BÖHME, H. BUNKHOLT, G.B. CROSTA,
H. DAHLE, G. DEVOLI, L. FISCHER, M. JABOYEDOFF, S. LOEW, S. SÆTRE & F.X. YUGSI MOLINA

score, ρ (Equation 1):

$$\rho = \sum_i v_{ij} \quad (1)$$

with j corresponding to the chosen condition χ_{ij} for criterion κ_i .

Using the nine criteria, the hazard score, ρ , can range from 0 to 12. It is assumed that the likelihood of an unstable rock slope to fail increases with ρ .

CONDITION UNCERTAINTIES

Unstable rock slopes are complex landslide phenomena and it may often be difficult to choose only one of the conditions (χ_{ij}) for a given criterion (κ_i). In order to include these uncertainties, probabilities (p_{ij}) for each condition can be given. The average (expected) hazard score, $\bar{\rho}$, is obtained by summing all the scores (v_{ij}) multiplied by the conditions probabilities (Equation 2):

$$\bar{\rho} = \sum_i \sum_j p_{ij} v_{ij} \quad (2)$$

However, this average hazard score does not express the uncertainties on the individual criteria and therefore on the hazard score. In order to compute the entire range of possible outcomes, the criteria are organized in a decision tree. Each criterion, κ_i , represents a node of the decision tree and each condition, χ_{ij} , forms a branch of the tree. For each path of the tree, its hazard score, ρ_{path} , and its probability, ϕ_{path} , can be calculated using Equations (1) and (3), respectively:

$$\phi_{path} = \sum_i p_{ij} \quad (3)$$

with j corresponding to the chosen condition χ_{ij} for criterion κ_i .

Using scores and conditions for the nine criteria shown in Fig. 2 leads to 48'600 possible paths and probabilities for individual paths may be very low. However, several paths may lead to the same path hazard score, ρ_{path} . Therefore, the total probability of having a given hazard score corresponds to the sum of

1. Back-scarp	Score	Rel. prob.	Norm. prob.
Not developed	0	0	33.3 %
Partly open over width of slide body (few cm to m)	0.5	0	33.3 %
Fully open over width of slide body (few cm to m)	1	0	33.3 %
2. Potential sliding structures	Score	Rel. prob.	Norm. prob.
No penetrative structures dip out of the slope	0	0	33.3 %
Penetrative structures dip on average < 20 degree or steeper than the slope	0.5	0	33.3 %
Penetrative structures dip on average > 20 degree and daylight with the slope	1	0	33.3 %
3. Lateral release surfaces	Score	Rel. prob.	Norm. prob.
Not developed	0	0	20.0 %
Partly developed on 1 side	0.25	0	20.0 %
Fully developed or free slope on 1 side or partly developed on 2 sides	0.5	0	20.0 %
Fully developed or free slope on 1 side and partly developed on 1 side	0.75	0	20.0 %
Fully developed or free slope on 2 sides	1	0	20.0 %
4. Kinematic feasibility test	Score	Rel. prob.	Norm. prob.
Kinematic feasibility test does not allow for planar sliding, wedge sliding or toppling	0	0	20.0 %
Failure is partly kinematically possible (movement direction is more than $\pm 30^\circ$ to slope orientation)	0.5	0	20.0 %
Failure is kinematically possible (movement direction is less than $\pm 30^\circ$ to slope orientation)	0.75	0	20.0 %
Failure is partly kinematically possible on persistent discontinuities (movement direction is more than $\pm 30^\circ$ to slope orientation)	0.75	0	20.0 %
Failure is kinematically possible on persistent discontinuities (movement direction is less than $\pm 30^\circ$ to slope orientation)	1	0	20.0 %
5. Morphologic expression of the rupture surface	Score	Rel. prob.	Norm. prob.
No indication on slope morphology	0	0	33.3 %
Slope morphology suggests formation of a rupture surface (bulging, concavity-convexity, springs)	0.5	0	33.3 %
Continuous rupture surface is suggested by slope morphology and can be mapped out	1	0	33.3 %
6. Displacement rates	Score	Rel. prob.	Norm. prob.
No significant movement	0	0	16.7 %
0.2 - 0.5 cm/year	1	0	16.7 %
0.5 - 1 cm/year	2	0	16.7 %
1 - 4 cm/year	3	0	16.7 %
4 - 10 cm/year	4	0	16.7 %
> 10 cm/year	5	0	16.7 %
7. Acceleration (if velocity is >0.5 cm/yr and <10 cm/yr)	Score	Rel. prob.	Norm. prob.
No acceleration or change in displacement rates	0	0	50.0 %
Increase in displacement rates	1	0	50.0 %
8. Increase of rock fall activity	Score	Rel. prob.	Norm. prob.
No increase of rock fall activity	0	0	50.0 %
Increase of rock fall activity	1	0	50.0 %
9. Past events	Score	Rel. prob.	Norm. prob.
No post-glacial events of similar size	0	0	33.3 %
One or several events older than 5000 years of similar size	0.5	0	33.3 %
One or several events younger than 5000 years of similar size	1	0	33.3 %

Fig. 2 - Nine criteria describing the present state of the slope: For each criterion several conditions are possible to choose from and a score is assigned to each condition

HAZARD AND RISK CLASSIFICATION FOR LARGE UNSTABLE ROCK SLOPES IN NORWAY

all ϕ path with the same ppath.

We have developed a macro in Microsoft Visual Basic 6.5 (implemented in Microsoft Excel® 2007) that is downloadable at the same website as the report (see HERMANN *et alii*, 2012 in the references). It computes all possible paths of the decision tree including ppath and ϕ path and creates the sum of all ϕ path leading to the same ppath. Using the scores presented in Figure 2, the path hazard score, ppath, ranges from 0 to 12 with steps of 0.25. The final outcome is a probability for each of these 49 different hazard scores, ϕ score. The probability distribution of ϕ score allows obtaining the minimum and maximum hazard scores, ρ , using the chosen probabilities, p_{ij} . The modal value indicates the most probable ρ located at the peak of the probability distribution, while the mean value is computed using Equation 2.

HAZARD CLASSES

Simplified to allow for effective communication, the hazard score is divided into five hazard classes using equal intervals (Fig. 3). Equal intervals are preferred over expert-knowledge-based class limits, because the latter are more controversial and need to be supported by calibrations of past rock slope failures. For example, one could define the very low hazard class by slopes that move since more than 10,000 years and that did not yet fail catastrophically; hence

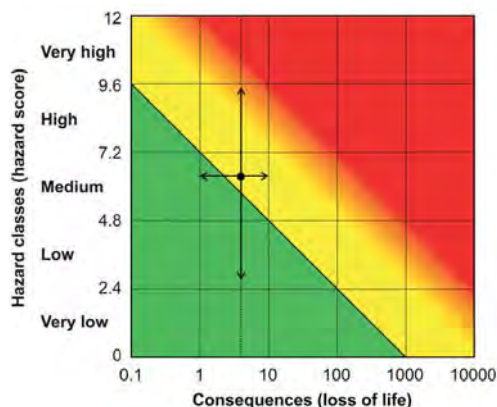


Fig. 3 - Risk classification matrix for follow-up with monitoring and further investigations of unstable rock slopes in Norway: green = low risk; yellow = moderate risk; red = high risk. The risk of an unstable rock slope is represented by its mean value, the minimum and maximum consequences (horizontal arrows), the 5% and 95% percentiles of the hazard score (vertical arrows) and the minimum and maximum scores of the hazard analysis (dotted line)

dating the deformation could solve the problem. However this information from the geological past does not necessarily indicate anything on the performance of the slope in future and continuous fatigue of rock in the past 10,000 years could have led to a critical stability today. Similarly, rock slopes that failed catastrophically could define the very high hazard class, if the slope conditions in the period of months/years prior to the catastrophic failure are used. Unfortunately, there is generally not enough information available on past catastrophic rock slope failures, in order to assess their hazard score with satisfying reliability.

The advantage of this decision tree analysis is obvious: instead of giving a single hazard score for an unstable rock slope, the proposed technique with the decision tree analysis gives a range of probable hazard classes.

Note that due to the use of probabilities in the classification system, it can also be used to determine whether more detailed analyses are necessary. For example, often during early site investigations, no information is available on the displacement rate of the slide. Hence, this high level of uncertainty should be expressed in the analyses. If the result of the analyses indicates that there is a probability that the sites might be defined to be of moderate or high risk, then more investigations become necessary focusing on defining the velocity. If also under the worst case assessment the site remains a low risk object, no further investigations are required.

CONSEQUENCE AND RISK ANALYSIS AND SUGGESTED SURVEILLANCE OF UNSTABLE ROCK SLOPES

FELL *et alii* (2008) define risk as "a measure of the probability and severity of an adverse effect to health, property or the environment". We focus in our consequence/risk analyses on loss of life only. "Risk is often estimated by the product of probability of a phenomenon of a given magnitude times the consequences" (p. 86). The risk, R , can be calculated using the widely used risk equation (modified from LEROI, 1996; FELL *et alii*, 2005) (Equation 4):

$$R = P_F \times P_P \times P_E \times V \times E \quad (4)$$

with P_F = probability of failure; P_P = probability of propagation (probability of the landslide and its secondary effects reaching the element at risk); P_E =

R.L. HERMANN, T. OPPIKOFER, E. ANDA, L.H. BLIKRA, M. BÖHME, H. BUNKHOLT, G.B. CROSTA,
H. DAHLE, G. DEVOLI, L. FISCHER, M. JABOYEDOFF, S. LOEW, S. SÆTRE & F.X. YUGSI MOLINA

probability of presence of the element at risk; V = vulnerability of the element at risk to the landslide event (degree of loss from 0% to 100%); E = element at risk (i.e. exposed population).

Several of the factors of Equation 4 are difficult to quantify within the framework of this hazard and risk classification for unstable rock slopes in Norway, especially the probability of failure, P_F , which cannot be assessed with today's technical understanding of large unstable rock slopes within the timeframe of hundreds to thousands years. For this hazard and risk classification system the hazard score is used as a qualitative measure of P_F .

PRELIMINARY CONSEQUENCE AND RISK ANALYSIS

The preliminary risk analysis is a first, rough analysis aiming to distinguish between low risk objects and medium to high risk objects that require more detailed risk analyses. Therefore, a worst case scenario is assumed for the preliminary risk assessment and P_F , P_E and V are set to 1 and E is the maximum number of persons living and being present or transit in the affected area.

This means that the entire area computed in the run-out assessment will be reached by the rock avalanche or displacement wave ($P_F = 1$), all the population and persons that transit are present in the affected area ($P_E = 1$) and their loss of life is certain ($V = 1$). The number of potential life losses is thus equal to E .

DETAILED CONSEQUENCE AND RISK ANALYSIS

For potential medium to high risk objects based on the preliminary risk assessment a detailed consequence analysis becomes necessary (Fig. 1). This includes a more detailed quantification of the parameters in Equation 4. Detailed run-out modeling (and displacement wave assessment if relevant) allows the determination of P_F . The parameter P_E is mainly depending on the building type (house, office, shop, school etc.) and can be determined roughly at a national level. Different vulnerabilities can be defined, depending if a building is hit directly by a rock avalanche and loss of life is nearly certain ($V=1$) or if it is hit by a displacement wave that have an assumed survival rate of 30% ($V=0.7$) (BLIKRA *et alii*, 2006b). The number of potential life losses is then obtained by

multiplying P_F , P_E , V and E for each building and summing over the entire area affected by a rock avalanche and its secondary effects. Areas frequently visited by tourists and all infrastructure with persons in transit are assessed in the same manner as buildings (e.g., BLIKRA *et alii*, 2013).

An exception from the approach outlined above, is up- and downstream flooding related to rockslide dams. In contrast to the direct impact of a rockslide on a building or the impact of a rockslide-triggered displacement wave on a building, people affected by upstream and downstream flooding related to landslide damming and subsequent dam breaching can be evacuated from the building. Hence this secondary effect is treated as a flood hazard and in these cases the evaluation of hazard and risk related to dam formation and dam failure should be included as outlined in DAHLE *et alii* (2011a) and HERMANN *et alii* (2013b). However, the final risk classification will mainly be based on the number of people which might lose their life in a potential event.

RISK MATRIX AND RISK CLASSES

This classification system combines the hazard score and the potential life losses in a risk matrix (Fig. 3). Isorisk lines are often used in a risk matrix to distinguish between acceptable, tolerable and unacceptable risks as proposed for example for landslides and rock falls from natural slopes in Hong Kong (GEOTECHNICAL ENGINEERING OFFICE, 1998). However, these isorisk lines are not applicable for the present risk classification system, since the hazard score is only a qualitative measure of the probability of failure and the classification focuses on rock slope failures preceded by an acceleration phase only, thus excluding earthquake-triggered rock slope failures. The risk can therefore not be expressed in terms of number of casualties per year, and this is not a risk management tool in its own but a support for risk management.

The purpose of the risk matrix is helping to decide on follow-up actions for unstable rock slopes including monitoring, further field investigations, and/or possible mitigation measures. For that reason the risk matrix is divided into three risk classes: low (green), medium (yellow) and high (red). The limit between the low and medium risk classes is set along the diagonal going from the high hazard class with very low consequences (0.1 to 1 casualties) down to very low hazard class with high consequences (100 to 1000 cas-

HAZARD AND RISK CLASSIFICATION FOR LARGE UNSTABLE ROCK SLOPES IN NORWAY

ualties). It is expected that most of the sites in Norway fall into the low risk class. Those sites are either considered to have low consequences and further follow up is not economically sustainable, or the site would require dramatic changes in the geological conditions prior to failure. Such changes could be captured with a scanning of geological conditions by means of field visit or remote sensing data interpretation every 10 to 20 years. Medium risk sites are expected to be less common in Norway. However, potential consequences are higher or the probability of failure is higher so that a low-level follow up is recommended to reduce the risk level. The limit between the medium and high risk classes is not precisely defined and is shown as a yellow to red gradient. In this transition zone between medium and high risk, in general further site-specific geological criteria are needed to be studied in order to have a good enough understanding for a final classification. These sites will generally require additional expert judgement that will be used to classify the risk.

REPRESENTING UNSTABLE ROCK SLOPES IN THE RISK MATRIX

An unstable rock slope can be placed in the risk matrix based on the hazard analysis and the consequence analysis. As both factors have uncertainties, the minimum and maximum values for hazard and consequences can also be plotted in addition to the mean value (Fig 3).

The uncertainties on the hazard score and the consequences can have an influence on the risk classification and on the decision on follow-up activities. An unstable rock slope might for example be classified as low risk based on the most likely hazard class, but there might be a certain probability that it ends up as a medium risk. If this probability exceeds 5%, more site investigations should be considered in order to reduce the uncertainties on the assessment of conditions for the different criteria. If this is not feasible, the unstable rock slope might be classified with the higher risk class. The 5% and 95% percentiles of the hazard score are therefore also shown in the risk matrix (Fig. 3). Similarly, there is uncertainty related to the consequences and more detailed consequence analyses could be considered in order to reduce the uncertainty. The decision on follow-up activities will be made after a thorough discussion of the uncertainties related to both hazard and consequences.

IMPLICATION OF THE RISK CLASSIFICATION

The risk classification of unstable rock slopes in Norway will be used by the NGU and the NVE in order to decide on follow-up investigations and mitigation measures. It will also help municipalities and other stakeholders as a basis for land use planning and contingency planning.

A document describing the implications of the risk classification related to the low, medium and high risk classes will be presented in due time by NVE. This will include implications related to land use planning, monitoring and early-warning, contingency planning and structural measures. All decisions on mitigation measures will be based on cost-benefit reasoning that will be explained in more detail in the NVE document.

In general, low risk objects will not be followed up except a routine scanning in the field or based on remote sensing data (air photos, satellite data) every 10 to 20 years. For medium risk objects, periodic monitoring is recommended and the techniques used and the measurement intervals applied will depend on geological conditions on the site, applicability of the various methods under cost-benefit reasoning. For high-risk objects mitigation measures are recommended that will often be coupled monitoring and early warning techniques. This has to be discussed among risk owners and geoscientists.

SUMMARY AND DISCUSSION

Due to the geomorphologic conditions of Norway with high mountains deeply penetrated by fjords, large rock slope failures occurred repeatedly in the past, often accompanied by secondary effects such as displacement waves. Therefore, in contrast to other mountain belts in the world, these rock slope failures resulted in disasters with a high death toll far from the source area of the rock slope failure. As such events will also occur in the future, systematic mapping of rock slopes has been started in the first decade of the 21st century and today more than 300 unstable rock slopes are known. This high number necessitated a quantitative classification system based on hazard and risk related to the potential failures that should help deciding on follow-up activities. This system was elaborated in a large effort combining national and international experts from various disciplines in earth sciences. During the elaboration of this system it became obvious that today there

R.L. HERMANN, T. OPPIKOFER, E. ANDA, L.H. BLIKRA, M. BÖHME, H. BUNKHOLT, G.B. CROSTA,
H. DAHLE, G. DEVOLI, L. FISCHER, M. JABOYEDOFF, S. LOEW, S. SÆTRE & F.X. YUGSI MOLINA

is not enough scientific knowledge to predict the timing of large rock slope failures, and that more research is needed and much can be learned from rock slope failures that have been monitored in the years prior to failure. Therefore, we qualitatively classified the probability of failure in very high, high, moderate, low and very low.

Our hazard classification is based on two sets of criteria: 1) Structural site investigations including analysis of the development of a back-scarp, lateral boundaries and basal sliding surface. This includes a kinematic analysis that tests if rock sliding or toppling is kinematically feasible with respect to the slope orientation, the persistence of main structures and the morphologic expression of the sliding surface. 2) The analysis of the activity of the slope is primarily based on the slide velocity, but also includes the change of deformation rates (acceleration), observation of rock-fall activity and historic or prehistoric events. For each criterion several observations are possible to choose from. Each observation is associated to a score and the sum of all scores gives the total score for a scenario. The weighting of these scores has changed from the first proposal of the classification system (HERMANN *et alii*, 2010) over a preliminary usage of it (DAHLE *et alii*, 2011b) to this final version. For example, in this final version the historic and prehistoric events are weighted much lower than in the first proposal. This seemed necessary as the occurrence of a prehistoric event alone should not raise a site by one hazard class without any signs of present day activity. Furthermore, the displacement rates and morphological expressions/kinematic feasibility of failure are weighted equally. This weighting should be revised once statistically adequate information becomes available.

As all these observations are connected to uncertainties, the classification system is organized in a decision tree where probabilities to each observation can be given. All possibilities in the decision tree are computed and the individual probabilities giving the same total score are summed. Basic statistics show the minimum and maximum total scores of a scenario, as well as the mean and modal value. The final output is a cumulative frequency distribution divided into several classes, which are interpreted as hazard classes.

Within the completion time of this document a rock slope failure occurred in Switzerland that has been monitored for more than a decade (LOEW *et alii*,

2012). The analysis of pre-failure conditions indicated a high hazard for that slope (in HERMANN *et alii*, 2012). We take this as a first positive test of our classification system. Furthermore, the probability of the Åknes rock slope in Norway was assessed earlier, and independently of this system, and the results are comparable (BLIKRA *et alii*, 2005; HERMANN *et alii*, 2012). Nevertheless we want to highlight that this classification system should be updated once more scientific knowledge becomes available, and that more research is necessary to better understand failure processes of large rock slope failures through time. These efforts will then hopefully allow replace the qualitative hazard analysis with a quantitative hazard analysis.

The consequence analysis is focused on number of loss of lives only and we start with a conservative approach by assuming that all people that might be hit by a rock avalanche or a rockslide-triggered displacement wave are likely to lose their lives. For potential high-risk objects a more detailed analysis is carried out that includes the probability of surviving the rockslide triggered displacement wave. Both the qualitative hazard analysis and the quantitative consequence analyses are combined in a risk matrix for a risk analysis. Three different risk classes are defined. Low risk where no further follow up is needed, medium risk where periodic monitoring of the rock slope is suggested and high risk that suggest for further follow up. Follow up for high risk objects has to be discussed with the risk owners and could be resettlement, periodic monitoring, continuous monitoring coupled with early warning or any other mitigation measure that has to be decided after cost-benefit reasoning. Often additional geological information to those summarized in this classification has to be assembled for optimal monitoring practices and a thorough slope stability analysis. This might include subsurface information obtained from core logging, geophysics and hydrological investigations.

Finally we want to stress again that the hazard and risk classification system is not a risk management tool in itself as it does not include seismically triggered rock slope failures. It is thus a support tool for risk management that will help to decide on follow up (e.g. no follow up necessary, periodic monitoring is recommended to reduce the risk, more studies are required and/or risk mitigation measures should be taken). This is also not a guideline for early warning practices as these are regulated in Norway by the

HAZARD AND RISK CLASSIFICATION FOR LARGE UNSTABLE ROCK SLOPES IN NORWAY

building code TEK 10 § 7.4 (Byggeteknisk forskrift, 2010) and we thus do not include a discussion on triggering mechanism here.

ACKNOWLEDGEMENTS

The authors gratefully thank Norwegian Water and Energy Directorate that made a workshop possible in 2010 that started the discussion on the document. Numerous scientist (Jordi Corominas, Ollianne

Eikenæs, Corey Froese, Jarle Hole, Aline Saintot) are thanked that initially have been in the discussion of elaborating the classification system that later voluntarily dropped out as the discussion was very time consuming. Also Carl Harbitz (Norwegian Geotechnical Institute) and Hallvard Berg (NVE) contributed to the classification system over a long period.

REFERENCES

- AA A.R., SJÅSTAD J., SØNSTEGAARD E. & BLIKRA L.H. (2007) - *Chronology of Holocene rock-avalanche deposits based on Schmidt-hammer, relative dating and dust stratigraphy in nearby bog deposits, Vora, inner Nordfjord, Norway*. The Holocene, **17**: 955-964.
- BLIKRA L.H., BÖHME M., DEHLS J., HERMANN R.L., OPPIKOEFER T., REDFIELD T.F., RØNNING J.S., YUGSI MOLINA F., DOMAAS U., PFAFFHUBER A., HENRIKSEN H., HOLE J. & KRISTENSEN L. (2013) - *The unstable phyllitic rocks in Stampa –Flåm, western Norway: compilation, scenarios, risk and recommendations*. NVE report no. x, in press.
- BLIKRA L.H., LONGVA O., BRAATHAN A., ANDA E., DEHLS J.F. & STALSBERG K. (2006a) - *Rock slope failures in Norwegian fjord areas; examples, spatial distribution and temporal pattern*. In: EVANS S.G., SCARASCIA MUGNOZZA G., STROM A. & HERMANN R.L. *Landslides from massive rock slope failures*. 475-496. NATO Science Series IV (49), Earth and Environmental Sciences, Springer, Dordrecht, Netherland.
- BLIKRA L.H., ANDA E., BELSBY S., JOGERUD K. & KLEMPPE Ø. (2006b) - *Åknes/Tafjord prosjektet, Statusrapport for Arbeidsgruppe 1 8undersøking og overvakning*. Åknes/Tafjord-Prosjektet, 57 pp.
- BLIKRA L.H., LONGVA O., HARBITZ C. & LØVHOLT F. (2005) - *Quantification of rock-avalanche and tsunami hazard in Storfjorden, western Norway*. In: SENNESET K., FLAATE K. & LARSEN J.O. (EDS.). *Landslides and Avalanches ICFL 2005 Norway*. Taylor & Francis Group, London.
- BUNGUM H., LINDHOLM C.D., DAHLE A., HICKS E., HØGDEN H., NADIM F., HOLME J.K. & HARBITZ C. (1998) - *Development of seismic zonation for Norway*. Report for Norwegian Council for Building Standardization (on behalf of a consortium of industrial partners). NORSAR and Norwegian Geotechnical Institute, Oslo, 187 pp.
- BUNGUM H., LINDHOLM C.D., DAHLE A., WOO G., NADIM F., HOLME J.K., GUDMESTAD O.T., HAGBERG T. & KARTHIGEYAN K. (2000) - *New seismic zoning maps for Norway, the North Sea and the UK*. Seismological Research Letters, **71**: 687-697.
- BUNGUM H., LINDHOLM C. & FALEIDE J.I. (2005) - *Postglacial seismicity offshore mid-Norway with emphasis on spatio-temporal-magnitudinal variations*. Marine and Petroleum Geology, **22**: 137-148.
- BUNKHOLT H., NORDAHL B., HERMANN R.L., OPPIKOEFER T., FISCHER L., BLIKRA L.H., ANDA E., DAHLE H., & SÆTRE S. (2013) - *Database of unstable rock slopes of Norway*. In: MARGOTTINI C., CANUTI P. & SASSA K. (EDS.). *Landslide science and practise*. Springer Verlag, Berlin. in press.
- BYGGETEKNISK FORSKRIFT (Tek 10) (2010) - <http://www.lovdata.no/cgi-wift/lides?doc=/sf/sf-20100326-0489.html>.
- DAHLE H., BJERKE P.L., CROSTA G., HERMANN R.L., ANDA E. & SAINTOT S. (2011a) - *Faresoner for utløp, oppdemming og flom som følge av fjellskredfare ved Mannen*. NGU rapport 2011.058, 41 pp.
- DAHLE H., ANDA E., SÆTRE S., SAINTOT A., BÖHME M., HERMANN R.L., OPPIKOEFER T., DALSEGG E., RØNNING J.S. & DERRON M.H. (2011b) - *Risiko og sårbarhetsanalyse for fjellskred i Møre og Romsdal*. 105 pp.
- EVANS S.G. & HUNGR O. (1993) - *The assessment of rockfall hazard at the base of talus slopes*. Canadian Geotechnical Journal, **30** (4), 620-634.
- FELL R., COROMINAS J., BONNARD C., CASCINI L., LEROI E. & SAVAGE W.Z. (2008) - *Guidelines for landslide susceptibility, hazard and risk zoning for land use planning*. Engineering Geology, **102** (3-4): 85-98.
- FELL R., HO K.K.S., LACASSE S. & LEROI E. (2005) - *A framework for landslide risk assessment and management*. In: HUNGR O., FELL R., COUTURE R. & EBERHARDT E. (EDS.). *Landslide Risk Management*: 3-26, Taylor & Francis, London.
- FURSETH A. (2006) - *Skredulykker i Norge*. Tun Forlag, Oslo.

R.L. HERMANN, T. OPPIKOFE, E. ANDA, L.H. BLIKRA, M. BÖHME, H. BUNKHOLT, G.B. CROSTA,
H. DAHLE, G. DEVOLI, L. FISCHER, M. JABOYEDOFF, S. LOEW, S. SÆTRE & F.X. YUGSI MOLINA

- GEOTECHNICAL ENGINEERING OFFICE (1998) - *Landslides and boulder falls from natural terrain: interim risk guidelines*. GEO report no. 75: ERM-Hong Kong, Ltd.
- GLASTONBURY J. & FELL R. (2008) - *A decision analysis framework for the assessment of likely post-failure velocity of translational and compound natural rock slope landslides*. Canadian Geotechnical Journal, **45**: 329-350.
- HANTZ D., DUSSAUGE C. & VENGEON J.-M. (2002) - *Méthode historique, géomécanique, probabiliste: approche probabiliste par combinaison d'études géomécaniques et statistique d'éboulements (LIRIGM)*. In: CARERE K., RATTO S. & ZANOLINI F. (EDS.), *Prévention des mouvements de versants et des instabilités de falaises: confrontation des méthodes d'étude des éboulements rocheux dans l'arc alpin*. Programme Interreg IIC - "Falaises", Aosta, Italy: 132-154.
- HERMANN R.L., BLIKRA L.H., ANDA E., SAINTOT A., DAHLE H., OPPIKOFE T., FISCHER L., BUNKHOLT, H., BÖHME M., DEHLS J., LAUKENS T.R., REDFIELD T.F., OSMUNDSEN P.T. & EIKEN T. (2013a) - *Systematic mapping and hazard and risk classification of unstable rock slopes with the potential of forming rock avalanches in Norway*. In: MARGOTTINI C., CANUTI P. & SASSA K. (EDS.), *Landslide Science and Practise*. Springer, Berlin. in press.
- HERMANN R.L., DAHLE H., BJERKE P.L., CROSTA G.B., ANDA E., BLIKRA L.H., SAINTOT A., LONGVA O. & EIKEN T. (2013b) - *Rock slide dams in Møre og Romsdal county, Norway: examples for the hazard and potential of rock slide dams*. In: MARGOTTINI C., CANUTI P. & SASSA K. (EDS.), *Landslide Science and Practise*. Springer, Berlin. in press.
- HERMANN R.L., OPPIKOFE T., ANDA E., BLIKRA L.H., BÖHME M., BUNKHOLT H., CROSTA G.B., DAHLE H., DEVOLI G., FISCHER L., JABOYEDOFF M., LOEW S., SÆTRE S., & YUGSI MOLINA F. (2012) - *Recommended hazard and risk classification system for large unstable rock slopes in Norway*. NGU-rapport 2012.029, <http://www.ngu.no/no/hm/Publikasjoner/Rapporter/2012/2012-029/>
- HERMANN R.L., HANSEN L., SLETTEN K., BÖHME M., BUNKHOLT H.S.S., DEHLS J.F., EILERTSEN R.S., FISCHER L., L'HEUREUX J.S., HØGAAS F., NORDAHL B., OPPIKOFE T., RUBENSDOTTER L., SOLBERG I.-L., STALSBERG K. & YUGSI MOLINA F.X. (2012) - *Systematic geological mapping for landslide understanding in the Norwegian context*. In: EBERHARDT E., FROESE C., TURNER K. & LEROUËL S. (EDS.), *Landslides and engineered slopes: protecting society through improved understanding*: 265-271, Taylor & Francis Group, London.
- HERMANN R.L. & LONGVA O. (2012) - *Rapid rock-slope failures*. In: CLAGUE J.J. & STEAD D. (EDS.), *Landslides: Types, Mechanisms and Modeling*: 59-70, Cambridge University Press.
- HERMANN R.L., ANDA E., HENDERSON I., DAHLE H., SAINTOT A., BLIKRA L.H., BÖHME M., DEHLS J., REDFIELD T. F. & EIKEN T. (2010) - *Towards a hazard classification system for large rock slope failures in Norway*. European geosciences Union, 02-07 Mai 2010. Vienna, Austria. Geophysical Research Abstracts. 12: EGU2010-13657.
- HERMANN R.L., BLIKRA L.H., NAUMANN M., NILSEN B., PANTHI K.K., STROMEYER D. & LONGVA O. (2006) - *Examples of multiple rock-slope collapses from Köfels (Ötztal valley, Austria) and western Norway*. Engineering Geology, **83** (1-3): 94-108.
- HERMANN R.L., NIEDERMANN S., VILLANUEVA GARCIA A., SOSA GOMEZ J., & STRECKER M.R. (2001) - *Neotectonics and catastrophic failures of mountain fronts in the southern intra-Andean Puna Plateau, Argentina*. Geology, **29** (7): 619-623.
- HØST J., DERRON M.H. & SLETTEN K. (2013) - *Digital rockfall and snow avalanches susceptibility mapping in Norway*. In: MARGOTTINI C., CANUTI P. & SASSA K. (EDS.), *Landslide science and practise*. Springer, Berlin. in press.
- HUNGR O. & EVANS S.G. (2004) - *The occurrence and classification of massive rock slope failure*. Felsbau, **22** (1): 1-12.
- KEEFER D.K. (1984) - *Landslides caused by earthquakes*. Geological Society of America Bulletin, **95**: 406-421.
- JABOYEDOFF M., DERRON M.-H., PEDRAZZINI A., BLIKRA L.H., CROSTA G.B., FROESE C., HERMANN R.L., OPPIKOFE T., BÖHME M., STEAD D. (2012) - *Fast assessment of susceptibility of massive rock instabilities*. In *Landslides and engineered slopes: Protecting society through improved understanding*. In: *Landslides and engineered slopes: protecting society through improved understanding*. 459-465, Taylor & Francis Group, London.
- LEROI E., BONNARD C., FELL R., MCINNES R. (2005) - *Risk assessment and management*. In: HUNGR O., FELL R., COUTURE R. & EBERHARDT E. (EDS.), *Landslide risk management*: 159-198, Taylor & Francis, London.
- LOEW S., GISCHIG V., MOORE J.R. & KELLER-SIGNER A. (2012) - *Monitoring of potentially catastrophic rockslides*. In: *Landslides and engineered slopes: protecting society through improved understanding*: 101-116, Taylor & Francis Group, London.
- STANDARD NORGE (2008) - *Eurokode 8: Prosjektering av konstruksjoner for seismiske påvirkning. Del 1: Allmenne regler, seismiske laster og regler for bygninger*. NS-EN 1998-1: 2004+NA.2008, p. 229.
- WILLENBERG H. (2004) - *Geologic and kinematic model of a complex landslide in crystalline rock (Randa, Switzerland)*. Ph.D thesis, Earth Sciences Department, Swiss Federal Institute of Technology, Zurich.

APPENDIX 3: SAINTOT ET AL. (2012) LARGE GRAVITATIONAL ROCK SLOPE DEFORMATION IN ROMSDALEN VALLEY (WESTERN NORWAY)

Full citation: Saintot, A., Oppikofer, T., Derron, M.-H. and Henderson, I. (2012) Large gravitational rock slope deformation in Romsdalen valley (Western Norway). *Revista de la Asociación Geológica Argentina*, **69**, 3, 354-371.

LARGE GRAVITATIONAL ROCK SLOPE DEFORMATION IN ROMSDALEN VALLEY (WESTERN NORWAY)

Aline SAINTOT^{1,2*}, Thierry OPPIKOFER¹, Marc-Henri DERRON³ and Iain HENDERSON¹

¹Geological Survey of Norway (NGU), Postbox 6315 Sluppen, 7491 Trondheim, Norway

²Department of Endogenous Geology, Ruhr University Bochum, Universitätsstr. 150, 44780 Bochum, Germany

³Institute of Geomatics and Risk Analysis, University of Lausanne, Amphipôle, 1015 Lausanne, Switzerland

(*)Corresponding author: aline.saintot@rub.de

ABSTRACT

Large gravitational rock slope deformation affects Precambrian gneisses at four localities of the Romsdalen valley of Western Norway. At each locality, detailed studies have allowed to determine the mechanism of deformation and to assess the degree of susceptibility for failure. 1) Svarttinden is a 4.3 Mm³ translational rockslide. Its single basal detachment developed along a foliation-parallel cataclastic fault. Although a rockslide occurred along the same detachment and the deposits reached the edge of the plateau, no displacement of the current instability is detected. 2) At Flatmark distinct 2-25 Mm³ blocks detached from the edge of the plateau by an opening along the steep foliation. The collapse of the blocks is explained by a complex mechanism of sliding and toppling. No displacement is actually detected on the instabilities. 3) At Børa blocks located at the edge of the plateau deformed by the same mechanism as at Flatmark. They have a maximum volume of 0.5 Mm³ and displacement rates of 0.2-2 cm/year. The deformation at Børa has affected a large part of the plateau and the entire deformed volume would be of 50-200 Mm³ but it is currently inactive. 4) A wedge failure at the edge of Mannen plateau is inferred to allow the 4-5 cm/year downward displacement of a 2-3.5 Mm³ instability. The high susceptibility of failure led to a permanent monitoring of the site since 2009.

Keywords: *rockslide, structural analysis, mechanism.*

RESUMEN

Deformación gravitacional de las vertientes rocosas del valle de Romsdalen (Noruega occidental).

Una gran deformación gravitacional afecta unidades gnéissicas precámbricas en cuatro localidades del valle Romsdalen, Oeste de Noruega. En cada localidad, estudios detallados permitieron determinar el mecanismo de deformación y evaluar el grado de susceptibilidad al colapso. 1) Svarttinden es un deslizamiento translacional de 4.3 Mm³. Su plano basal se desarrolló a lo largo de una falla paralela a planos con deformación cataclástica. Si bien un deslizamiento tuvo lugar a lo largo del mismo plano basal, y los depósitos alcanzaron el borde del *plateau*, no se detecta desplazamiento en la zona inestable. 2) En Flatmark, bloques de 2-25 Mm³ se desprendieron del borde de la meseta a partir de la apertura de planos de foliación de gran inclinación. El colapso de bloques es explicado por un complejo mecanismo de deslizamiento y volcamiento. No se detecta actualmente desplazamiento en las zonas inestables. 3) En Børa, bloques ubicados en el borde de la meseta fueron deformados por el mismo mecanismo que en Flatmark. Los mismos tienen un volumen máximo de 0.5 Mm³ y tasas de desplazamiento de 0.2-2 cm/a. La deformación en Børa ha afectado gran parte de la meseta y el total del volumen deformado sería de 50-200 Mm³, si bien se encuentra actualmente inactiva. 4) Un colapso en cuña en el borde de la meseta Mannen permitiría un desplazamiento de 4-5 cm/a pendiente abajo, de 2-3.5 Mm³. La alta susceptibilidad al colapso, dio lugar a un monitoreo permanente del sitio desde el año 2009.

Palabras clave. *deslizamiento, análisis estructural, mecanismo.*

INTRODUCTION

Western Norway is a region of important topographic gradient. Like in the Andes and other mountain regions in the world, the relief is prone to large rock slope failures. As the latter may have catastrophic

consequences in terms of life loss, the Norwegian government launched a long term program to map and study the sites of large gravitational rock slope deformation. The large instabilities that directly endanger the community are under investigation for detection of displacements. Aside, geologi-

cal investigations for a better understanding of the major features that control these instabilities are carried out. This is the case for the four large gravitational rock slope instabilities at Svarttinden, Flatmark, Børa and Mannen, in Romsdalen valley for which the susceptibility for failure has to

be accurately determined (Figs. 1 and 2). Hence, multi-disciplinary studies of these instabilities are carried out for approximately 10 years and rock slope displacements are detected at Børa and Mannen. The 30 km long Romsdalen valley is an over-deepened U-shaped glacial valley, typical of the extreme alpine relief of Western Norway (Etzelmüller *et al.* 2007; Fig. 1). It is characterized by the highest spatial density of past, including historical, rock slope failures in Norway. The present contribution focuses on the structural development of the four instabilities with the principal aim of understanding the failure mechanism. All four developed on the southern slope of the valley in a suite of intensively tectonized high-grade metamorphic Precambrian gneisses. Studies of large rock slope instabilities in similar intrinsically strong rocks have demonstrated the quasi-systematic reactivation of inherited structures in the gravity-driven deformation and large volumes of these types of rocks effectively destabilize where the pre-existing structures favorably dip relatively to the slope (e.g. Cruden 1976, Mahr 1977, Varnes 1978, Giraud *et al.* 1990, Guzzetti *et al.* 1996, Julian and Anthony 1996, Sauchyn *et al.* 1998, Hermanns and Strecker 1999, Agliardi *et al.* 2001, Kellogg 2001, Eber-

hardt *et al.* 2004, Brideau *et al.* 2005, 2009, El Bedoui *et al.* 2008, Jaboyedoff *et al.* 2009, Welkner *et al.* 2010). The same conclusion is drawn from extensive studies on the development of large rock slope instabilities over Western Norway with, in many cases, the metamorphic foliation accommodating a prominent part of the deformation (e.g. Braathen *et al.* 2004, Henderson *et al.* 2006, Ganerød *et al.* 2008, Oppikofer 2009, Böhme *et al.* 2011, Jaboyedoff *et al.* 2011; Oppikofer *et al.* 2011, Saintot *et al.* 2011b). Field studies (Henderson and Saintot 2007) combined with the inspection of aerial photographs and analyses of meter-scale resolution Digital Elevation Model (DEM) from airborne laser scanning (ALS) and terrestrial laser scanning (TLS; see in Oppikofer *et al.* (2012, this volume) for an exhaustive description of the latter) result in detailed structural maps and dataset collections, which allow us to determine the type of slope deformation as well as to assess the kinematics of the potential failure at each site. With the help of independent data (occurrence of previous failures, monitoring of displacement by differential Global Positioning System (dGPS), etc.) a qualitative assessment of the susceptibility for failure is attempted. The term “susceptibility for failure” is used here instead for “hazard”,

because for the investigated rock slope instabilities there are no temporal constraints on the likelihood of failure, which according to Fell *et al.* (2008) are necessary for a thorough “hazard” assessment.

REGIONAL BEDROCK AND QUATERNARY GEOLOGY

Romsdal valley cuts into the crystalline basement of the Western Gneiss Region of Norway. The bedrock belongs to the severely deformed and tectonized Precambrian autochthon (or para-autochthon) of the Caledonides (Roberts and Gee 1985). Three geological basement units are identified along the Romsdalen valley by Tveten *et al.* (1998). Most of the area is covered by the typical, and probably the oldest, granitic to dioritic gneiss unit of the basement (Fig. 2). The instabilities at Svarttinden, Flatmark and Børa developed in this unit. A lens of coarse-grained granitic and augen gneisses of meso- and neo-Proterozoic ages (1600-542 Ma) crops out north-east of the studied area (Fig. 2). A widespread unit consists of a quartz-rich gneiss unit characterized by sillimanite and kyanite of uncertain ages spanning from Proterozoic to Paleozoic. The instability at Mannen developed in this unit.

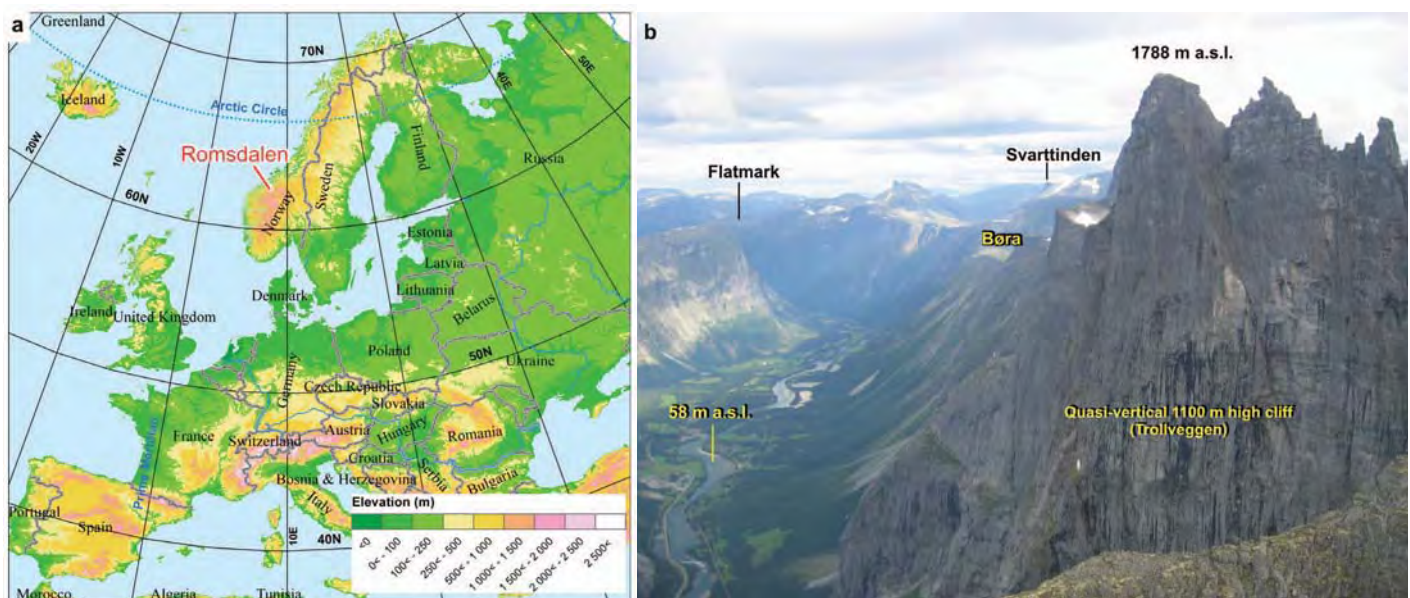


Figure 1. a) Topographic map of Europe with Norway showing an Alpine relief and location of Romsdalen valley. b) View of Romsdalen to the east displaying the typical U-shape of the over-deepened glacial valley (Børa, Svarttinden and Flatmark are three of the unstable slopes described in the present contribution).

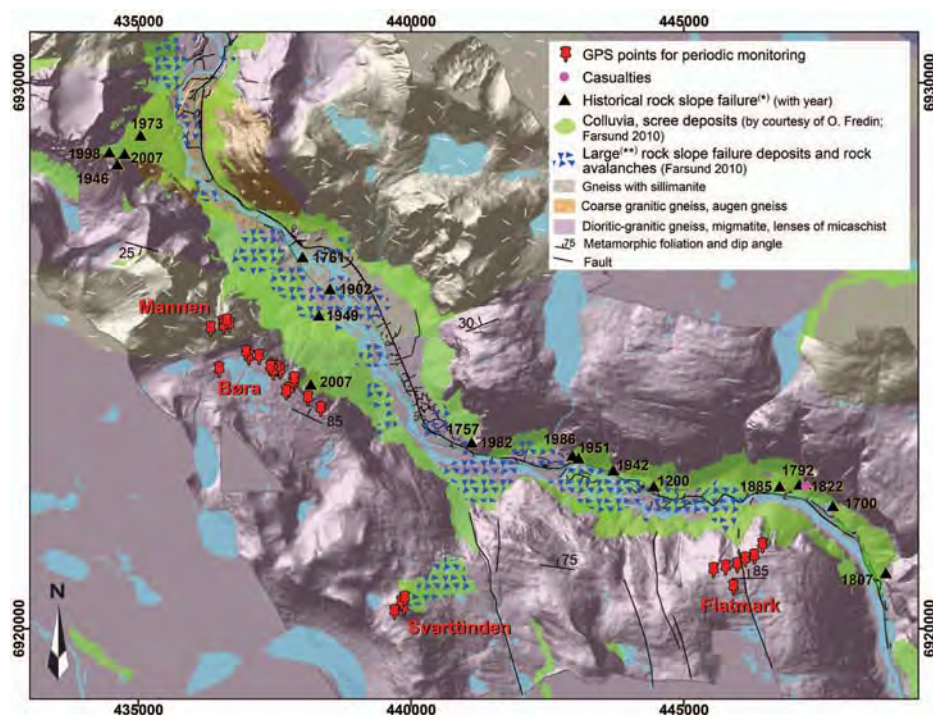


Figure 2. Geological map of Romsdalen (from Tveten *et al.* 1998) on a hillshaded ALS-DEM (coordinates in UTM zone 32). Romsdalen is characterized by the highest density of past and historical rock slope failures in Western Norway and by four current large gravitational rock slope instabilities: Flatmark, Svarttinden, Bora and Mannen. (*), either placed at the source areas or at the deposits (Dahle *et al.* 2008, Skrednett 2012), (**), > 100 000 m³.

After the Caledonian Orogeny, the basement of the Western Gneiss region significantly exhumed during the Devonian collapse of the chain (Hossack and Cooper 1986; Roberts 2003). The age of the major brittle structures observed on Romsdalen valley (Fig. 2) is not constrained. They can pertain to this Devonian tectonic phase as well as to other brittle tectonic phases that are known to have affected the Western Gneiss Region (i.e. for the most significant, the Permo-Trias and Jurassic rifting episodes; Torsvik *et al.* 1997, Valle *et al.* 2002, Mosar 2003). The (still ongoing) uplift of the basement started at a debated time. Anyway, the drainage river system was surely installed during the Tertiary and already shaped the present-day landscape. The Quaternary geology of the region is marked by glaciation episodes. The ice extended to the outer part of the continental shelf during the maximum of the last glaciation in the Weichselian (Mangerud 2004). During the Younger Dryas last severe cooling event, the glaciers re-advanced close to the coast and frost wedging into preexisting fractures is thought to have been a primary

factor of rock slope instability development (Blikra *et al.* 2006).

The ice cap melting generates a regional isostatic rebound and large-magnitude earthquakes (Olesen *et al.* 2000, 2004). Combined with the sudden unloading of the steep slopes due to the rapid glacier retreat an important amount of large rock slope failures occurred shortly (1000 to 2000 years) after the deglaciation (Blikra *et al.* 2002, 2006, Longva *et al.* 2009).

The work of glaciers enhanced the relief to produce the spectacular landscape (fjords, cirques, lakes) of Western Norway and the typical U-shaped Romsdalen valley was carved by the retreated glaciers. Moraines and tills of the last Younger Dryas ice sheet are conspicuous in Romsdalen valley that was probably free of ice some 10 000 years ago or so (Mangerud 2004). No rock slope failure deposits linked to the ice debuttressing of the slopes are preserved in Romsdalen valley bottom. If rock slope failures occurred at that time, the associated deposits were likely far transported by the remnant glacier and/or covered by deltaic and marine fine-sand, silt and clay

deposits that filled the valley in postglacial Holocene times.

More than 15 rock avalanche deposits (larger than 100 000 m³) are mapped in the 30 km long Romsdalen valley (Fig. 2, Blikra *et al.* 2006, Farsund 2010) and are therefore the most recent significant infill of the valley bottom. This is among the highest concentrations of rock avalanches on land in Norway (Blikra *et al.* 2002). They occurred during the last 5,000 years (Blikra *et al.* 2006). Charcoal below one of these rock avalanche deposits yielded an age younger than 2,000 years BP (Blikra *et al.* 2006). Nineteen historical rock slope failures (Skrednett 2012; Dahle *et al.* 2008) are recorded over the study area of Romsdalen valley (Fig. 2).

METHODS

Structural analysis and kinematic feasibility tests

To assess the kinematic (geometric) feasibility of failure of rock slope instability, a detailed structural analysis is performed. The main different kinematic models of rock slope failure are toppling, planar sliding and wedge sliding (e.g. Varnes 1978, Hoek and Bray 1981, Cruden and Varnes 1996, Braathen *et al.* 2004). Most of the large rock slope instabilities in the hard gneissic rocks of Western Norway deformed by planar or wedge sliding (Braathen *et al.* 2004, Henderson *et al.* 2006, Oppikofer 2009, Henderson and Saintot 2011, Oppikofer *et al.* 2011, Saintot *et al.* 2011b). It is also well known that in hard gneissic rocks the gravitational deformation reactivates the pre-existing structures of the rock mass. Therefore, the structural analysis at a site consists to collect the different sets of preexisting discontinuities in the aim to identify the ones which may accommodate the gravitational deformation (that lead to the development of the instability). The collection of discontinuity sets is a priority during fieldwork. However, due to the steepness of the slopes, measurements are often spatially restricted to few zones of the entire instability.

ALS and TLS data and derived DEM permit to measure the orientation of discontinuities of large parts of the instability (e.g. Jaboyedoff *et al.* 2009, Oppikofer *et al.*

2009, 2011, Pedrazzini *et al.* in press). The assumption is that the topographic surfaces of steep rock slopes are shaped by the major fracture surfaces in the rock mass. Therefore, the orientation of these fractures can be extracted from the local orientation of the topographic surface. Here we use two raster models, slope aspect and slope angle, calculated from the ALS-DEM in ArcGIS® system (ESRI 2010). The values of the slope aspect and of the slope angle for the same DEM cell give the full orientation (dip direction and dip angle) of the topographic surface and hence of the rock discontinuity. The high resolution of the ALS-DEM (1 m cell size), which is available in the Romsdalen valley, ensures an accurate measurement of the fracture orientations. Selecting regions with homogeneous orientation allows computing the mean orientations of the discontinuities of the rock mass, which in turn leads to distinguish the sets that mechanically account for the failure and to define the mode of failure.

Volume estimation

The preferred method to accurately define the volume of the rock slope instability is to compute the differences between the present topography and the supposed basal failure surface (Jaboyedoff *et al.* 2004a, b, Oppikofer 2009, Oppikofer *et al.* 2012, this volume). Therefore, the goodness of the volume estimation of the rock slope instability depends of the degree of knowledge of its geometry, i.e. of the spatial extent in 3D of the basal failure surface. In many cases, it is difficult to estimate the depth of deformation even though the gravitational deformation can be well delimited on a map (in 2D). For example, the rough estimation of the volumes of the instabilities at Børa is due to the uncertainty in the depth of deformation, i.e. the accurate determination of the basal failure surface. In turn, the basal failure surface of Svarttinden rock slide crops out and an accurate calculation of the volume can be performed. In such cases, a 3D model of the possible failure surface is built in the software PolyWorks® (InnovMetric 2012) by following the present morphology in the surroundings of the rock slope instability and extending the observed structures underneath the instability

(Oppikofer 2009). With the analysis of the high-resolution DEM of Romsdalen, the location of potential basal surfaces may be recognized by geomorphological signs on the slope where the surfaces should daylight. The latter are somehow well displayed at Mannen and moreover the proposed failure surfaces fit with zones of severe deformation observed along a core drilled from the top of the instability. At Flatmark, the geomorphological signatures of the structures on which may accommodate the deformation at the base of the instabilities are not enough pronounced on the slope to ascertain their location. It results a rough estimation of the unstable volumes.

SVARTTINDEN

Svarttinden is a 1600 m altitude mount, located at 1.2 km inward the plateau from the cliff (Fig. 2). The whole mount is a translational rockslide lying on a single moderately NE-dipping basal detachment (Figs. 3 and 4, Henderson and Saintot 2007).

A large volume already failed from the eastern part of the basal detachment and the deposits reached the edge of the plateau but not the valley floor. Rock avalanche deposits in the valley likely originated from scars at the edge of the plateau (Fig. 3). Smaller failures from the three free faces of the remaining instability followed and the relat-

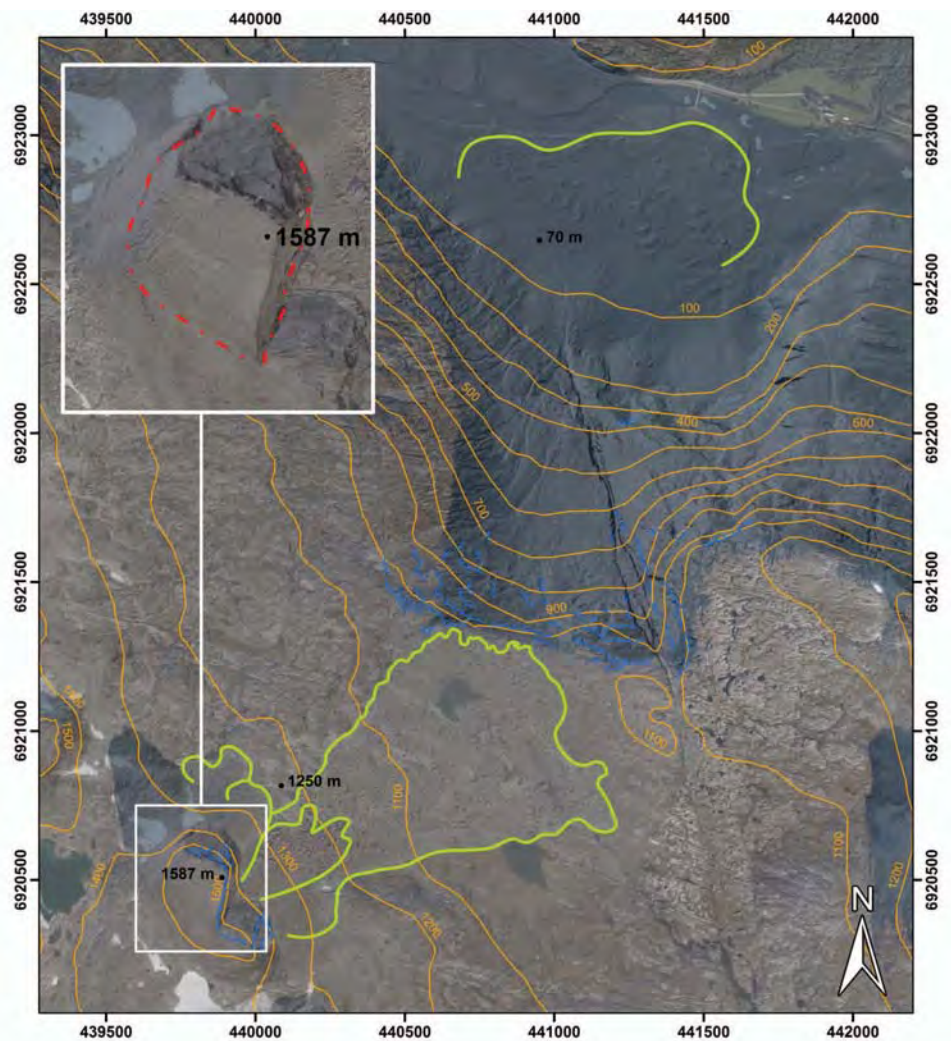


Figure 3. Svarttinden: a large remaining rock slope instability west of a previous failed slope (in white frame). Blue lines: scars of previous rock slope failures; green lines: limits of deposits of previous failures; red dashed line: trace of the single basal detachment of the translational rockslide.

ed deposits are clearly superimposed on the large deposit of the previously failed eastern volume (Fig. 3).

The background fracturation of the gneiss corresponds to steep-to-vertical NW-SE and NE-SW/NNE-SSW trending sets and foliation-parallel sets (Fig. 4). The foliation is moderately to steeply dipping to the NE and NNE. The foliation steepens toward the frontal part of the instability (Fig. 4). A prominent NNE-SSW steep planar fracture forms the border between the failed slope and the remaining block (Fig. 5a). The basal detachment crops out well due to the previous failure east of the rockslide and can be plainly characterized (Figs. 4 and 5). It developed along a metamorphic foliation surface. Its surface is rough and displays meter-scale amplitude undulation which corresponds to the ductile fabric of

the foliation (Fig. 5a, b). It is also stepped by rupture along the NW-SE steep joints (Figs. 4 and 5).

Field observations result in the assumption that sliding of the instability has occurred. On the eastern side of the block, tensile minor structures in the hanging wall of the basal detachment and a 20 cm thick layer of silty-grained unconsolidated breccia observed along the detachment are both inferred to be the products of the gravity-driven displacement of the block (Hen-

derson and Saintot 2007; Fig. 5c, d). On the western side of the block, gravitational deformation is expressed by large cracks which vertically developed from the top surface of the block and parallelized downward to the valley-dipping metamorphic foliation (Henderson and Saintot 2007; Fig. 6a). Cavities are also visible and elongated along the basal detachment. They may either be due to an offset along the undulated basal detachment or to the removal of uncemented breccia material from lenses

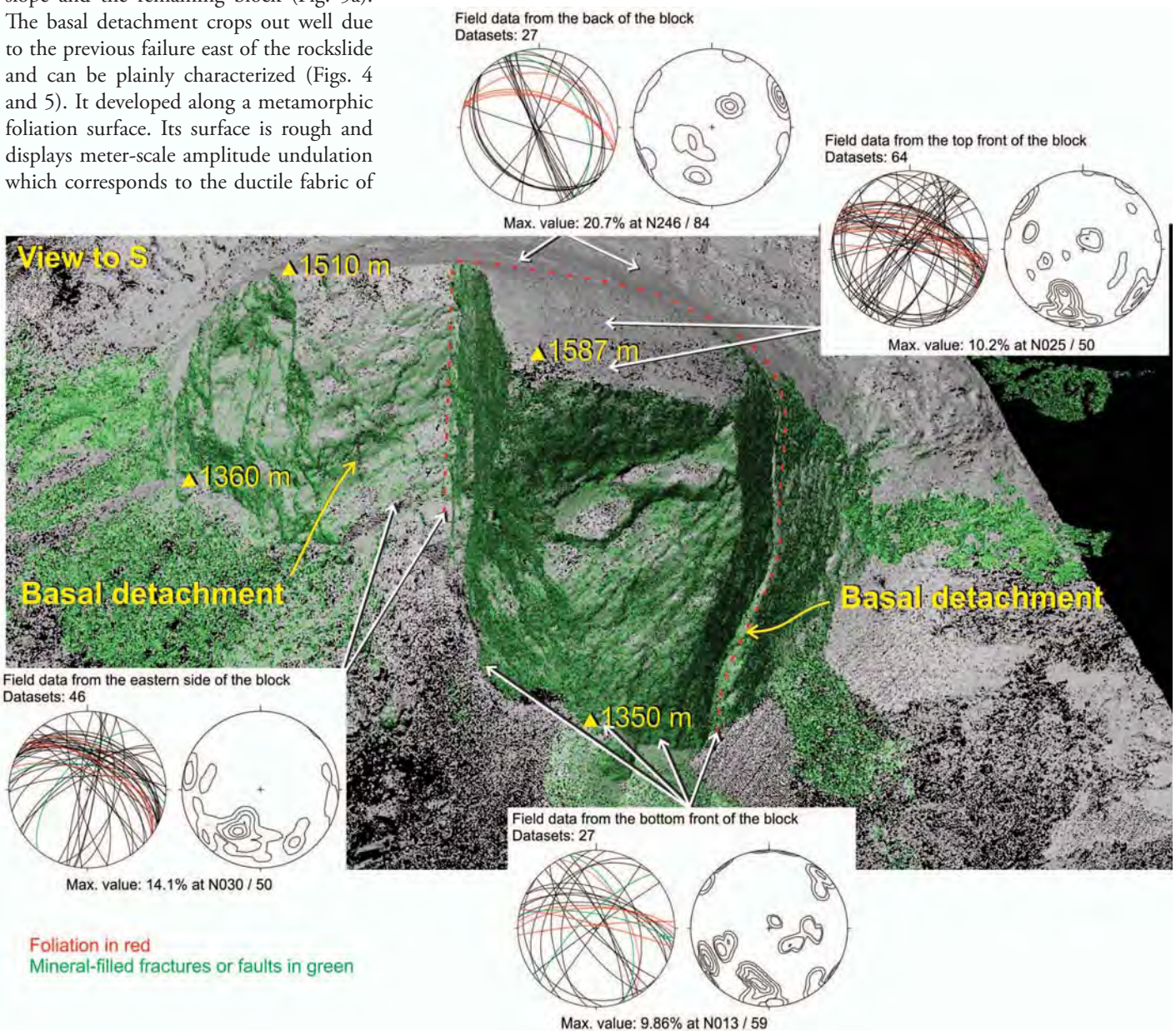


Figure 4. Stereoplots of structural field measurements at locations shown on a 3D view of Svarttinden. The green dots are the TLS point cloud superimposed on the hill-shaded ALS-DEM in gray; the red dashed line is the trace of the single basal detachment of the translational rockslide.

(Fig. 6a, b). The current rockfall source areas are the western and eastern steep sides of the instability as well as the hinges of recumbent tight folds of the northern face (Figs. 5a, b and 6a, b).

The basal detachment developed along an ancient ductile shear zone as indicated by the deflection of the foliation to become parallel to it (Fig. 6a). This zone was the locus of a later tectonic reactivation in the brittle regime to become a chlorite- and epidote-coated cataclastic fault zone (Fig. 6c). Hence, the gravity-driven deformation occurred along a brittle fault zone that has likely developed along a pre-existing ductile shear zone. The observation at Svarttinden gives further support to the hypothesis that the gravitational structures in hard gneissic rocks commonly develop on distinct weak zones created by tectonic forces.

The mean orientation of the basal detachment was extracted from the numerical topographic surface orientation (slope gradient and direction derived from a 1 m resolution DEM) and is of 44° to N034 and of 46° to N048, east and west of the block respectively (Fig. 7). These two orientations

are confirmed by scattered field measurements on the outcropping basal detachment, east and west of the current instability (Fig. 4). These are mean orientations and the 3D view of Svarttinden indeed displays the undulations of the basal detachment and specifically of its western outcropping part which steepens and rotates toward the front of the block to be ENE-directed (Fig. 4). Nevertheless, the fitting of the eastern and western outcropping parts of the basal detachment identified on the DEM resulted in a similar mean orientation with a plane dipping 50° to N040. This good morphologic and structural control of the basal failure surface made the Svarttinden instability propitious for 3D modeling and volume estimation. Using a single plane as basal failure surface yields a volume of 4.3 Mm³ for the remaining rock slope instability. The volume that failed east of the instability was probably of the same order or less.

The Svarttinden rockslide is monitored by dGPS since 2006 because of the occurrence of (1) a well-developed basal sliding surface, with locally the occurrence of a fine-

grained breccia lowering the friction, (2) a previous failure of similar size along the same surface and (3) rockfall activity from the remaining block. However, the rockfall activity may be simply due to the steepness of the faces of the block rather than induced by motion of the block. Indeed, no significant displacement of the rockslide is detected until now. This is in agreement with the field survey at the back of the block, which reveals that no conspicuous recent disturbance of the rocks is observed where the basal detachment intersects the topographic surface (see for example on the aerial photograph of Fig. 7). The high roughness and the undulations of this basal surface is a primary factor that may explain the absence of motion of the instability. A second factor may be the change of orientation of this surface. As mentioned above, its orientation is approximately of 45° dipping to the NE except at the bottom frontal part of the block where the surface steepens and shifts to an ENE dip direction. It cannot be ruled out that the change of orientation of the basal detachment toward the toe zone avoids it from day lighting the topography

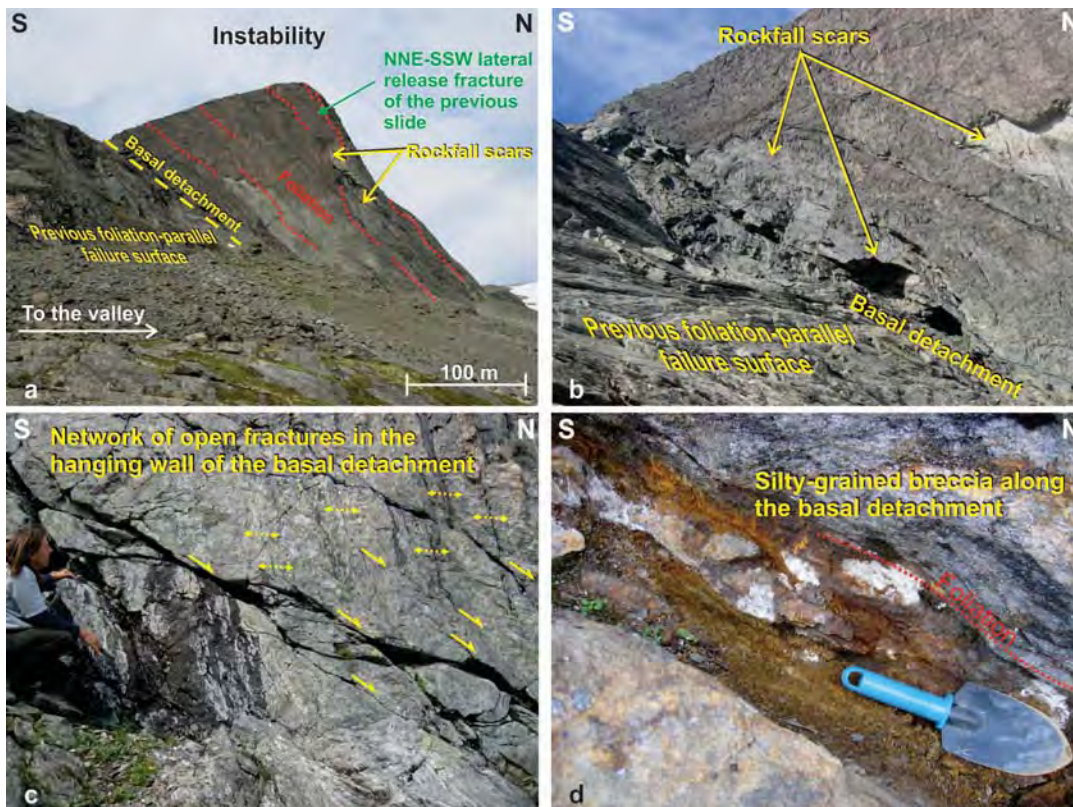


Figure 5. Svarttinden: photographs of the eastern side of the current unstable block. a) View of the remaining instability over the basal detachment of the previous rock slope failure. b) Roughness of the basal detachment (undulation and steps) and rockfall activity from the remaining instability. c) Deformation in the hanging wall of the basal detachment interpreted to accommodate the gravity-driven displacement of the remaining instability. d) Unconsolidated breccia along the basal detachment interpreted to be the product of past displacements.

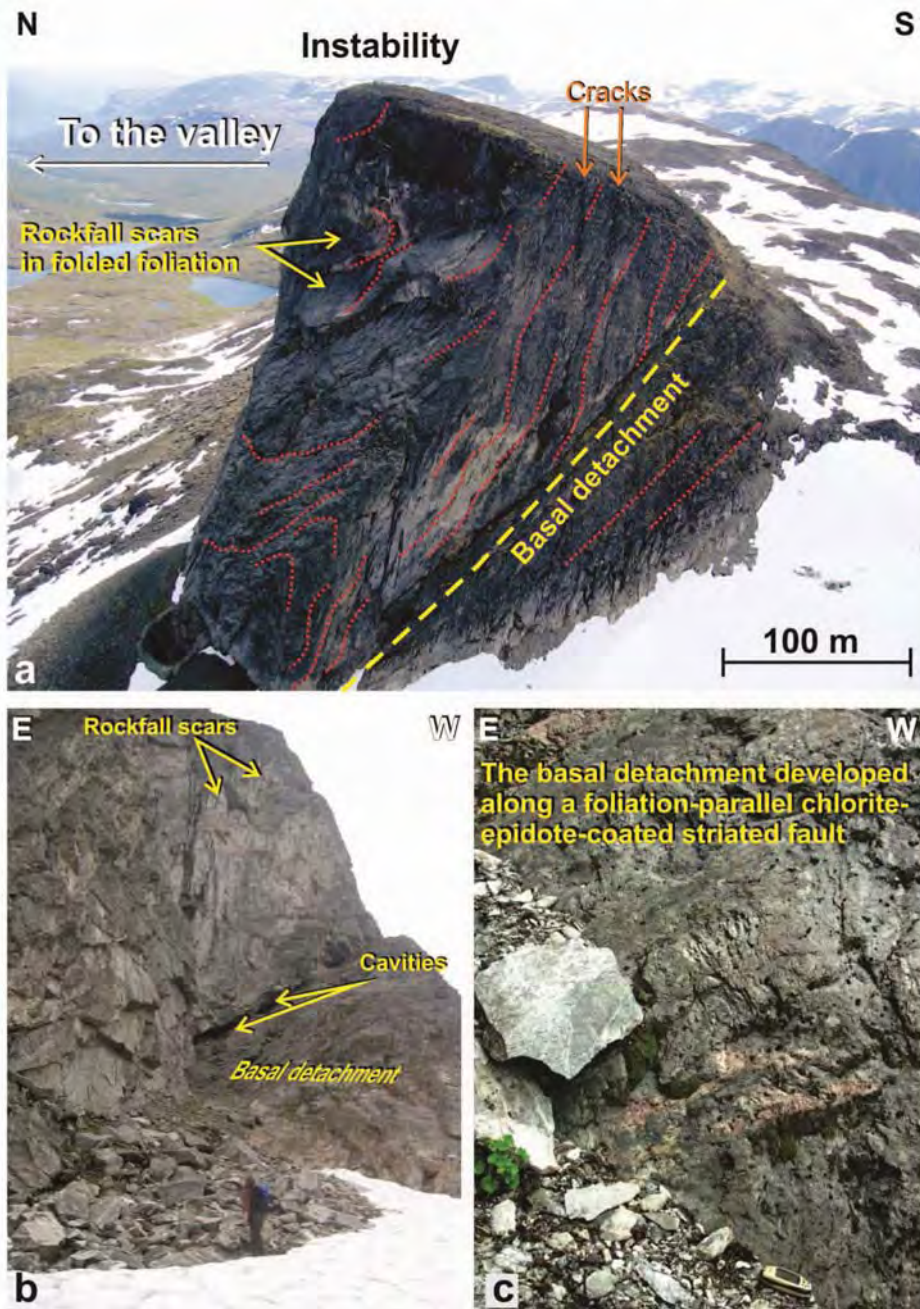


Figure 6. Svarttinden: photographs of the western side of the remaining instability. a) View from helicopter showing (1) the sources of rockfalls at the hinges of recumbent folds and (2) the ductile deformation of the metamorphic foliation and the pre-existing ductile shear along the present-day basal detachment. b) Rockfall activity from the remaining instability and elongated cavities along the detachment (seen also on (a)). c) The basal detachment of the rockslide is a pre-existing foliation-parallel chlorite- and epidote-coated cataclastic fault.

and thus acts against the sliding of the total block by a buttressing effect.

FLATMARK

At Flatmark (Fig. 2), a series of rock slope instabilities extends from the edge of the

plateau at 900 to 1050 m a.s.l. to large parts of the slope downward (Fig. 8). A succession of rock avalanches and large rock slope failure deposits, including historical ones, are mapped on the valley floor at the bottom of Flatmark (Fig. 2). Flatmark is expected to be the source area of most of them.

The rock slope instabilities at Flatmark are delimited by wide vertical back-cracks that have partly smooth walls parallel to the quasi-vertical metamorphic foliation and partly stepped walls shaped by the same foliation and steep quasi-meridian joints (Fig. 8). For the uppermost and largest instability the width of the back-crack is 20–25 m. Only few opened fractures of small amplitude are observed inward the plateau at the back of the rock slope instabilities. This testifies of the important localization of the large gravitational deformation at the edge of the plateau (see also discussion in Böhme *et al.* 2011).

The structures that may represent the basal failure surfaces of the instabilities are not yet clearly identified, the fieldwork being unfortunately restricted to the plateau edges due to the steepness of the slope (Fig. 9). At the base of small surficial displaced blocks two favorably orientated, valley-dipping planes were collected (Fig. 9), which might represent a fracture set forming also a larger basal sliding surfaces at depth. However, the scarcity of field measurements questions about their real significance at the scale of the entire slope. Nonetheless, a set of joints can be observed that systematically developed perpendicular to the dip line of the metamorphic foliation (Fig. 8). The field study on the plateau has indeed permitted to observe the variation of the metamorphic foliation from quasi-vertical to clearly dipping toward the mountainside (Figs. 8g and 9). At the locations where the foliation dips into the slope, the joints that formed perpendicular to its dip line are so favorably orientated toward the valley that they may act as basal sliding surface. The sharp topographic surfaces of the slope downward the largest instability may actually reflect the foliation dipping into the mountain and moderately valley-dipping topographic surfaces would correspond to such a joint set (Fig. 8h).

The analysis of the topography (Fig. 10) tends to assign basal limits of the instabilities on shallow to moderately valley-dipping surfaces (Fig. 10b, c). The possible failure mechanism of the large rock slope instabilities at Flatmark is likely a sliding and/or a sagging on these valley-dipping basal failure surfaces yielding back-crack

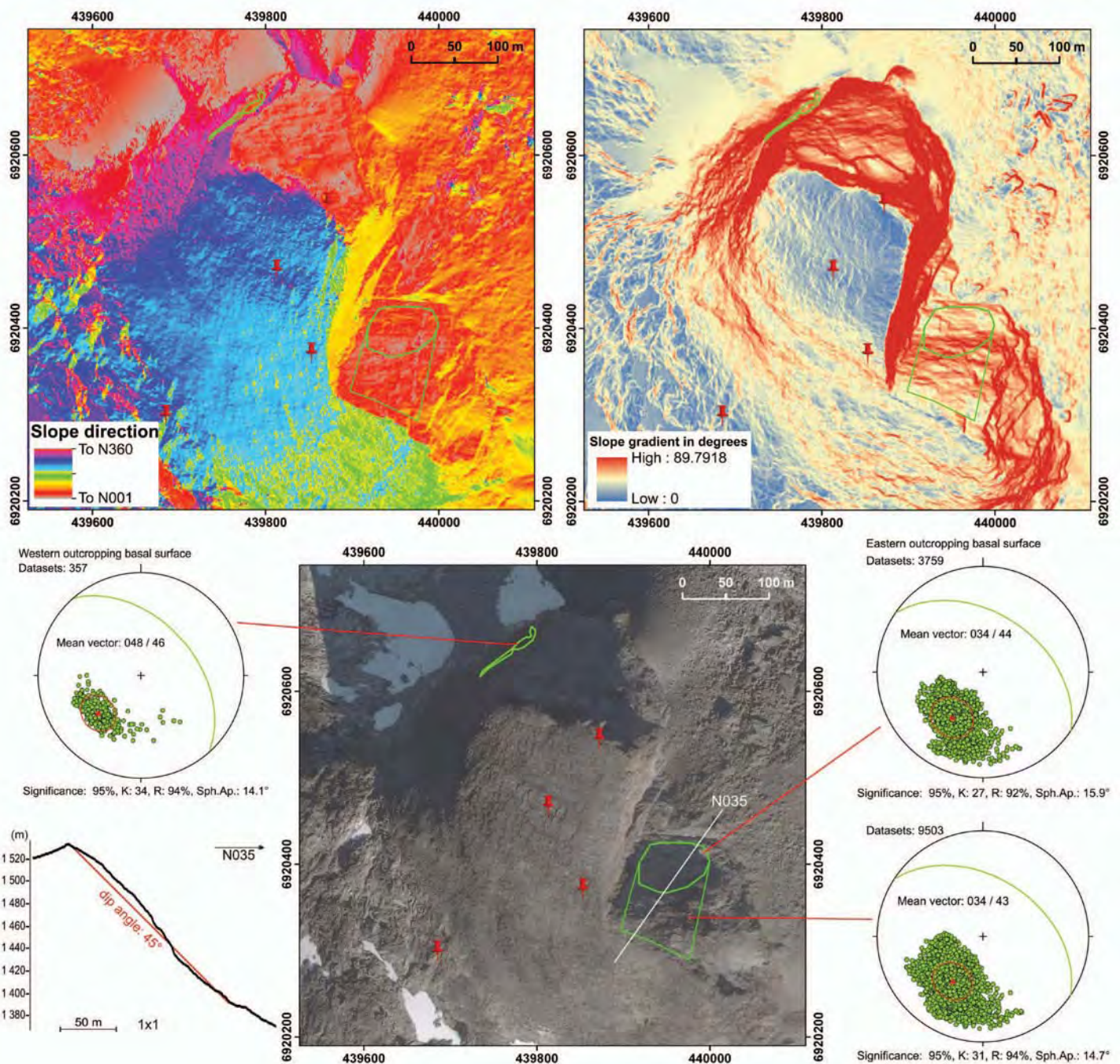


Figure 7. Top: maps of the slope direction (left) and gradient (right) derived from the ALS-DEM. Areas limited by green lines: western and eastern outcropping sides of the basal surface of the Svarttinden rockslide. Bottom: Stereoplots of the slope orientations of the western and eastern sides of the basal sliding surface (1 point per DEM cell). Slope profile directed to N035 across the eastern outcropping basal sliding surface (along which occurred the previous failure) and indicating an average dip angle of 45°; aerial photograph of Svarttinden rockslide with location of the profile. Note on the mean vector calculation: *Mean vector*, azimuth/plunge; *Significance* (%), prediction probability of the cone of confidence; *K*, concentration parameter (closeness, precession) after Fisher (1953) ranging between 2 (uniform distribution) and infinity (parallel fabrics); *R* (%), concentration parameter from Wallbrecher (1986) ranging from 0% (uniform distribution) to 100% (parallel fabrics); *Spherical aperture* (°), radius of a small circle of a spherical normal distribution with equal *R*-value as the given data.

opening along the cliff-parallel steep meta-morphic foliation planes. Locally, a toppling mechanism clearly affects small pieces of rock at the top of the blocks (Fig. 8). However, the vertical extents of the back-

cracks and the continuity of the basal failure surfaces are speculative and stepped surfaces cannot be ruled out (Fig. 10b). Nevertheless, one of the instabilities has by contrast well-defined borders that stick,

eastward and westward, to a vertical N-S cataclastic fault and its east-dipping branch respectively, and follow, backward, an E-W vertical foliation plane (Fig. 9).

The total deformed volume would reach



Figure 8. a) Flatmark: 3D view of the hillshaded ALS-DEM showing rock slope instabilities of various sizes (back-cracks at the edge of the plateau as blue dashed lines, limits of instabilities on the slope as yellow lines, traces of the steep metamorphic foliation as red dashed lines; locations of photos in (b) (h) are shown). b)h) photographs of the rock slope instabilities at Flatmark with the trace of the metamorphic foliation (red dashed lines) and shallow to moderately valley-dipping joints that developed perpendicular to the foliation dip line (yellow arrows). b) View from helicopter of the largest instability with a back-crack opening partly guided by a pre-existing quasi-vertical metamorphic foliation. c) close view to the east of the 20 m wide back-crack largely filled by debris; the instability is affected by toppling. d) Close view to the west of the largest instability. e) And f) toppling displacements observed at the top of two instabilities in the eastern part of the Flatmark plateau. g) Shallow to moderately valley-dipping topographic surfaces on the largest rock slope instability corresponding to joints that systematically developed perpendicular to the foliation dip line; these are favorably orientated toward the valley where the foliation steeply dips into the mountain and where the basal sliding surfaces of the instabilities are expected to daylight.

155 Mm³ with subsidiary blocks of volumes ranging between 2 and 25 Mm³ (Henderson and Saintot 2007, Longchamp *et al.* 2010). Because of the large degree of deformation observed at Flatmark and because the site was the source area of large deposits lying on the valley floor (Fig. 10a), the unstable blocks are monitored since 2006 by dGPS measurements but no displacements are detected until now. This is in agreement with (1) the important infill of the back-cracks with deposits (Fig. 8a, b) and with (2) the absence of rockfall activity at the front of the deformed volumes as well as of well-developed bulges due to advancing slopes. The latter is confirmed by the regularity of the topography as displayed on profiles crossing the instabilities (Fig. 10b). A slight bulge might have nevertheless developed across the lowest unstable block which also shows the highest rate of rock dislocation (see topography along profile 5 on Fig. 10b, Fig. 8e).

BØRA

The geological and geomorphological settings at Børa (Fig. 11) are the same as at Flatmark with the exception of a large paleo-glacial perched valley at Børa trending parallel to the slope. Otherwise, both sites comprise identical gneissic rocks characterized by a steep to vertical foliation, shaping parts of the cliff at the edge of the plateau. Like at Flatmark, several rock slope instabilities developed along foliation-parallel back-cracks at the edge of the cliff at 1000 m altitude and are the sources of frequent rockfalls (Fig. 11a-c). At least 5 previous large rock slope failures occurred from the cliff of Børa including historical events (Fig. 2; Blikra *et al.* 2002). The last rockfall dates from 2007 and involved a significant volume of 30 000 to 50 000 m³ (Dahle *et al.* 2008) with deposits that reached the valley bottom.

Contrary to Flatmark where the severe

gravitational deformation is restrained to blocks at the edge of the plateau, the gravity-driven deformation encompassed a large area at Børa, going well inward the plateau. The limit of the deformed rock slope is marked by a one kilometer long, several meters wide and deep, foliation-parallel, back-bounding crevasse. The crevasse is particularly well-developed in its eastern part (Fig. 11d) and dies out westward (Fig. 12) leading to a decrease in past deformations from east to west.

Two conspicuous sets of structures accommodate the gravitational deformation by opening and comprise the quasi-vertical WNW-ESE foliation and a vertical NNW-SSE fracture set (Fig. 12a, b). They both shape the edge of the plateau. A toppling mechanism along these two geometries is impossible given the importance of the deformed volume, and a third set of discontinuities may exist to limit the deformation at depth. The general background of dis-

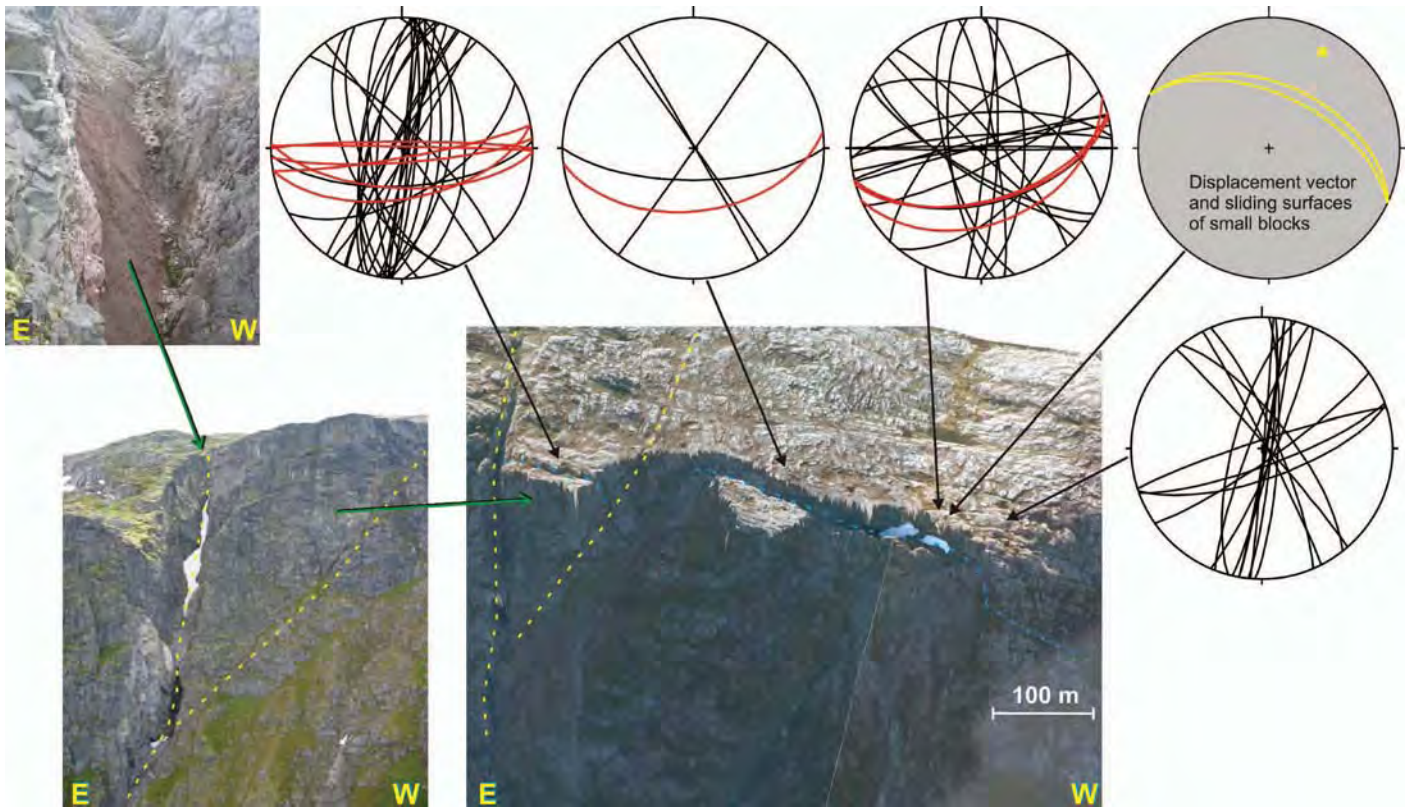


Figure 9. Stereoplots of field measurements at the edge of the Flatmark plateau where the largest instability developed: metamorphic foliation in red and joints in black, two planes at the base of small detached blocks have an orientation favorable for sliding. Locations of field measurements on a 3D view of the top of the largest instability (aerial photograph draped on DEM). Photographs taken from helicopter of one of the instabilities, delimited by a foliation-parallel back-crack (blue line) and two preexisting tectonic faults (yellow lines), one being largely hematite-rich cataclastic (located on Fig. 8a).

continuity geometry in the gneiss of Western Norway is the occurrence of a joint set perpendicular to the dip line of the metamorphic foliation (although their origin is still poorly understood; e.g. Weinberger *et al.* 2010). At Børa, it would correspond to a flat-lying joint set as identified by Braathen *et al.* (2004). The development of the instability would be then better explained by a mechanism of sagging along such flat-lying discontinuities, accompanied by an opening along the vertical sets of discontinuities. As such, Børa is classified as a planar styled complex field (Braathen *et al.* 2004). The large-scale gravitational deformation at Børa would involve between 50 and 200 Mm³ of rocks (Braathen *et al.* 2004). The uncertainty in the volume estimation

is due to the unknown extent in depth of the instability. The volumes of local instabilities located at the edge of the plateau (Fig. 12c) are roughly estimated to be of approximately half a Mm³.

Three of these local instabilities show displacement rates between 0.2 and 2 cm/yr based on periodic dGPS measurements (Fig. 12). No displacements are measured for the entire unstable rock slope at Børa indicating that the active deformation takes place at the frontal cliff leading to the creation of the mentioned localized instabilities.

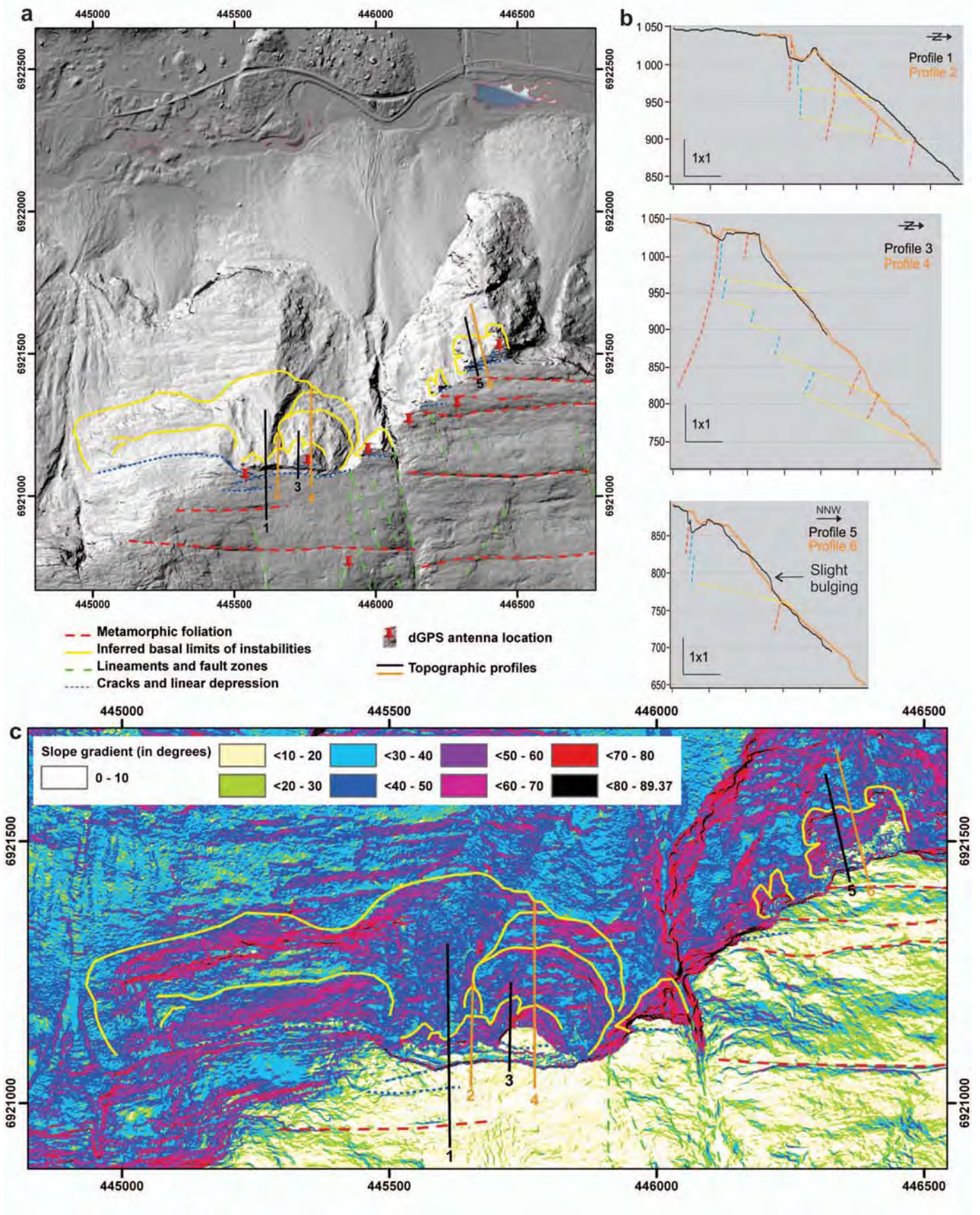
MANNEN

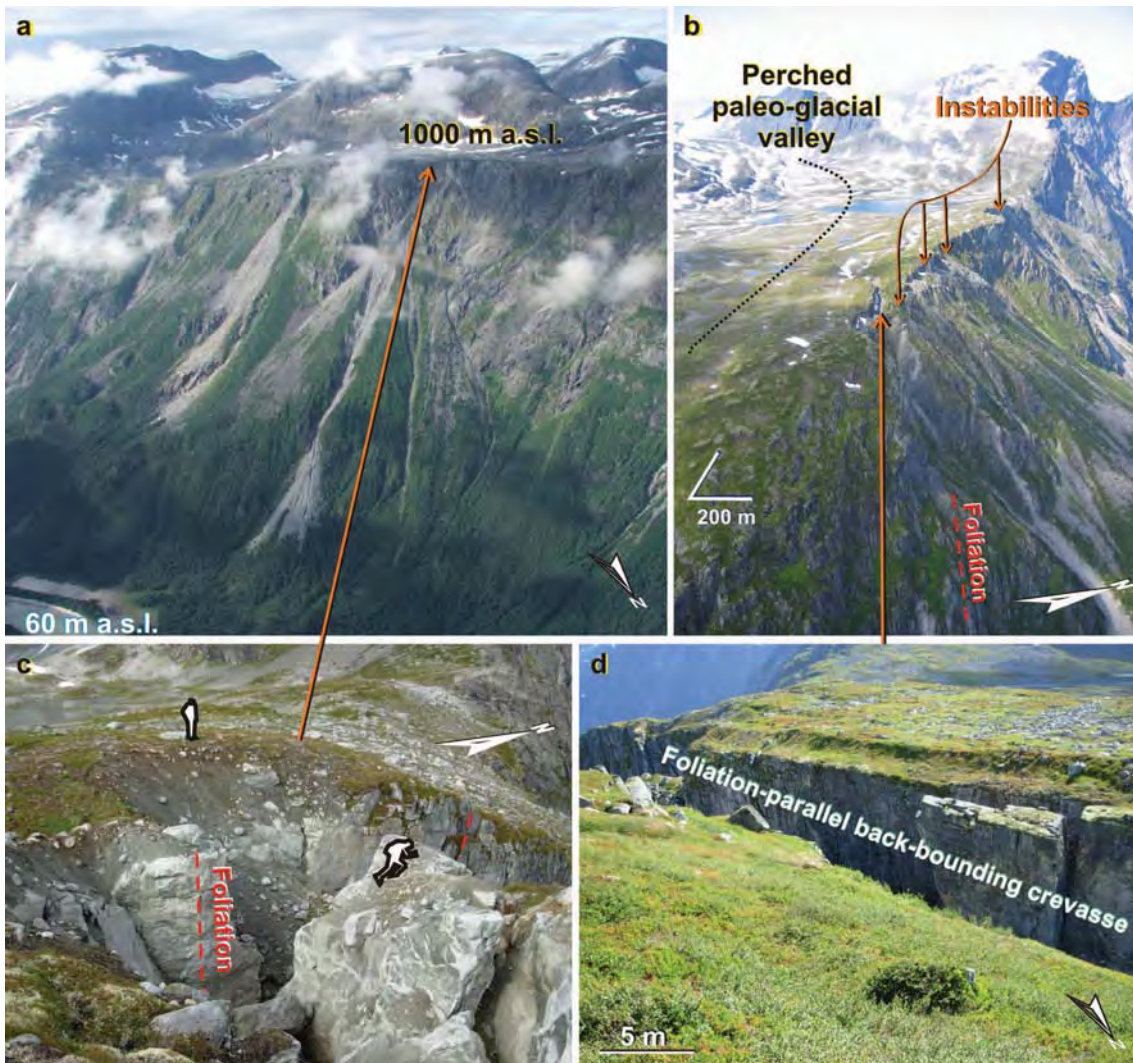
The Mannen rock slope displays a widespread gravitational deformation and com-

prises a collapsing instability at the edge of the 1300 m elevated plateau (Fig. 13a). Abundant scars of previous failures of various sizes are observed at Mannen and two related large deposits are preserved on the valley floor (Fig. 2; Blikra *et al.* 2002). Minor rockfalls are reported every year since the site is studied from 2007.

Contrary to the three other localities in Romsdalen valley where gravitational instabilities are encountered in the dioritic-granitic gneiss basement unit of the valley, the Mannen rock slope instabilities developed in a singular high-grade metamorphic unit made of intensively folded alternating sillimanite-bearing dioritic and muscovite-sillimanite granitic gneisses, amphibolites and pegmatites (Fig. 2; Saintot *et al.* 2011a).

Figure 10. a) Map of the rock slope instabilities at Flatmark on a hillshaded DEM and location of the slope profiles shown in (b); note the deposits of large rock slope failures in the valley bottom that are assumed to be from Flatmark. b) Topographic profiles across the instabilities; yellow lines: basal limits with uncertain dip angles; blue lines: back-cracks with unknown depth; red dashed lines: attitude of the metamorphic foliation. c) Map of the slope gradient at Flatmark showing the moderately valley-dipping topographic surfaces.



**Figure 11.**

a) Photograph of the Børa unstable rock slope (by courtesy of Tor Farsund) displaying the frequent rockfall events. b) Photograph of the perched paleo-glacial valley trending parallel to the cliff. The cliff is shaped by the steep metamorphic foliation planes. c) Photograph of one of the moving local instabilities at the edge of Børa plateau. d) The eastern end of the back-bounding crevasse of the gravitational deformation at Børa.

The field studies on the plateau behind the unstable rock slope has allowed recognizing widespread gravitational deformation by opening of the penetrative steep E-W metamorphic foliation and a set of nearly perpendicular vertical N-S/NNE-SSW fractures (Fig. 13a-c). The latter are copies of a regional tectonic fault displaying an epidote- and chlorite-rich fault core inherited from a ductile shear zone (Fig. 13a, d, e). This fault makes a clear boundary between the unstable parts of the slope in the east and the stable parts in the west (Fig. 13a, d).

The geomorphological DEM analysis coupled with aerial photographs has allowed defining the limits of the deformed rock slope. Three instabilities based upon different deformed volumes are retained (Dahle

et al. 2008, 2010). The first volume corresponds to the moving upper part of the unstable rock slope and may reach a volume of 2–3.5 Mm³ (Fig. 14a; Farsund 2011). Due to motion a topographic bulge is visible at its front (Fig. 14b). At the base of the instability a surface underlined by frequent rockfalls satisfies the geometry of a sliding surface (Fig. 14b). The continuation of this surface within the mountain intersects a vertical borehole that was drilled from the top of the unstable block (Fig. 14b) at c. 75 m depth. At this depth the drill core is formed by a c. 15 m thick zone of much damaged rocks, which comprises layers of crushed rocks, clay-rich gouges and fine-grained breccias (Saintot *et al.* 2011a). However, the attitude of this sliding surface extracted from the ALS-DEM (dip

direction/dip angle: N110/48°; Fig. 14c) is highly oblique to the slope and a planar failure along this surface only seems to be unlikely. With the help of the 3D model of the slope a second sliding surface (N023/59°) was identified permitting the development of a wedge sliding mechanism (Dahle *et al.* 2010; Farsund 2011). The intersection of these two sliding surfaces, i.e. the possible sliding direction, fits well with the displacement vectors determined by dGPS measurements that plunges of 50° toward N060-070 (Fig. 14c).

The unstable rock slope at Mannen has been classified as instability with high susceptibility for failure when a movement of 4–5 cm/year of the 2–3.5 Mm³ instability at the edge of the plateau was detected by dGPS measurements (Dahle *et al.* 2008).

Because of the catastrophic consequence of a failure, this block is under continuous monitoring since 2009 and multi-disciplinary studies follow each other (Dahle *et al.* 2008, 2010, 2011, Saintot *et al.* 2011a). The second unstable volume includes the first volume and would reach 25–30 Mm³ (Fig. 14a; Farsund 2011). Its basal limits are not clearly visible in the field or on the ALS-DEM or aerial photographs. A severely damaged zone identified along the drill core at 113–115 m depth might correspond to the basal failure surface of this second unstable volume (Saintot *et al.* 2011a). Its lateral and upper boundaries partly coincide with those of the first instability, but they are not underlined by signs of activity (openings, rockfall activity, etc.; Fig. 14a). Since the structural limits of this deformed volume are not accurately defined, its kinematics is not fully understood. Therefore, this second unstable volume is considered to have a lower susceptibility for failure than the first volume (Dahle *et al.* 2010). The third potential instability encompasses the entire gravitationally deformed slope far inward the plateau and has a volume of 80–100 Mm³ (Fig. 13a). The lateral and basal limits of this third instability are visible neither in the field, nor on the ALS-DEM and aerial photographs. In addition there are no ongoing displacements or other signs of activity and therefore is this third volume considered as stable (Dahle *et al.* 2010; Fig. 14a).

DISCUSSION WITH CONCLUSIVE REMARKS

The four sites of Svarttinden, Flatmark, Børa and Mannen display large gravitational deformation that evoke the normal process of slope denudation: the deformation occurs on knick-points of the slope and the total failure will smooth the slope to a steady state (Ahnert 1987, Selby 1993, Böhme *et al.* 2011).

The kinematic feasibility of failure is clearly determined for Svarttinden rockslide. It is a planar failure on an ideally 45° valley-dipping basal surface. However, it is noticed that the surface is rough and undulated and that, at the toe zone of the rockslide, its change in dip direction may act as a buttress to sliding.

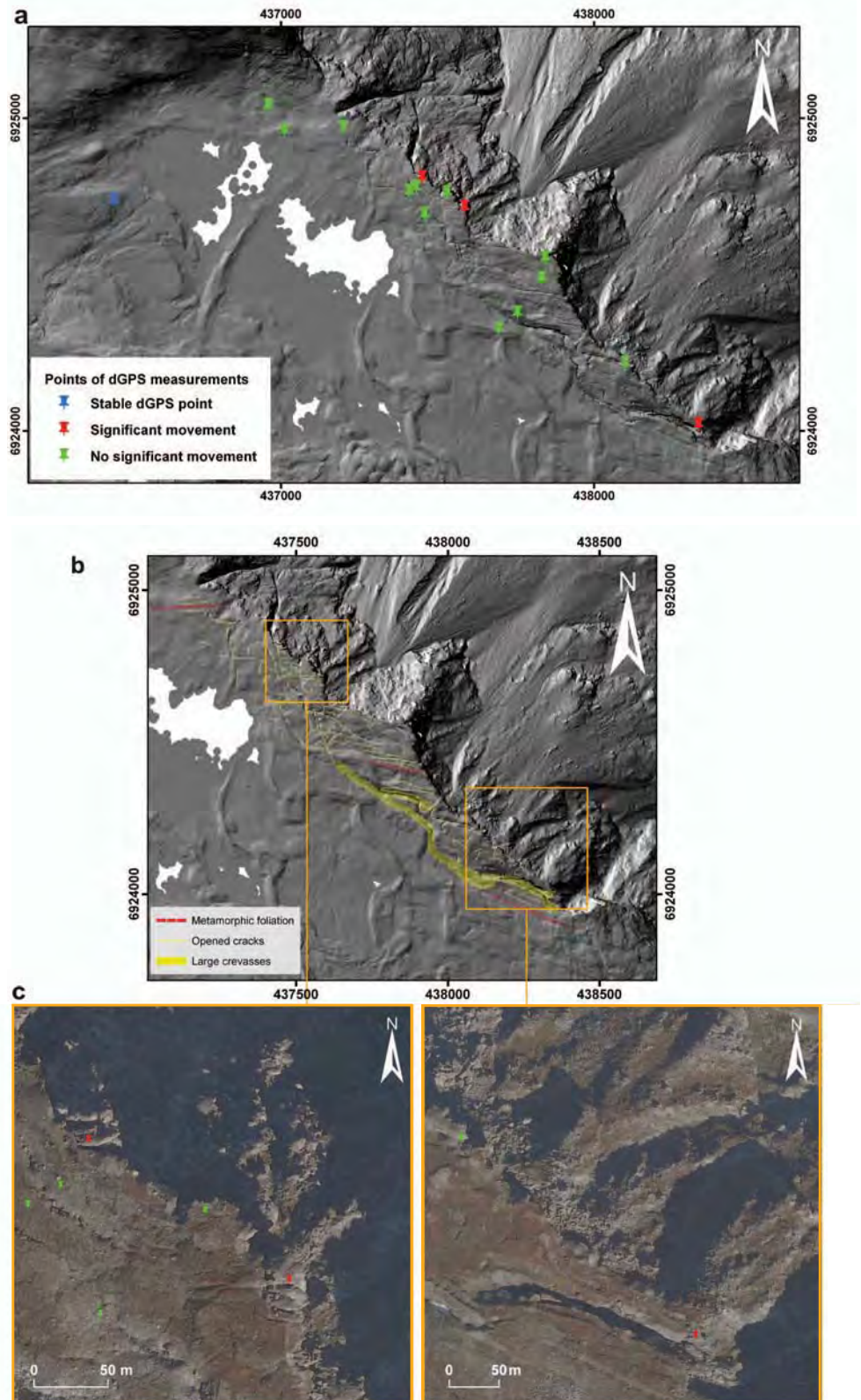


Figure 12. a) Hillshaded ALS-DEM of the Børa plateau with dGPS antenna positions and associated detection of movements. The movements are significant on 3 local instabilities at the edge of Børa plateau and range between 0.2 and 2 cm/yr. b) Structural map of the deformed edge of Børa plateau from the analysis of the ALS-DEM. c) And d) detailed aerial photographs of the three local instabilities.

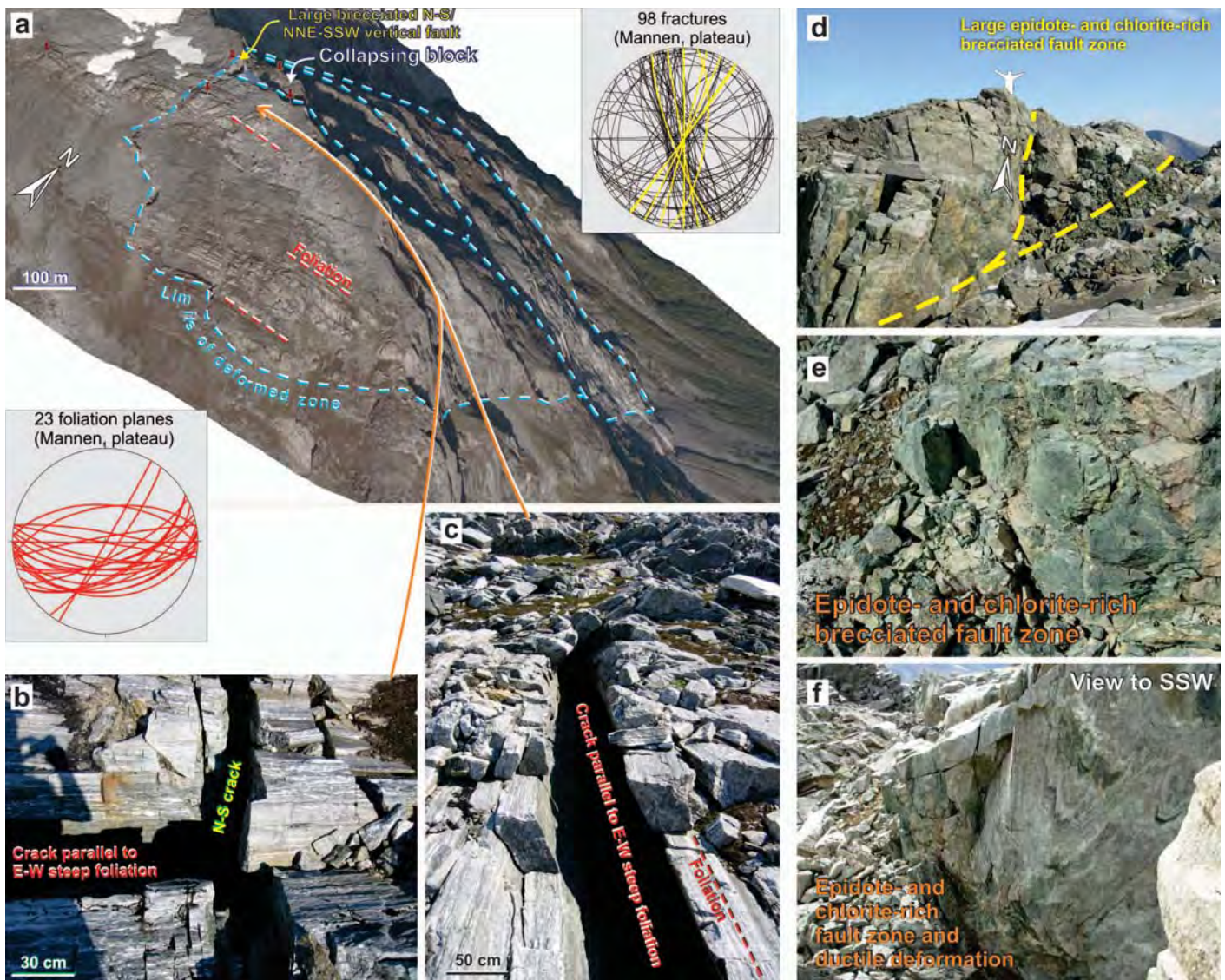


Figure 13. a) Aerial photograph draped on the ALS-DEM of the deformed edge of Mannen plateau (view from above) and stereonet of field data (in yellow, mineralized fracture surfaces); red pins mark the location of dGPS antennas. b) And c) photographs of E-W cracks and N-S cracks that respectively opened parallel to the steep metamorphic foliation and along N-S fractures. d) and e) A roughly N-S trending epidote-rich cataclastic fault limits the instability to the west. f) The epidote-rich cataclastic fault (shown in (d) and (e)) is also a pre-existing discrete zone of high ductile strain.

The failure mechanism at the edge of Flatmark and Børa plateau is less clearly understood. The only well developed and identifiable structures are the back-cracks, which largely follow the steep foliation surfaces and their opening by tension is indubitable. The involvement of such large slope volumes (several Mm^3) in the gravitational deformation would require deformation on basal surfaces rather than toppling, but no conspicuous basal sliding surfaces are detected so far at Flatmark and Børa. At Flatmark, shallow valley-dipping joints exist that may

allow a sliding of the rock mass. At Børa, the joints would be flat-lying and a sagging of rock volumes at the edge of the plateau is the retained mechanism of deformation. In itself, the entire deformed volume at Børa typically resembles the complex fields that developed at edges of plateaus in Norway (Braathen *et al.* 2004, Böhme *et al.* 2011). At the uppermost instability of Mannen, two basal surfaces identified through an analysis of the ALS-DEM form a wedge along which the sliding of the instability may occur. One of the basal surfaces is the

locus of frequent rockfalls and may also fit with a thick zone of severely damaged rocks at c. 70-80 m depth identified in the borehole drilled from the top of the instability. Large tectonic fault zones when intersecting the slopes are prone to be reactivated under gravity. An epidote- and chlorite-rich cataclastic fault is the basal detachment of the Svarttinden rockslide. At Flatmark and Mannen, large cataclastic vertical faults are the lateral limits of the instabilities. At Mannen and Svarttinden, these prominent brittle structures were also the locus of high

ductile strain. Such discontinuities have a protracted geological history and are likely zones of weakness within the hard gneissic rocks of Romsdalen valley.

As already mentioned, Mannen is located in a specific rock unit of the basement that comprises a range of petrology and displays an intense ductile deformation (with disharmonic and recumbent close to tight folds being common). The conspicuous difference in the bedrock at Mannen and in its structural pattern might partly explain the large finite gravitational deformation of Mannen slope and its subsequent present-day state of high activity (Henderson and Saintot 2007, Dahle *et al.* 2008). It is a qualitative assessment which aims at ex-

plaining the specific case of Mannen based on the rheological contrast of the bedrocks along the southern side of the Romsdalen valley.

While the local instabilities at Børa are susceptible for failure, the large deformed area inward the plateau is not. However, it cannot be ruled out that a very low, not detectable, rate of opening of the back-bounding crevasse may have very important effect on the free border of the rock volume, i.e. on the highly unstable structures at the edge of the plateau. The comparison with the site of Flatmark, where no large gravitational structures developed inward the plateau and no displacement are recorded on the instabilities at the edge of the plateau, lets

envisage that a link exists between the occurrence of widespread gravitational deformation affecting the Børa plateau far from its edge and the present movements of local instabilities at the edge. Further investigations are required to better understand this possible link, even though the imbrications of localized, small instabilities within large gravitational slope deformations are quite common (e.g. Agliardi *et al.* 2001, Ambrosi and Crosta 2006).

A conceptual model to explain the large-scale gravitational deformation at Børa involving maybe more than 200 Mm³ of rocks considers the presence of a paleoglacial valley trending parallel to the cliff (and which may actually be the only geomor-

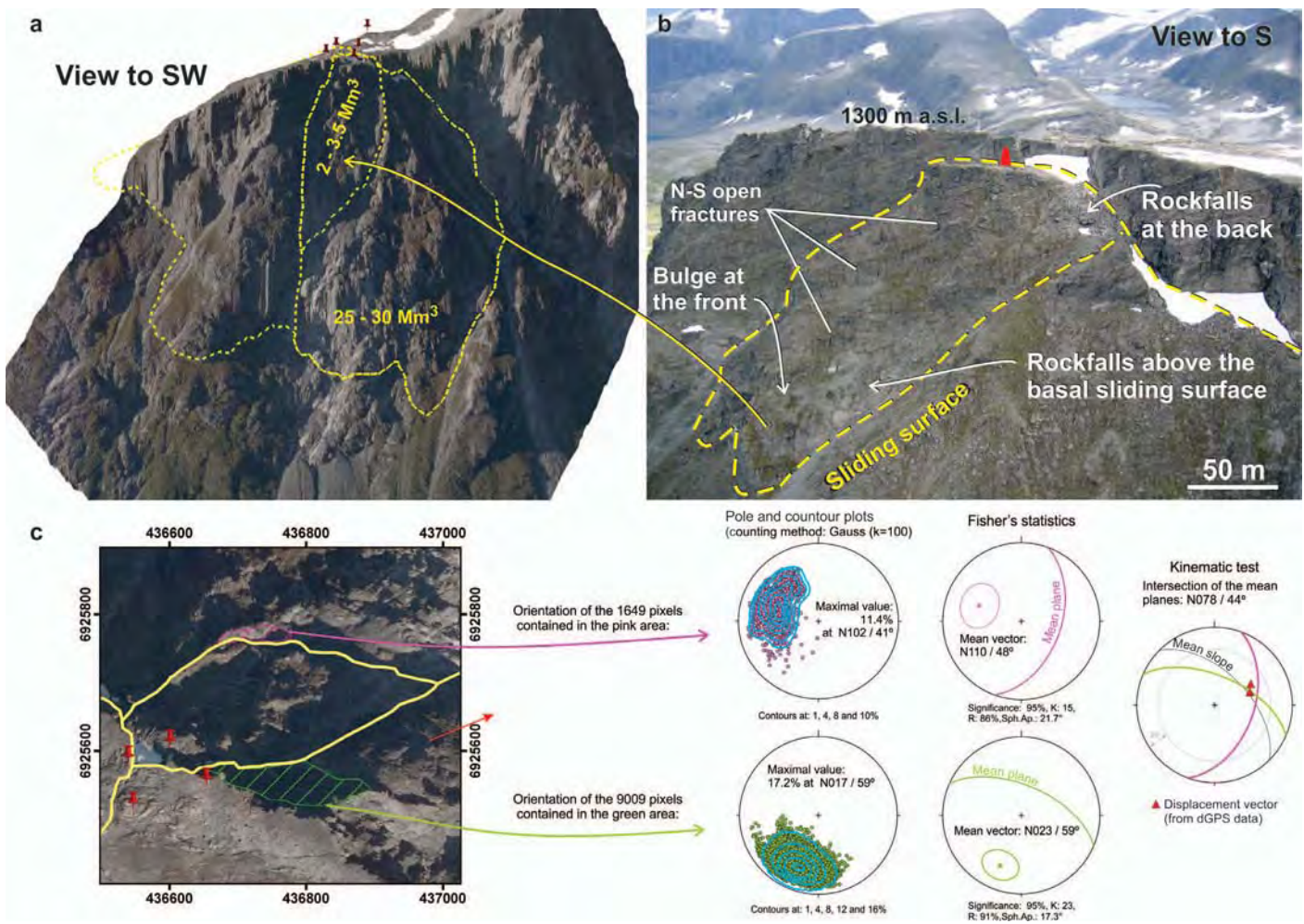


Figure 14. a) Aerial photograph draped on the ALS-DEM of the Mannen rock slope. Yellow lines: inferred limits of the instabilities; red pins: location of the dGPS antennas. b) Photograph from helicopter of the uppermost instability at Mannen with an important set of N-S trending opened fractures, a bulge at the front and a sliding surface underlined by rockfall events. The red cone marks the location of the drilling site. c) Determination of a wedge sliding mechanism on two outcropping surfaces at the limit of the uppermost instability at Mannen. The mean planes matching the mean orientations of these surfaces are extracted from the ALS-DEM and the wedge intersection line fits well with the displacement vector obtained from dGPS measurements.

phological difference with Flatmark area). Assumption is made that, at the base of the glacier, the vertical foliation would have weakened either by opening of these vertical planes by ice loading or by weathering of mica-rich foliation layers due to water circulation or both (e.g. Saintot *et al.* 2011b). It is also noticeable that the finite deformation along the km long bounding crevasse appears to have been larger eastward, where the paleoglacial valley intersects the edge of the plateau toward the Romsdal valley. The question is opened if more flowing water at this location and thus more weathering could have favored more deformation later on (e.g. Bachmann *et al.* 2004).

The large potential rock slope instabilities presented in this contribution are on the southern side of Romsdalen valley. No such large gravitational instability is nowadays observed on the northern slope of the Romsdalen valley, while some scars and deposits of previous large events are visible. The detailed geometrical characterization of these scars is expected to reveal parameters that may count for the difference of behavior of the two slopes of the Romsdalen valley. As the field study is avoid due to the steepness of the slopes, this will be mainly based on the analyses of the ALS-DEM and of its derivatives.

The four unstable rock slopes may be ranked in terms of susceptibility for failure. The uppermost instability at Mannen has without any doubt the highest susceptibility for failure with 5 decisive parameters: (1) velocity of the moving block of 4-5 cm/year, (2) rockfall activity along the sliding surface, (3) bulging of the topography at its front, (4) structures that kinematically explain the failure and (5) weak layers along the probable basal failure surface. The 3 local instabilities at the edge of Børa plateau have medium to high susceptibility for failure with velocities of 0.2-2 cm/yr and frequent rockfall activity, even though the failure mechanisms are not fully understood. The Svarttinden rockslide is structurally well defined and displays indications of past displacements with a well-developed frictional product along its single basal sliding surface. East of the remaining instability, a large volume already failed along the same basal sliding surface. However, there

are no sign of current displacement of the instability and rockfalls are restrained to its very steep faces, which cannot be interpreted as sign of activity for the rock slope instability. Therefore, the Svarttinden rock slope instability has a medium susceptibility for failure. The instabilities at Flatmark are well detached from the edge of the plateau but no conspicuous activity is observed from the deformed slope. Thus, the rock slope instabilities at Flatmark are considered having a low susceptibility for failure. The instabilities at Svarttinden and Flatmark are nonetheless under periodic monitoring because of the severe consequences of a catastrophic failure. Repetitive TLS surveys are performed in the aim to supplement the dGPS method in the detection of eventual displacements. Any increase in displacements or other signs of activity will lead to a reassessment and likely to an increase of the susceptibility for failure of these instabilities.

The present study strengthens the importance of a geological understanding of the rock slope deformation. The detailed structural analysis of gravitational rock slope instabilities leads to accurately carry out the kinematic feasibility of failure. It is also a necessary step for further advanced studies. Among other possibilities, it may allow the construction of geometrically correct numerical modeling on slope stability including the implementation of the discontinuity sets and the good localization of the borders of the deformed rock mass. The latter leads to a good estimation of the unstable volumes used to assess propagation scenarios.

ACKNOWLEDGEMENTS

The authors thank the Norwegian Water and Energy Resources Directorate for funding this study through the national plan for mapping unstable rock slopes. M. Jaboyedoff and R. Hermanns are kindly acknowledged for their review. This work is International Centre for Geohazards (ICG) contribution No. 382.

LIST OF REFERENCES

Agliardi, F., Crosta, G. B. y Zanchi, A. 2001. Structural constraints on deep-seated slope

deformation kinematics. *Engineering Geology* 59: 83-102.

Ahnert, F. 1987. Process-response models of denudation at different spatial scales. *Catena Supplement* 10: 31-50.

Ambrosi, C. y Crosta, G.B. 2006. Large sackung along major tectonic features in the central Italian Alps. *Engineering Geology* 83: 183-200.

Bachmann, D., Bouissou, S. y Chemenda, A. 2004. Influence of weathering and pre-existing large scale fractures on gravitational slope failure: insights from 3-D physical modeling. *Natural Hazards and Earth System Sciences* 4: 711-717.

Böhme, M., Saintot, A., Henderson, I., Henriksen, H. y Hermanns, R.L. 2011. Slope instabilities in Sogn og Fjordane County, Norway. In Jaboyedoff, M. (ed.) *Slope Tectonics*, Geological Society, London, Special Publications 351: 97-111.

Blikra, L.H., Braathen, A., Anda, E., Stalsberg, K. y Longva, O. 2002. Rock avalanches, gravitational bedrock fractures and neotectonic faults onshore northern Norway: Examples, regional distribution and triggering mechanisms. *NGU Report 2002.016*, Geological Survey of Norway, Trondheim, Norway.

Blikra, L.H., Longva, O., Braathen, A., Anda, E., Dehls, J. y Stalsberg, K. 2006. Rock slope failures in Norwegian fjord areas: examples, spatial distribution and temporal pattern. In Evans, S.G., Scarascia Mugnozza, G., Strom, A. y Hermanns, R.L. (eds.) *Landslides from Massive Rock Slope Failure*, NATO Science Series, IV. Earth and Environmental Sciences 49, Springer: 475-496, Dordrecht, Netherlands.

Braathen, A., Blikra, L.H., Berg, S.S. y Karlsen, F. 2004. Rock slope failures in Norway; type, geometry, deformation mechanisms and stability. *Norwegian Journal of Geology* 84: 67-88.

Brideau, M.-A., Stead, D., Kinakin, D. y Fecova, K. 2005. Influence of tectonic structures on the Hope Slide, British Columbia, Canada. *Engineering Geology* 80: 342-359.

Brideau, M.-A., Yan, M. y Stead, D. 2009. The role of tectonic damage and brittle rock fracture in the development of large rock slope failures. *Geomorphology* 103: 30-49.

Cruden, D.M. 1976. Major slides in the Rockies. *Canadian Geotechnical Journal* 13: 8-20.

- Cruden, D.M. y Varnes, D.J. 1996. Landslide types and processes. In Turner, A.K. and Schuster, R.L. (eds.) *Landslides: Investigation and Mitigation*. Special Report 247, Transportation Research Board, National Research Council, Washington DC: 36-75.
- Dahle, H., Anda, E., Saintot, A. y Sætre, S. 2008. Faren for fjellskred fra fjellet Mannen i Romsdalen. NGU Report 2008.087, Geological Survey of Norway, Trondheim, Norway [in Norwegian].
- Dahle, H., Saintot, A., Blikra, L.H. y Anda, E. 2010. Geofagleg oppfølging av ustabilt fjellparti ved Mannen i Romsdalen. NGU Report 2010.022, Geological Survey of Norway, Trondheim, Norway [in Norwegian].
- Dahle, H., Bjerke, P.L., Crosta, G., Hermanns, R.L., Anda, E. y Saintot, A. 2011. Faresoner for utløp, oppdemming og flom som følge av fjellskredfare ved Mannen, NGU Report 2011.058, Geological Survey of Norway, Trondheim, Norway [in Norwegian].
- Eberhardt, E., Stead, D. y Coggan, J.S. 2004. Numerical analysis of initiation and progressive failure in natural rock slopes – the 1991 Randa Rockslide. *International Journal of Rock Mechanics and Mining Sciences* 41: 69-87.
- El Bedoui, S., Guglielmi, Y., Lebourg, T. y Pérez, J.-L. 2008. Deep-seated failure propagation in a fractured rock slope over 10,000 years: the La Clapière slope, the south-eastern French Alps. *Geomorphology* 105: 232-238.
- ESRI (Environmental Systems Research Institute) 2010. ArcGIS [software]. Version 10, Environmental Systems Research Institute Inc., Redlands, CA.
- Etzelmüller, B., Romstad, B. y Fjellanger, J. 2007. Automatic regional classification of topography in Norway. *Norwegian Journal of Geology* 87: 167-180.
- Farsund, T.Ø. 2010. Geology, DEM analysis and geohazard assessment of the Romsdalen valley. Unpublished MSc project thesis TGB4500, Department of geology and mineral resources engineering, Norwegian University of Sciences and Technology, Trondheim.
- Farsund, T.Ø. 2011. Geological and numerical stability modelling of Mannen, Romsdalen MSc thesis in Petroleum Geosciences and Engineering, Norwegian University of Sciences and Technology, Trondheim.
- Fell, R., Corominas, J., Bonnard, C., Cascini, L., Leroi, E. y Savage, W.Z. 2008. Guidelines for landslide susceptibility, hazard and risk zoning for land use planning. *Engineering Geology* 102: 85-98.
- Fisher, R.A. 1953. Dispersion on a sphere. *Proceedings of the Royal Society of London, Series A*, 217: 295-305.
- Ganerød, G.V., Grøneng, G., Rønning, J.S., Dal-segg, E., Elvebakk, H., Tønnesen, J.F., Kveldsvik, V., Eiken, T., Blikra, L.H. y Braathen, A. 2008. Geological model of the Åknes rockslide, western Norway. *Engineering Geology* 102: 1-18.
- Giraud, A., Rochet, R. y Antoine, P. 1990. Processes of slope failure in crystallophyllian formations. *Engineering Geology* 29: 241-253.
- Guzzetti, F., Cardinali, M. y Reichenbach, P. 1996. The influence of tectonic setting and lithology on the landslide type and pattern. *Environmental and Engineering Geoscience* 2: 531-555.
- Henderson, I.H.C. y Saintot, A. 2007. Fjellskredundersøkelser i Møre og Romsdal. NGU Report 2007.043, Geological Survey of Norway, Trondheim, Norway [in Norwegian].
- Henderson, I.H.C., Saintot, A. y Derron, M.-H. 2006. Structural mapping of potential rockslide sites in the Storfjorden area, Western Norway: the influence of bedrock geology on hazard analysis. NGU Report 2006.052, Geological Survey of Norway, Trondheim, Norway.
- Henderson, I.H.C. y Saintot, A. 2011. Regional spatial variations in rockslide distribution from structural geology ranking: an example from Storfjorden, western Norway. In Jaboyedoff, M. (ed.) *Slope Tectonics*. Geological Society Special Publication 351, p. 79.
- Hermanns, R.L. y Strecker, M.R. 1999. Structural and lithological controls on large Quaternary rock avalanches (sturzstroms) in arid northwestern Argentina. *Geological Society of America Bulletin* 111: 934-948.
- Hoek, E. y Bray, J. 1981. *Rock slope engineering*, revised 3rd edition. The Institution of Mining and Metallurgy, London: 37-63.
- Hossack, J.R. y Cooper, M.A. 1986. Collision tectonics in the Scandinavian Caledonides. *Geological Society of London. Special Publication* 19: 287-304.
- InnovMetric 2012. PolyWorks: 3D scanner and 3D digitizer software from InnovMetric Software Inc. <http://www.innovmetric.com/polyworks/3D-scanners/home.aspx?lang=en>, accessed 20.01.2012.
- Jaboyedoff, M., Baillifard, F., Couture, R., Locat, J. y Locat, P. 2004a. New insight of geomorphology and landslide prone area detection using Digital Elevation Model(s). In Lacerda, W.A., Ehrlich, M., Fontoura, A.B. y Sayão, A. (eds.) *Landslides: Evaluation and Stabilization*, Taylor & Francis Group: 191-198, London.
- Jaboyedoff, M., Baillifard, F., Couture, R., Locat, J. y Locat, P. 2004b. Toward preliminary hazard assessment using DEM topographic analysis and simple mechanical modeling by means of sloping local base level. In Lacerda, W.A., Ehrlich, M., Fontoura, A.B. and Sayão, A. (eds.) *Landslides: Evaluation and Stabilization*, Taylor & Francis Group: 199-205, London.
- Jaboyedoff, M., Couture, R. y Locat, P. 2009. Structural analysis of Turtle Mountain (Alberta) using digital elevation model: Towards a progressive failure. *Geomorphology* 103: 5-16.
- Jaboyedoff, M., Oppikofer, T., Derron, M.-H., Blikra, L.H., Böhme, M. y Saintot, A. 2011. Complex landslide behaviour and structural control: a three dimensional conceptual model of the Åknes rockslide, Norway. In Jaboyedoff, M. (ed.) *Slope Tectonics*, Geological Society, London, Special Publications 351: 147-162.
- Julian, M. y Anthony, E. 1996. Aspects of landslide activity in the Mercantour Massif and the French Riviera, southeastern France. *Geomorphology* 15: 275-289.
- Kellogg, K.S. 2001. Tectonic controls on a large landslide complex: Williams Fork Mountains near Dillon, Colorado. *Geomorphology* 41: 355-368.
- Longchamp, C., Delasoie, F., Carrea, D., Derron, M.-H., Oppikofer, T. y Jaboyedoff, M. 2010. Analysis of groundbased Lidar data from Møre og Romsdal County (Norway), Unpublished Report IGAR – UNIL.
- Longva, O., Blikra, L.H. y Dehls, J. 2009. Rock avalanches – distribution and frequencies in the inner part of Storfjorden, Møre og Romsdal County, Norway. NGU report 2009.002, Geological Survey of Norway, Trondheim, Norway.

- Mahr, T. 1977. Deep-reaching gravitational deformations of high mountain slopes. *Bulletin of the International Association of Engineering Geology* 16: 121-127.
- Mangerud, J. 2004. Ice sheet limits in Norway and on the Norwegian continental shelf. In Ehlers, J. y Gibbard, P.L. (eds.) *Quaternary Glaciations Extent and Chronology Part I: Europe*, Elsevier: 271-294.
- Mosar, J. 2003. Scandinavia's North Atlantic passive margin. *Journal of Geophysical Research* 108: NO. B8, 2360, doi:10.1029/2002JB002134.
- Olesen, O., Dehls, J., Bungum, H., Riis, F., Hicks, E., Lindholm, C., Blikra, L.H., Fjeldskar, W., Olsen, L., Longva, O., Faleide, J.I., Bockmann, L., Rise, L., Roberts, D., Braathen, A. y Brekke, H. 2000. Neotectonics in Norway, Final Report. Geological Survey of Norway, Report 2000.002, Geological Survey of Norway, Trondheim, Norway.
- Olesen, O., Blikra, L.H., Braathen, A., Dehls, J.F., Olsen, L., Rise, L., Roberts, D., Riis, F., Faleide, J.I. y Anda, E. 2004. Neotectonic deformation in Norway and its implications: a review. *Norwegian Journal of Geology* 84: 3-34.
- Oppikofer, T. 2009. Detection, analysis and monitoring of slope movements by high resolution digital elevation models, PhD thesis, Institute of Geomatics and Analysis of Risk, University of Lausanne, Lausanne, Switzerland.
- Oppikofer, T., Jaboyedoff, M., Blikra, L.H. y Derron, M.-H. 2009. Characterization and monitoring of the Åknes rockslide using terrestrial laser scanning. *Natural Hazards and Earth System Sciences* 9: 1003-1019.
- Oppikofer, T., Jaboyedoff, M., Pedrazzini, A., Derron, M.-H. y Blikra, L.H. 2011. Detailed DEM analysis of a rockslide scar to improve the basal failure surface model of active rockslides. *Journal of Geophysical Research* 116: F02016. doi:10.1029/2010JF001807.
- Oppikofer, T., Hermanns, R.L., Redfield, T.F., Sepúlveda, S.A., Duhart, P. y Bascuñán, I. 2012. Morphologic description of the Punta Cola rock avalanche and associated minor rockslides caused by the 21 April 2007 Aysén earthquake (Patagonia, southern Chile). *Revista de la Asociación Geológica Argentina*, this volume.
- Pedrazzini, A., Froese, C.R., Jaboyedoff, M., Hunger, O. y Humair, F. 2012. Combining digital elevation model analysis and run-out modelling to characterize hazard posed by a potentially unstable rock slope at Turtle Mountain, Alberta, Canada. *Engineering Geology* DOI:10.1016/j.enggeo.2011.03.015.
- Roberts, D. 2003. The Scandinavian Caledonides: event chronology, palaeogeographic settings and likely modern analogues. *Tectonophysics* 363: 283-299.
- Roberts, D. y Gee, D.G. 1985. An introduction to the structure of the Scandinavian Caledonides. In Gee, D.G. and Sturt B.A. (eds) *The Caledonide Orogen - Scandinavia and related areas* 55-68. John Wiley and Sons, Chichester.
- Saintot, A., Elvebakk, H., Ganerød, G.V., Oppikofer, T. y Farsund, T. 2011a. Mannen unstable rock slope (Romsdal, Møre & Romsdal County): Logging of drill hole and core KH-01-10, geomorphological interpretation of a 1 m resolution digital elevation model and terrestrial laser scan displacement analysis. *NGU Report* 2011.026, Geological Survey of Norway, Trondheim, Norway.
- Saintot, A., Henderson, I. y Derron, M.-H. 2011b. Inheritance of ductile and brittle structures in the development of large rock slope instabilities: examples from Western Norway. In Jaboyedoff, M. (ed.) *Slope Tectonics*, Geological Society, London, Special Publications 351: 27-78.
- Sauchyn, D.J., Cruden, D.M. y Hu, H.Q. 1998. Structural control of the morphometry of open rock basins, Kananaskis region, southwestern Alberta. *Geomorphology* 22: 313-324.
- Selby, M.J. 1993. *Hillslope Materials and Processes*. Oxford University Press, New York.
- Skrednett 2012. Skreddata på nett. <http://www.ngu.no/kart/skrednett>, accessed 06.02.2012 [in Norwegian].
- Torsvik, T.H., Andersen, T.B. Eide, E.A. y Walderhaug, H.J. 1997. The age and tectonic significance of dolerite dykes in western Norway. *Journal of Geological Society of London* 154: 961-973.
- Tveten, E., Lutro, O. y Thorsnes, T. 1998. Geologisk kart over Norge, berggrunnskart Ålesund, 1:250,000. Geological Survey of Norway, Trondheim [in Norwegian].
- Valle, P., Faereth, R. B. y Fossen, H. 2002. Devonian-Triassic brittle deformation based on dyke geometry and fault kinematics in the Sunnhordland region, SW Norway. *Norwegian Journal of Geology* 82: 3-17.
- Varnes, D.J. 1978. Slope movement types and processes. In Schuster, R.L. and Krizek, R.J. (eds.) *Landslides, Analysis and Control*. Transportation Research Board Special Report, 176. National Research Council, Washington, DC: 11-33.
- Wallbrecher, E. 1986. Tektonische und gefügebanalytische Arbeitsweisen. Enke-Verlag, Stuttgart [in German].
- Weinberger, R., Eyal, Y. y Mortimer, N. 2010. Formation of systematic joints in metamorphic rocks due to release of residual elastic strain energy, Otago Schist, New Zealand. *Journal of Structural Geology* 32: 288-305.
- Welkner, D., Eberhardt, E. y Hermanns, R.L. 2010. Hazard investigation of the Portillo Rock Avalanche site, central Andes, Chile, using an integrated field mapping and numerical modelling approach. *Engineering Geology* 114: 278-297.

Recibido: 11 de febrero, 2012

Aceptado: 23 de abril, 2012

APPENDIX 4: SCHLEIER ET AL. (2013) SPATIAL DISTRIBUTION OR ROCKSLIDE DEPOSITS AND THEIR MORPHOLOGICAL FEATURES SUGGEST TIMING AND PALEO-ENVIRONMENTAL CONDITIONS FOR ROCK SLOPE FAILURES IN INNERDALEN AND INNFJORDDALEN, MØRE OG ROMSDAL COUNTY, WESTERN NORWAY

Full citation: Schleier, M., Hermanns, R.L. and Rohn, J. (2013) Spatial distribution or rockslide deposits and their morphological features suggest timing and paleo-environmental conditions for rock slope failures in Innerdalen and Innfjorddalen, Møre og Romsdal County, Western Norway. In: Genevois, R. and Prestininzi, A. (eds.) *International Conference Vaiont, 1963-2013 - thoughts and analyses after 50 years since the catastrophic landslide*, Italian Journal of Engineering Geology and Environment - Book Series 6, Sapienza University, Rome, Italy, pp. 493-505.

**SPATIAL DISTRIBUTION OF ROCKSLIDE DEPOSITS AND THEIR
MORPHOLOGICAL FEATURES SUGGEST TIMING AND
PALAEO-ENVIRONMENTAL CONDITIONS FOR ROCK SLOPE
FAILURES IN INNERDALEN AND INNFJORDDALEN,
MØRE OG ROMSDAL COUNTY, WESTERN NORWAY**

MARKUS SCHLEIER^(*), REGINALD L. HERMANN^(**) & JOACHIM ROHN^(*)

^(*)University of Erlangen-Nuremberg, GeoZentrum Nordbayern - Schlossgarten 5 - D-91054 Erlangen, Germany
Email: markus.schleier@gzn.uni-erlangen.de / Phone: 004991318522723

^(**)Geological Survey of Norway (NGU) - Trondheim, Norway

ABSTRACT

Rock avalanches dropping into a fjord or lake, initiating displacement waves or damming narrow valleys, are severe hazard scenarios in glacial overprinted mountain areas and have strong influence on the quaternary valley development. Several investigations show, that the collapse of a rock avalanche increases the probability for prospective similar events at the same rock slope. Moreover, data for the Storfjord area in Western Norway indicates that catastrophic rockslides were more frequent during late Pleistocene than in Holocene. This study is to test these hypotheses, to reconstruct the palaeo-environmental conditions of multiple landslide deposits, and to study the effect of rock avalanches on decaying ice bodies and landforms influenced by isostatic rebound. For investigation, the two valleys of Innerdalen and Innfjorddalen in Western Norway were chosen, where multiple landslide deposits have developed on the valley floor. Its spatial and temporal distribution is studied by detailed field investigations, including morphological and sedimentological analyses. In Innerdalen glacial and postglacial rock avalanches have occurred, whereas the first was partly deposited on the decaying ice body. In Innfjorddalen several post glacial rock avalanches occurred, whereas the first was deposited on highly water saturated valley fill sediments. In both valleys distinct morphological features have developed.

KEY WORDS: multiple landslide deposits, rock avalanche, morphological analyses, palaeo-environmental conditions, Western Norway

INTRODUCTION

In glacial overprinted mountain areas like in Western Norway, important hazards are large rock slope instabilities that might develop into large rock avalanches. The most severe scenarios are large volumes of rock dropping into a fjord or lake, causing displacement waves or damming narrow valleys causing upstream and potential downstream flooding, (HERMANN *et alii*, 2004; EVANS *et alii*, 2011; HERMANN *et alii*, 2011a; HERMANN *et alii*, 2012; HERMANN & LONGVA, 2012).

Furthermore, large rock avalanches and their deposits which developed across valleys and built dams play a major role in late quaternary landscape evolution (HEWITT *et alii*, 2011). The detailed study of multiple landslide deposits as for example presented in (HERMANN *et alii*, 2006; WELKNER *et alii*, 2010; BLAIS-STEVENS *et alii*, 2011) provides important information to understand palaeo-environmental conditions, failure mechanisms, activity of steep rock slopes, and to estimate recurrence periods for similar events which is important for hazard assessments.

Data on the temporal distribution of rockslide deposits in Storfjord (Møre og Romsdal County, Western Norway) suggest that catastrophic rockslides were larger and more frequent during the late Pleistocene than in

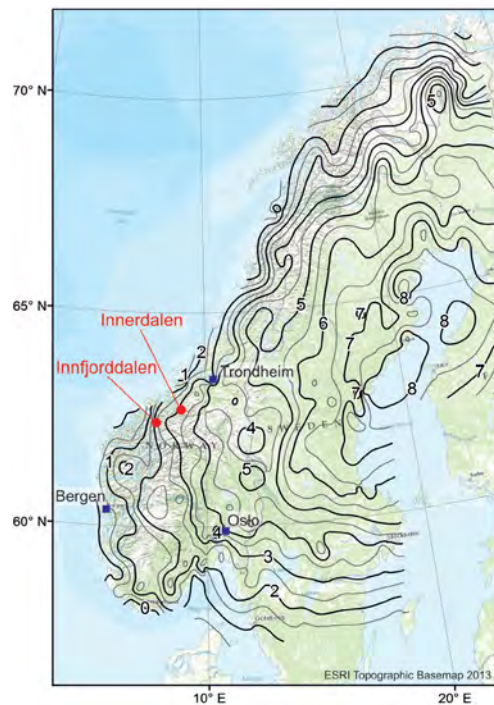


Fig. 1 - Map of Norway showing the locations of the study areas (red dots) and the current apparent uplift of Fennoscandia. Values are uplift rates in mm/yr following DEHLS *et alii* (2000)

the Holocene (HERMANN & LONGVA, 2012). With this study we want to test if similar temporal pattern can also be expected for other valleys in Norway. In addition we aim to study the effect of rock avalanching on decaying ice bodies and landforms subjected to isostatic rebound.

We selected the Innerdalen and Innfjorddalen in Møre og Romsdal County in western Norway, where multiple rock avalanche deposits occur. During field investigations the spatial distribution of the multiple rockslide deposits, soft sediments and the morphological structures were mapped. The different sediments were described by plotting grain size and grain shape. Furthermore, samples for dating the different deposits with in-situ terrestrial cosmogenic nuclides were taken to determine the exact chronological distribution.

The main aims of this publication are:

- 1) to distinguish the multiple rock avalanche deposits spatially and stratigraphically,
- 2) to reconstruct the palaeo-environmental conditions under which all events formed,
- 3) to describe the facies of rock avalanches onto different type of substrate.

STUDY AREA

The two study areas, the valleys of Innerdalen and Innfjorddalen, are located in Møre og Romsdal County in Western Norway (Fig 1).

These areas are located in the Western Gneiss Region of Norway. The exposed rocks are Proterozoic gneisses, mainly orthogneisses, partly overlain by continental and oceanic sediments which have been affected by the Caledonian orogeny (HACKER *et alii*, 2010). The bedrock and the deposits in the study areas are composed out of the typical hard gneisses of this region. Based on the geological map of Ålesund (TVETEN *et alii*, 1998), the main rock types can be described as follows:

In the Innerdalen area, the disclosed rocks consist of three main lithologies, 1) coarse-grained granitic gneiss, augengneiss, gneissic granite, 2) meta-arkose, quartzite and 3) coarse to fine-grained granitic to dioritic, biotite containing gneiss. The additional quartzitic rock layers in Innerdalen are located at the border of a main thrust fault. The multiple landslide deposits contain all of these lithologies.

The disclosed lithologies in the Innfjorddalen area are 1) coarse-grained granitic gneiss, augengneiss, gneissic granite, 2) sillimanit containing quartzitic gneiss, partly containing kyanite and 3) undifferentiated gneiss, mostly quartzdioritic, partly migmatitic.

The quaternary landscape evolution is also important for the presented study of rock avalanches onto different substrates. In Western Norway the present distribution of marine sediments at elevations up to 220 m a.s.l. show that the land mass near the shoreline partly raised up for several hundred meters since the Last Glacial Maximum (HERMANN *et alii*, 2012). This development is part of the dome-like postglacial uplift of Fennoscandia, which is explained generally as movements of solid earth originated in glacioisostatic rebound due to melting of the thick ice sheets and attended unloading of the crust (FJELDSKAAR *et alii*, 2000). This uplift is a still ongoing process and following the neotectonic map of Norway (DEHLS *et alii*, 2000), the present apparent uplift rates are up to 8 mm/yr, showing values of 2 to 3 mm/yr for the study areas (Fig 1).

Therefore, the glaciation during the last ice age and the following deglaciation, the crustal uplift and sea level changes have enormous influence on the landscape evolution due to deep valley incisions, changes in sedimentation, erosion, and stress fields in rock slopes as well as induced seismicity.

SPATIAL DISTRIBUTION OF ROCKSLIDE DEPOSITS AND THEIR MORPHOLOGICAL FEATURES SUGGEST TIMING AND PALAEO-ENVIRONMENTAL CONDITIONS FOR ROCK SLOPE FAILURES IN INNERDALEN AND INNFJORDDALEN, MØRE OG ROMSDAL COUNTY, WESTERN NORWAY

Both, the Innerdalen and the Innfjorddalen are steep glacial affected valleys which show high topographic relief with mean elevation differences of around 1,000 m between valley bottom and surrounded mountain crests.

METHODS

In order to determine and describe the different multiple landslide deposits in the two study areas and to reconstruct the palaeo-environmental conditions an area of ~16 km² was mapped in the valley of Innerdalen and ~4 km² in Innfjorddalen (Fig. 2, Fig. 5).

We mapped the spatial distribution of Late Pleistocene and Holocene deposits and their geomorphological features and, described their grain size and shape by statistically sampling of 100 randomly connected boulders. We used the six roundness classes after Folk as described in (BOGGS, 2001). For Innerdalen such data was collected at 75 sample sites, distributed in the different landslide and moraine deposits and 13 sample sites for the multiple deposits in Innfjorddalen.

We also assessed the mean thickness of the deposits to estimate volumes of different events.

The Fahrböschung angle (angle between the horizontal and the connecting line of main scarp's upper limit and the deposit's most distal part) was calculated for the rock avalanche deposits, showing the apparent friction angle (HEIM, 1932).

In order to determine the absolute ages of the multiple deposits and therefore to reconstruct the valley history and to estimate the recurrent period, surface exposure dating with in-situ terrestrial cosmogenic nuclides using ¹⁰Be were taken in both valleys. Results are not yet available.

RESULTS AND DISCUSSION

DEPOSITS WITHIN THE INNERDALEN

In Innerdalen multiple deposits composed of rock boulders several meter in diameter occur. They can be divided in two groups: a) continuous rock avalanche deposits with typical lobate shapes with boulders several meters to tens of meters in diameter that cover the entire surface of the deposits, b) suspicious discontinuous boulder deposits that form various morphological units, and that are separated from each other by several km, and that are covered by almost identi-

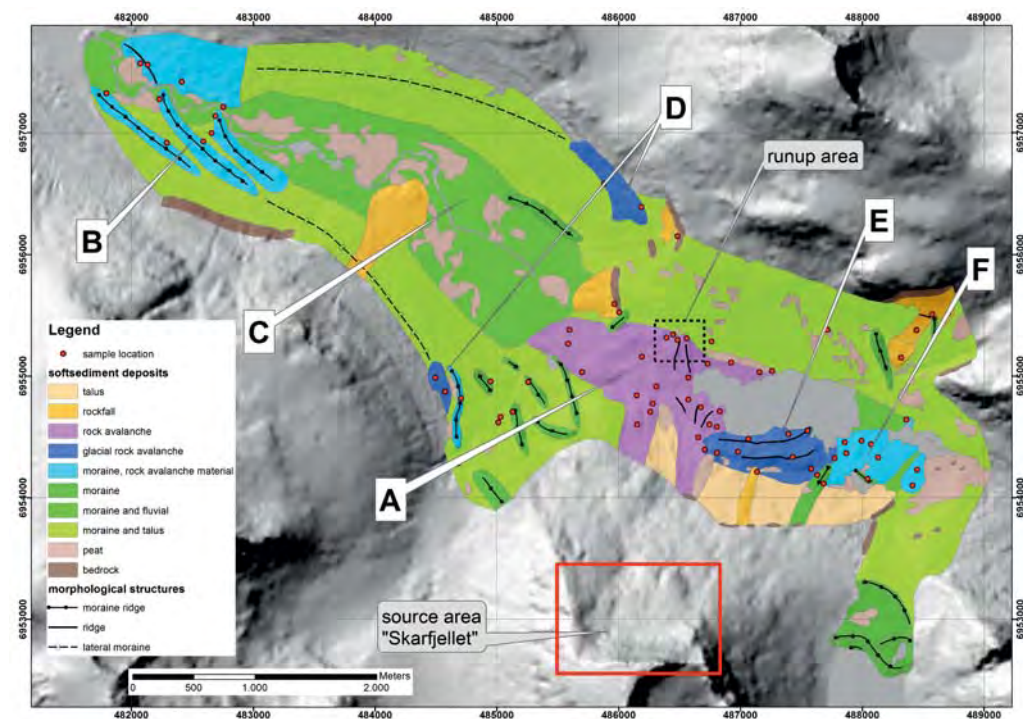


Fig. 2 - Map of multiple landslide deposits in Innerdalen. A-F mark the main deposits described in the text. The source area of the multiple landslides is marked with red rectangle. The runup area is marked with dotted rectangle

495

cal boulders. We divided all deposits in six units, A-F (Fig. 2, Fig. 3).

A) This is a typical lobate rock avalanche deposit spanning the valley bottom and impounding a lake, B) three prominent frontal moraine ridges in the outer valley, C) scattered isolated hills composed of boulders on the valley floor in the lower part of Innerdalen, D) isolated patches of boulders on the slope several 100 m above the valley floor, E) distinctive valley parallel ridges along and F) flat boulder patches in the upper Innerdalen. In total an area of around 2.4 km² is covered by these deposits and their total estimated volume is ~64x10⁶ m³. The main geometrical characteristics of the

multiple landslide deposits are summarized in Tab. 1.

ROCK AVALANCHE DEPOSIT ALONG VALLEY BOTTOM THAT IMPOUNDS A LAKE (A)

The rock avalanche deposit (A) stretches on the valley floor over a length of ~1700 m and a width of 1100 m in the upper part and 270 m (mean 800 m) in the most distal part, covering an area of around 1,303,000 m². That represents a volume of ~39x10⁶ m³ (Tab. 1). The deposit shows lateral levees and frontal rims. It covers the valley on its whole width and indicates a runup on the opposite valley slope of around 65 m. The deposit forms a natural dam that impounds a lake. Furthermore the deposit part-

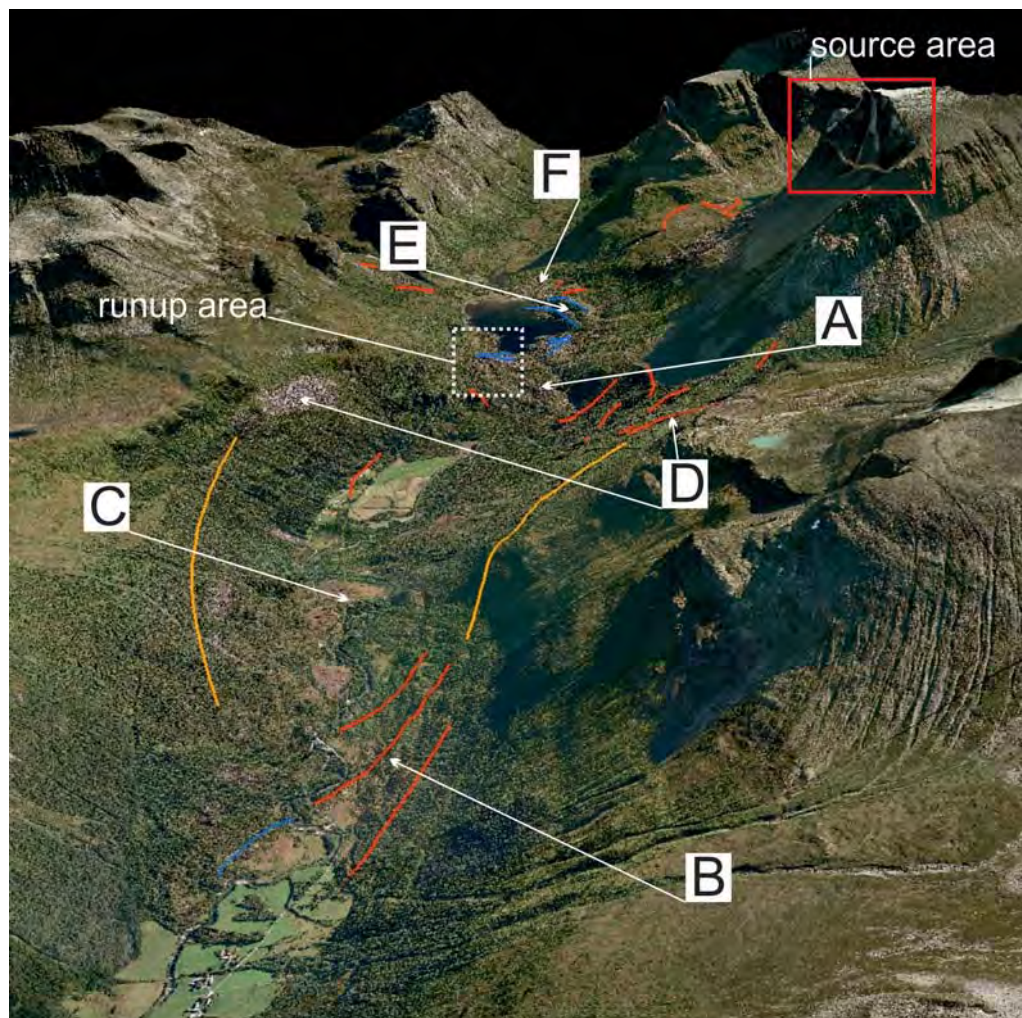


Fig. 3 - Oblique view of Innerdalen valley showing the main part of the multiple landslide deposits. View direction to WSW. A - F mark the main deposits described in text. The rock face of the source area is marked with red rectangle, the runup with dotted rectangle. Orange lines mark lateral moraines, red lines mark the frontal moraines

SPATIAL DISTRIBUTION OF ROCKSLIDE DEPOSITS AND THEIR MORPHOLOGICAL FEATURES SUGGEST TIMING AND PALAEO-ENVIRONMENTAL CONDITIONS FOR ROCK SLOPE FAILURES IN INNERDALEN AND INNFJORDDALEN, MØRE OG ROMSDAL COUNTY, WESTERN NORWAY

ly covers moraine deposits. The source area of this event is located at the steep northern rock face of the “Skarfjellet” south of the lake (Fig. 3). The horizontal distance of the top of the scarp to the end of the runup deposit is ~3270 m and the elevation difference is ~1290 m. Therefore the Fahrböschung angle is 21.5°. The distal part of the deposit has a distance from the source of 3320 m and an elevation difference of 1460 m, therefore is the Fahrböschung angle 23.7°. The mean grain size of this rock-avalanche deposit is 1.5 m. The distribution shows a concentration between 0.5 and 2 m with maximum size boulders >10 m in diameter. The mean roundness is subangular (57%) to angular (37%).

PROMINENT FRONTAL MORAINES RIDGES IN THE OUTER VALLEY (B)

In the outer part of the valley three distinct frontal moraines (B) occur that are closely spaced. These are one km long and have elevations of 12 to 15 m above the current valley floor. The mean width of the deposits ranges from 100 to 140 m. These moraine deposits cover an area of around 395,000 m² and contain an estimated volume of 7.3×10⁶ m³. The sedimentological features of the three ridges are identical. They are entirely covered by boulders several meters to tens of meters in size with no finer grained material (matrix) visible. However in fluvial cuts the core is visible that contains a sandy matrix with angular but also well rounded grains (Fig. 4). The deposits have a mean grain size of ~1 m with clasts that exceed 5 m in diameter. According to the grain roundness they show normal distribution with a peak for subangular boulders (54%). Angular (25%) and subrounded (21%) boulders are almost equal distributed.

SCATTERED ISOLATED HILLS ON VALLEY FLOOR (C)

Within the area between deposit (A) and (B) the valley floor is characterized by scattered single isolated hills (C) of boulder accumulations only few meters high and several meters in diameter which occur scattered on the normal valley sediments. These boulders are surrounded by valley fill material.

ISOLATED BOULDER PATCH ON THE SLOPE ABOVE THE VALLEY FLOOR (D)

Within the slope and ~270 m to 370 m above the valley floor several-100-m²-large boulder fields occur on both sides of the valley that are separated from each other. These patches lower towards the outer valley and terminate in the frontal moraines. The most prominent boulder patch is located on the northern valley slope. It covers an area of 147,000 m². Its estimated volume is 2.2×10⁶ m³ (Tab. 1). Another isolated boulder patch is located on the opposite southern valley slope at similar elevation but it has a smaller extent (Fig. 2). It is obvious that there exists no connection to any possible scarp upslope at any of the localities (Fig. 3). The grain size distribution of these deposits shows a mean diameter of ~1 m with maximum clast size reaching >10 m. The deposit shows a relatively wide and not distinct grain roundness distribution with angular (46%) and subangular (43%) boulders with a tendency towards very angular boulders (12%).

PROMINENT VALLEY PARALLEL RIDGES ALONG THE LAKE (E)

There are two prominent morphological ridges parallel to the valley along the southern shore of the lake. The lower one (E1), has a length of 870

Area	Description	Mean est. thickness [m]	Measured area [m ²]	Est. Volume [m ³]	Fahrböschung angle [°]
A	Rock avalanche deposit	30	1,302,884	39,086,520	21.5 (runup), 23.7 (distal)
B	1 st moraine	20	115,496	2,309,920	
	2 nd moraine	20	152,147	3,042,940	
	3 rd moraine	15	127,646	1,914,690	
D	Isolated boulder patch	15	146,669	2,200,035	
E..1	1 st ridge	40	101,559	4,062,360	
...2	2 nd ridge	50	167,523	8,376,150	
F	Flat boulder patch	10	264,592	2,645,920	
Sum			2,378,516	63,638,535	

Tab. 1 - Geometrical characteristics of multiple landslide deposits in Innerdalen

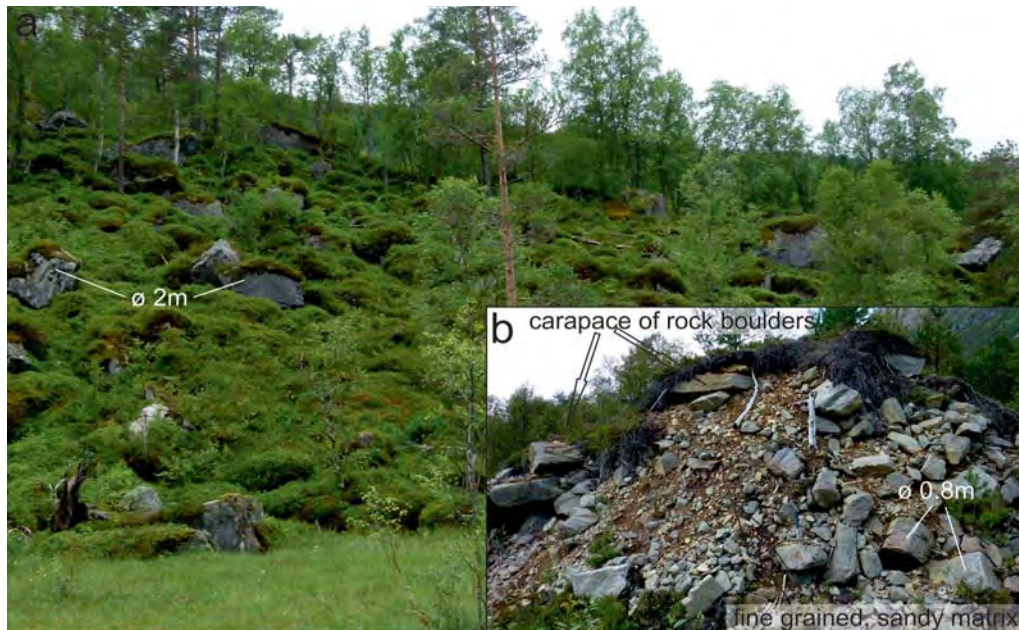


Fig. 4 - Morphological end moraine ridge in Innerdalen, around 12 meter high (a). Four meter high fluvial cut (b) shows fine grained sandy matrix in subsurface. For scale consider mean diameter of visible boulders marked in (a) and (b)

m and a mean width of 110 m and a mean height of 30 m above the lake (water level 395 m a.s.l.). Its deposit covers an area of 102,000 m². The second higher ridge (E2) is 1060 m long, 150 m wide and 50 m higher than the shoreline. The deposit spans an area of around 168,000 m². The depth of the lake is at least 18 m in the front part (west). Therefore the mean thickness of the deposit of the lower ridge can be estimated to be 40 m and 50 m for the higher ridge. This results in a volume of 4×10^6 m³ for the lower and 8.4×10^6 m³ for the upper ridge (Tab. 1). No deposits of similar composition can be found on the opposite (northern) shore of the lake. The material of the ridges (deposit E) is similar. They show a mean grain size of surficial boulders of around 1.5 m. The roundness of boulders for both ridges shows a distinct peak for subangular boulders (76% for E1 and 60% for E2). In addition also angular boulders occur whereas its amount is higher in E2 (34%) and there also few subrounded boulders exist.

FLAT BOULDER PATCH SE OF LAKE (F)

At the SE boarder of the lake patches of boulder deposits occur (F). Morphologically these patches are relatively flat (no ridges). The depo-

sit covers an area of ~265,000 m² and its mean thickness is estimated with 10m, therefore it is containing a volume of $\sim 2.6 \times 10^6$ m³. The mean grain size of deposit (F) is around 1 m with no distinct concentration. This deposit shows a widely distribution of grain roundness with a peak for subangular (58%) and angular boulders (30%), but also subrounded (10%) and less very angular (2%) boulders occur.

DISCUSSION OF DEPOSITS WITHIN THE INNERDDALEN

In this glacial affected, U-shaped valley, multiple landslide deposits occur that have similar sedimentological features of their bouldery carapace (grain size, grain roundness). However, they show strong differences in the morphology of the deposits thus strongly differing palaeo-environmental conditions of their formation.

The post glacial event is a very distinct rock avalanche deposit (A). It shows the typical morphological characters of a rock avalanche with the carapace composed of large rock boulders of subangular (57%) and angular (37%) forms. This indicates that the deposit was not reworked after deposition. In addition, the lateral levees and frontal rim (DUFRESNE & DAVIES, 2009) with a run-up of 65 meters indicate the typical high mobility

SPATIAL DISTRIBUTION OF ROCKSLIDE DEPOSITS AND THEIR MORPHOLOGICAL FEATURES SUGGEST TIMING AND PALAEO-ENVIRONMENTAL CONDITIONS FOR ROCK SLOPE FAILURES IN INNERDALEN AND INNFJORDDALEN, MØRE OG ROMSDAL COUNTY, WESTERN NORWAY

of a rock avalanche. The source area can be located at the steep northern rock face of the "Skarfjellet" mountain. Evidence for its postglacial origin is that the deposit partly covers some moraine deposits and that it fills the valley floor over its whole width. This deposit dams a lake that is evidently stable since formation. Following the description of rockslide dams of (HERMANN *et alii*, 2011b) this dam can be classified as an IIa ii 2 event.

Grain sizes of the carapaces of other landforms as well as grain roundness suggest a further rock avalanche event in the valley. For example are the three closely spaced distinct morphological moraine ridges (B) also covered by a carapace of rock boulders several meters in diameter. These deposits (B) show the smallest mean grain size of boulders (chiefly <0.5 to 1 m) and mainly subangular (54%) forms however with a trend towards subrounded forms (21%). This suggests more reworking and mixture of material during transport has taken place. In fluvial cuts it gets visible that the moraine material is not pure rock avalanche material but that the boulders are imbedded in fine grained, sandy matrix. Suspicious are also the isolated hills composed of rock boulders surrounded by fluvial sediments (C) that are scattered in the whole valley bottom between the post glacial rock avalanche deposit (A) and the moraine ridges (B).

The isolated boulder patches on both sides of the valley (D) suggest that these landforms formed when a landform occupied that valley that does not exist anymore. The mean elevation of around 350 m above valley suggests the thickness of that landform at that time. The high amount of angular (46%) and even very angular boulders shows less reworking of those boulder patches.

Both of the valley parallel ridges (E) are also entirely covered by subangular boulders (76%) and no subrounded boulders could be found, that indicates no significant transportation. Their location at only one side of the lake suggests a process that leads to concentration of sediments into these ridges.

Therefore we interpret that a rock avalanche occurred in this valley, when it was filled by a glacier at the end of the Younger Dryas. This rock avalanche would have traveled over the glacier and deposited the bouldery patches above the valley floor on unglaciated ground, thus marking the thickness of the ice body at that time. However most of the material would have been deposited onto the glacier where it was redeposited with the

normal supra- and subglacial load into the three closely spaced frontal moraine ridges. According to (HEWITT, 2009; SHUGAR & CLAGUE, 2011) rock avalanche material that covers the glacier protects the ice from melting. In addition fine grained material is washed out by supraglacial processes and therefore rock boulders are concentrated. Following our model, the formation of the two morphological ridges (D) is related to that process. A decaying ice body as at the end of the Younger Dryas is rather stagnant. Insulation on the N side and hence S-facing side of a valley would cause such a stagnant ice body decay asymmetrically leading to the concentration of boulders on the S (and thus N facing) valley side.

We see the boulder patch (deposit F) east and up-valley disconnected to this process, although composed of similar material (grain size and grain roundness). Due to its relatively flat surface, and its coincidence with moraine deposits, we suspect that this material is related to retransported rock fall and rock avalanche material from higher up in the catchment as catastrophic landslides are also very abundant in the upper catchment (HERMANN *et alii*, 2013).

DEPOSITS WITHIN THE INNFJORDDALEN

In the lower Innfjorddalen a succession of multiple rock avalanche deposits with lobate forms overly each other. These are covered with rock boulders, meter to several meters in diameter. The second of those deposits is damming a lake, however also the older deposits span the entire width of the valley suggesting that similar dams also existed before (Fig. 5).

Several distinguishable morphological features can be mapped: a marine terrace deposit (A), a first stratigraphically lowest rock avalanche deposit that can be divided into a continuous deposit (B) in the upper valley and a distal part (E). In between there are an area of deformed (C) and an area of undeformed (D) valley fill deposits. The proximal part of the stratigraphically lowest rock avalanche deposit is overlain by a second rock avalanche deposit with a smaller extension (F) and these are overlain by a third rock fall deposit with much smaller extension (G).

MARINE TERRACE DEPOSITS (A)

A distinct terrace occurs in the inner part of the valley. This deposit (A) is composed out of fine grained material, chiefly rounded and well rounded sand and gravel and shows typical graded and with

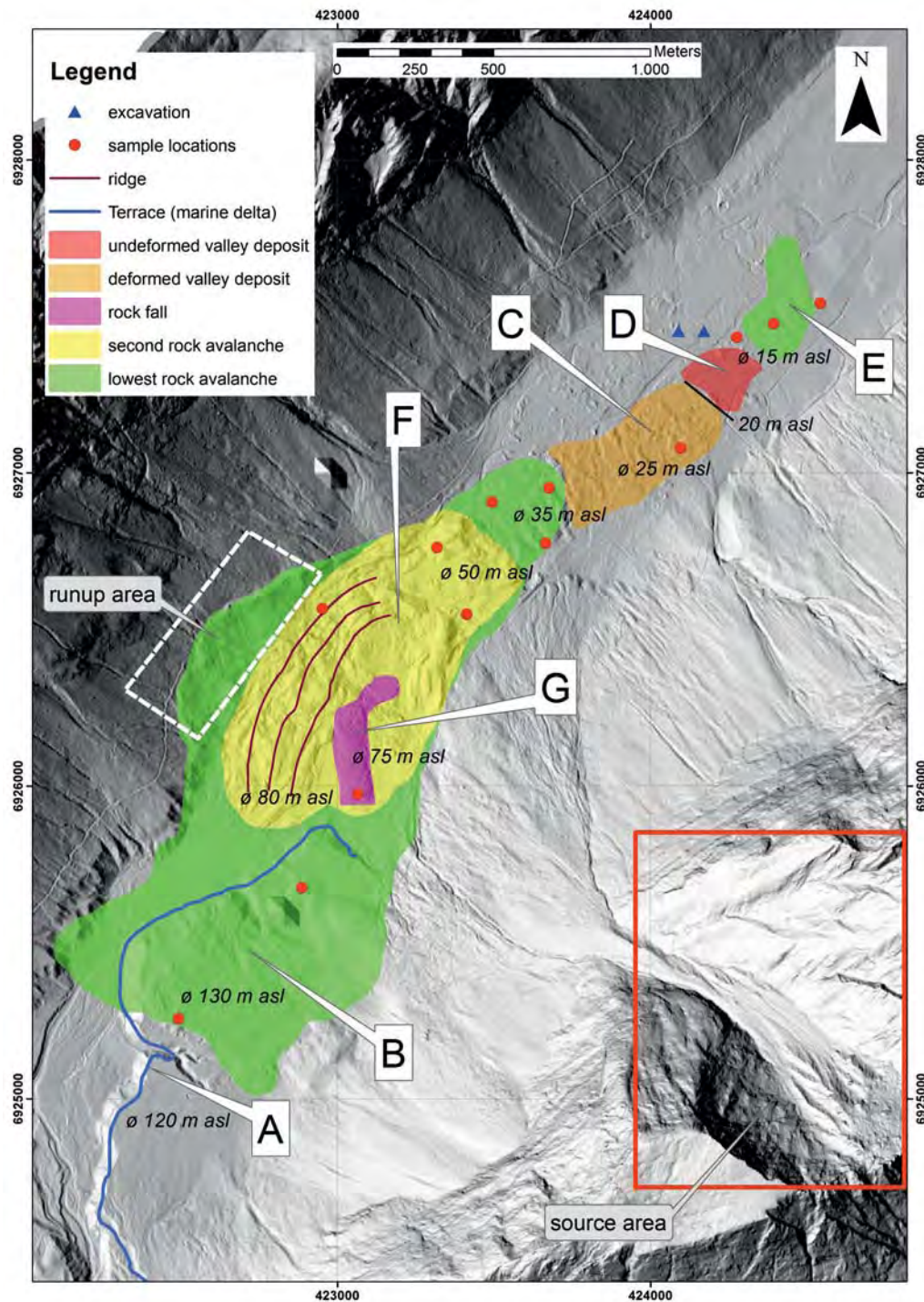


Fig. 5 - Map of multiple Holocene deposits in Innfjordalen. A - G mark the areas which are described in the text. The source area of the multiple rock avalanches and rock falls is marked with red rectangle. The runup area (~110 m above valley floor) is marked with a dotted rectangle. Values showing mean elevation of deposits above sea level

SPATIAL DISTRIBUTION OF ROCKSLIDE DEPOSITS AND THEIR MORPHOLOGICAL FEATURES SUGGEST TIMING AND PALAEO-ENVIRONMENTAL CONDITIONS FOR ROCK SLOPE FAILURES IN INNERDALEN AND INNFJORDDALEN, MØRE OG ROMSDAL COUNTY, WESTERN NORWAY

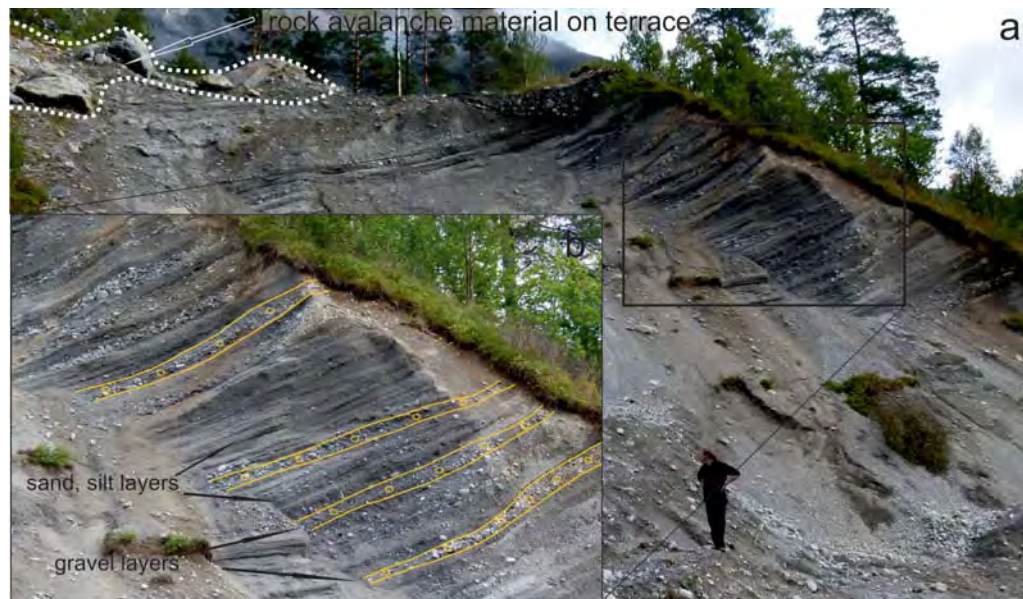


Fig. 6 - Marine terrace deposit in Innfjorddalen valley. Rock avalanche material is deposited on top of the terrace at 120 m a.s.l. (upper left corner) (a). Typical bedding structures of a propagating delta are visible in (b). View towards SSE. For scale consider Geologist in lower right of (a)

Area	Description	Mean est. thickness [m]	Measured Area [m ²]	Est. Volume [m ³]	Mean Elevation [m asl]	Fahrböschung angle [°]
B	Continuous deposit of lowest rock avalanche	15	1,407,376	21,110,640	130 to 35	22.3
E	Distal part of lowest rock avalanche deposit (isolated hills)	5	50,393	251,965	15	19.6
F	Second rock avalanche	10	542,555	5,425,550	80 to 50	25.1
G	Rock fall	5	38,999	194,995	75	28.8
Sum			2,039,323	48,351,180		

Tab. 2 - Geometrical characteristics of multiple landslide deposits in Innfjorddalen

25 degrees inclined bedding structures of a propagating marine delta (Fig. 6). This terrace surface lies at an altitude of 120 m a.s.l., marking an isostatic rebound of that area of at least 120 m. All rock-avalanche deposits lie on top of this terrace.

SUCCESSION OF MULTIPLE ROCK AVALANCHE AND ROCK FALL DEPOSITS (B, F, G)

The deposits of the lowest (B) and intermediate (F) rock avalanche and the upper (G) rock fall deposit are composed of rock boulders, several meters in diameter building a typical carapace. The deposit (B) covers an area of 1,407,000 m² and has an estimated volume of 21×10^6 m³ (Tab. 2). This deposit shows a runup of 110 m on the opposite valley slope. It is the largest deposit and has

a Fahrböschung angle of 22.3° (only including the continuous deposit B), which is smaller than those of the other events. The elevations above sea level of the deposits in the inner valley (proximal part) are 130 m and only 35 m in the outer valley (most distal part).

The intermediate rock avalanche deposit (F) is the second largest with a volume of 5.4×10^6 m³ covering an area of 542,500 m². The Fahrböschung angle of this deposit is 25.1°. Altitude of this deposit above sea level is 80 m down to 50 m. This deposit is damming a lake.

The uppermost deposit (G) that partly covers the intermediate is much smaller with an area of 39,000 m², and a volume of 0.19×10^6 m³. This deposit is thus a rock fall deposit. This is also indicated by the Fahrböschung angle of 28.8° and therefore that of a rock fall. It is lo-

501

cated at 75 m a.s.l.

Deposit (B) has a mean grain size of surficial boulders of 1.5 m in diameter with a spread from <0.5 to 10 m. The grain roundness is subangular with (60%) to angular and subrounded boulders with 20% each. Deposit (F) has a mean grain size of 2 m. Boulders also range from <0.5 to 10 m. These boulders are similarly to deposit (B) subangular (around 65%) with 26% of angular and 5% of subrounded clasts. In contrast to deposits (B) and (F) the rock fall deposit (G) shows a different distribution. The mean grain size of large boulders is 4.5 m. Although there is a concentration of boulders between 2-5 m in this deposit all of the grain sizes are well distributed in the range between <0.5 up to 10 m. Compared to the other deposits they show a relatively high amount of boulders >5 m. Angularity of boulders is more pronounced with 68% angular and 23% subangular boulders.

DEFORMED (C) AND (D) UNDEFORMED VALLEY FILL DEPOSITS

The stratigraphically lowest rock avalanche deposit is split into two parts by valley fill deposits that are deformed valley deposits (C) between 30 and 20 m a.s.l. and undeformed below 20 m a.s.l. In the deformed area (C) no connected boulder deposits occur, however isolated boulders could be found. The surface is undulated with small “valleys and ridges” that are oriented perpendicular to the axis of the valley. Within those deposits and along its frontal part where the undulated valley floor deposits limit towards the undeformed valley fill deposits (D), two excavations (see Fig. 5 for location)

were opened to describe the deformation of valley fill deposit (see Fig. 7 as an example). The excavation shows five different units which are composed of silt, sand, pebbles and gravel. Layered silt and sand (E1) is covering the top of most of the excavation including a channel (E2) that occurs only in one part. Most of the excavation is characterized by well homogenized deposits without any sedimentological structures such as layering. Within this matrix there float two islands of gravelly deposits E3 and E5 also without any layering. The homogenized deposit and the islands of gravel deposits are underlain by layered sand and silt E4.

The lower part of the valley fill deposit (15 m a.s.l.) is undeformed (D). Again no rock boulders are present.

The mean diameter of the boulders imbedded in this undulated surface (C) is 1m. Its grain size distribution shows a characteristic peak for grain sizes <0.5 to 1 m. Biggest boulders found are 6m in diameter. Boulders are subrounded (58%) and subangular (33%).

ISOLATED ISLANDS OF ROCK AVALANCHE MATERIAL (E)

Isolated hills composed of rock avalanche boulders (E) lie in the outer part of the valley at 15 m a.s.l.. This deposit covers an area of 50,000 m² and has a volume of 0.25×10⁶ m³ (Tab. 2). The deposit shows rather isolated centric hills, which are composed out of rock boulders of meters to several meter diameter embedded in fine grained material. These hills are up to three meters high and

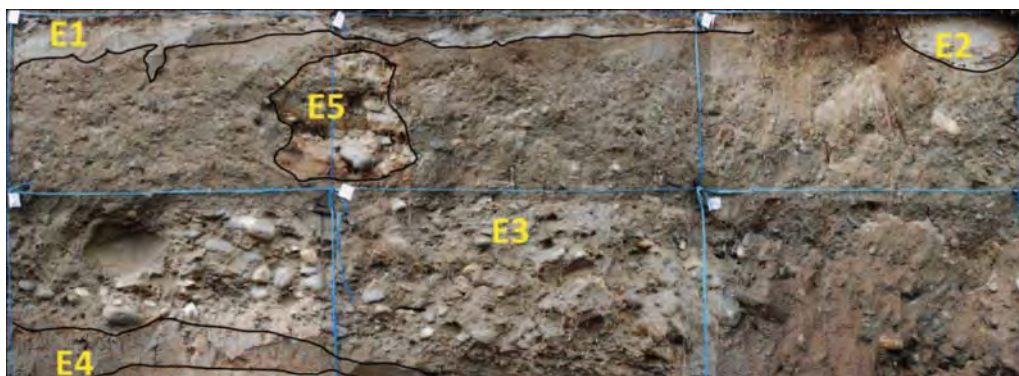


Fig. 7 - Exemplary excavation of the deformed valley fill deposits at the border between deformed and undeformed valley sediments. The blue raster shows 6 cells (1 m length, 0.5 m width). (E1, E2: layered silt and sand; E3, E5: islands of gravelly deposits without layering; E4: layered sand and silt)

SPATIAL DISTRIBUTION OF ROCKSLIDE DEPOSITS AND THEIR MORPHOLOGICAL FEATURES SUGGEST TIMING AND PALAEO-ENVIRONMENTAL CONDITIONS FOR ROCK SLOPE FAILURES IN INNERDALEN AND INNFJORDDALEN, MØRE OG ROMSDAL COUNTY, WESTERN NORWAY

its mean thickness is estimated in the field to be 5 m (Fig. 8). The grain size distribution of deposit (E) is similar to (B) and (F). The mean grain size is 1m, with a peak at 0.5-2 m. Boulders >3.5 m are less common but exceptional boulders are 10 m large. The boulders are subrounded (57%) to subangular (29%) with also some rounded boulders (14%) present.

DISCUSSION OF DEPOSITS WITHIN THE INNFJORDDALEN

The multiple landslide deposits in Innfjorddalen show a simple succession where the different rock avalanche deposits and the rock falls are deposited on top of each other. The timing of the events is poorly understood. However a historical rock failure in 1665 is described in historical records from that valley in the church books as the event caused the death of farmers, not by the direct impact but due to suffocation due to the enormous dust (FURSETH, 2006). We interpret that this age is the age of the youngest rock slope failure that forms deposit (G).

Further constrain on the age of the oldest deposits can be derived from the valley fill deposits and their elevation a.s.l. This deposit split into two parts. While the proximal deposit is continuous the

distal part occurs in form of separated island hills of rock avalanche material. Following this interpretation the Fahrböschung angle of the whole event is 19.6°. Such island hills have been also described in the distal part of the Flims rock avalanche deposits in the Swiss Alps and called there “Toma-hills” (VON POSCHINGER, 2002). The Flims rock-avalanche is interpreted to have dropped into a lake (VON POSCHINGER *et alii*, 2006) and also at that site the frontal hills (Toma-hills) are separated from the main body of the rock avalanche by valley fill deposits that have no sedimentary structure and are strongly homogenized (Bonaduz gravel). Similarly to Flims the deformed valley fill deposits in Innfjorddalen are strongly homogenized and lack sedimentary structure. Therefore, we interpret that similar to the Flims rock avalanche also the oldest rock avalanche in the Innfjorddalen dropped in its distal part into a water body. As no morphological landforms as moraine dams or rockslide dams exist in the lower Innfjorddalen valley the only water body could have been the fjord itself. The lower limit of deformation structures in the valley fill lie at 20 m a.s.l. This line is interpreted to represent the sea level at the time of the oldest rock avalanche. Following this interpretation, this rock avalanche would have dropped into



Fig. 8 - Isolated island hill deposits of rock avalanche material in Innfjorddalen at the border to the undeformed valley fill deposits (view towards NNE). For scale consider Geologist in the center

the valley and made a 90 degree turn after a run-up of 110 m at the opposite valley site. The remaining mass would have run down the valley strongly liquefying and deforming the valley fill deposits in those areas where they have strongly been water saturated close to the former shore line of the fjord. Here the rock avalanche may have split into two bodies, one coming to rest onshore and another running out into the shallow fjord. An alternative interpretation is that both bodies are connected below the surface and that the undeformed valley fill deposits have been deposited later under water level covering the connection of both parts.

In Innfjorddalen the sea level drop due to isostatic rebound of Scandinavia is not well dated throughout the Holocene, however in other areas of western Norway the sea level was at ca. 25 m around 3000 years ago (MAIFORTH, 2010). Therefore the limit between undeformed and deformed deposits suggests that this event occurred ca. 3000 years ago.

CONCLUDING REMARKS

Although isolated hills made up of rock avalanche material are similar in the Innerdalen and Innfjorddalen valley, the interactions with other landforms allow to interpret the genesis of these landforms differently:

INNERDALEN

- 1) Several rock avalanches occurred in late Pleistocene and Holocene age.
- 2) At least one large rock avalanche occurred in late glacial age onto the decaying ice body, creating distinct morphological features (isolated boulder patches above the valley, moraine ridges composed of rock avalanche material, hills on the valley floor composed of rock avalanche material surrounded by valley fill deposits, and valley parallel ridges of rock avalanche material).

INNFJORDDALEN

- 1) Several rock avalanches occurred after deglaciation towards the end of the Holocene, sourcing from the same area.
- 2) The oldest event was deposited onto highly water saturated valley fill sediments above, partly below and close to sea level, that also created isolated island hills of rock avalanche material.

ACKNOWLEDGEMENTS

The authors gratefully thank the Norges geologiske undersøkelse (NGU) for great financial and scientific support and acknowledge the help from colleagues and friends during field work and discussion. We thank the anonymous reviewer for the suggestions.

REFERENCES

- BLAIS-STEVENS A., HERMANN R.L. & JERMYN C. (2011) - *A ³⁶Cl age determination for Mystery Creek rock avalanche and its implications in the context of hazard assessment, British Columbia, Canada*. *Landslides*, **8**: 407-416.
- BOGGS S.JR. (2001 Ed) - *Principles of sedimentology and stratigraphy*. Prentice Hall.
- DEHLS J.F., OLESEN O., BUNGUM H., HICKS E.C., LINDHOLM C.D. & RIIS F. (2000) - *Neotectonic map: Norway and adjacent areas*. Geological Survey of Norway, Trondheim.
- DUFRESNE A. & DAVIES T.R. (2009) - *Longitudinal ridges in mass movement deposits*. *Geomorphology*, **105** (3-4): 171-181.
- EVANS S.G., HERMANN R.L., STROM A. & SCARASCIA-MUGNOZZA G. (2011 Eds.) - *Natural and artificial rockslide dams*. Lecture Notes in Earth Sciences 133, Springer, Berlin-Heidelberg.
- FURSETH A. (2006) - *Skredulykker i Norge*. Tun Forlag, Oslo.
- HACKER B.R., ANDERSEN T.B., JOHNSTON S., KYLANDER-CLARK A.R.C., PETERMAN E.M., WALSH E.O. & YOUNG D. (2010) - *High-temperature deformation during continental-margin subduction and exhumation: The ultrahigh-pressure Western Gneiss Region of Norway*. *Tectonophysics*, **480** (1-4): 149-171.
- HEIM A. (1932) - *Bergsturz und Menschenleben*. Beiblatt zur Vierteljahrsschrift der Naturforschenden Gesellschaft in Zürich, **77**: 218.
- HERMANN R.L., BLIKRA L.H., ANDA E., SAINTOT A., DAHLE H., OPIKOFE T., FISCHER L., BUNKHOLT H., BÖHME M., DEHLS J.F., LAUKNES T.R., REDFIELD T.F., OSMUNDSEN P.T. & EIKEN T. (2011a) - *Systematic mapping of large unstable rock slopes in Norway*. *Proceedings of the 2nd World Landslide Forum, Rome*.
- HERMANN R.L., BLIKRA L.H., NAUMANN M., NILSEN B., PANTHI K.K., STROMEYER D. & LONGVA O. (2006) - *Examples of multiple rock-slope collapses from Köfels (Ötztal valley, Austria) and western Norway*. *Engineering Geology*, **83** (1-3): 94-108.
- HERMANN R.L., DAHLE H., BJERKE P.L., CROSTA G.B., ANDA E., BLIKRA L.H., SAINTOT A., LONGVA O. & EIKEN T. (2013) - *Rock*

SPATIAL DISTRIBUTION OF ROCKSLIDE DEPOSITS AND THEIR MORPHOLOGICAL FEATURES SUGGEST TIMING AND PALAEO-ENVIRONMENTAL CONDITIONS FOR ROCK SLOPE FAILURES IN INNERDALEN AND INNFJORDDALEN, MØRE OG ROMSDAL COUNTY, WESTERN NORWAY

- slide dams in Møre og Romsdal county, Norway: examples for the hazard and potential of rock slide dams.* In: MARGOTTINI C., CANUTI P. & SASSA K. (Eds.). *Landslide science and practise*. Springer, Berlin. in press.
- HERMANN S. R.L., HANSEN L., SLETTEN K., BÖHME M., BUNKHOLT H.S.S., DEHLS J.F., EILERTSEN R.S., FISCHER L., L'HEUREUX J.S., HOGAAS F., NORDAHL B., OPIKOFE T., RUBENDOTTER L., SOLBERG I.-L., STALSBERG K. & YUGSI MOLINA F.X. (2012) - *Systematic geological mapping for landslide understanding in the Norwegian context*. In: EBERHARDT E., FROESE C., TURNER K. & LEROUEIL S. (Eds.). *Landslides and engineered slopes: protecting society through improved understanding*: 265-271, Taylor & Francis Group, London.
- HERMANN S. R.L., HEWITT K., STROM A., EVANS S.G., DUNNING, S.A. & SCARASCIA-MUGNOZZA G. (2011b) - *The Classification of Rockslide Dams*. In: EVANS S.G., HERMANN S. R.L., STROM A. & SCARASCIA-MUGNOZZA G. (Eds.). *Natural and artificial rockslide dams*. Lecture Notes in Earth Sciences, **133**: 581-593, Springer, Berlin-Heidelberg.
- HERMANN S. R.L. & LONGVA O. (2012) - *Rapid rock-slope failures*. In: CLAGUE J.J. & STEAD D. (Eds.). - *Landslides: types, mechanisms and modeling*: 59-70, Cambridge University Press.
- HERMANN S. R.L., NIEDERMANN S., IVY-OCHS S. & KUBIK P.W. (2004) - *Rock avalanching into a landslide-dammed lake causing multiple dam failure in Las Conchas valley (NW Argentina) - Evidence from surface exposure dating and stratigraphic analyses*. *Landslides*, **1** (2): 113-122.
- HEWITT K. (2009) - *Rock avalanches that travel onto glaciers and related developments, Karakoram Himalaya, Inner Asia*. *Geomorphology*, **103** (1): 66-79.
- HEWITT K., GOSSE J. & CLAGUE J.J. (2011) - *Rock avalanches and the pace of late Quaternary development of river valleys in the Karakoram Himalaya*. *Geological Society of America Bulletin*, **123** (9/10): 1836-1850.
- MAIFORTH J. (2010) - *Kulturminner på Flakk*. Master Thesis, pp. 23. NTNU, Trondheim
- SHUGAR D.H. & CLAGUE J.J. (2011) - *The sedimentology and geomorphology of rock avalanche deposits on glaciers*. *Sedimentology*, **58** (7): 1762-1783.
- TVETEN E., LUTRO O. & THORSNES T. (1998) - *Geologisk kart over Norge, berggrunnskart Ålesund, 1:250,000*. Geological Survey of Norway, Trondheim.
- VON POSCHINGER A. (2002) - *Large rockslides in the Alps: A commentary on the contribution of G.Abele (1937-1994) and a review of some recent developments*. In: EVANS S.G. & DEGRAFF J.V. (Eds.). *Catastrophic landslides: effects, occurrence and mechanisms*. Geological Society of America Reviews in Engineering Geology, **XV**: 237-255, Boulder, Colorado.
- VON POSCHINGER A., WASSMER P. & MAISCH M. (2006) - *The Flims Rockslide: History of interpretation and new insights*. In: EVANS S.G., SCARASCIA MUGNOZZA G., STROM A. & HERMANN S. R.L. (2006). *Landslides from massive rock slope failure*. NATO Science Series IV: Earth and Environmental Sciences, **49**: 329-356, Springer, Netherlands.
- WELKNER D., EBERHARDT E. & HERMANN S. R.L. (2010) - *Hazard investigation of the Portillo Rock Avalanche site, central Andes, Chile, using an integrated field mapping and numerical modelling approach*. *Engineering Geology*, **114** (3-4): 278-297.

**APPENDIX 5: KRIEGER ET AL. (2013) THE BERILL FAULT AND ITS
RELATION TO A DEEP-SEATED GRAVITATIONAL SLOPE
DEFORMATION (DSGSD)**

Full citation: Krieger, I., Hermanns, R.L., Schleier, M., Yugsi Molina, F.X., Oppikofer, T., Rønning, J.S., Eiken, T. and Rohn, J. (2013) The Berill fault and its relation to a deep-seated gravitational slope deformation (DSGSD). In: Genevois, R. and Prestininzi, A. (eds.) *International Conference Vaiont, 1963-2013 - thoughts and analyses after 50 years since the catastrophic landslide*, Italian Journal of Engineering Geology and Environment - Book Series 6, Sapienza University, Rome, Italy, pp. 265-273.

THE BERILL FAULT AND ITS RELATION TO A DEEP SEATED GRAVITATIONAL SLOPE DEFORMATION (DSGSD)

INGVAR KRIEGER^(*), REGINALD L. HERMANN^(**), MARKUS SCHLEIER^(***),
FREDDY XAVIER YUGSI MOLINA^(**), THIERRY OPIKOFE^(**), JAN STEINAR RØNNING^(**),
TROND EIKEN^(****) & JOACHIM ROHN^(***)

^(*)University of Erlangen-Nuremberg - GeoZentrum Nordbayern - Erlangen, Germany Now Isofer AG - Knonau, Switzerland

^(**)Geological Survey of Norway - Trondheim, Norway

^(***)University of Erlangen-Nuremberg - GeoZentrum Nordbayern - Erlangen, Germany

^(****)University of Oslo - Oslo, Norway

ABSTRACT

Within the Innfjorddalen valley (Møre og Romsdal, Norway) a 1.5 km long linear NNE-SSW striking feature, forming a 3-4 m high step in the topography, occurs on the SE facing slope of the Middagstinden mountain and was previously discussed as a Holocene reverse fault, called the "Berill fault". Our intense structural field mapping and a high resolution digital elevation model based on LiDAR data derived from airborne and terrestrial laser scanning indicate that the "Berill fault" is a normal fault that has the orientation of the collapse of the Caledonian orogen, that is today reactivated as a limiting structure of a Deep Seated Gravitational Slope Deformation (DSGSD). Differential Global Navigation Satellite System (dGNSS) surveys over the instability indicate velocities of the DSGSD of ca. 0.6 cm/yr. Three electric resistivity profiles on the valley floor attest that the fault is a structure with regional extend. Three trenches with a total length of 100 m parallel to the electric resistivity profiles although down to glacial deposits or the underlying bedrock do not indicate any Holocene activity of the fault. Hence reactivation of the fault by the DSGSD produces the linear feature oblique to the slope.

KEY WORDS: normal fault, rock slope instability, LiDAR, kinematic analyses, Western Norway

INTRODUCTION

Several km-long linear features that build a ver-

tical step in high mountain terrain have often been discussed to be either related to faulting or to deep seated gravitational slope deformation (THOMPSON *et alii*, 1996; HIPPOLYTE *et alii*, 2006; LI *et alii*, 2010). The slope of the investigation area shows a prominent 1.5 km long linear feature, that strikes NNE-SSW and therefore in a 30 degree angle with the SE facing slope. It forms a 3-4 m high step in the topography and was previously discussed as a Holocene reverse fault called the "Berill fault" (ANDA *et alii*, 2002). Only on the western side of the fault a massive rock slope instability has developed. Here occur slope parallel, up to 20 meter deep up-hill facing scarps (counter scarps) with active rock fall and shallow translational sliding of single rock blocks and unconsolidated rock (e.g. shallow landslides). East of the lineament called the "Berill fault" no slope deformation is visible. Hence the fault seems to be a limiting factor for the slope instability.

In order to better understand the relation of the slope deformation with the proposed Holocene reverse fault, an intensive structural analyses of the slope and electric resistivity profile measurements along the valley floor were implemented and the deformation was monitored over the past 5 years with differential Global Navigation Satellite System (dGNSS) surveys. The investigation area is located on the south-east exposed slope of the Middagstinden mountain right above the Berrilvatnet lake in the Møre og Romsdal county in West Norway (Fig. 1) and

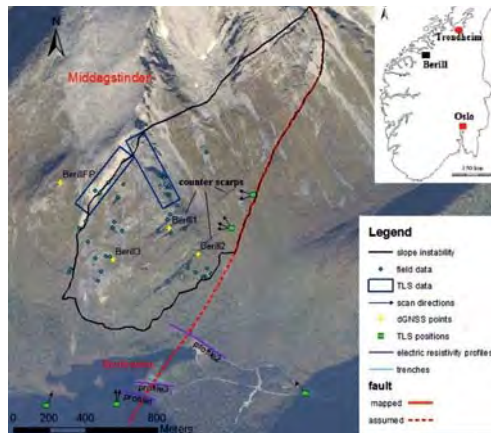


Fig. 1 - Orthophoto of the Berill instability (NGU) showing the different observation points for field data, TLS data and dGNSS measurements, the position of the trenches and the electric resistivity profiles and the morphological trace of the fault; The investigation is limited to the western part of the instability with rock outcrops, since the rest is covered by surficial glacial deposits that do not allow the implementation of structural analyses of the bedrock

herein it is described as the “Berill instability”. The instable slope is part of the Innfjorddalen, a glacial U- valley, where several post glacial mass movements have taken place (SCHLEIER *et alii*, this issue).

GEOLOGICAL SETTING

The Berill instability is located in the Western Norwegian Gneiss Region (WNGR). The bedrock of this area consists mainly of proterozoic gneisses with a magmatic origin, which is locally covered with oceanic and continental sediments. The deformation and metamorphisation of the neo- and mesoproterozoic rocks took place during the Caledonian orogeny (GANERØD, 2008). In the geological map sheet the gneisses are described as undifferentiated and locally migmatitic in composition (TVETEN *et alii*, 1998). The most prevalent rock types in the WNGR are tonalitic and granodioritic gneisses (HACKER *et alii*, 2010). The bedrock disclosed in the investigation area is marked of quartz-dioritic gneiss with a sporadically well distinct foliation. Locally migmatitic structures are present (TVETEN *et alii*, 1998).

METHODS

DATA USED

A detailed structural field mapping over the whole investigation area with rock outcrops was undertaken and about 1500 structural measurements at

35 locations were taken. Furthermore the main features and the limiting structures in the instability were mapped in order to estimate the size of the individual blocks (Fig. 1 and 2).

Supplementary data for structural analyses was gained from airborne- and ground based LiDAR- (Light Detection and Ranging) data in order to create a high resolution digital elevation model (DEM). To create a DEM by terrestrial laser scanning (TLS) the site was scanned with the long range ILRIS Optech 3D Scanner (OPTECH, 2008) from several positions with different lines of sight (Fig. 1) to get a preferably dense 3D point cloud. To keep the vegetation as a disturbing factor to a minimum only the last reflected impulse of the pulsed laser was recorded. The LiDAR point clouds were cleared of disturbing factors like vegetation and georeferenced in the PolyWorks software (INNOVMETRIC, 2011; OPPIKHOFER *et alii*, 2012). In addition, to gain a better overview over the site and its prominent structures and to improve the field investigations (mapping and structural measurements) detailed Orthophotos as well as a DEM based on airborne laser scanning (ALS) with a resolution of 2 meters were used. The DEM suits very well as input data for differently exposed hillshades for a better understanding and identifying of the large morphological structures in the instability.

STRUCTURAL ANALYSES

The data collected in the field and the values gained by the Coltop3D analyses were stored and analysed with the software Dips6.0 (ROSCIENCE, 2012). The orientations of the planes are displayed by its great circles and pole points in the Stereonet (lower hemisphere, equal area). Furthermore, kinematic tests for planar and wedge sliding as well as direct flexural toppling were performed to determine the possible failure modes.

In order to analyse the orientation of the discontinuity sets in the DEMs the Coltop3D software (TERRANUM, 2011) was applied (JABOYEDOFF *et alii*, 2007). The software computes surface normals out of the point cloud DEM and provides them with an orientation-specific colour. In the next step, by selecting surfaces with the same colour, Coltop3D was used to illustrate the orientations of the defined planes in a spherical projection (lower Stereonet) and to export the results as dip and dip direction in a text file (OPPIKHOFER *et alii*, 2012).

THE BERILL FAULT AND ITS RELATION TO A DEEP SEATED GRAVITATIONAL SLOPE DEFORMATION (DSGSD)

For a better understanding of the possible movements within the rock, a comprehensive recording of persistence, spacing and roughness of the discontinuity sets according to WYLLIE & MAH (2004) was accomplished during the fieldwork.

DISPLACEMENT MEASUREMENTS

Displacements within the instability have been measured yearly by dGNSS surveys since 2008 (no measurement possible in 2012 because of bad weather conditions). Therefore three rover points were installed in the apparent instable parts of the mountain slope and one fixed point (Fig. 1) in a stable part above the main scarp, to receive a network of vectors which shows the point movement relative to each other. For this method, uncertainties in horizontal directions of 3-6 mm and in the vertical direction of 10-20 mm are assumed (HERMANN *et alii*, 2011). Thus in this paper

a movement is expected to be significant when it is larger than the uncertainty. Because of large height differences between the rover points and the fix point as well as annual systematic trends from un-modelled meteorological effects, the vertical uncertainty is much higher than the horizontal (BÖHME *et alii*, 2012) and hence must be interpreted carefully.

GEOELECTRIC

Three 2D resistivity profiles were measured in the valley bottom (Fig. 1) using the Lund system (DAHLIN, 1993) gradient electrode configuration and an ABEM SAS Terrameter 4000 (ABEM, 1999). Electrode separation was two meters (profile 1 and 2) and five meters (profile 3) giving a penetration depth of 25 and 60 meters respectively. This method has proven to be a powerful tool for mapping of drift deposits and fracture zones in bedrock (SOLBERG *et alii*, 2008; RØNNING *et alii*, 2009).

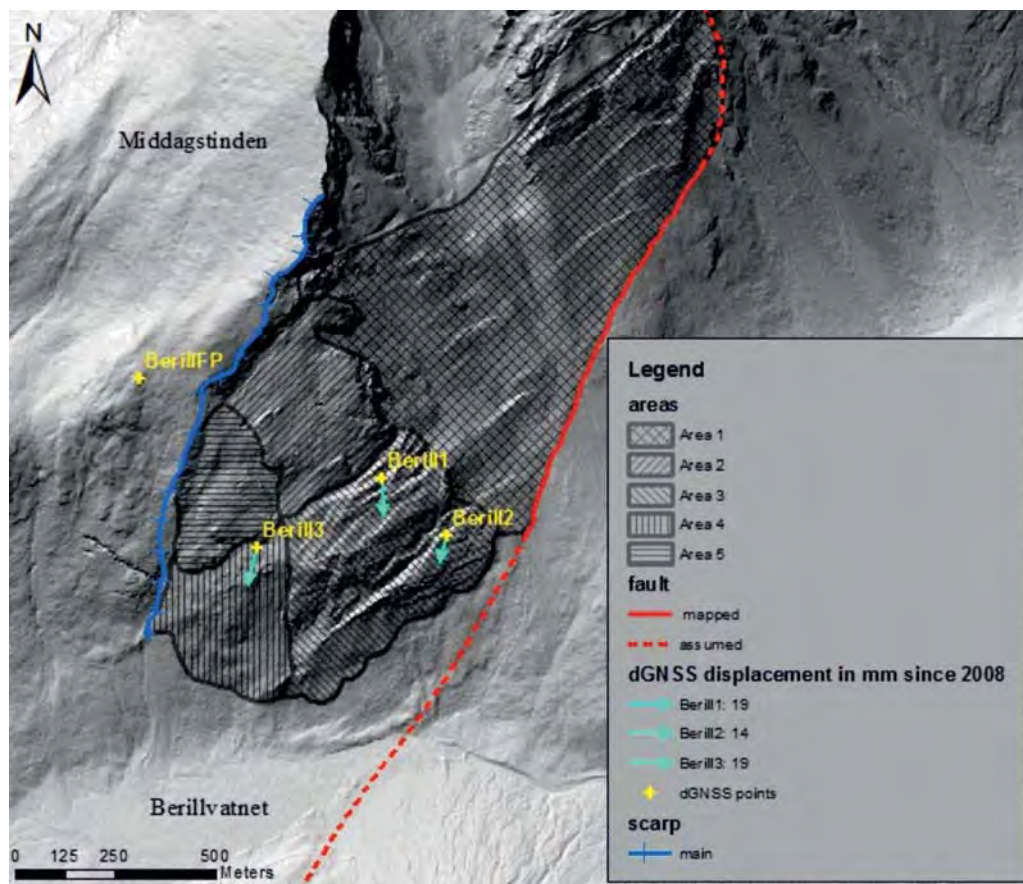


Fig. 2 - Hillshade of the Berill instability with the different kinematic areas, morphological trace of the fault the main scarp and the relative movement of the dGNSS rover points

RESULTS

MORPHOLOGY ON SLOPE

Based on the field mapping and ALS as well as Orthophoto analyses, four main areas (area 2-5) within the rock slope (Fig. 2) can be distinguished showing different types and/or amount of deformation. Similar deformation is suggested by counter scarps in surficial deposits E of the described rock slope and NW of the linear feature described as "Berill fault" (area 1).

EASTERN PART COVERED BY SURFICIAL DEPOSITS (AREA 1)

This area shows 3-4 meter deep depressions, which strike in the same direction as the counter scarps and the main scarp and deform the surficial deposits and limit towards the fault. Furthermore lateral moraines associated to younger Dryas glaciations can be found in this part of the slope instability. The fault strikes NNE-SSW and can be traced morphologically by a convex lineation along the slope which is 3-4 meters high and 1.5 km long but disappears in the valley.

UPPER MIDDLE PART (AREA 2)

Area 2 shows one coherent block with active rock fall at the lateral and frontal margins. Here large block fields have developed with up to several-meter- sized blocks.

LOWER MIDDLE PART (AREA 3)

Area 3 displays very prominent, up to 20 meter deep uphill facing scarps (counter scarps) with regular rock fall at the rockfaces. Hence the scarps are filled with meter sized blocks, so the real depth is masked. The distance between the individual rockfaces varies between 10 and 50 meters.

LOWER WESTERN PART (AREA 4)

Area 4 is characterised by large block fields with local repositioning structures. Where the blocks get smaller and mix with soil, surficial mass movements (e.g. shallow landslides) are present. Outcrops of the bedrock can only be found in some few parts and even then they are highly weathered and fractured. The transition to area 5 shows an accumulation of outcrops imbedded in large block fields.

UPPER WESTERN PART (AREA 5)

Area 5 shows one coherent block with defined lateral limits and many single, randomly distributed outcrops of the bedrock at the western and frontal margins that are surrounded by large blockfields. Since the major part of blocks in the deposits does not show repositioning structures (angular –partly very angular blocks) and there are highly fractured outcrops within the blockfields, the blocks are suggested to come from fragmentation on site but not by rock falls from above.

The horizontal displacements at the main scarp of the rock slope instability above area 2 and area 5 to the moving mass below is approximately 50 meters while the height of the scarp amounts to ~ 60 meters. The main scarp forms the back bounding limit both of area 2 and area 5.

STRUCTURAL ANALYSES

By analysing the structural data of the field and the DEMs, four main discontinuity sets have been identified (Tab. 1). The persistence, spacing and roughness descriptions refer to the classification of WYLLIE & MAH (2004).

FOLIATION (JS)

The foliation JS plunges with a mean dip/dip direction of 156/47 (field value) and varies over the whole area of the instable slope. In area 2 and area 5 the foliation forms distinct discontinuity surfaces with a high persistence, a close-moderate spacing and shows very little variability in the orientation. The surface of the foliation is here smooth and planar-undulating and both the main scarp and the frontal limit of area 2 are formed by the foliation. In the lower parts, especially in the counter scarps in area 2, the occurrence and the orientation are not constant. Here, the orientation of the foliation (dip direction) varies between NNE and SSW with

discontinuity set	DEM	Field data	spacing	persistence	roughness
J1	80/315±8	74/320±23	wide-very wide	high	rough, planar (undulating)
J2	81/048±14	78/45±20	wide-very wide	high	rough, planar (undulating)
JS	50/160±11	47/150±28	close-moderate	high	smooth, planar-undulating
JF		44/270±20	moderate-extremely wide	high	clinkered, planar
Lineation on JF groove marks on JS		31/245±11			
		42/138±16			

Tab. 1 - Summary of the main discontinuity sets. The orientation data are presented as dip/dip direction with $\pm 1\sigma$ variability in degrees; the spacing, persistence and roughness descriptions refer to the classification of WYLLIE & MAH (2004)

THE BERILL FAULT AND ITS RELATION TO A DEEP SEATED GRAVITATIONAL SLOPE DEFORMATION (DSGSD)

shallower inclinations between 5° and 40° with higher spacing and lower persistence values than in the upper area. This is because of folding in centimeter but also in meter scale with a fold axis towards the east.

JOINTS (J1, J2)

Two prominent joint sets are developed (J1, J2) that are both steep dipping with mean dip/dip direction values of 74/320 for J1 and 78/045 for J2 (field values). The spacing is wide – very wide, the persistence is high and the discontinuity surfaces are rough, planar, occasionally undulating. Most of the prominent structures like big fractures, cracks or lineaments visible in the field and on the DEM develop along these joint sets and single blocks or outcrops in the instability are limited by J1 and J2 or a combination of both. At the main scarp the occurrence of these joint sets is not as frequent as in the deforming parts and their persistence is much lower. This gets confirmed both by field observations and the analyses of the DEMs.

FAULT PLANE (JF)

The fault plane dips with a mean dip/dip direction of 44/270. The surface shows a quartz–feldspar remineralisation with lineation and frequent break offs that indicate normal fault movement. These lineaments do not occur continuously on the surface of the plane and the planes are partly undulated with varying orientations. Therefore the fault plane might follow a pre-existing discontinuity that was used as a preconditioned zone of weakness in the course of faulting. Because of its relative shallow orientation dipping into the mountain slope it can not be found in the DEMs, but the field investigation yield high, occasionally even very high persistence values. The spacing varies very much depending on the area. In some parts the outcrops of the surface recur in meter scale, in other parts it does not exist and in the lower parts (counter scarps) it plunges about 16° shallower than further up on the slope.

DISPLACEMENT MEASUREMENTS

All rover points show a significant horizontal movement towards the south with a mean displacement rate of ~ 0.6 cm/year. The vertical movements over the last four years are not higher than the uncertainty and therefore are not discussed. The rover point Berill1 moves straight towards the south (176°) with a total displace-

ment of 19 mm since 2008, while Berill2 and Berill3 indicate a movement towards SSW (194° and 193°) with a displacement of 14 mm (Berill2) and 19 mm (Berill3) since 2008. Especially Berill1 and Berill2 show high variations in the east-west displacement, while Berill3 moves mainly constantly towards SSW (Fig. 3)

GEOELECTRIC

All resistivity profiles show low resistivity on the surface and higher resistivity at few meters depth. In addition, in all profiles there is one pronounced zone of low resistivity that separates areas of high resistivity that is ca. 10 m wide and dips either vertical or in the proposed dip direction of the fault. A second less pronounced zone of lower resistivity runs parallel to the former zones (Fig. 4).

DISCUSSION*GENESIS OF THE FAULT*

The fault plane shows significant quartz-feldspar remineralisation with quartz/feldspar lineation that indicates that the fault was active in depth prior to exhumation to its present position. Moreover frequent break offs indicate a down-dip direction and hence a normal fault process (Fig. 5). The orientation of the lineation is parallel to the direction of the collapse of the Caledonian orogen. The low resistivity zone within the valley dips in the same direction and is thus interpreted to represent the prolongation of the fault in the valley. NGU opened trenches along the resistivity profiles that went

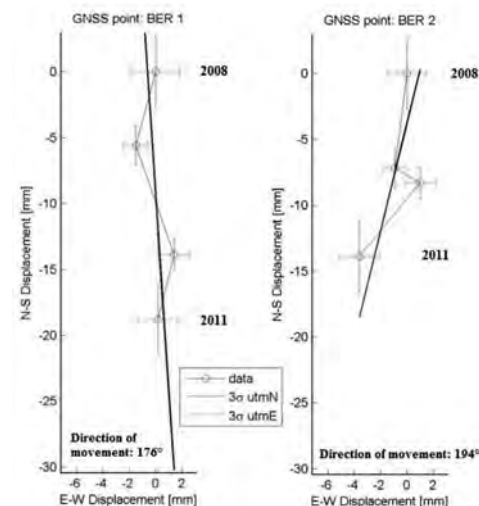


Fig. 3 - Horizontal displacement rates of Berill 1 and Berill 2 since 2008

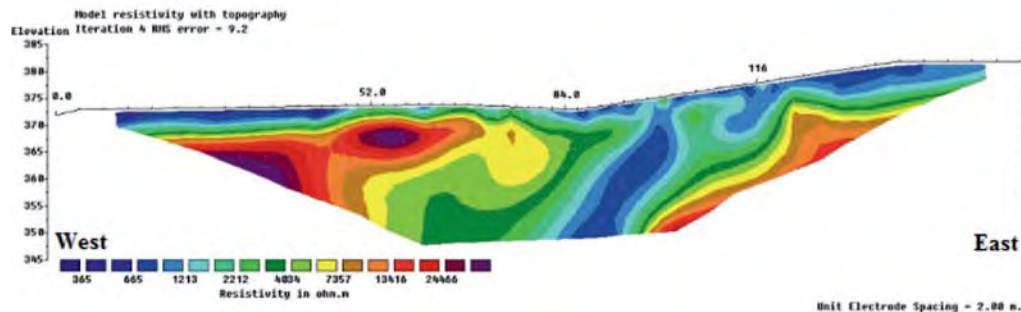


Fig. 4 - Resistivity results along profile P1; low resistivity (blue colours) represent peat material at the surface and a 10 meter wide fractured zone in the bedrock dipping towards the west

down into glacial deposits or down to the basement. No fault offsets or any soft sediment deformation features indicating seismic activity within the trenches were observed. Thus we interpret that the fault represents a fault active during the Caledonian collapse that has not been seismically reactivated in post glacial times.

INFLUENCE OF THE FAULT TO THE SLOPE DEFORMATION

The field data and the additional TLS data show, that the main scarp is mainly formed by the foliation JS which

plunges with a mean value of 52/154 (data taken in the field at the main scarp) and therefore does not daylight on the slope. However groove marks (Tab. 1) on the main scarp indicate a rockslide towards SSE. As the foliation is not daylighting, this movement becomes only possible because the foliation intersects with the fault plane forming an intersection lineament with the orientation 22/205 (Fig. 6). This orientation is 50° obliquely towards the orientation of the slope that strikes N 065° E with an average slope angle of 45°. The orientation of the sliding rock mass therefore moves out of the slope as a wedge failure with an angle of 50° relative to slope direction producing a positive offset along its SE boundary forming a step in the relief similar to thrusting along the fault plane in an eastward direction (Fig. 5). Thus the Caledonian fault gets reactivated through the slope instability in form of an "apparent reverse fault". This direction is identical with the movement direction documented with the dGNSS rover stations Berill 1-3. Because the fault and the foliation are not present over the entire slope and their orientations are variable, also other deformation styles have developed on the slope in various sectors.

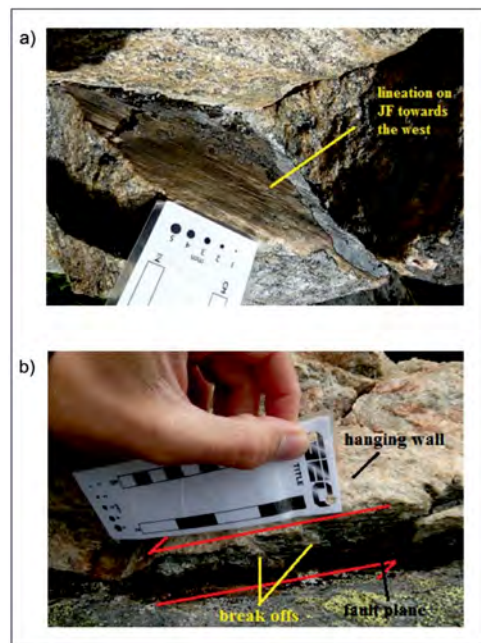


Fig. 5 - Pictures of the fault plane JF taken in the field
a) lineation plunging 33/241; b) breakoffs on the hanging wall of the fault plane indicating a down dip direction

AREA 1

The bedrock of this area is covered by surficial glacial deposits and therefore it was neither possible to collect applicable structural data nor to install representative dGNSS points. But since area 1 also shows depressions, which strike in the same direction as the counter scarps in area 3, this part of the slope might follow a similar slope deformation process.

AREA 2

This coherent block has a surface area of 130.000 m² and is delimited by the joint set J1 in the front and

THE BERILL FAULT AND ITS RELATION TO A DEEP SEATED GRAVITATIONAL SLOPE DEFORMATION (DSGSD)

by J2 at its lateral limits. This block moves SSE along the foliation as shown by the groove marks at the back bounding scarp and therefore nearly in direction of the inclination of the slope. This movement builds up stress in the lower part of the slope in area 2.

AREA 3

dGNSS measurements and the kinematic analyses show, that area 2 is moving SSW that is therefore parallel to the intersection line of JS and JF (Fig. 6). However, as the foliation is less developed in this area deformation is also taken up by J1 by toppling towards SE (Fig. 7). This produces the counter scarps and might explain the varying east-west displacement rates of Berill1 and Berill2, which are installed at the top of the rock faces of the counter scarps. An SE direction of toppling and in combination with the SSW direction of wedge sliding on the intersection line of the foliation and the fault of this part of the unstable slope results in the observed S movement of the dGNSS points. Area 2 and area 3 are described here as two different areas since the kinematic processes differ from each other, but still both areas outline one coherent block in the hillshade.

AREA 4

In area 4 no dGNSS point could be installed, because there are neither coherent blocks nor unfractured outcrops. The few existing outcrops are highly fractured with wide opened discontinuities likely related to high strain rates from the surrounding coherent blocks that “push” on this part of the slope.

AREA 5

The dGNSS measurements of the rover point Berill 3 and the Stereoplots indicate that the coherent block in the upper western part moves SSW and therefore differs from the moving direction of the upper eastern block. This block is separated from the block of area 2 along the joint set J2 and it moves parallel to intersection line of JS and JF towards SSW. The highly fractured outcrops of the bedrock at the western and frontal margins are assumed to be the result of varying movement directions of surrounding blocks.

CONCLUDING REMARKS

In conclusion after our thorough structural mapping in combination with dGNSS and geophysical

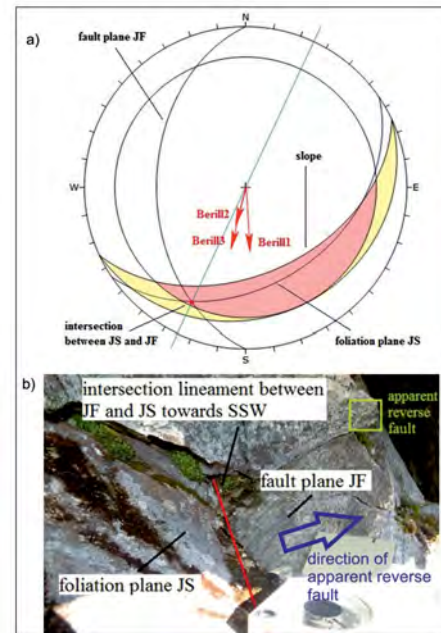


Fig. 6 - a) wedge sliding along the intersection line of the foliation JS and the fault JF; The input data are mean values of JF and JS taken in the lower parts (area 2) of the slope instability where the wedge developed; because of the slickensided surface of the fault and the smooth surface of the foliation the friction angle is estimated to be as low as 20°. The also plot shows the direction of the dGNSS rover points Berill1-3; b) field photo of the sliding on the intersection line between JF and JS with measured value of 21/201 (plunge/trend)

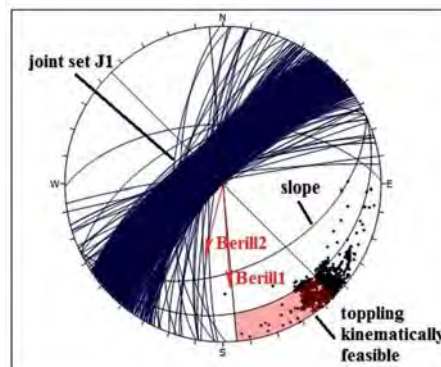


Fig. 7 - Toppling along the joint set J1 with the directions of the dGNSS rover points Berill1-2; the friction angle is with 25° higher than in Figure 3 because of a rougher discontinuity surface; the slope has a mean orientation of 45/155 (dip/dip direction)

investigations we summarize:

1. The fault plane is supposed to be a pre-existing

- discontinuity which was exploited as a weakness zone in the course of faulting.
2. The quartz-feldspar remineralisation with lineation and break offs indicate a normal fault process towards the west.
 3. Since the fault is parallel to the direction of the collapse of the Caledonian orogen and there was no evidence of fault deformation in the soft sediments in the trenches, we assume that the fault was active during the Caledonian collapse and was not reactivated in post glacial times.
 4. The fault plane intersects with the foliation forming a wedge with an intersection lineament plunging SSW that takes part of the deformation. This direction coincides with dGNSS measurement of Berill3.
 5. Due to different orientations of the slope and the wedge, the sliding rock mass produces a positive offset along its SE boundary and reactivates the fault plane locally in form of an “apparent reverse fault”.
 6. As the fault plane and the foliation plane do not occur constantly over the unstable slope, also other deformation styles developed on the slope, which are all terminated by the joint sets J1 and J2 and result in localized toppling towards the SE.

ACKNOWLEDGEMENTS

This investigation was funded by the Geological Survey of Norway, which contributed both with physical and intellectual work very much to this paper.

REFERENCES

- ABEM (1999) - ABEM Terrameter SAS 4000/SAS 1000. *Instruction Manual*. ABEM Printed Matter 93101.
- ANDA E., BLIKRA L.H. & BRAATHEN A. (2002) - *The Berill Fault - first evidence of neotectonic faulting in southern Norway*. Norwegian Journal of Geology, **82**: 175-182.
- BÖHME M., HERMANN R.L., FISCHER L., OPPIKHOFER T., BUNKHOLT H., DERRON M.H., CARREA D., JABOYEDOFF M. & EIKEN T. (2012) - *Detailed assessment of the deep-seated gravitational deformation at Stampa above Flåm, Norway*. In: EBERHARDT E., FROESE C., TURNER K. & LEROUÉIL S. (Eds.). *Landslides and engineered slopes: protecting society through improved understanding*: 647-652. Taylor & Francis Group, Canada.
- DAHLIN T. (1993) - *On the automation of 2D resistivity surveying for engineering and environmental applications*, Department of Engineering Geology, Lund Institute of Technology. ISBN 91-628-1032-4. Lund University.
- GANERØD G.V. (2008) - *Structural mapping of the Åknes Rockslide, Møre and Romsdal County, Western Norway*. Geological Survey of Norway, Trondheim.
- HACKER B.R., ANDERSEN T.B., JOHNSTON S., KYLANDER-CLARK A.R.C., PETERMAN E.M., WALSH E.O. & YOUNG D. (2010) - *High-temperature deformation during continental-margin subduction & exhumation: the ultrahigh-pressure Western Gneiss Region of Norway*. Tectonophysics **480** (1-4): 149-171.
- HERMANN R.L., BLIKRA L., ANDA E., SAINTOT A., DAHLE H., OPPIKHOFER T., FISCHER L., BUNKHOLT H., BÖHME M., DEHLS J., LAUKNES T., REDFIELD T., OSMUNDSEN P. & EIKEN T. (2011) - *Systematic mapping of large unstable rock slopes in Norway*. Proceedings of the Second World Landslide Forum, Rome.
- HIPPOLYTE J.-C., TARDY M., NICOU D., BOURLES D., BRAUCHER R., MENARD, G. & SOUFACHE B. (2006) - *The recent fault scarps of the western Alps (France): Tectonic surface ruptures or gravitational sacking scarps? A combined mapping geomorphic, leveling and ¹⁰Be-dating approach*. Tectonophysics, **418** (3-4): 255-276.
- INNOVMETRIC (2011) - PolyWorks, p. 3D scanner and 3D digitizer software from InnovMetric Software.
- JABOYEDOFF M., METZGER R., OPPIKHOFER T., COUTURE R., DERRON M.-H., LOCAT J. & TURMEL D. (2007) - *New insight techniques to analyze rock-slope relief using DEM and 3D-imaging cloud points: COLTOP-3D software*. Rock mechanics: Meeting Society's challenges and demands. Proceedings of the 1st Canada - U.S. Rock Mechanics Symposium: 61-68. Taylor & Francis, Vancouver, Canada.
- LI Z., BRUHN R.L., PAVLIS T.L., VÖRNING M. & ZENG Z. (2010) - *Origin of sacking uphill-facing scarps in the Saint Elias orogen, Alaska: LIDAR data visualization and stress modeling*. Geological Society of America Bulletin, **122**: 1585-1595.
- OPPIKHOFER T., BUNKHOLT H.S.S., FISCHER L., SAINTOT A., HERMANN R.L., CARREA D., LONGCHAMP C., DERRON M.-H., MICHOU D. & JABOYEDOFF M. (2012) - *Investigation and monitoring of rock slope instabilities in Norway by terrestrial laser scanning*. In: EBERHARDT E., FROESE C., TURNER K. & LEROUÉIL S. (Eds.). *Landslides and engineered slopes: protecting society through improved understanding*: 1235-1241. Taylor & Francis Group, Canada.

THE BERILL FAULT AND ITS RELATION TO A DEEP SEATED GRAVITATIONAL SLOPE DEFORMATION (DSGSD)

- OPTECH (2008) - *ILRIS-3D. Intelligent Laser Ranging and Imaging System*.
- ROCSCIENCE (2012) - *Dips 6.0. Graphical and Statistical Analysis of Orientation Data*.
- RØNNING J.S., DALSEGG E., ELVEBAKK H., GANERØD G.V. & HEINCKE B.H. (2009) - *Characterization of fracture zones in bedrock using 2D resistivity*. Proceedings from 5th Seminar on Strait Crossings, Trondheim: 439-444.
- SOLBERG I.L., RØNNING J.S., DALSEGG E., HANSEN L., ROKOENGEN K. & SANDVEN R. (2008) - *Resistivity measurements as a tool for outlining quick clay extents and valley fill stratigraphy: feasibility study from Buvika, Central Norway*. Canadian Geotechnical Journal, **45**: 210-225.
- TERRANUM (2011) - *Coltop3D. LIDAR data processing and analyzing software for geologists*.
- THOMPSON S.C., CLAGUE J.J. & EVANS S.G. (1997) - *Holocene activity of the Mt. Currie scarp, Coast Mountains, British Columbia, and implications for its origin*. Environmental & Engineering Geosciences, **3** (3): 329-348.
- TVETEN E., LUTRO O. & THORSNES T. (1998) - *Geologisk kart over Norge, berggrunskart ÅLESUND, 1:250,000*. Geological Survey of Norway, Trondheim, Norway.
- WYLLIE D.C. & MAH C.W. (2004 EDS.) - *Rock slope engineering: civil and mining*. 4th ed. Spon, London.

APPENDIX 6: BLIKRA & KRISTENSEN (2012) MANNEN (NORWAY)

Full citation: Blikra, L.H. and Kristensen, L. (2012) Mannen (Norway). In: Baron, I., Supper, R. and Ottowitz, D. (eds.) *SafeLand deliverable D4.6 - Report on evaluation of mass movement indicators*, SafeLand European project, pp. 271-283, available at <http://www.safeland-fp7.eu>.

4.9 MANNEN (NORWAY)

L.H. Blikra & L. Kristensen

Åknes/Tafjord Early Warning Centre, Norway

ABSTRACT

Mannen is one of only four high-risk rock instabilities in Norway. It has the potential of creating a rock avalanche of 2 - 20 million m³ with catastrophic consequences for houses and infrastructure in the valley, in particular as a landslide dam may be formed. An early warning system has been established, which is based on measurements of displacement in the instability and a well-defined alarm chain. The monitoring sensors are a GPS network, lasers, extensometers, a ground-based radar system and a borehole instrument; all data are checked daily. Construction of the early warning system was nearly complete in 2010 and over one year's worth of measurements are reported here. During this time the velocity in the upper part of the instability was about 2 cm/year. A seasonal trend with increased velocities during the snowmelt and summertime is seen. The active rockslide body is highly fractured and has no groundwater, and the increased movement is interpreted to be an effect of water coming into the fine-grained and brecciated detachment zones. This will saturate the sliding planes and reduce their shear strength.

Presented parameters: displacement, velocity, precipitation, air temperature.

4.9.1 GENERAL DESCRIPTION OF THE TEST SITE

Geological and geomorphic settings

The Mannen rock slope instability is located in Møre and Romsdal County in western Norway (Figure 4.9-1). The instability is developed at the edge of a 1295 m elevated plateau southwest of the steep, glacially eroded valley called Romsdalen.

The bedrock consists of Proterozoic sillimanite-bearing gneisses with inherited structural weaknesses from the tectonic deformation. Specifically, the metamorphic foliation surfaces are prone to be reactivated where favorable orientation occurs in regards to the gravitational forces (Saintot et al. 2011).

At the top, where the main backcrack is developed, foliation is near-vertical. In the upper part of the moving area, a borehole showed foliation dipping about 30° to the north and downslope, but further down the pattern is more complex as the gneisses are intensely folded. Inside the instability the bedrock is extremely fractured and weathering products of soil cover much of the surface. The morphology is characterized by the well-defined backscarp and numerous smaller slide scars (Figure 4.9-1). The scars bear witness to multiple recent rockfalls or smaller rock avalanches on the slope; the latest occurred on November 7, 2011, which destroyed a cable to one of the GPS antennas.

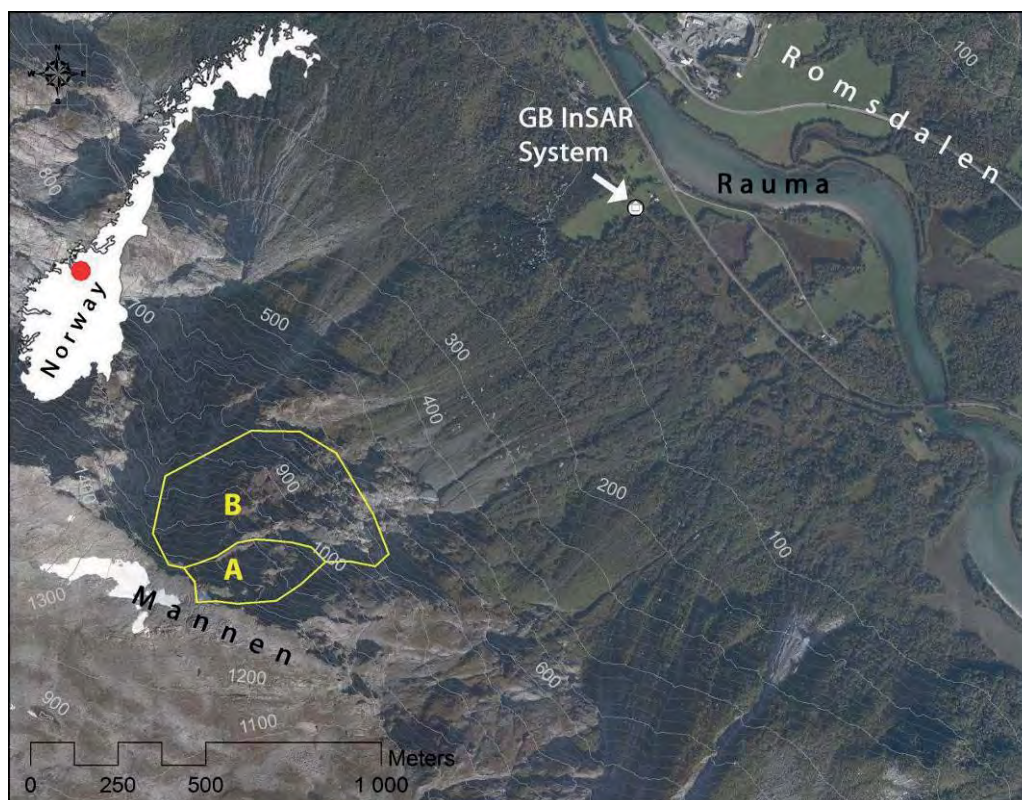


Figure 4.9-1. The location of Mannen and the mapped scenarios, with estimated annual likelihood of A: 1/100 and B: 1/1000.

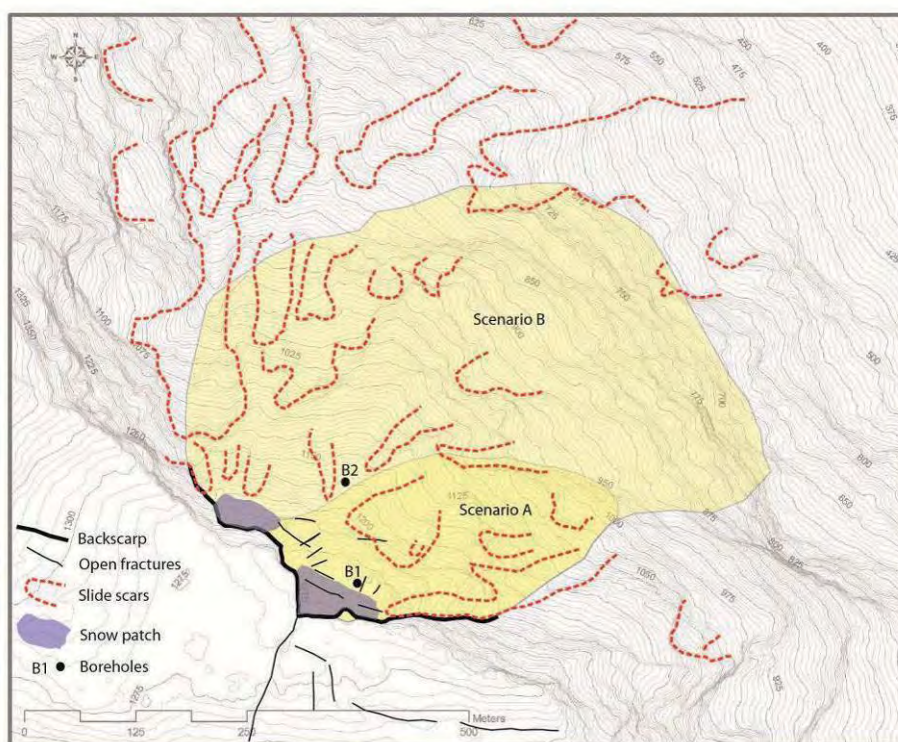


Figure 4.9-2. Morphological map of the Mannen rockslide.

Characterization of the site

A part of the plateau towards the valley (100 million m³) is bounded by deep clefts indicating past movement, but most of this appears inactive today (Figure 4.9-2). A block of possibly 15-20 million m³ has been lowered 15-20 m from the plateau (Figure 4.9-2 and Figure 4.9-3), and a block in its upper part (of 2-3 million m³) has been measured periodically with DGPS, showing a yearly movement of 4-5 cm dipping 45-50° against ENE. These two blocks are the basis of scenarios (A & B) drawn in Figure 4.9-1 and Figure 4.9-2. The Norwegian Geological Survey and the county governor have estimated that the annual probability of a rock avalanche of scenario A is about 1/100. Following structural and geological analysis of the surrounding areas, Henderson and Saintot (2007) deduced a translational sliding as a mechanism of deformation of the rock slope instability.

Modelling work shows that a rock avalanche of a magnitude of either scenarios A or B would destroy the road and railroad at the valley bottom as well as several houses. Furthermore, the rock debris may dam the river Rauma, with a subsequent risk of dam collapse and flooding downstream of the river.



Figure 4.9-3. Photo of the upper part of Mannen, showing the block that has been lowered from the plateau. Some instruments from the upper part of the rock slope instability are shown.

Description of the history of the mass movement

Deposits of more than 15 large rock avalanches postdating deglaciation have been mapped over a 25 km stretch in Romsdalen. In historic times, numerous rockfalls and smaller rock avalanches have occurred in the valley, many of which cost human lives. Most appear to have

occurred during spring and summer time (www.skrednett.no), but a possible correlation to precipitation or other environmental factors has not been tested. A rockfall event inside the instability occurred on November 7, 2011 after several days of fine weather, though unusually high temperatures probably led to some snowmelt. Large active talus fans (Figure 4.9-1) bear evidence of high slope activity.

4.9.2 DESIGN OF THE MONITORING NETWORK

Investigations at the site were initiated in 2004 by annual measurements of fixed points using differential GPS, and more points were added in 2006. The measurements showed a total displacement of 4-5 cm/yr with a dip of 45° towards ENE in the most active block (Dahle et al 2008). Detailed geological mapping followed in 2006. Based on the high displacement rate, the past slope displacement, and the large potential consequences of a rock avalanche, the instability was classified as a high-risk object in 2009 (Dahle et al., 2008; Saintot et al., 2011) and the construction of an early warning system was initiated the same year by Åknes Taffjord Early Warning Centre. Meanwhile, investigations continued in 2010 with the core-drilling of a 139 m deep borehole (location Figure 4.9-2 and Figure 4.9-3). The core was carefully logged for rock type and deformation structures, and the borehole was photographed using a televiewer that makes it possible to see all fractures and breccias inside the borehole in detail and study their relation to foliation (Saintot et al 2011). Afterwards, the borehole was instrumented with a DMS column that both identifies sliding planes and is used in the early warning system to monitor displacement. In 2011, another borehole was drilled further down the slope (Figure 4.9-2) which will also be instrumented with a DMS column. Also in 2011, a 800 m long 2D resistivity profile was surveyed across the upper part of the instability, in an attempt to find slope parallel sliding structures to better delineate the depth of the instability.

Investigations are now more or less complete, though a model that better links the structural information with observed patterns of displacement is yet to be constructed. The day to day monitoring data works both to provide information to be used for early warning and to be included in the rock instability investigation.

Instrumentation at the Mannen instability consists of two lasers, seven extensometers, eight GPS antennas, one DMS borehole instrument, and a meteorological station. At the valley bottom, a ground-based radar system is in place that measures displacement of the entire slope and provides the only information we obtain from the lower, inaccessible part of the rock instability. A diesel generator inside a bunker at the top provides power to the sensors, and the data signals are collected in dataloggers in the bunker as well.

The bunker is connected to the internet by a radio link to the valley. Thus, the generator control system, dataloggers, routers and other equipment in the bunker are accessible from everywhere via VPN. The data is transferred to a database and this database has a web-interface that permits a display of the measurements of flexible intervals.

All sensors are checked daily in order to identify failure of instrument or communication as well as unusual movement. An online steerable camera at the top often provides a first indication of the cause of a problem – it could be fog, obscuring the view from the lasers, ice placed on the reflectors, or snow that distorts the GB InSAR measurements. In the event of a bigger problem, such as a broken cable from a rockfall or an avalanche, it is repaired as fast as possible. However, access to several sensors on the slope is difficult and dangerous during the

winter, and it may be impossible to find and fix an instrument or cable below a very thick snow cover in any case. The generator is maintained according to schedule.

4.9.3 ANALYSIS OF MONITORING DATA

4.9.3.1 Surface displacement: DGPS network

A permanent GPS (GNSS) network has been in place since November 3, 2010. It consists of eight antennas, of which two are placed at assumed stable locations as references (Figure 4.9-4). Data is processed using a RTK (Real Time Kinematic) technique every 15 minutes and post-processed for 12-hour averages.

The six antennas in the active part of the instability have moved between 0 and 22 mm in 3D within one year of measurement. The fastest antenna is GPS 3 and a plot of the recordings in north, east and height (z) directions is seen in Figure 4.9-5. On Figure 4.9-4, a summary of all antennas and their velocity and direction is shown.

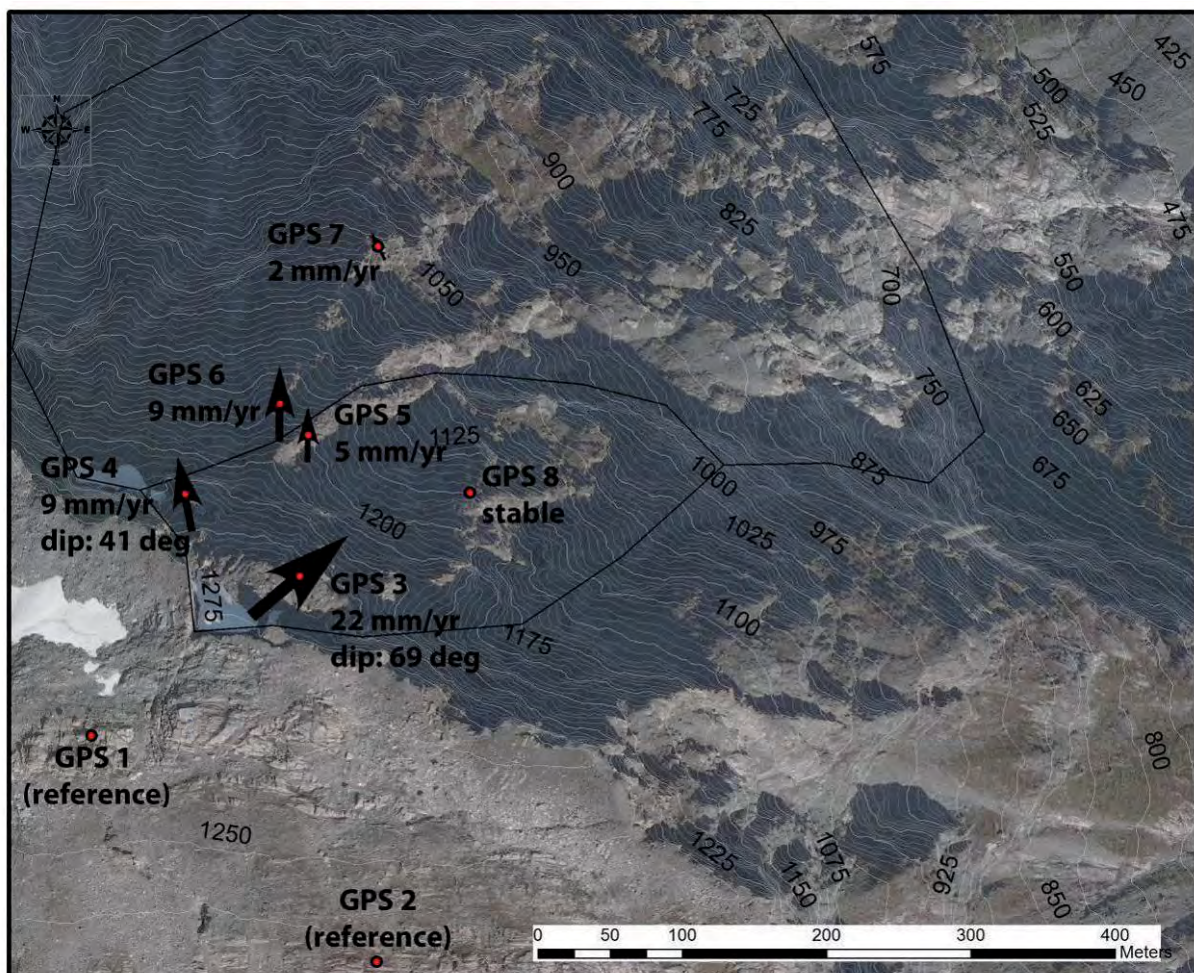


Figure 4.9-4. The location of the GPS antennas and an overview of their velocities and directions.

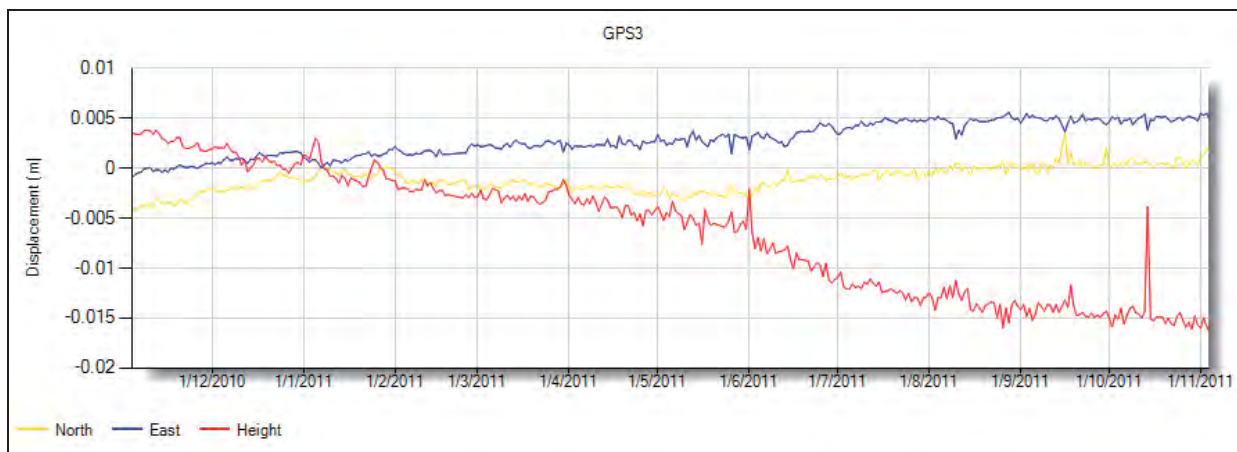


Figure 4.9-5. Movement in three directions of GPS 3 between November 3, 2010 and November 3, 2011.

The 12-hour post-processing are more precise than the RTK processing, with fluctuations of about 2 mm in the north and east directions and 10 mm in the z direction. The RTK data fluctuate about 10 mm in the north and east directions and 30 mm in the z direction. No automatic filtering is applied.

The GPSs provide reliable data, but apart from GPS 3, the recorded movement is not much bigger than the level of random fluctuations so far. GPS 3 was fastest in the summer from June to August (Figure 4.9-3), in particular in the z direction.

The GPSs directly show the magnitude of surface displacement and thus mass movement. As they are distributed in the upper part of the instability they may also help delineate zones moving with different velocities and stable areas.

The GPS antennas are very important parts of the EW system. They will provide reliable data in an acceleration phase up to a certain level; however, they are dependant on cables to the bunker both for power and data transmission, and the cables will probably fail in the last stages before a rock avalanche.

4.9.3.2 Surface displacement: lasers

Two lasers measure the distance across the main back crack (location: Figure 4.9-2) and have been operational since October 21 2009. Once every five minutes, 10 measurements are taken, the data quality checked, and the average value logged. The lasers use visible light and depend on free sight to the reflectors, therefore fog or heavy precipitation can disturb the measurements. They measure in the Line Of Sight (LOS) which may underrepresent the true displacement vector. In most cases the values fluctuate within a couple of millimeters, but regularly meteorological conditions create fluctuations of >20 mm. Some noise is removed by using daily averages when plotting a longer time series.

The lasers have measured about 40 mm displacement in their two years of operation (Figure 4.9-6), corresponding to 20 mm/yr. Some fluctuations in velocity are present in the data and probably linked to seasonal variation, but the variation is slightly different between the two lasers.

The lasers directly measure displacement and thus mass movement. They are important parts of the early warning system, due to their frequent and reliable measurements across the main back scarp. As the sensors are placed at stable ground, and the reflectors are passive, no

cables are required inside the instability (except some heating during winter). In case the reflectors move out of sight from the lasers, they are easy to adjust from the top.

4.9.3.3 Displacement: extensometers

Seven extensometers measure movement across different cracks in the upper part of the instability. Apart from extensometer 2, they have all measured less than 2 mm displacement since since August 25, 2010. Extensometer 2 is placed behind a block with the highest rate of displacement in the instability (Figure 4.9-3). When this block fails, it will fall onto the main block instability, but it is probably too small to trigger a larger rock avalanche.

Extensometer 2 has recorded displacement in the crack of a total of 56 mm in 14 months (Figure 4.9-6), which is more than twice the velocity of the lasers and GPS 3. The movement of extensometer 2 displays a strong seasonality, with high rates of displacement in summer and autumn, and a marked slowdown in winter (Figure 4.9-6). The other extensometers are not catching significant crack openings, and seem to be placed across more or less passive fractures on the moving block.

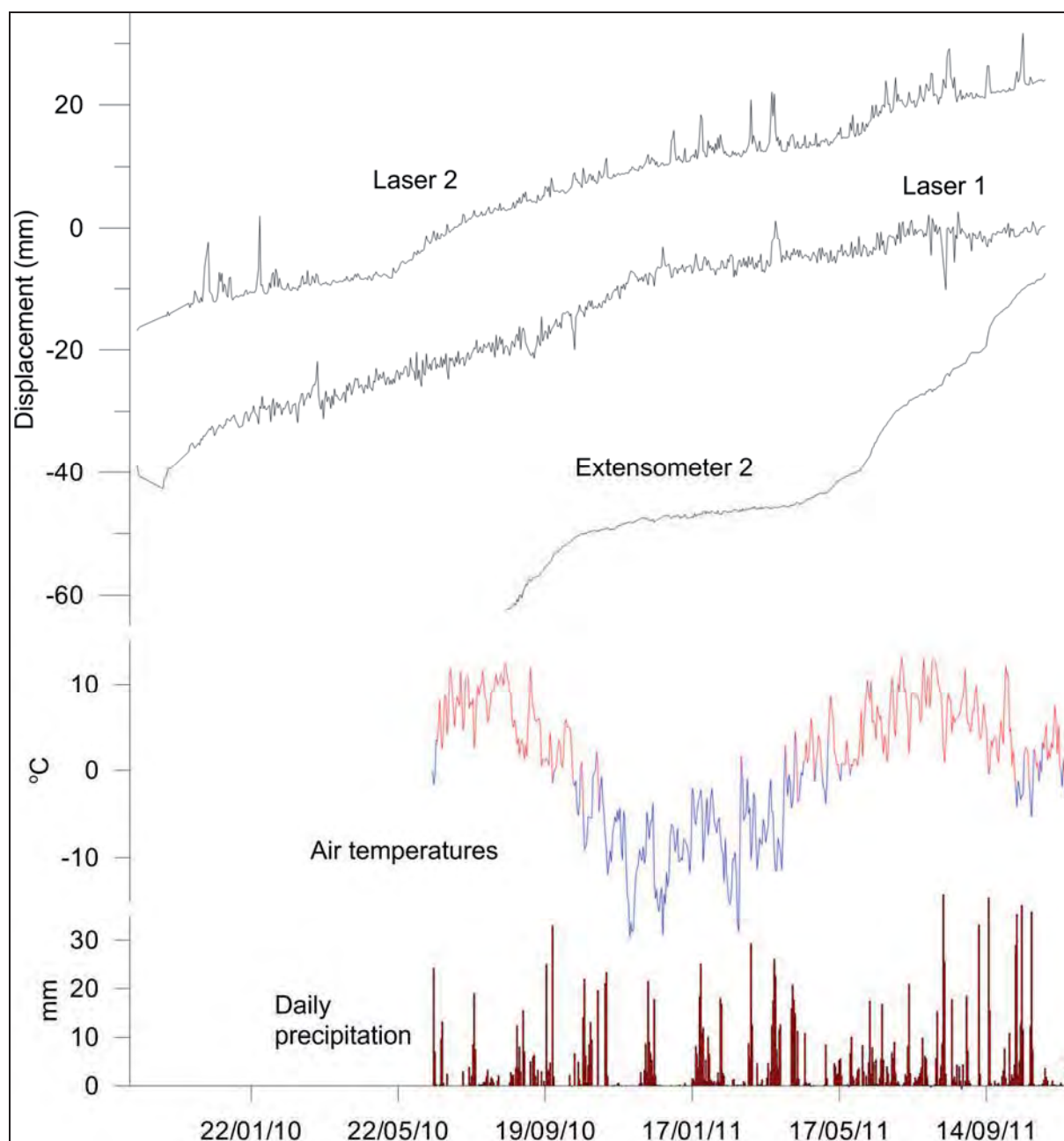


Figure 4.9-6. Displacement of lasers and extensometer 2. Air temperature and daily precipitation is also shown.

4.9.3.4 Displacement: Ground-based Interferometric Synthetic Aperture Radar System (GB InSAR)

A GB InSAR system is placed at the valley bottom (location: Figure 4.9-1), measuring distributed displacement of the entire mountainside on a continuous basis. Movement is measured in the Line of Sight (LOS) to the radar, which is often smaller than the real movement. Measurements from August 2010 to August 2011 are georeferenced and plotted on Figure 4.9-7. The velocity is quite well defined to the upper part of scenario A and compares well to the measurements by the GPS antennas (also drawn). The northern

movement shown by GPS 4 to 7 is difficult to pick up by the radar system due to the LOS (Figure 4.9-7).

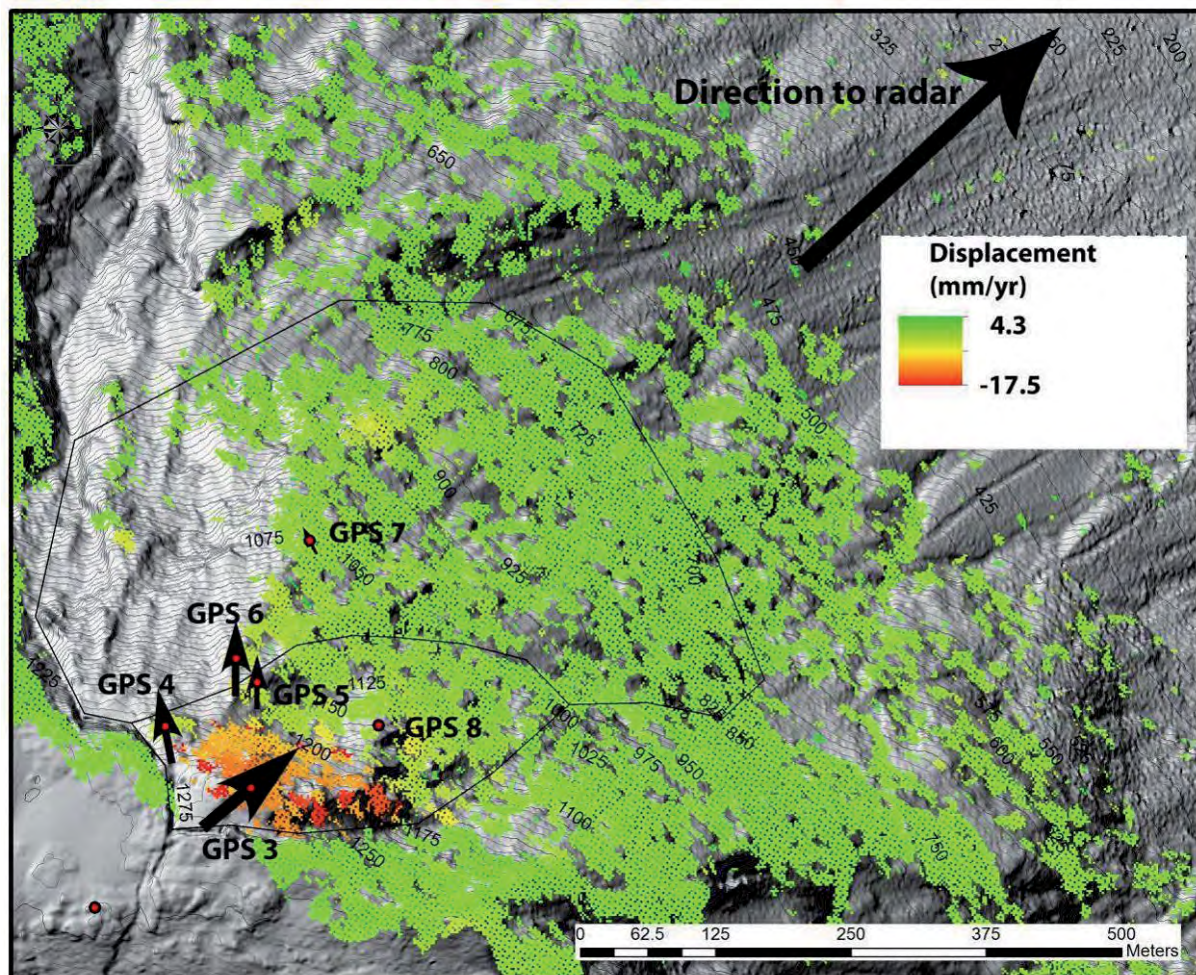


Figure 4.9-7. Displacement measured by the radar in from August 2010 to August 2011. Negative values are displacement towards the radar. Arrows show displacement vectors from the GPS antennas.

4.9.3.5 Displacement: DMS

A 139 m deep borehole was drilled in the upper part of the instability (see Figure 4.9-2 and Figure 4.9-3). It was instrumented with a 120 m long DMS column, measuring displacement or tilt for every meter. The DMS instrumentation is important in the investigations as it provides information of sliding planes in depth. It is also very important in the early warning system, as we obtain hourly updates of movement inside the instability. Figure 4.9-8 (left) shows the northward displacement measured during a 2.5 month period. The main sliding plane is clearly defined to 24 m depth (6.5 mm in 2.5 months), where the recovered borehole core and the televiewer revealed a thick breccia (Figure 4.9-8 right). A secondary sliding plane with a northern component is located at 86-89 m depth (2.1 and 1.2 mm movement in

2.5 months). Piezometers are placed in the DMS instrument, but no water is present in the borehole at Mannen.

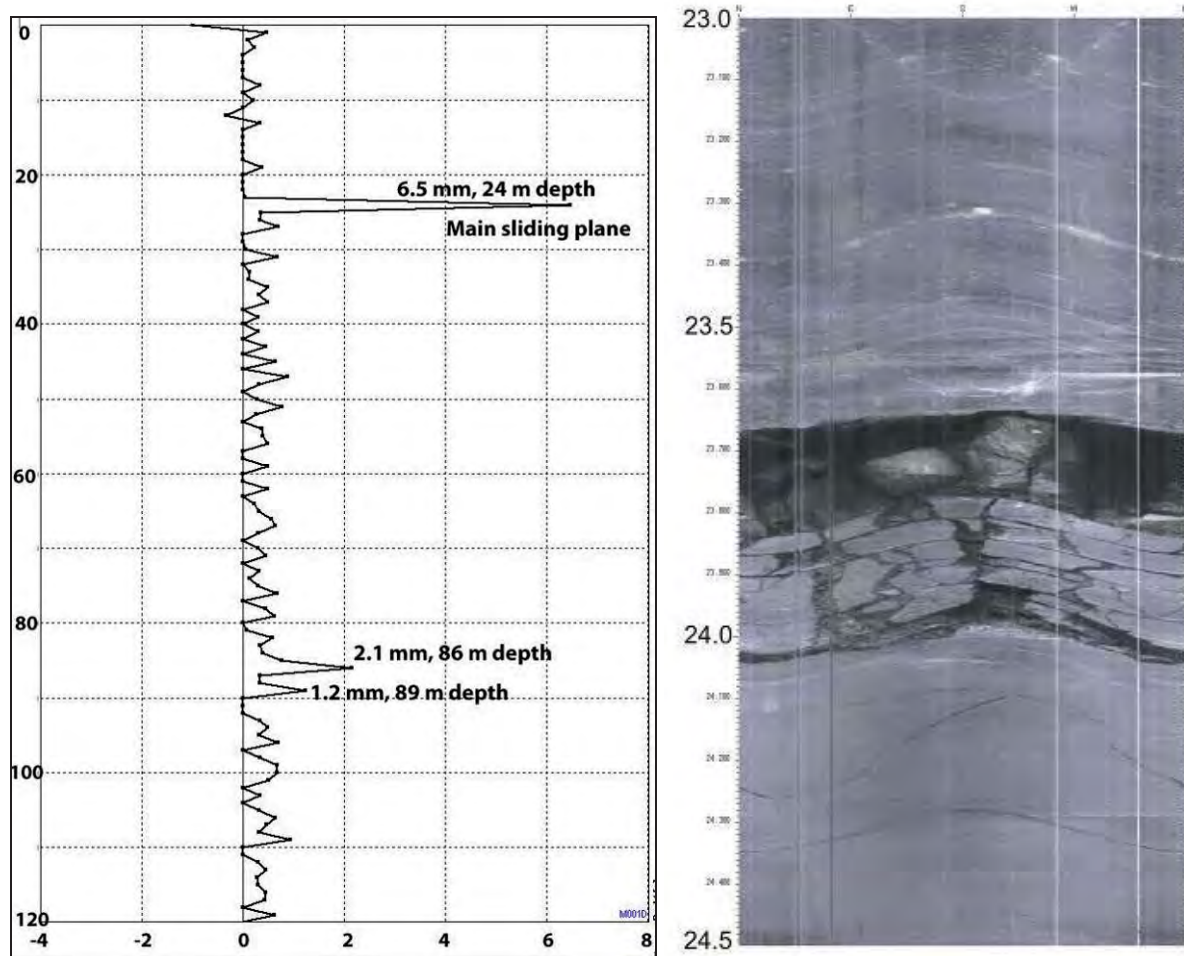


Figure 4.9-8. Left: Displacement in north direction in mm (main downhill direction) measured in the DMS column in the period: September 2 to November 25, 2011. Right: Televier image of the main sliding plane, found at 24 m depth. A 35 cm thick silty to gravelly breccia was recovered in this zone.

4.9.3.6 Meteorological station

A meteorological station is located at the plateau near the bunker, outside the instability. It records air temperature, wind speed and direction, precipitation, humidity and snow depth. Average daily temperatures and daily precipitation can be seen in Figure 4.9-6. Events of high precipitation or snowmelt are known to be linked to landslides of various types, but for the Mannen instability, we have not observed a clear pattern between precipitation and displacement rate. However, we move to blue alarm level when precipitation exceeds 70 mm/day or 200 mm/week.

4.9.4 END-USER INVOLVEMENT AND ALARM CHAIN

The total early warning system for the Mannen rockslide and other monitored rockslides in Norway involves all responsible partners or end-users that may be affected by the potential rockslide and tsunami. A systematic end-user involvement includes local, regional and

national official levels, police, and all other sectors like road authorities, health authorities, the coast guard, power companies, etc. A national emergency plan is being implemented to secure the communication chains and quality of the system. National tests have been organized, including both table-top and field-based.

The early warning levels are based on the velocity level and the stability situation at the monitored sites (Figure 4.9-9). The normal situation at Mannen is the green level, with movements typically about $0.1\text{-}0.25\text{ mm/day}^{-1}$ (Figure 4.9-9). The next level (blue) is in effect when the velocity increases substantially due to seasonally wet weather, and the yellow level is reached when the velocity increases beyond the seasonal fluctuations. The orange level is reached when movements accelerate, and the red level is reached when a catastrophic failure is imminent, at which time an evacuation is ordered. Specific actions are implemented for the different warning levels and involve the Early Warning Center, police, county governor, municipalities, road authorities, coast guard, and power companies.

The operational system is based on the following routines: (1) daily check of all sensors and data by the geologist on duty; (2) daily technical checks by the technical person on duty; (3) mobile phone text messages (SMS) on data acquired from selected sensors and technical system failures; and (4) long-term contracts with monitoring companies that have different operational responsibilities. The use of the SMS and e-mail messages is difficult due to the different types of noise in the data. It is important to use thresholds that do not result in too many false alarms, but rather provide warning of real events. SMS messages alone are never used to change warning levels, but provide important support for the people on duty. One of the challenges is that sensors with large noise levels, for example the single lasers, create a large number of messages and cannot be used alone to raise the warning level.

The structure of the communication chain between the Early Warning Centre, the responsible organizations, and all involved partners are written in detailed documents and plans. The Early Warning Centre has the responsibility to inform the responsible organization when the early warning level is changed. The county governor has the responsibility for the coordination during the yellow level, while the police take over this role during orange and red level. The implementation of warnings and evacuation is done by the police. Two different methods are used to issue warnings; first, a system of phone messages is generated based on a continuously updated database, in addition to automatic SMS messages based on regional coverage from the mobile network companies. Second, an electronic warning siren in all the villages situated in the hazard zone can be activated.

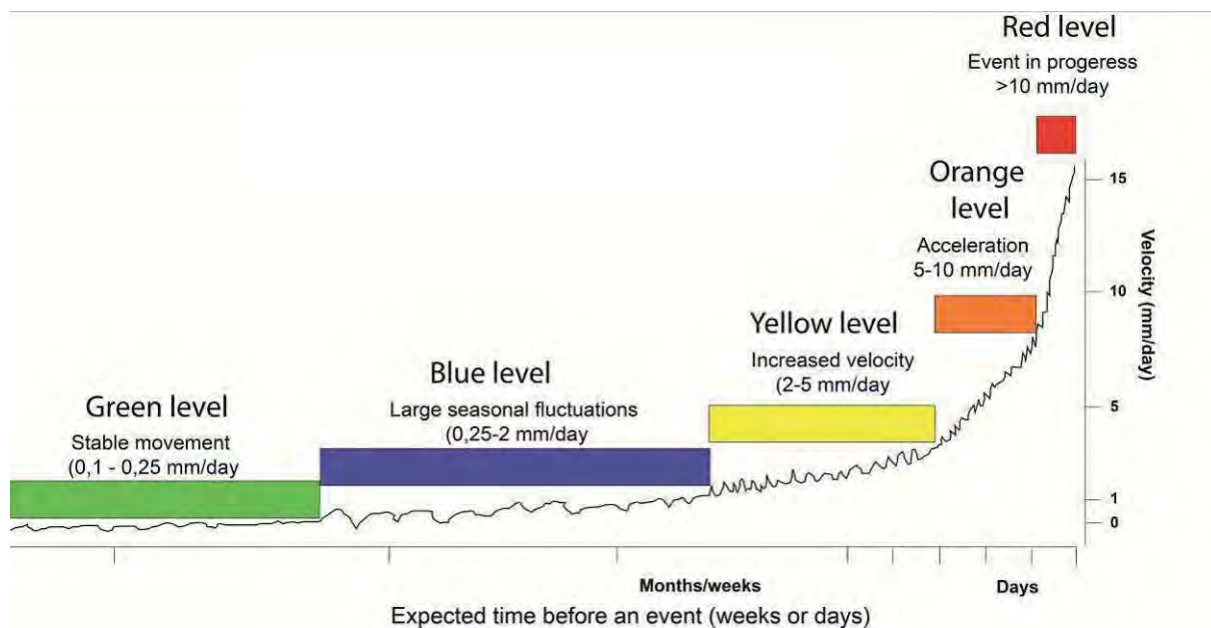


Figure 4.9-9. Early-warning levels for the Mannen rockslide

4.9.5 SUMMARIZED EVALUATION OF PARAMETERS

All sensors (GPS 3, Laser 1 & 2 and the GB radar) show movement of the upper part of the instability of about 2 cm/yr. The GPS indicates the displacement vector to be dipping 69° NE, close to the direction of the radar but much steeper. Further north, the GPS antennas show a smaller velocity and movement towards the north, which also corresponds well to the GB radar measurements. The movement in the upper block is smaller than what was measured by periodic (annual) fixed-point measurements. However, these were also varying considerably from year to year, and we assume the smaller movement can be caused by variations from year to year. Both measurements from the GB radar and the GPS antennas suggest that the area of biggest displacement is smaller than the mapped scenario A, and the scenarios should be redrawn on the basis of this information.

A seasonal trend with increased velocities during the snowmelt and summertime is seen, in particular at extensometer 2. The active rockslide body is highly fractured and has no groundwater, and the increased movement is interpreted to be an effect of water coming into the fine-grained and brecciated detachment zones. This will saturate the sliding planes and reduce their shear strength.

The threshold values that increase the alarm level from green to blue are about 1 mm/week for the upper block in the instability (excluding extensometer 2). Several instruments must be evaluated in combination, as 1 mm is less than the noise level for the lasers and GPS.

The depth of the main sliding plane is 24 m while a secondary zone of movement is found at 86-89 m depth. Some movement is seen throughout the borehole, which can be due to the highly fractured bedrock at all depths and subsidence in the main back crack which forms a graben-like structure.

A considerable effort has been put into the instrumentation of the Mannen instability, and we will consider the instrumentation to be more or less complete once the lower borehole has been instrumented with a DMS column. It has been a challenge to instrument the lower parts of the instability, and the lowermost GPS antennas and in particular as their cable connections

are at risk of snow avalanches and rockfalls. The lowermost part of the slope is inaccessible and only monitored with the GB radar.

All the instrument sensors are working fine and give the monitoring centre continuous data. However, bad weather is a major problem for getting good quality data from the laser systems and the ground-based radar.

The future outlook includes building a more complete model of the instability, which combines measurements of displacement with structural information and geophysical measurements. This will improve our understanding of processes and mechanisms of failure, which will give us better confidence in forecasting a rockslide event. Furthermore, a significant task for the monitoring centre is to maintain all instruments and systems in good working order, to ensure timely early warnings can be given.

References

Dahle et al. 2008. Faren for fjellskred fra fjellet Mannen i Romsdalen. NGU rapport nr: 2008.087

Henderson & Saintot, 2007. Fjellskredundersøkelser i Møre og Romsdal. NGU rapport nr: 2007.043

Saintot et al. 2011. Mannen unstable rock slope (Møre & Romsdal): Logging of borehole and drill core KH-01-10, geomorphologic digital elevation model interpretation & displacement analysis by terrestrial laser scanning. NGU report no. 2011.026.

www.skrednett.no: National skreddatabase på internett. (National database of avalanches, landslides, rock avalanches and rockfall). NVE & NGU.

**APPENDIX 7: KRISTENSEN & BLIKRA (2013) MONITORING DISPLACEMENT
ON THE MANNEN ROCKSLIDE IN WESTERN NORWAY**

Full citation: Kristensen, L. and Blikra, L.H. (2013) Monitoring displacement on the Mannen rockslide in Western Norway. In: Marggottini, C., Canuti, P. and Sassa, K. (eds.) *Landslide Science and Practice*, Springer, Berlin Heidelberg, pp. 251-256.



Monitoring Displacement on the Mannen Rockslide in Western Norway

Lene Kristensen and Lars Harald Blikra

Abstract

In Norway, four large rock slides are considered high-risk objects and equipped with real time early warning system. The mountain Mannen is the most recently instrumented of those. Construction and instrumentation was started in 2009 and was almost completed in 2010. To ensure redundancy, several types of instruments are used, such as lasers, realtime DGPS, extensometers, ground based InSAR system, borehole instrumentation and a meteorological station. The surface displacement is about 3 cm/year, with the largest velocity in the upper part, where the annual probability of failure estimated to 1/100. Strong subsurface deformation is measured in a 120 m borehole, suggesting a complex movement in a graben structure at the back-crack.

Keywords

Rockslide • Monitoring • Displacement

Introduction and Site Description

In Norway large rock slides are rare, but have historically cost many lives – in particular tsunamis created from rockslides have been deadly (Fylkesmannen i Møre og Romsdal 2011). Large rockslides are usually being pre-warned by accelerated movement, seen as opening and widening of cracks and increased rockfall activity. Monitoring these parameters allows for “forecasting” a rockslide event (Blikra 2008; Crosta and Agliardi 2003). The Geological Survey of Norway (NGU) has identified four high-risk objects in Norway, where both the probability and consequence of a failure is large, and an early warning system thus necessary.

L. Kristensen (✉)
Åknes/Tafjord Early Warning Centre, Stranda, Ødegårdsvegen 176
N-6200, Norway
e-mail: Lene.Kristensen@aknes.no

L.H. Blikra
Åknes/Tafjord Early Warning Centre, Stranda, Ødegårdsvegen 176
N-6200, Norway

Sogn og Fjordane University College, P.O. Box 133, Sogndal,
N-6851, Norway

The mountain Mannen, Møre and Romsdal, western Norway (Fig. 1) is the most recently identified and instrumented of the four high risk objects, and Åknes/Tafjord Early Warning Centre is responsible for the instrumentation and monitoring.

Mannen is a 1,295 m high mountain which is a part of a plateau above the steep, glacial eroded valley Romsdalen. A part of the plateau (100 mill. m³) towards the valley is bounded by deep clefts indicating past movement, but most of this appear inactive today. A block of possibly 15–20 mill. m³ has been lowered 15–20 m from the plateau, and a block in the upper part of this (2–3 mill. m³) has been measured periodically with DGPS, showing an yearly movement of 5–6 cm dipping 45–50 against ENE. These blocks are the basis of the scenarios (A and B) drawn in Fig. 1. NGU and the County Governor have estimated that the yearly probability of A; a 2–3 mill. m³ rock slide is about 1/100.

Modelling work shows that a rockslide of such magnitude would destroy the road and railroad at the valley bottom as well as several houses. Furthermore, the rock debris may dam the river Rauma, with a subsequent risk of dam collapse and flooding downstream of the river.



Fig. 1 The mountain of Mannen and the valley Romsdalen. The two scenarios, A and B are indicated in yellow as well as the position of the GB InSAR system in the valley

This paper presents the first results of the displacement measurements, which is the basis of the monitoring work at the Early Warning Centre. The displacement measurements are also important input to the understanding of the geological evolution of the rockslide.

Measurements of Displacement

The instrumentation and monitoring of Mannen is focused on identifying surface and subsurface deformation using state of the art technology. Several types of instruments are used, such as lasers, realtime DGPS, extensometers, a DMS borehole column that in real time measures detailed displacement for every meter between 0 and 120 m depth. At the valley bottom, a Ground Based Interferometric Radar system (GB INSar) measures spatially distributed displacement of the mountain side, and also ensure redundancy in case of loss of power or communication on the mountain. A meteorological station record controlling factors for the landslide such as heavy precipitation, snow melt etc.

The lasers have measured since October 2009, the GB InSAR system since February 2010, the climate station since June 2010, the extensometers since August 2010, the DMS column and the GPS's since November 2010. The different start time of the data series is evident in the plots.

The data is send to the Åknes Early Warning Centre using radiolink and stored. For the daily work we have web-based solutions for display of all data collected in the mountain, meaning that it is possible to access the data from everywhere. For selected sensors automatic alarms are sent, if the displacement is greater than pre-defined thresholds.



Fig. 2 Photo of the upper back-crack area and the plateau which has sunk 15–20 m. The position of some instruments is drawn

Extensometers and Lasers

Seven extensometers are located inside various cracks in the upper part of the landslide. They are steel rods fixed to the bedrock on either side of the cracks, and they measure extension as increased electric resistance. The extensometers are reliable instruments which provide data with little noise. A challenge at Mannen is to find unfractured bedrock to attach the instrument.

The largest movement of the extensometers is found in extensometer 2. It is located in a large crack behind a tilting block, as clearly seen in Fig. 2. Extensometer 2 has measured 25 mm of displacement in 10 months, corresponding to 30 mm/year (Fig. 3). The movement is clearly dependent on season, with a velocity of 6 mm/month in August and September 2010, a slowdown in mid October to about 0.5 mm/month in January to March 2011. As the snow started to melt again in spring 2011 the velocity increased again to 9 mm/month in May and June. Figure 3 shows the close coupling between the movement recorded by this extensometer and air temperature. The controlling factor of the variation of velocity is probably snow melt in the spring and wet conditions throughout the summer, rather than temperature itself.

Five other extensometers have recorded less than 2 mm total displacement.

Two lasers measure distance across the main back crack and down to the depressed plateau (Fig. 2). They send a laser beam to a passive reflector and record the two way travel time to measure the distance. In 19 months they have recorded a displacement of 30 and 36 mm for laser 1 and 2 respectively (Fig. 3) corresponding to 19 and 23 mm/year.

There seem to be periods of higher and lower velocity of both lasers, but they do not coincide. The measured displacement is smaller than previously seen by periodic GPS measurements. This may be explained by the fact that the

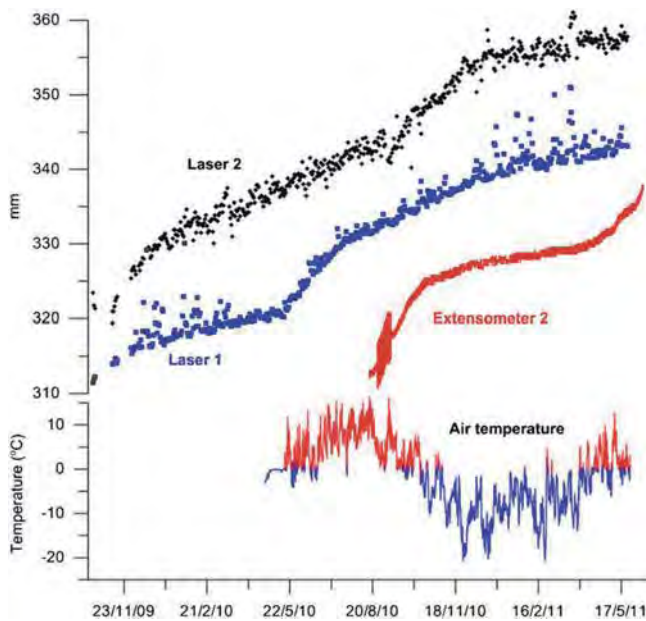


Fig. 3 Measurement of displacement of the two lasers and extensometer 2. Also shown is the air temperature, red are positive and blue are negative temperatures

direction of the laser beam is different than the direction of displacement. Their velocities are also smaller than that of extensometer 2, but this extensometer is placed at a block which was identified as the fastest in the rock slide (Fig. 2).

Differential GPS

Eight GPS antennas are placed at Mannen to record absolute displacement in 3D. Two of those are placed at assumed stable location and works as reference stations. The analyzed period covers the stable time from November 2010 to the end of May 2011, which judging from extensometer 2 is a quiet period. GPS 3 on the sunken plateau (position Figs. 2 and 5) is the fastest of the GPS antennas, with a movement of 9 mm down and 3 mm east, corresponding to a velocity of 17 mm/year. From November to January it appeared to move 4 mm north (as expected), but after that it moved somewhat towards south (Fig. 4).

GPS 4, 5, 6 and 7 moved north, with velocities between 3 and 8 mm/year. The movement is statistically significant, but quite small compared to the level of uncertainty of the method. GPS 8 was stable in the time interval. The locations, velocities and horizontal direction of the GPS antennas are summarized in Fig. 5.

Ground Based InSAR Measurements

A Ground Based Interferometric Synthetic Aperture Radar (GB InSAR) is located at the bottom of Romsdalen,

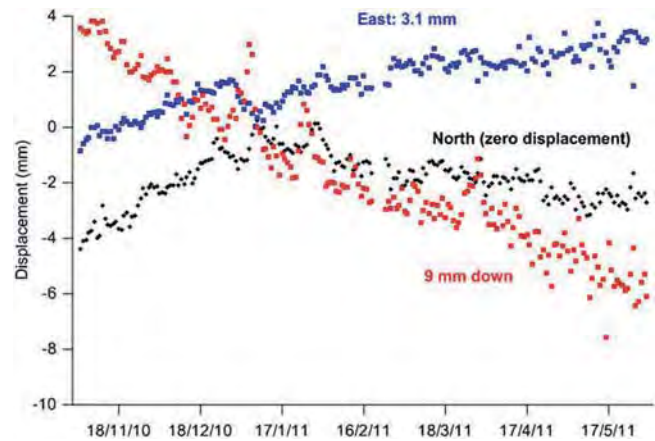


Fig. 4 The displacement of GPS 3 in three directions

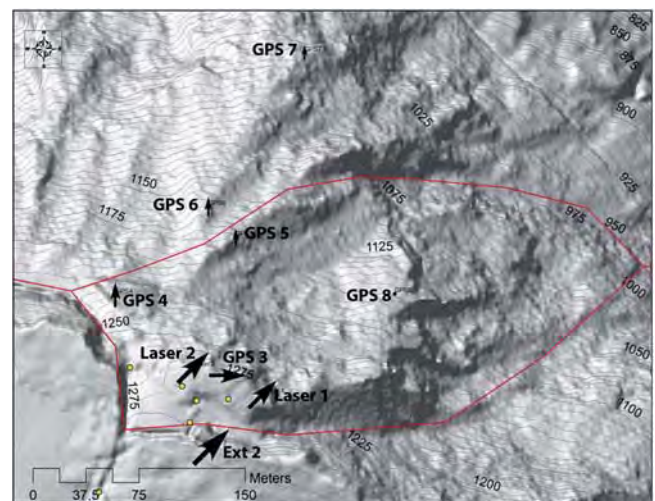


Fig. 5 The velocity measured by the GPS antennas, the lasers and extensometer 2. The direction of movement of the GPS antennas is reflected by the arrows, while the direction of the two lasers and extensometer 2 is set to NE, as this is expected

measuring displacement of the large parts of the mountain side (Fig. 6). For the principle of radar interferometry, see Ferretti et al. (2007). The system used is a LiSALab radar from Ellegi Srl.

Figures 6 and 7 show radar measurements of displacement from February to early November 2010 projected on a DEM. Positive numbers mean movement away from the system and negative numbers towards the system. This mean that red and orange is movement downhill and green/yellow are stable areas.

The areas without data-coverage are in topographic shade and not seen by the radar. The measured displacement is in the line of sight to the radar, which may be shorter than the real displacement.

Large parts of block A is seen to move about 20 mm towards the radar in 9 months, corresponding to 27 mm/year.

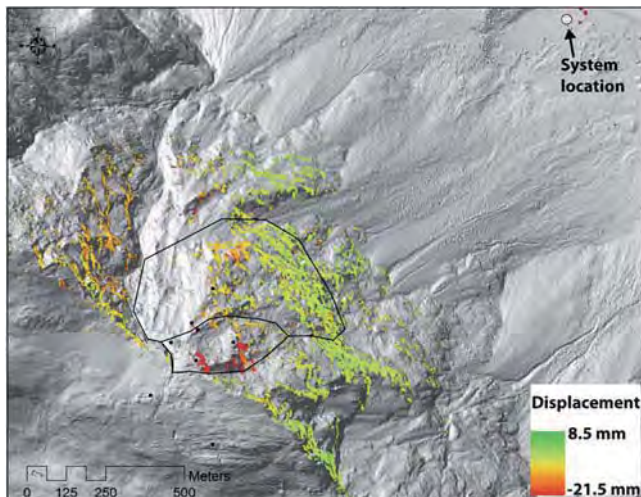


Fig. 6 The distribution of the GB InSAR measurements on Mannen. The system location and the scenations are drawn

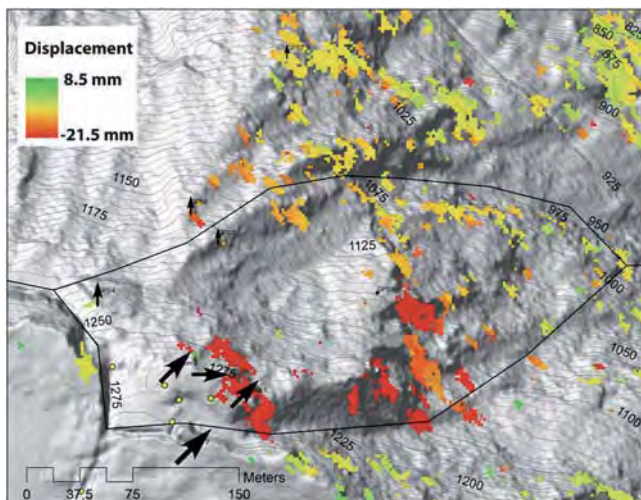


Fig. 7 Close up of the upper part of Mannen, with the radar measurements and the velocity arrows from Fig. 5

Measurements of Surface Displacement

With about a year of data from most sensors of surface displacement the data seem to correspond well with typical rates of displacement of 2–3 cm/year. This is a little less movement than previously found by periodic GPS measurements of about 5 cm/year. Some of this may be because the direction of measurement does not completely correspond to the direction of movement. Probably longer time series are important to evaluate the pattern of displacement as for instance the GPS's have only been working since November 2010.



Fig. 8 Crushed bedrock at 28 m depth

In general the GB InSAR measurements seem to fit well with the measurements. However, it measured quite high velocity last summer at the location of GPS 8, which in turn was stable this winter. We need coinciding time interval in order to evaluate such discrepancies better. The GB InSAR measurements also support the suggested scenarios with the highest rates of displacement within scenario A (2–3 mill. m³). Some displacement is also seen further down the slope, in areas where it is very difficult to place other instruments.

Mechanisms of Displacement

Evidence from a Borehole

Measurements within the ground are necessary to understand the processes in a rockslide. A 137 m deep borehole was drilled at the sunken plateau in the Autumn 2011. Logging of the core proved that the bed-rock is highly fractured to a depth of 113 m, with several levels of breccia as well as bedrock crushed to silt fraction (Fig. 8).

A 120 m DMS column from C.S.G. S.r.l. was installed in the borehole. The column consists of 120 modules with flexible joints, and each module records displacement in two directions and temperature. A few modules record the water pressure.

In the borehole, no water was found. Two modules showed movement of more than 2 mm; they are in 24 and 28 m depth (Fig. 9). At these depths crushed bedrock were logged and they are important sliding zones. The cumulated northward displacement in the time interval is almost 50 mm. This is an order of magnitude more than recorded by the nearby GPS in the same time interval. A possible explanation for this is discussed at the end of the paper.

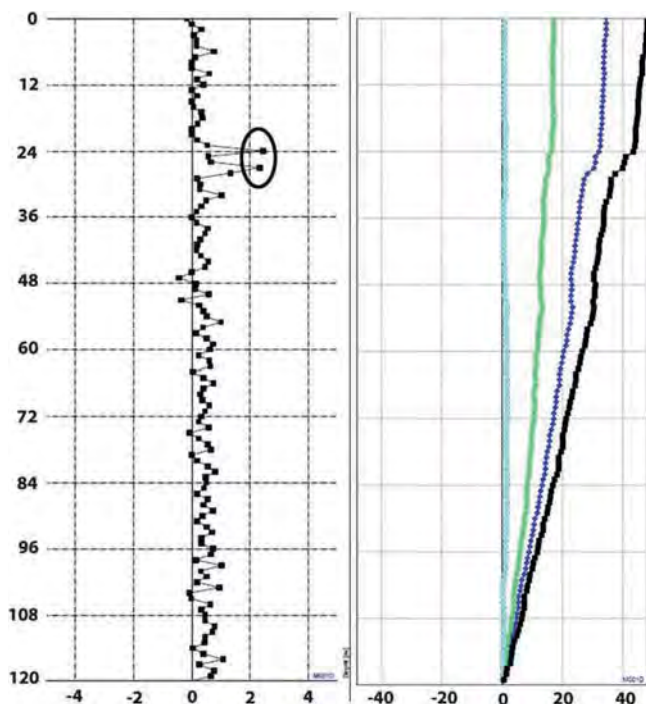


Fig. 9 Displacement of the DMS column in the period 24 February 2011 to 2 June 2011. The x-axis is in millimeters and positive is movement towards north. *Left*: Differential plot showing displacement in each module *Right*: Cumulative displacement at four time intervals

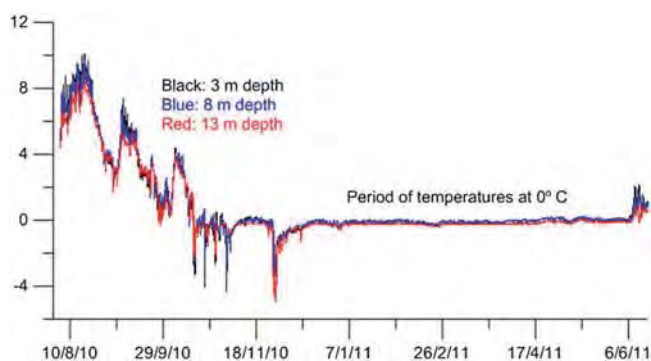


Fig. 10 Temperature in a deep open crack at the plateau at Mannen. Temperatures at three different depth intervals are shown

Possibility for Permafrost

It has been suggested that permafrost at the north facing 1,295 m high Mannen might be a factor to consider. Little is known of alpine permafrost in western Norway. Frost and ice segregation within bedrock can be a powerful mechanism for weathering rock (Murton et al. 2006) and perhaps for further crack opening.

The measurements collected so far, however, suggest that permafrost is not present at Mannen. In the borehole,

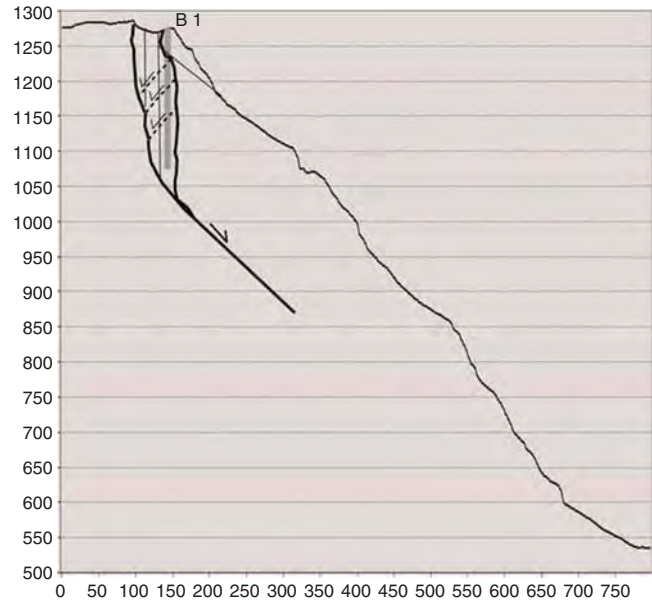


Fig. 11 The borehole at the sunken plateau. Some of the northward movement is suggested to take place as backward sliding into a graben structure at the back crack

temperatures down to 120 m are around +1 °C. Measurements from August 2010 to June 2011 in a deep open crack at the top of the plateau with sensors from 3 to 13 m below the surface, show that by early January the crack is isothermal at 0 °C (Fig. 10). If permafrost is present the temperature would be lower than 0 °C.

It is possible that isolated “cold pockets” of permafrost are found in the upper parts of the north facing Mannen. However, as seen in Fig. 3 most of the crack opening takes place in the snow melt season and summer. It is not likely that refreezing in the cracks is responsible for the crack development during this season, as the temperature is not cold enough to facilitate substantial refreezing.

Sliding Planes and Backward Tilt into a Graben Structure

The DMS measurements and the core logging show clearly active sliding zones in 24 and 28 m depth. However, a northward displacement is seen in most modules and cumulative the displacement is much larger than what is recorded by the surface instruments.

The mechanism we propose is responsible for the movement is a periodic backward sliding into open space in a graben structure in the back-crack area (Fig. 11).

It also fit well with the sudden “southward” shift in direction of GPS 3, seen in early January (Fig. 4). We need

to make more investigations to understand this hypothesised process better. First steps to be carried out in the summer 2011 are drilling of a second borehole further down the slope as well as geophysical investigations.

Conclusions

Displacement has been measured using various instruments at the active rock slide Mannen, western Norway for about a year. In general the surface displacement is in agreement with earlier periodic GPS measurements. Local measurements on the mountain fit well with GB InSAR measurements from the valley bottom, and also support the failure scenarios proposed before the detailed monitoring was initiated. Measurements in a 120 m borehole instrument show two clear sliding planes in 24 and 28 m depth. At both these depths, core logging show that bands of the bedrock was crushed to silt fraction. However, the entire core was highly fractured to 113 m depth, and the borehole instrument has measured a cumulated northward displacement 10 times higher than what was measured on the surface by a GPS antenna.

We suggest that backward sliding into a graben structure at the back-crack may be responsible for this displacement. Another borehole and geophysical investigations are planned for this summer, to better understand the processes in the subsurface.

References

- Blikra LH (2008) The Åknes rockslide; monitoring, threshold values and early-warning. In: Proceedings of the 10th international symposium on landslides and engineered slopes, 30 June–04 July 2008, Xi'an, China, Taylor & Francis
- Crosta GC, Agliardi F (2003) Failure forecast for large rock slides by 306 surface displacement measurements. *Can Geotech J* 40: 176–191
- Ferretti A, Monti-Guarnieri A, Prati C, Rocca F (2007) InSAR principles: guidelines for SAR interferometry processing and interpretation. ESA Publications, Noordwijk, The Netherlands. ISBN: 92-9092-233-8
- Fylkesmannen i Møre og Romsdal, Møre og Romsdal fylkeskommune, NGU (2011) Risiko-og sårbarhetsanalyse for fjellskred i Møre og Romsdal. Molde, p 106
- Murton JB, Peterson R, Ozout JC (2006) Bedrock fracture by ice segregation in cold regions. *Science* 314(5802):1127–1129

APPENDIX 8: HERMANNNS ET AL. (2013B) ROCKSLIDE DAMS IN MØRE OG ROMSDAL COUNTY, NORWAY

Full citation: Hermanns, R., Dahle, H., Bjerke, P., Crosta, G., Anda, E., Blikra, L., Saintot, A. and Longva, O. (2013b) Rockslide Dams in Møre og Romsdal County, Norway. In: Margottini, C., Canuti, P. and Sassa, K. (eds.) *Landslide Science and Practice*, Springer, Berlin Heidelberg, pp. 3-12.



Rockslide Dams in Møre og Romsdal County, Norway

Reginald L. Hermanns, Halgeir Dahle, Per L. Bjerke, Giovanni B. Crosta, Einar Anda, Lars H. Blikra, Aline Saintot, and Oddvar Longva

Abstract

Eleven rockslide dams exist in Møre og Romsdal county in Norway. Geological evidences indicate that more of such dams existed during the Holocene. Eight of those dams formed in prehistoric times, while two rockslide dams formed in historical time. One of the rockslide dams failed partially at the beginning of the Holocene eroding 45,000 m³ from the dam, however the remaining dam is stable and it is used for hydropower generation. Present hazard of rockslide dams is represented by the Mannen unstable rockslope. This site has a volume of 15–25 × 10⁶ m³ and is moving up to >4.5 cm/year on measurement points. A failure of the slope would dam the Rauma valley and few farms would be flooded upriver. However, due to the large discharge of the river the dam would only prevail a short time and dam failure is likely to cause inundation downstream. Here we present a probability analysis for this scenario.

Keywords

Landslide dam • Rock avalanche • Dam breach • Flooding • Probability analysis • Hydrological modelling

Introduction

Large rockslides have formed natural dams in all mountain environments and volumes involved vary significantly from several million cubic meters up to several cubic kilometers

R.L. Hermanns (✉) • H. Dahle • A. Saintot • O. Longva
Landslide Department, Geological Survey of Norway,
Leiv Eirikssons vei 39, Trondheim, Norway
e-mail: Reginald.Hermanns@NGU.NO

P.L. Bjerke
Landslide Department, Norges Vassdrags Og Energi Direktorat,
Trondheim, Norway

G.B. Crosta
Dipartimento Di Scienze Geologiche E Geotecnologie, UMB,
Milan, Italy

E. Anda
The County of Møre og Romsdal, Molde, Norway

L.H. Blikra
Åknes Tafjord Beredskapsenteret, Stranda, Norway

(Evans et al. 2011). Impounded lakes can have capacities up to more than 10 km³ with lake Sarez, impounded by the Usoy dam in Tajikistan, being with a volume of 16 km³ the largest rock slide dam reservoir known on Earth (Ischuk 2011). Despite the large volume forming those dams they are not necessarily stable and of all dams formed in the 20th century with a volume in excess of 20 × 10⁶ m³ half have breached within the following 7–3,435 days (Evans 2006) causing catastrophic floods downriver from the dams often releasing nearly the entire stored water (e.g. Costa and Schuster 1988) and have resulted in significant destruction and loss of life (e.g., Groeber 1916; Zevallos et al. 1996; Evans et al. 2011). In history the landslide hazards with highest reported numbers of victims was the result of the breach of a dam along the Dadu river in Sichuan, China, on June 11th 1786 which had only formed 10 days earlier after being triggered by an earthquake of ~ M 7.75. Reports indicated a death toll up to 100,000 (Dai et al. 2005). In general, there is an agreement that those dams which fail catastrophically, are usually new and ~80 % of catastrophic

dam failures occur within the first year of dam existence (Costa and Schuster 1988; Ermini and Casagli 2003; Evans et al. 2011). However, rockslide dams which remain a few years can become stable landforms controlling the geomorphic development of valleys for thousands of years (e.g. Hermanns et al. 2004a; Schuster 2006). Nevertheless, also older dams have breached and have caused catastrophic floods (e.g., González Díaz et al. 2001; Hermanns et al. 2004a, b). Therefore, Ermini and Casagli (2003) suggested a geomorphic index based on the dam volume, the dam height and the catchment size which indicates stabilities of dams. Other indexes were proposed later (Korup 2004; Jia-Jyun et al. 2009).

Due to the large water volume stored and the steep gradient in the river profile these dams have been often used for hydro-power generation (e.g. Duman 2009; Hermanns et al. 2009), and rockslides have been artificially triggered by explosives in the former Soviet Union to construct dams in remote areas rapidly and at low cost (e.g. Adushkin 2005; Korchevskiy et al. 2011). Nevertheless, also dams with longevity have breached causing catastrophic floods (e.g. Hermanns et al. 2004a, b; Costa and González Díaz 2007).

Most of the landslide dams fail by overtopping (Costa and Schuster 1988; Evans et al. 2011) when the landslide dammed basin has filled up with water and erosion of the dam crown starts down cutting into the deposit. However, overtopping by displacement waves caused by a rock avalanche into the landslide dammed lake has also been reported and is considered a serious threat when large unstable slope areas exist in a slope above the lake (Hermanns et al. 2004a; Stone 2009). Other failure modes are piping (e.g., Meyer et al. 1985; Quenta et al. 2007), progressive upstream erosion (Hancox et al. 2005), and sliding collapse of the downstream face of the dam (Dunning et al. 2006). All of these processes are self accelerating because the larger the water escape growth, the higher the outflow velocity becomes and the more material can get eroded from the landslide deposit. Hence, the landslide dam erosion results often in its breach. Peak discharges during such failures can often be several times fold the seasonal peak discharge of a river and have volumes of several tens or more than 100 thousands cubicmeters per second (e.g., Abbott 1848; Zevallos et al. 1996; González Díaz et al. 2001; Evans et al. 2011). Such a discharge can flood large portion of the river valleys downstream and lead to the damage and destruction of bridges, villages, agricultural land and hydro-power facilities.

In this paper we will describe selected rockslide dams and related deposits as well as a potential rockslide in Møre og Romsdal which most likely will dam one of western Norway largest valleys in the next few hundred years in order to describe the hazard but also the potential of rockslide dams.

Geological Setting

The landscape of western Norway is characterised by an extreme alpine relief with steep slopes, heavily oversteepened U-shaped glacial valleys. The bedrock comprises mainly metamorphic rocks of Precambrian to Palaeozoic age. The bedrock is highly tectonized due to protracted intense ductile and brittle tectonics acting since Precambrian times over the entire region. In the Quaternary, multiple glacial cycles covered the landscape with kilometre thick ice caps and eroded into the fault-controlled valleys and causing loading, and subsequent isostatic rebound. The high concentration of structures, due to tectonics and glacial unloading in the bedrock and the steepness of the relief, would be the two main parameters that render a slope susceptible to development of large rock-slope failures (e.g. Braathen et al. 2004; Saintot et al. 2011) which can develop as rock avalanches (Blikra et al. 2006; Hermanns et al. 2006). In the narrow valleys of Norway rock-avalanche deposits often formed rockslide dams (Fig. 1) (e.g., Hermanns et al. 2009; Fenton et al. 2011).

Existing Rock Slide Dams

Rock-avalanche deposits exist throughout the entire Møre og Romsdal county (Blikra et al. 2006) as the province is everywhere characterized by high relief contrasts. Except in the Storfjord region where rockslide deposits have been systematically mapped on bathymetric data, and 107 individual deposits have been characterized (Longva et al. 2009), these deposits have been extensively described (Blikra et al. 2006) but not systematically mapped in Norway yet. Therefore we mark on our map (Fig. 1) only those deposits which impound a water body today.

The geography of the NW part of the county is characterized by mountain surrounded by deep fjords extending several tens to more than hundred kilometres into the mountains, so most rockslide dams concentrate in the SE part beyond the limit of the fjords (Fig. 1).

The Onilsavatnet Rockslide Dam (Norddal Municipality)

The prehistoric rock avalanche deposit forming the rockslide dam and impounding Onilsavatnet in Tafjord has a volume of $\sim 200 \times 10^6 \text{ m}^3$ and is one of the largest postglacial rock avalanches reported so far in Norway (Blikra et al. 2006) (Fig. 1). The rock avalanche formed at the end of Tafjord from the western slope composed of Precambrian ultramafic and gneissic rock. It occurred shortly after deglaciation

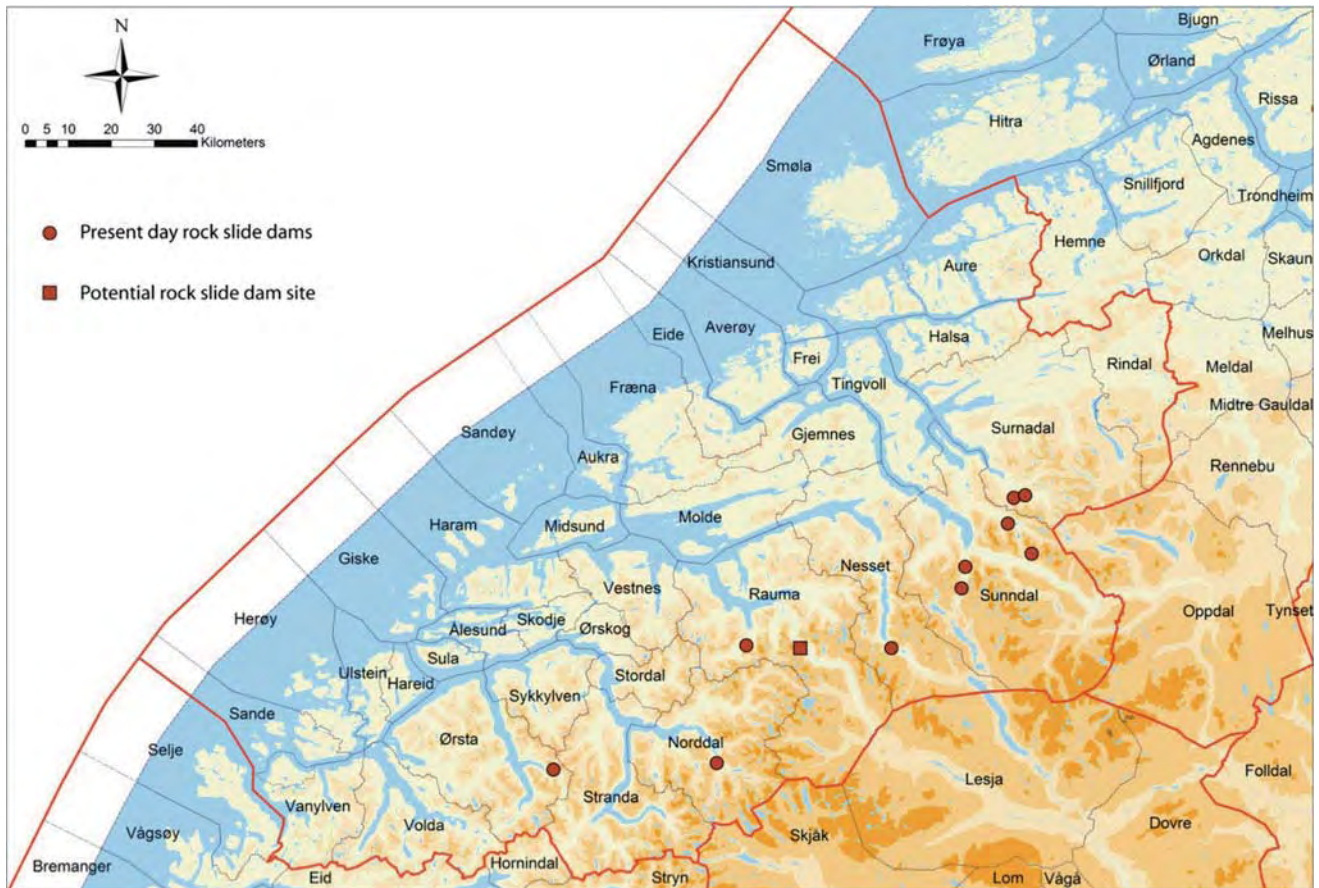


Fig. 1 Distribution of rockslide dams and the site of a potential near future dam in Møre og Romsdal in western Norway

about 10 ka ago as indicated by ^{10}Be cosmogenic nuclide ages (Hermanns et al. 2009). The valley geometry at that site is symmetrical due to glacial erosion (Fig. 2) and the thalweg of the valley has a low gradient. The rock avalanche was a single event and formed a lake within the Onilsa valley. In addition, with a total run out length of only 2,500 m and a vertical drop of 870 m between the rockslide scar and the rockslide toe, giving a *Fahrböschung* (H/L) of 0.35, the rock avalanche deposit is considered as massive and the event has been of relative low mobility. This is also in agreement with the distribution of the deposit seen on a cross valley profile with the main body of the displaced rock mass lying at the foot of the collapsed slope adjacent to the breakaway scarp (Fig. 2).

Today Onilsavatnet is only 1.3 km long and covers an area of 0.7 km². The lake surface lies at 177 m a.s.l. and the maximum depth is 152 m. This vertical drop is used by the hydropower company 'Tafjord-kraft' to generate an average of 72,2 GWh per year.

A breach eroded close to the eastern slope into the dam. This breach exposes the underlying bedrock and river discharge today is over the bedrock (Fig. 3). In front of the breach a massive debris fan expands north of the rock

avalanche deposit covering 2.5 km² of a marine terrace (Fig. 2). The debris fan between the present day coast line and the rock avalanche is composed of large boulders varying in size from several decimetres to up to 3 m. Volume calculations indicate that the breach has a volume of 45,000 m³ while the debris fan has a volume of 30,000 m³. The remaining 15,000 m³ were not deposited onshore.

A seismic profile of the marine deposits of Tafjord shows an unstratified layer with no internal reflectors spanning over a distance of 16 km (Fig. 4) away from the fjord end. Seismic stratigraphy of this fill facies layer indicates an early Holocene age (Longva et al. 2009), hence the age of the fill facies coincides closely with the age of the rockslide dam formation. At that time sea level was about 80 m higher in this part of Norway due to glacial loading of the Scandinavian shield, the shore line therefore coincided with the marine terrace in Tafjord. The restriction of the debris fan to this terrace also indicates that dam formation, dam breach, and deposition of debris fan and distal deposit in the fjord occurred within a small interval of time.

This lake has a small catchment of only 265 km² and using the geomorphological dimensionless index as suggested by Ermini and Casagli (2003) this dam should have been stable.

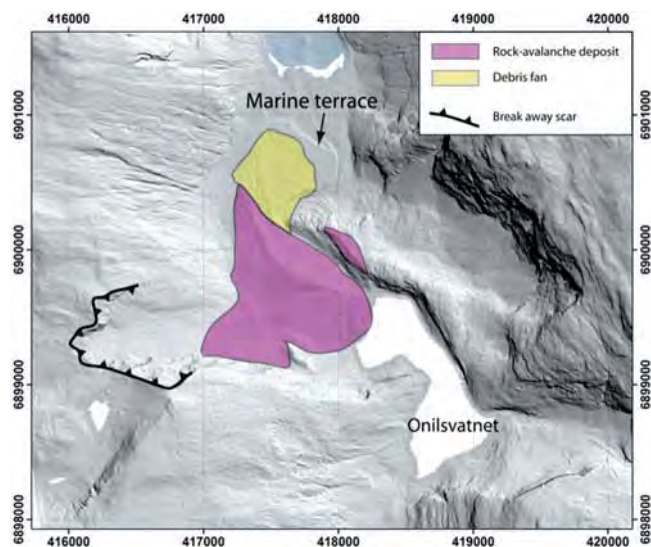


Fig. 2 Digital elevation model of the end of Tafjord showing the rock avalanche deposit which dams the Onilsvatnet. Note the breach eroded into the dam and the debris fan lying in front of this breach on top of the marine terrace. (UTM coordinates, zone 32 N)

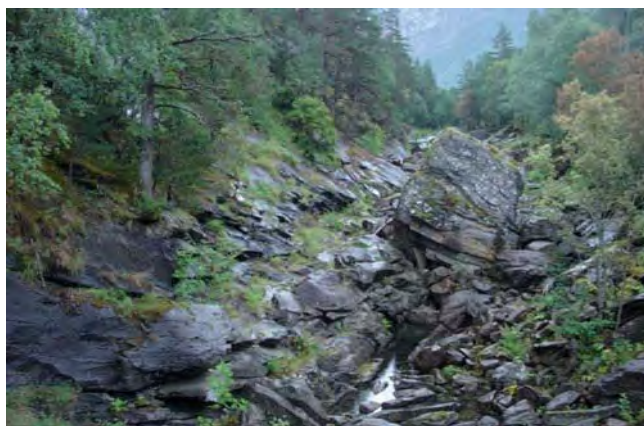


Fig. 3 Drainage of Onilsvatnet over bedrock. The rock avalanche deposit has been eroded away from the east side (left) of the slope

However due to melting of the ice cap in Norway, water budget of rivers at that time were much higher than today's situation.

We argue that the Onilsvatnet lake rockslide dam only partially breached releasing a minor portion of the lake volume and leaving behind stable rockslide dams due to the asymmetry of the rockslide deposit within the valley profile. Such asymmetric dams are as vulnerable to failure due to overtopping by river discharge or displacement waves as symmetric dams. However downcutting of the dam and breach development is restricted by the underlying rock

(Hermanns et al. 2011a). This case shows that down cutting of the dam and breach development is restricted to the rockslide deposit, but underlying rocks resist further breach development.

Rockslide Dam at Lyngstøylvatnet in Norangsдалen

The dam in Norangsdal, Østra municipality (Fig. 1) was formed by a large rockslope collapse with a volume of ca. 100,000 m³ on 26th of May 1908. This event did not had the mobility of a rock avalanche, however the valley is very narrow at that site and the deposit formed a lake 40 m deep and 408 m long (Furseth 2006). Although this rockslide did not cause any casualty or direct destruction in the 40-m-deep lake behind the dam, 8–9 mountain farms have been submerged by the lake (Fig. 5).

The lake lies close to the divide of the water shed and the discharge of this lake is restricted. Hence geomorphic parameters indicate a rather stable lake.

Potential Rockslide Dam in the Rauma Valley

One of the most actively deforming rock slopes identified in the last years in Norway is the rockslope at Mannen above the Rauma valley. This site shows significant signs of deformation (Saintot et al. 2011), has deformation velocities up to 4.5 cm/year, and is characterized by frequent rock falls. Two different scenarios of failure have been proposed based upon the distribution of slide velocities and structures. The first one (A) involves a volume of 2–4 million m² and the second (A + B) involving a volume of 15–25 million m² (Fig. 6) (Dahle et al. 2011).

Based upon these observations and frequent rock avalanches in the prehistoric past in this valley section, the probability of failure of scenario A was estimated to 1/100 and for the scenario A + B to a probability of 1/500 years in a preliminary assessment (Dahle et al. 2011). This was based upon principles outlined in Hermanns et al. (2011, this volume).

In this paper we do not deal with a discussion of slope stability of that slope and the related direct consequences (3 farms lie within the potential run out area) but with the analyses of geological consequences related to dam formation as this has an important impact on planning and development in the entire Rauma valley (Fig. 1). Due to the briefness of this publication we focus on the larger scenario A + B only, although the same type of analyses was also carried out for the smaller scenario A.

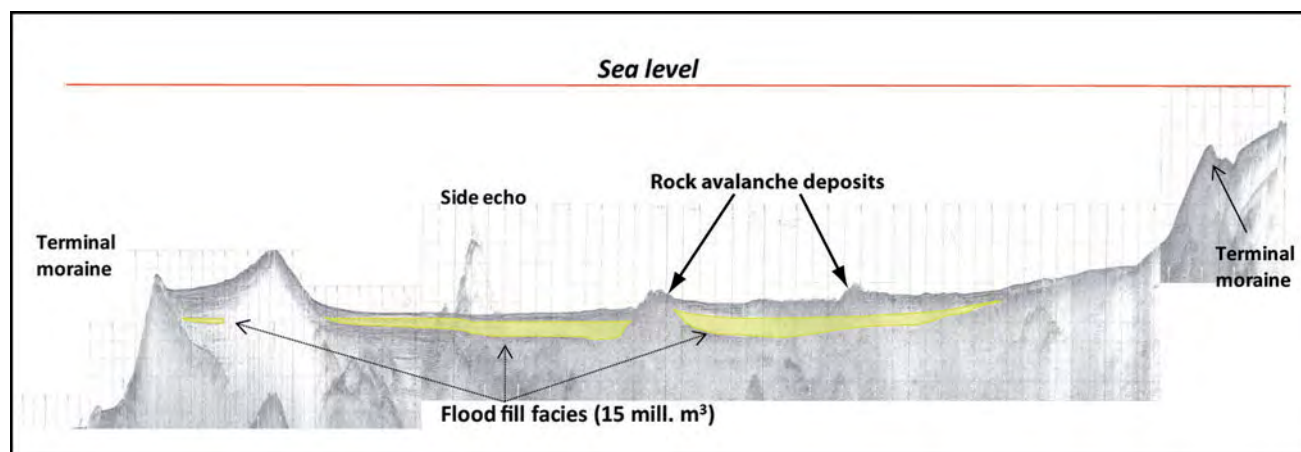


Fig. 4 Seismic profile of sediments of Tafjord spreading 16 km from the SE tip of the ford (*right*) to an important drop within the bathymetry of the fjord coinciding with a late Pleistocene

moraine. Note the unstratified fill facies within the middle part of the profile representing a fine grained layer which was rapidly deposited



Fig. 5 Old farm houses visible in rockslide dammed Lyngstøylvatnet (Photo by Astor Fuseth)

Run Out Modelling

In a first step the run out of a potential rockslide with a volume of 18.8 million m^3 was simulated using various 2D and fully 3D run out models and input parameters. All models indicated that the rock-avalanche would cross and hence dam the river. In a second step the maximum limit of all simulations were integrated into a map showing thicknesses of the deposit >2 m (Fig. 7).

The simulations indicate that the deposit at the position of Rauma river will have a thickness of 16–18 m rising the level of the present 59 m a.s.l. to 75 – 77 m a.s.l.. This gives the limit of the upstream inundation area (Fig. 8). Several more farms lie within this area. The possible dam height and inundation area allows determining how fast the basin would fill to the level of dam overtopping by taking into account various discharge rates of Rauma river (Table 1). With a

mean discharge a basin dammed up to 75 m a.s.l would fill up within 14 days while during a mean flood event within less than 2 days (Table 1).

The fast overtopping suggests that the dam would breach like most of the rockslide dams in the world (Costa and Schuster 1988) by overtopping. In addition applying the principles used by Ermini and Casagli (2003) and comparing to data from the Alps or Japan, the potential dam has to be considered as unstable.

Assessment of Downriver Flooding

In order to assess the downriver flood we used (A) an empirical approach in combination with a subjectively weighted decision tree analyses, and (B) a hydrological model Hec-Ras to assess the water level for various dam breach scenarios from the dam site down to the fjord, which did not included highly sediment-loaded floods or debris flows.

(A) Assessment of downriver flood based on empirical data

The peak discharge values, as well as the breach depth and volume of dammed lake basins of historical rockslide dam breaches have been collected by Manville (2001). He compared the relation of breach depth over basin volume (dam factor) against peak discharge and found a linear relation. However, data spread over one order of magnitude (Fig. 9). To assess peak discharge of the potential dam in Rauma valley we plotted the calculated dam factor for several dam heights to calculate potential peak discharges and calculated a mean, maximum and minimum peak discharge using the spread of the world wide data (Fig. 9). In addition we estimated that the dam would not breach entirely

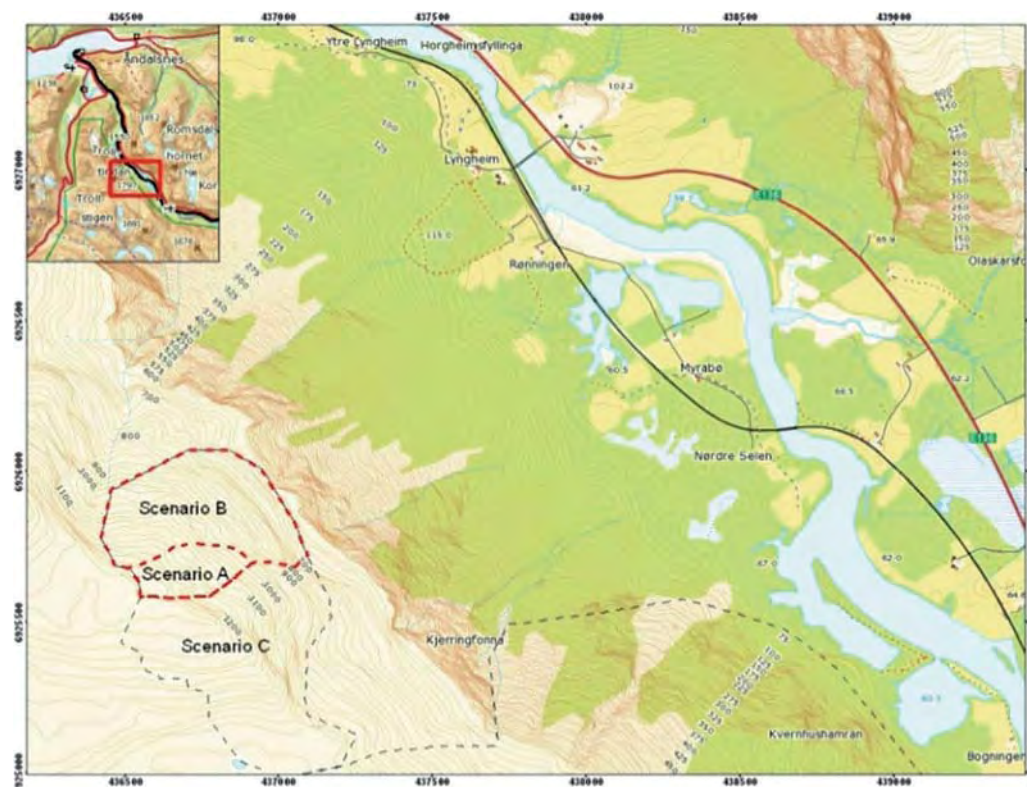


Fig. 6 Map showing the position of the unstable slope area above the Rauma valley

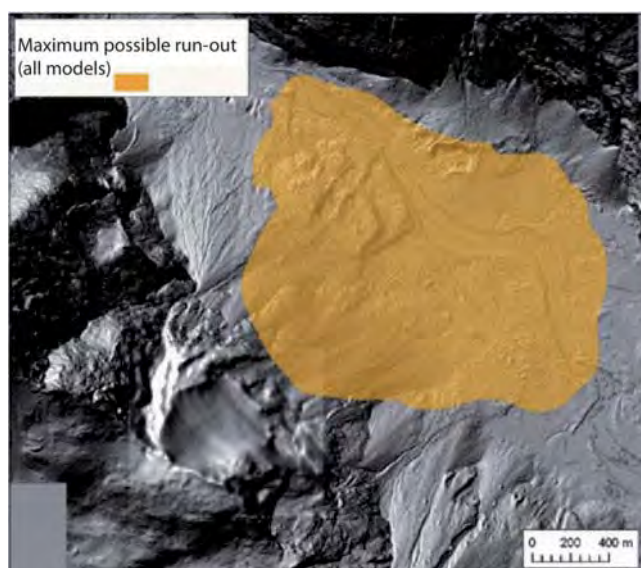


Fig. 7 Map showing the maximum expected extent of the rock avalanche deposit for the Mannen site, as obtained by enveloping the results of different numerical run out models. The failure surface is visible in the upper slope area just above the deposit. The thickness of the deposit is > 2 m

but a remnant lake would prevail. This is suggested by rest of prehistoric rockslides dam in Rauma valley where also remnant lakes exist (Fig. 10).

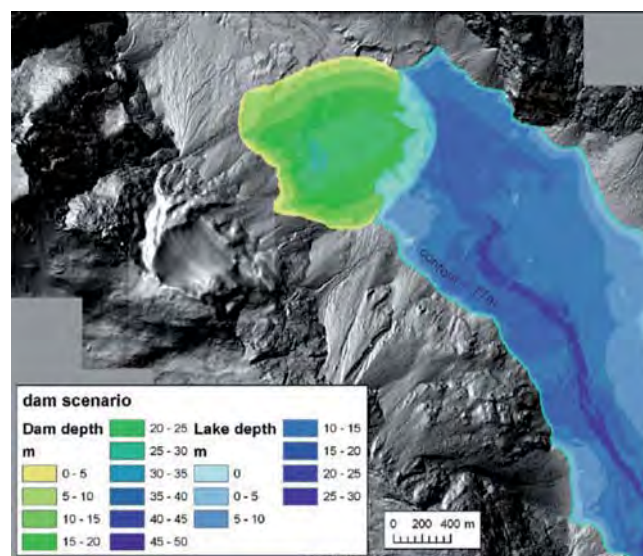
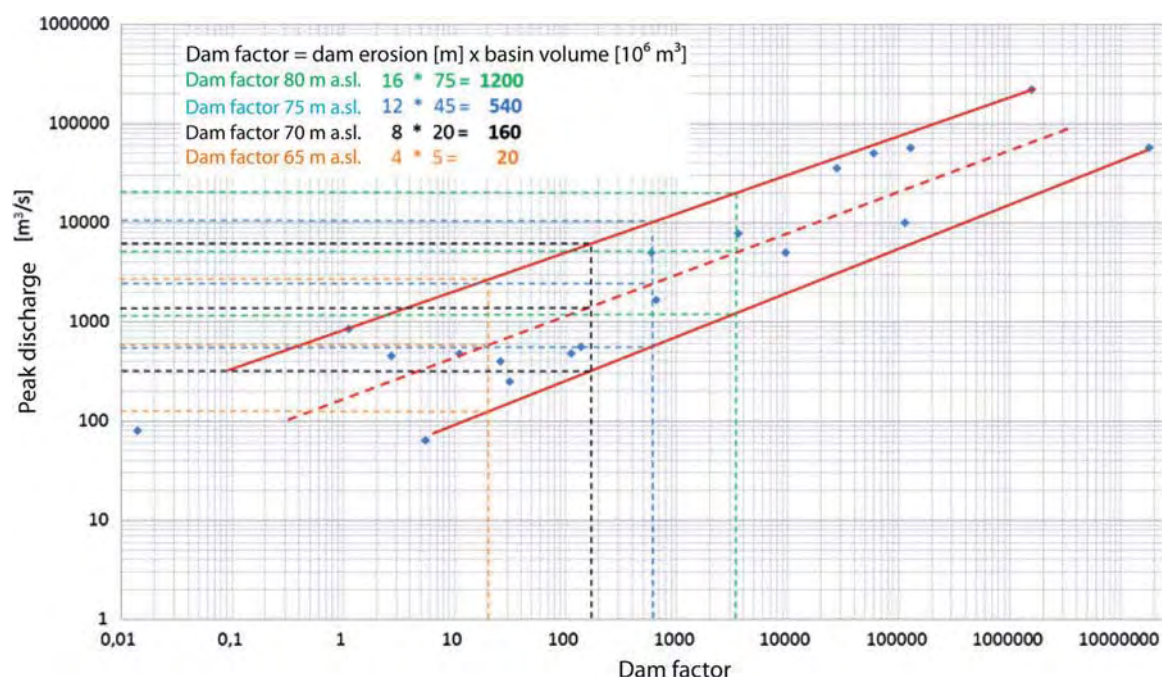


Fig. 8 Map showing one simulated scenario of the rock avalanche deposit for the Mannen site as well as the flooding area upriver the dam

In order to assess the likelihood of any given peak discharge we used as starting scenario the preliminary assessment of likelihood of failure of the rock slope (see above, Dahle et al. 2011) in a subjectively weighted decision tree. We considered several dam heights, a likelihood of 80 % that the dam would fail and 20 % that the dam

Table 1 Time needed to fill a basin behind a possible rockslide dam at Mannen, Rauma valley taking into account various discharge scenarios

Dam crest [m.a.s.l.]	Infill time			Capacity basin [10 ⁶ m ³]
	Normal discharge (38 m ³ /s)	Peak discharge (297 m ³ /s)	200 year flood (570 m ³ /s)	
80	23 days	70 h	36 h	75
75	14 days	42 h	22 h	45
70	6 days	19 h	10 h	20
65	39 h	5 h	3 h	5
60	3 h	0.5 h	0.2 h	0.4

**Fig. 9** Diagram showing empirical data (after Manville 2001) and estimation of peak discharge scenarios for various dam heights for potential dam heights in Mannen**Fig. 10** Remnant lake in Rauma valley behind prehistoric dam impounded by a rock avalanche

would be stable and a likelihood of 25 % that the peak discharge would be comparable to maximum and minimum peak discharge as compared to empirical data and a 50 % likelihood to be close to the mean values of empirical data (Fig. 11).

In a last step we combined both analyses from scenario A and scenario A + B and the likelihood of any flood events on Rauma river not related to any rockslide damming. This approach indicates a worst case scenario with a maximum discharge of 20,000 m³/s and a likelihood of 1 in 22,000 years and a most realistic scenario with a likelihood of 1 in 1,850 years and a discharge of 2,500 m³/s. All smaller discharge scenarios add up to a likelihood of 1 in 505 years (Fig. 12).

(B) Calculation of water level for various dam breach scenarios from potential dam site to ocean

The water level of Rauma river during dam failure was simulated for various dam breach scenarios using a hydrological model (Hec-Ras) based upon a digital elevation model with 1-m-resolution (Fig. 13). This model gives inundation depth value at each locality which allows mapping the houses which lie within the flood area for each scenario, here

Decision tree: Scenario A + B

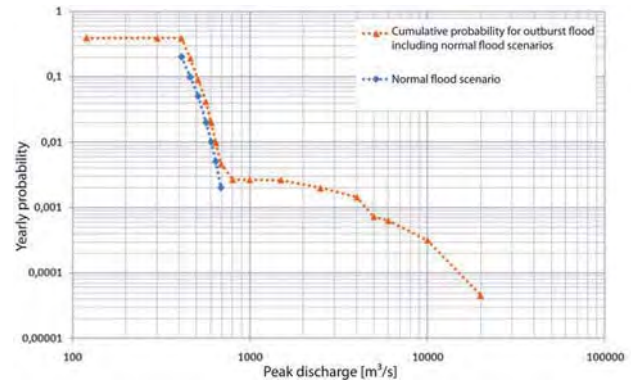
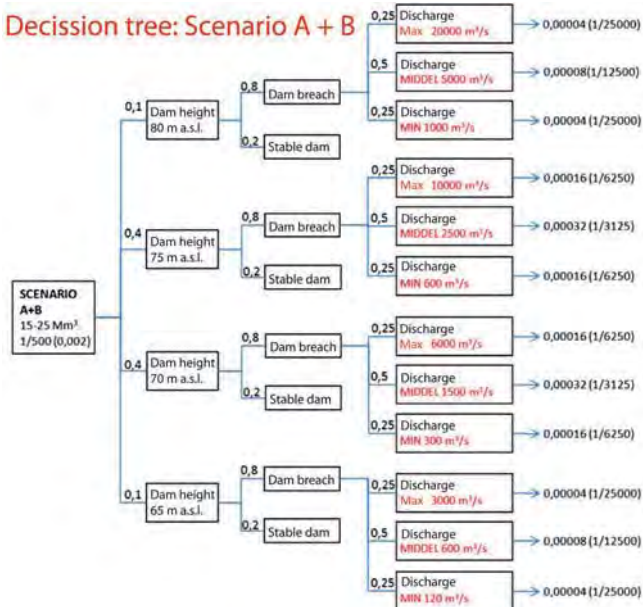


Fig. 12 Yearly probability for different dam heights (green is the sum of red and blue curve). In the building act likelihoods of 1/200 (0.005) and 1/1,000 (0.001) have legal consequences. Those relate to dam heights of 65 and 75 m a.s.l.

Fig. 11 Subjectively weighted decision tree to estimate likelihood of peak discharges deriving from dam breaching

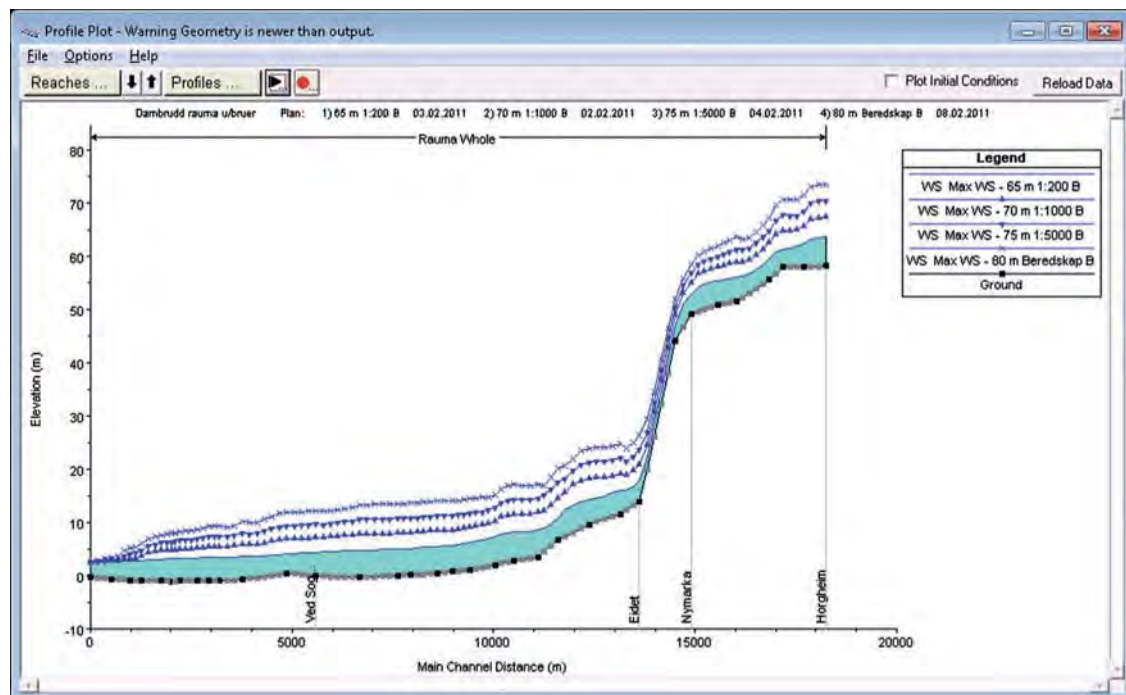


Fig. 13 Simulated water levels from potential rockslide dam down to the fjord

given for the one in 1,000 hundred years scenario (Fig. 14). As Rauma river enters the fjord at a delta on which the city of Åndalsnes is partly constructed, various flood scenarios

indicate that several hundred houses and touristic facilities would be flooded. This information is a necessary input for regional planning in the area.



Fig. 14 Map showing simulated flooding area of the lower river section related to an outburst flood with a 1 in 1,000 years probability. Area marked in red is estimated to be eroded in this scenario

Results and Conclusions

In the oversteepened narrow glacial valleys of the SE of Møre og Romsdal county rockslide damming is a likely secondary phenomena of larger rock slope failures. It has happened both in prehistoric and historical times and will likely happen related to future large rock slope failures. The direct impact of rockslope failures is often limited due to restricted settlement in the valleys. However, due to up- and potential down-stream flooding the hazard affects a much larger area than the run-out area of the rockslide itself and has to be considered during urban planning.

The main challenge in the presented analyses is the possibility of the generation of a highly sediment rich flood which behave different from a normal flood. However the case of the rockslide dam at Olinsavatnet demonstrates that rockslide dams do not only present a risk to society but that dams which are stable or can get stabilised can be used for hydropower generation.

Acknowledgments We want to acknowledge the financial support of this mapping program by the Norwegian Water and Energy Directorate (NVE) and namely Graziella Devoli and Ollianne Eikenæs for fruitful discussions throughout the years.

References

- Abbott J (1848) Inundation of the Indus, taken from the lips of an eye-witness A.D., 1842. *J Asiatic Soc Bengal* 17:230–232
- Adushkin VV (2005) Russian experiences of blast-fill dam erection. *Ital J Eng Geol Environ* 1(Special issue):199–202
- Blikra LH, Longva O, Braathen A, Anda E, Dehls JF, Stalsberg K (2006) Rock slope failures in norwegian fjord areas; examples, spatial distribution and temporal pattern, vol 49, NATO science series IV, Earth and environmental sciences. Springer, Dordrecht, pp 475–496
- Braathen A, Blikra LH, Berg SS, Karlsen F (2004) Rock-slope failures in Norway; type, geometry, deformation mechanisms and stability. *Norwegian J Geol* 84:67–88
- Costa CH, González Díaz EF (2007) Age constraints and paleoseismic implication of rock avalanches in the northern Patagonian Andes, Argentina. *J South Am Earth Sci* 24:48–57
- Costa JE, Schuster RL (1988) The formation and failure of natural dams. *Geol Soc Am Bull* 100:1054–1068
- Dahle H, Anda E, Sætre S, Saintot A, Böhme M, Hermanns RL, Oppikofer T, Dalsegg E, Rønning JS, Derron MH (2011) Risiko og sårbarhetsanalyse for fjellsred i Møre og Romsdal. 105 p
- Dai FC, Lee CF, Deng JH, Tham LG (2005) The 1786 earthquake-triggered landslide dam and subsequent dam-break flood on the Dadu River, southwestern China. *Geomorphology* 65: 205–221
- Duman TY (2009) The largest landslide dam in Turkey: Tortum landslide. *Eng Geol* 104:66–79
- Dunning SA, Rosser NJ, Petley DN, Massey CR (2006) Formation and failure of the Tsatichhu landslide dam, Bhutan. *Landslides* 3:107–113
- Ermini L, Casagli N (2003) Prediction of the behaviour of landslide dams using a geomorphologic dimensionless index. *Earth Surf Process Land* 28:31–47
- Evans SG (2006) The formation and failure of landslide dams: an approach to risk assessment. *Ital J Eng Geol Environ* 1(Special issue):15–20
- Evans SG, Delaney KB, Hermanns RL, Strom AL, Scarascia Mugnozza G (2011) The formation and behaviour of natural and artificial rockslide dams; implications for engineering performance and hazard management. In: Evans SG, Hermanns RL, Strom AL, Scarascia Mugnozza G (eds) *Natural and artificial rock slide dams. Lecture notes in earth sciences*, vol 133, Springer, Berlin, pp 1–76
- Fenton CR, Hermanns RL, Blikra LH, Kubik PW, Bryant C, Niedermann S, Meixner A, Groethals MM (2011) Regional ^{10}Be production rate calibration for the past 12 ka deduced from the radiocarbon-dated Grøtlandsura and Russenes rock avalanches at 69° N, Norway. *Quatern Geochronol.* doi:10.1016/j.quageo.2011.04.005
- Furseth A (2006) *Skredulykker i Norge*. Tun Forlag, Oslo, 207p
- González Díaz EF, Giaccardi A, Costa C (2001) La avalancha de rocas del río Barrancas (Cerro Pelán), norte del Neuquén: su relación con la catástrofe del río Colorado (29/12/1914). *Revista de la Asociación Geológica Argentina* 56:466–480
- Groeber P (1916) Informe sobre las causas que han producido las crecientes del río Colorado (Provincia de Neuquén, Argentina). *Dirección General de Minas, Geología e hidrogeología* 11:1–29
- Hancox GT, McSaveney MJ, Manville VR, Davies TR (2005) The October 1999 Mt Adams rock avalanche and subsequent landslide

- dam-break flood and effects in Poera River, Westland, New Zealand. *New Zeal J Geol Geophysics* 48:683–705
- Hermanns RL, Niedermann S, Ivy-Ochs S, Kubik PW (2004a) Rock avalanching into a landslide-dammed lake causing multiple dam failures in Las Conchas valley (NW Argentina) – evidence from surface exposure dating and stratigraphic analyses. *Landslides* 1:113–122
- Hermanns RL, Naumann R, Folguera A, Pagenkopf A (2004b) Sedimentologic analyses of deposits of a historic landslide dam failure in Barrancas valley causing the 1914 Rio Colorado flood, northern Patagonia, Argentina. In: Lacerda WA, Ehrlich M, Fontoura SAB, Sayão ASF (eds) *Landslides, evaluation and stabilization*. Balkema, Leiden, pp 1439–1445
- Hermanns RL, Blikra LH, Naumann M, Nilsen B, Panthi KK, Stromeyer D, Longva O (2006) Examples of multiple rock-slope collapses from Köfels (Ötztal valley, Austria) and western Norway. *Eng Geol* 83:94–108
- Hermanns RL, Blikra LH, Longva O (2009) Relation between rockslide dam and valley morphology and its impact on rockslide dam longevity and control on potential breach development based on examples from Norway and the Andes. In: *Proceedings of the 2nd international conference: long term behaviour of dams*, Graz, 12–13 Oct 2009, pp 789–794
- Hermanns RL, Blikra LH, Anda E, Saintot A, Dahle H, Oppikofer T, Fischer L, Bunkholt H, Böhme M, Dehls JF, Lauknes TR, Redfield TF, Osmundsen PT, Eiken T (2011) Systematic mapping of large unstable rock slopes in Norway. In: *Proceedings of the 2nd world landslide forum*, Rome, 3–7 Oct 2011, this volume
- Hermanns RL, Hewitt K, Strom AL, Evans S G, Dunning SA, Scarascia Mugnozza, G (2011) The classification of rock slide dams. In: Evans SG, Hermanns RL, Strom AL, Scarascia Mugnozza G (eds) *Natural and artificial rock slide dams*. Lecture notes in earth sciences, vol 133, Springer, Berlin, pp 581–594
- Ischuk AR (2011) Usoi rockslide dam and Lake Sarez, Pamir Mountains, Tajikistan. In: Evans SG, Hermanns RL, Strom AL, Scarascia Mugnozza G (eds) *Natural and artificial rock slide dams*, Lecture notes in earth sciences, vol 133, Springer, Berlin, pp 423–440
- Jia-Jyun D, Yu-Hsiang T, Chien-Chih C, Jyh-Jong L, Yü-Wen P (2009) Discriminant analysis of the geomorphic characteristics and stability of landslide dams. *Geomorphology* 110:162–171
- Korchevskiy VF, Kolichko AV, Strom A, Pernik LM, Abdrakhmatov KE (2011) Utilisation of data derived from large-scale experiments and study of natural blockages for blast-fill dam design. In: Evans SG, Hermanns RL, Strom AL, Scarascia Mugnozza G (eds) *Natural and artificial rock slide dams*. Lecture notes in earth sciences, vol 133, Springer, Berlin, pp 617–639
- Korup O (2004) Geomorphometric characteristics of New Zealand landslide dams. *Eng Geol* 73:13–35
- Longva O, Blikra LH, Dehls JF (2009) Rock avalanches – distribution and frequencies in the inner part of Storfjorden, Møre og Romsdal county, Norway. 2009.002, Norges Geologiske Undersøkelse, Trondheim, Norge, 32p
- Manville V (2001) Techniques for evaluating the size of potential dam-break floods from natural dams. Institute of Geological & Nuclear Sciences science, report 2001/28, 72p
- Meyer W, Sabol MA, Glicken HX, Voight B (1985) The effects of groundwater, slope stability, and seismic hazard on the stability of the South Fork Castle Creek blockage in the Mt. St. Helens area, Washington. USGS Professional Paper, 1345, pp 1–42
- Quenta G, Galaza I, Teran N, Hermanns R L, Cazas A, García H (2007) Deslizamiento traslacional y represamiento en el valle de Allpacoma, ciudad de La Paz, Bolivia. In: *Proyecto Multinacional Andino: Geociencias para las Comunidades Andinas*. Servicio Nacional de Geología y Minería, Publicación Multinacional, vol 4, pp 230–234
- Saintot A, Henderson I H C, Derron M-H (2011) Inheritance of ductile and brittle structures in the development of large rock slope instabilities: examples from Western Norway. In: Jaboyedoff M (ed) *Slope tectonics*, Geological Society, London, Special Publication, 351. (ISBN 978-1-86239-324-0), pp 27–78
- Schuster RL (2006) Impacts of landslide dams on mountain valley morphology. In: Evans SG, Scarascia Mugnozza G, Strom AL, Hermanns RL (eds) *Landslides from massive rock slope failures*. NATO Science Series IV. Earth and environmental sciences, vol 49, Springer, Dordrecht, pp 591–618
- Stone R (2009) Peril in the Pamirs. *Science* 326(5960):1614–1617
- Zevallos O, Fernandez MA, Plaza Nieto G, Klinkicht Sojos S (1996) Sin plazo para la esperanza, reporte sobre el desastre de La Josephina – Quito: Escuela Politécnica Nacional